1970

Dynamic adsorption of propane and propylene on activated carbon

Fred Baxter Smith Jr.
Iowa State University

DYNAMIC ADSORPTION OF PROPANE AND PROPYLENE ON ACTIVATED CARBON

by

Fred Baxter Smith, Jr.

A Dissertation Submitted to the
Graduate Faculty in Partial Fulfillment of
The Requirements for the Degree of
DOCTOR OF PHILOSOPHY

Major Subject: Chemical Engineering

Approved:

Signature was redacted for privacy.

In Charge of Major Work

Signature was redacted for privacy.

Head of Major Department

Signature was redacted for privacy.

Dean of Graduate College

Iowa State University
Ames, Iowa

1970

TABLE OF CONTENTS

ABSTRACT

A series of exchange adsorption runs were made between the gas-pair propane and propylene on Columbia LC 20/48, Grade H-63-11 activated carbon to determine the resulting isothermal breakthrough curves. These runs were made at 25° C and 1 atmosphere pressure.

The results of these runs were compared with the breakthrough curves predicted by mathematical models which assume isothermal adsorption in the bed and are applicable to this system. It was found that models proposed by Glueckauf and Coates and Eagleton and Bliss appeared to fit the experimental data. All other models tested failed to predict the shape of the breakthrough curve or the time of the breakpoint.

The gas flow rate and carbon particle size were varied and correlations obtained between the mass flow rate and the gas and solid phase mass transfer coefficients and the overall gas and solid phase mass transfer coefficients. It was found that the mass transfer coefficients increase as the mass flow rate increases.

Particle diffusivities were also calculated and a correlation found with the mass flow rate and particle size. Since the particle diffusivity varied with mass flow rate and particle size, it was concluded that these calculated diffusivities were not properties of the system but instead "effective" diffusivities since they appeared to be "structure sensitive."

In addition, equilibrium isotherms at 25° C were determined up to 760 mm Hg for propane and propylene on Columbia LC 20/48, Grade H-63-11, activated carbon. Comparison of experimental data with equilibrium isotherms predicted by several models indicated that the B.E.T. model fit the data best over the range of the isotherm determined.

A correlation was also found between the temperature rise in an adsorption bed due to heat of adsorption and the mole fraction of the adsorbate in a carrier gas stream of helium.

INTRODUCTION

A number of mathematical models have been proposed to describe the selective adsorption of gases on particulate solids. Each model attempts to reproduce the isothermal breakthrough curve which results when a given adsorbate is stripped from an inert carrier gas by an adsorbent. In addition to temperature, factors which affect the shape of the breakthrough curve are the adsorbent particle size, gas flow rate, equilibrium relationships, and column height.

Evaluation of the proposed models has been hampered by the lack of true isothermal data. Even though experiments are carried out in a constant temperature environment, heats of adsorption and desorption have a significant effect at the gas-solid interface.

In this project, very precise adsorption data were obtained for the gas pair propane-propylene where the respective heats of adsorption and desorption are essentially equal, thus assuring collection of essentially isothermal data. In addition, adsorbent particle size and gas flow rate were varied. From the rate data, diffusion coefficients and diffusivities were calculated and a comparison made between the nearly isothermal breakthrough curve observed and the breakthrough curve predicted by the appropriate models.

Previous Investigations of Isothermal Adsorption

There are currently two reports in which a similar method was used to investigate adsorption characteristics. The first, conducted by Norman (32), involved the exchange of propane and propylene on silica gel. In his investigation, Norman found diffusivities for the cases of propane replacing propylene and propylene replacing propane. Although his apparatus included thermocouples, no report was made of observed temperature rises in the adsorption bed. The preliminary findings of this research project, on the other hand, include large temperature rises measured in the bed. In addition, the small length (one inch) of adsorption bed used by Norman leads to questions concerning the applicability of his work to fixed-bed adsorption because of end effects in the flow pattern.

The other investigation was reported by v. Szirmay (41) who studied the exchange of ethane and ethylene on a fixed-bed of Pittsburgh activated carbon. Breakthrough data and diffusivities were obtained by v. Szirmay for a number of conditions involving this particular gas pair, but he did not conduct any tests for isothermal conditions in his adsorption bed during the adsorption process. In addition, no attempt was reported concerning fitting the experimental data to the various applicable models.

No other work concerned with obtaining isothermal breakthrough data was found having been reported.

Proposed Plan for Conducting Research

From preliminary data obtained, Columbia LC 20/48, Grade H-63-11 activated carbon was chosen as the primary adsorbent for this research. This was primarily due to the relatively low temperature rise observed in the bed compared to the temperature rise observed when initially saturating the bed with propane. In addition, the heat of adsorption data for this particular type of activated carbon was available (17).

The research was divided into three phases. They were: 1) determination of the equilibrium isotherms for propane and propylene on Columbia LC 20/48 activated carbon at 25° C, 2) determination of breakthrough data for propane replacing propylene and propylene replacing propane on Columbia LC 20/48 activated carbon, and 3) comparison of experimentally determined breakthrough curves with the breakthrough curves predicted by the applicable models.

The first two phases were concerned with obtaining the necessary data in order to test the applicability of the appropriate models planned for the third phase. The equilibrium data obtained in the first phase was an integral component of each model and varied with each type of activated carbon. Since all breakthrough curves were determined at 25° C, only the equilibrium isotherm of propane and propylene on Columbia LC 20/48 activated carbon at this temperature was determined.

The second phase involved very precise determinations of the breakthrough curves for propane being adsorbed by a bed of

Columbia LC 20/48 which had been previously saturated with propylene and vice versa. In addition, gas flow rate and bed particle size were varied and an attempt to correlate these variations was made. All runs were conducted at 760 mm Hg.

In the final phase, the data obtained in the first two phases were used to test the fit of various models, which assume isothermal conditions and are described later in this report, to the nearly isothermal data obtained. In addition, the diffusion coefficients and diffusivities for each system were determined.

ADSORPTION THEORY

Equilibria

The most widely used method of expressing adsorption data is to present the equilibria data of the system under study. Much of this type of presentation was originally intended to provide corroboration for one or another of the many theories postulated in an attempt to explain the adsorption phenomena. Since no one theory has been devised which satisfactorily explains even a majority of the observations, this discussion will consist of a description of several of the more commonly observed adsorption characteristics which are pertinent to the systems under study.

In the physical adsorption of a gas, the amount of gas adsorbed by a given adsorbent depends on the vapor pressure p, the temperature T, the nature of the gas, and the nature of the solid. Therefore, $X^* = f(p,T,gas,solid)$. A set of data representing measurement at constant temperature of the quantity adsorbed by a unit of adsorbent in equilibrium with a known concentration or pressure of the mobile phase, or an analytical expression representing such data, is called an adsorption isotherm. Other means of expressing equilibrium data are the isobar and isostere. However, the isotherm is generally regarded as the most useful means of equilibrium expression.

In many respects, the graphical presentation of adsorption isotherms of a gas or vapor on a solid resembles the equilibrium solubility of a gas in a liquid. These plots have

a wide variation of shapes and are therefore classified by this characteristic. Some of the isotherm shapes have been quantitatively classified and are shown in Figure 1 (4, 19).

The five most common types of isotherms are types A, B, C, D, and E shown in Figure 1. In type A, the adsorption isotherm is hyperbolic and approaches a constant asymptotic value at a relative saturation of unity. This is explained by the small size of the pores of the adsorbent in which there is space for only one monolayer on the walls of the pore. This type of isotherm conforms to the Langmuir (23) equilibrium concept and may represent favorable equilibrium.

In type B, the adsorption curve is S-shaped and increases to infinity as the relative saturation approaches unity. This is explained by the formation of a multimolecular layer of indefinite thickness.

Type C is distinguished by its curvature convex toward the adsorbate concentration axis. The second derivative of the curve is always positive and the amount of gas adsorbed increases without limit as its relative saturation approaches unity. In this case, as was noted for type B, an infinite molecular layer is feasible. The explanation for the convex curvature may be accounted for by heats of adsorption in the first layer becoming less than the normal heat of condensation due to interaction between molecules occurring in the first layer.

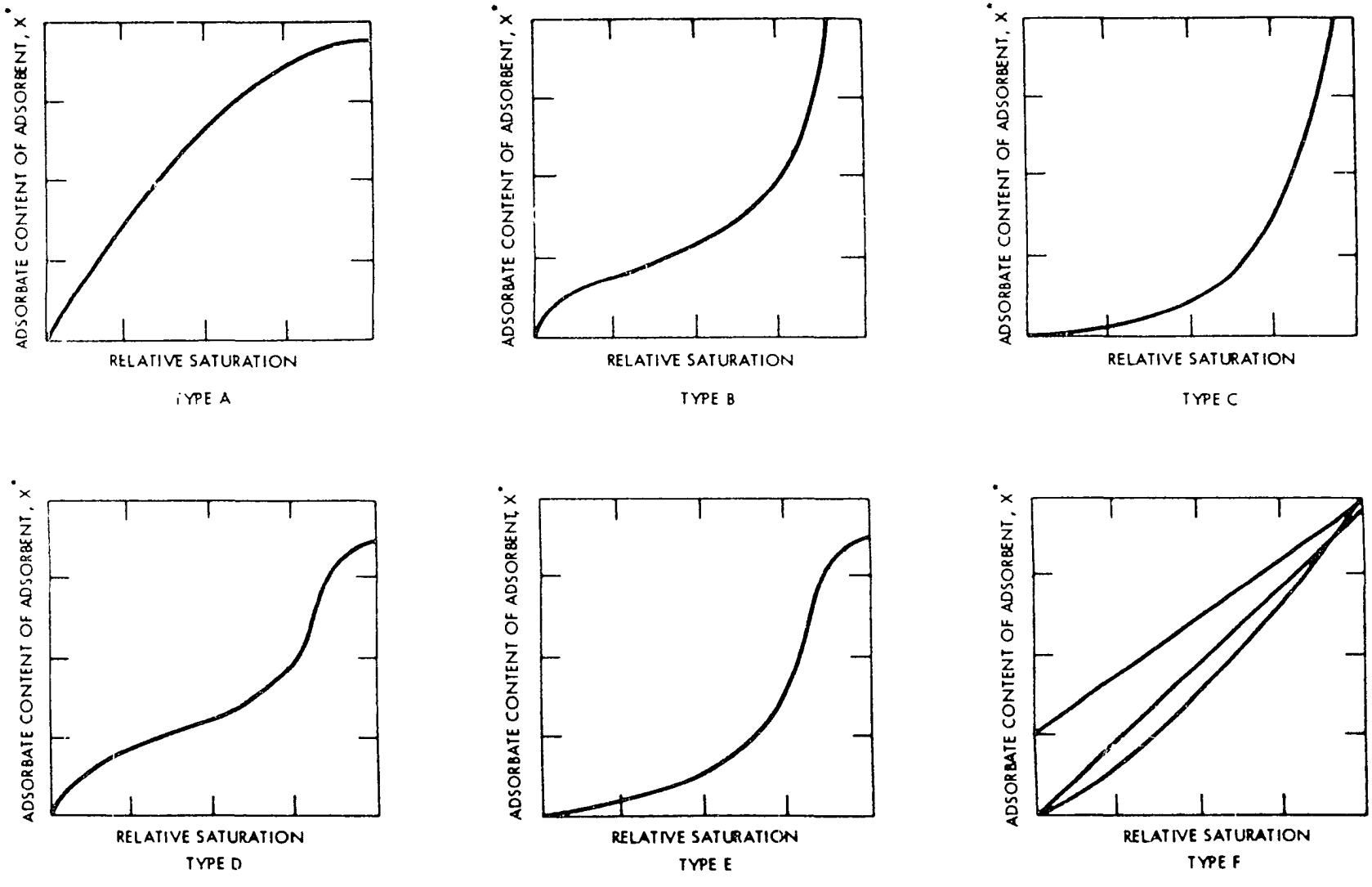

Figure 1. Typical equilibrium isotherms

Type D is similar to type B in the low and intermediate ranges of relative saturation of the adsorbate, but the curve approaches a maximum finite value at a relative saturation of unity. The high values of the relative saturation of the adsorbent are accounted for by capillary condensation with the maximum value indicating complete filling of the capillaries.

Type E is similar to type C at low and intermediate ranges of relative saturation, but approaches a maximum finite value for the relative saturation of the adsorbent as the relative saturation of the adsorbate approaches unity. This phenomena is due to capillary condensation and building up of a layer of finite thickness at saturation. The initial convex curvature can be accounted for by the heat of adsorption of the first layer becoming less than the heat of normal condensation due to interaction of molecules in the first layer as in type C.

The remaining isotherms, type F, are modifications of the five types discussed above and no attempt to discuss them will be made.

Figure 2 is a plot of the equilibrium isotherms of propane and propylene on an activated carbon. It is noted that both are type A isotherms which represent monolayer adsorption and favorable equilibrium.

Monolayer adsorption equilibria

For an "ideal" system in which all adsorbent sites are identical and in which there is no interaction between molecules

Figure 2. Equilibrium isotherms of propane and propylene on Columbia LC 20/48, Grade H-63-11, activated carbon at 25° C

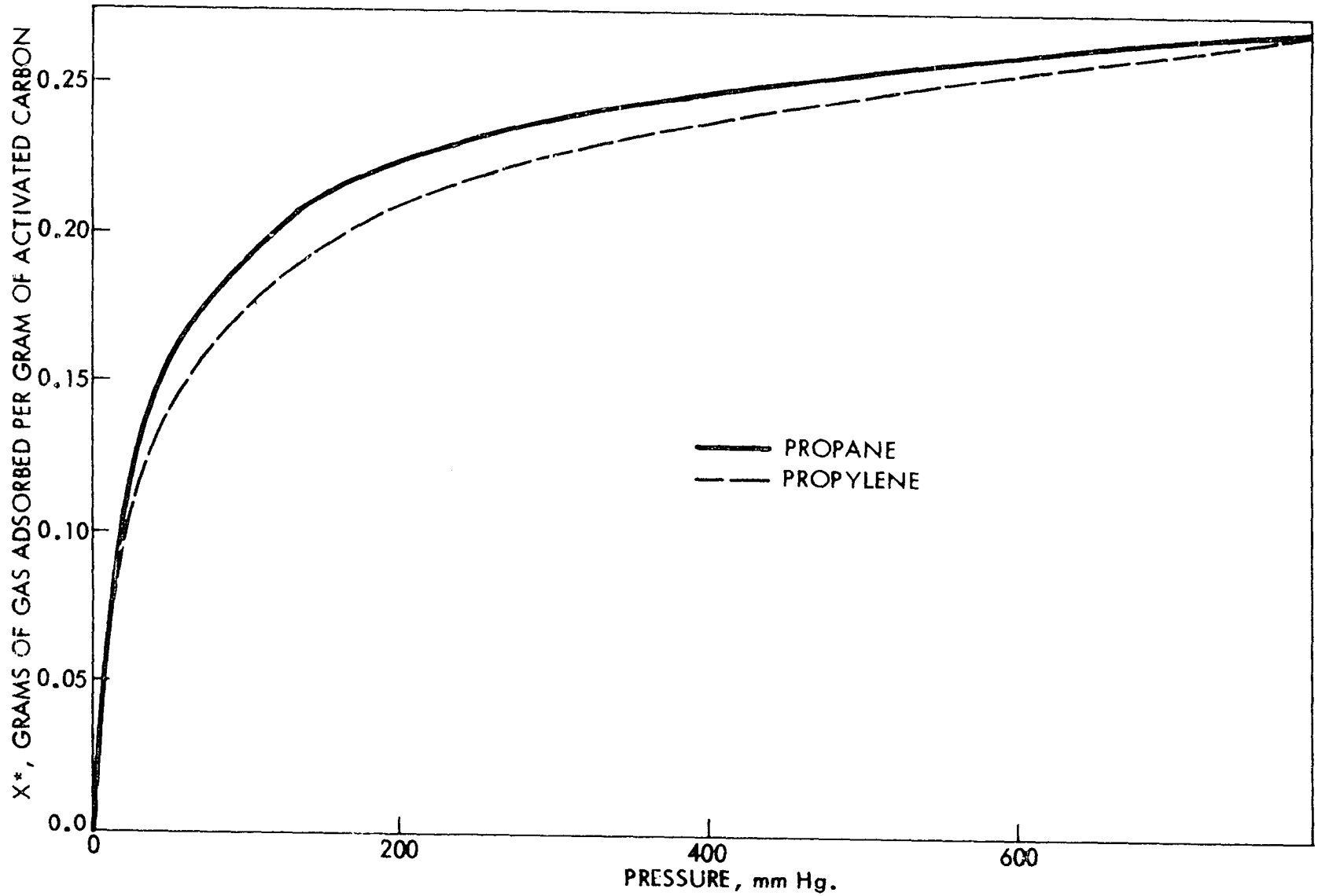
X*, GRAMS OF GAS ADSORBED PER GRAM OF ACTIVATED CARBON
0.25
0.20
0.15
0.10
0.05
0.0
0
200
400
600
PRESSURE, mm Hg.
PROPANE
PROPYLENE

adsorbed on adjacent sites, an equation which is perhaps the most important equation in the field of adsorption was developed by Langmuir (23) on a theoretical basis. Langmuir, believing that adsorption was a chemical process, and that the adsorbed layer was unimolecular, proposed that the equilibrium set up between the adsorbed monolayer gas and the adsorbent is a dynamic one in which the rate of condensation of a molecule on a bare site of adsorbent surface is equal to the rate at which they re-evaporate from the occupied sites. The isotherm derived by Langmuir is described by:

$$\frac{X^*}{X_m} = \frac{Bp}{1 + Bp} \qquad (1)$$

where: X_m = monolayer adsorbent capacity.

B = a temperature dependent constant characteristic of the adsorbent with units of pressure^{-1}.

p = vapor pressure of the adsorbate, mm Hg.

Some forms of the Langmuir equation show the gas phase concentration, C^*, substituted for the vapor pressure, p (20).

The shape of the graph of Equation 1 has the general form of the type A isotherm shown in Figure 1. An increase in the heat of adsorption causes the constant, B, to increase and results in the graph having a sharpened bend which is closer to the solid concentration or X^* axis.

The validity of the Langmuir equation for a particular system may be tested by three criteria: 1) whether the experimental data fit the equation, 2) whether the constant in the equation, representing independently measurable physical

quantities, has a reasonable value, and 3) whether the equation reproduces correctly the temperature dependence of the adsorption under study (4).

As stated previously, the Langmuir equation is a theoretical representation for equilibria data which does provide a useful standard for ideality. However, this equation is often not applicable for real systems which are often better represented by the Freundlich or "classical isotherm" described by (16):

$$X^* = kp^{1/n'} \qquad (2)$$

where: k = a constant.

n' = a constant with a value greater than one.

This classical isotherm was originally empirical, but has been derived since then by a suitable site distribution treatment which assumes no appreciable interaction between adjacent molecules of the adsorbent (4). The two constants may be found by plotting ln X^* versus ln p with the intercept giving ln k and the slope equaling 1/n'. Substitution of the solvent concentration, C^*, for the vapor pressure, p, is also found in some forms of this equation (20).

Another unimolecular adsorption theory was proposed by Magnus (26). He assumed that the forces of interaction between the surface of the adsorbent and gas were electrostatic in nature, and not chemical as assumed by Langmuir. In addition, he assumed that on the surface of the adsorbent, the molecules held behaved like a two-dimensional imperfect gas whose actions

conformed to the van der Waals equation of state. However, it was recently shown by deBoer (9) that this assumption leads to erroneous results. Therefore, Magnus' theory and resulting equation will not be further discussed.

Another quantitative description of adsorption equilibria is the B.E.T. equation (Brunauer, Emmett, and Teller equation) (6). The B.E.T. equation, with certain modifications (5), can be quantitatively used in the general case to reproduce types A through F isotherms in Figure 1, most of which assume multilayer adsorption. However, the general application of these equations is limited by the oversimplification of the basic assumptions. The theory does retain the concept of fixed adsorption sites, but allows for the formation of an adsorbed layer of more than one molecule thick in which the state of "dynamic equilibrium" is assumed to hold for each successive molecular layer.

The B.E.T. equation is (6):

$$\frac{p}{X^*(p_s - p)} = \frac{1}{X_m b} + \frac{(b - 1)p}{X_m b p_s} \qquad (3)$$

where: b = constant.

p_s = saturation vapor pressure at temperature T, mm Hg.

For monomolecular adsorption, the B.E.T. equation reduces to the following general form of the Langmuir equation:

$$\frac{X^*}{X_m} = \frac{Ap}{1 + (A - 1/p_s)p} \qquad (4)$$

where: A = empirical constant.

The quantitative failure of the Langmuir isotherm equation and the B.E.T. equation, when correlating with experimental data, is attributed to the variation in the site activation energies or surface nonuniformity (5, 6).

Theories of Adsorption Phenomena

Potential theory

The B.E.T. equation is one of several developed from theories proposed by Polanyi (34) which are based on the concept of adsorption potential. Polanyi believed that adsorption was a physical process and that the adsorbed phase was many layers thick in contrast to Langmuir's theory.

The model upon which Polanyi based his potential theory originated with de Saussure (10) who proposed the compressed film hypothesis. The Polanyi theory suggests that the adsorbent exerts a strong attractive force upon the gas in its vicinity which gives rise to adsorption. These forces of attraction are electrical in nature and are so strong that they can attract and hold many adsorbed layers on the surface of the solid. The first layers to form are under pressure, partly because of the layers on top of the layer under pressure, and partly because of the forces of attraction of the solid surface. The compression is greatest on the first adsorbed layer,

less on the second, and so on until the density decreases to that of the surrounding gas. Thus, the structure of the adsorbed phase, according to the "compressed film" theory, is similar to that of the atmosphere surrounding the earth.

The original theory which described the force of adsorption as an "intermolecular gradient" was conceived by Eucken (14). However, he had incorrectly formulated this theory quantitatively which was correctly formulated by Polanyi several years later. Polanyi defined the adsorption potential at a point near the adsorbent as the work done by the adsorption forces in bringing a molecule from the gas phase to that point. This work may be viewed as a work of compression, and is defined mathematically by the so-called hydrostatic equation (34):

$$\beta_i = \int_{\rho_x}^{\rho_i} V dp \qquad (5)$$

where: β_i = adsorption potential at a point where the density of the adsorbed substance is ρ_i.

ρ_x = density of the gas phase.

V = molar volume of adsorbate = M/ρ.

M = molecular weight of adsorbate.

In order to evaluate the integral in Equation 5, it is necessary to express the molar volume, V, or the density, ρ, as a function of the pressure of both the gas and adsorbed phases. Since the equation of state of the adsorbed phase is

unknown, Polanyi assumed the gas obeys the same equation of state in the adsorbed phase as in the gas phase. This assumption is based on the similarity between van der Waals adsorption and condensation.

The potential theory also assumes that the adsorption potential does not change with temperature. This means that the curve representing the potential distribution is the same for all temperatures. Thus, the validity of the potential theory can be tested by the ability to calculate isotherms for a particular system at different temperatures from one initial isotherm with a fair degree of accuracy (35).

Capillary condensation theory

The capillary condensation theory describes the adsorbate as condensing to an ordinary liquid in the pore of the solid, usually after the walls of the pores have become lined with an adsorbed monolayer. It was first proposed in 1911 by Zsigmondy (44) who, while examining the pore structure of silica gel under an ultramicroscope, came to the conclusion that the gel contained much finer capillaries than had been previously supposed by early investigators. Since silica gel was known to take up a large quantity of water, the idea occurred to him to correlate the adsorption of water with the capillary properties of the gel. Since it had been known for a long time that in a capillary immersed in a liquid which wets its walls, the liquid rises in the capillary and forms a meniscus

which is concave toward the vapor phase. The vapor pressure of the liquid over the meniscus is lower than the normal vapor pressure of the liquid by an amount equal to the pressure exerted by the column of liquid in the capillary. The vapor pressure lowering over a cylindrical capillary is described by the Kelvin equation (44):

$$\ln \frac{p}{p_s} = - \frac{2 \sigma V}{r_c RT} \cos \theta \qquad (6)$$

where: p = vapor pressure over the meniscus of the capillary.

p_s = saturation vapor pressure.

r_c = capillary radius.

σ = surface tension of the condensed vapor.

θ = angle of wetting. For complete wetting, $\theta = 0^\circ$ and $\theta = 180^\circ$ for absolute nonwetting.

From the above equation, the capillary radius, r_c, may be calculated. It is assumed in this calculation that the diameter of the molecules in the capillary is negligible in comparison to the capillary radius. It is apparent, therefore, that the smaller the capillary radius, the greater the vapor pressure lowering. This led Zsigmondy to conclude that in capillaries as small as the ones found in silica gel, a liquid would condense at pressures far below the normal vapor pressure.

This theory is still regarded as valid today as most investigators believe that capillary condensation plays some role in van der Waals adsorption. However, the degree to which

capillary condensation contributes to physical adsorption is a matter of disagreement.

Zsigmondy did distinguish between direct adsorption on the walls of the capillary and condensation and this was the theoretical basis which predecessors used in justifying the use of the Kelvin equations as the fundamental equation of their work. They assumed that capillary condensation became important only when adsorbents had capillaries at least several molecular diameters in width, and at pressures not very far from saturation pressure.

The major disagreement on the degree with which capillary condensation affected adsorption was published by McGavack and Patrick (28). Patrick's initial theory was that all physical adsorption was due to capillary condensation. Later he admitted the existence of unimolecular adsorption, but continued to believe that all other physical adsorption was due to capillary condensation. He also believed that the Kelvin equation was not valid down to pore diameters of molecular diameter.

McGavack and Patrick proposed an empirical equation with the basis of comparison the volume of liquid condensed in the capillaries at the relative pressure p/p_s instead of the volume of gas adsorbed at pressure p to use in place of the Kelvin equation. Starting with the Freundlich equation and rewriting it on the basis of relative pressure, they proposed the following equation (28):

$$X^* = k''(p/p_s)^{1/n'} \qquad (7)$$

where: k'' = an empirical constant.

n' = an empirical constant with a value greater than unity.

Equation 7 was tested by plotting ln X^* versus ln (p/p_s) for sulfur dioxide on silica gel from -80° to 100° C. Good straight lines resulted which intersected at a point where $p = p_s$ for all temperatures (4, p. 122) indicating that at saturation pressure, all capillaries of the adsorbent are filled with liquid. Since the total pore volume is constant, it is apparent that the value of X^* should be the same for all temperatures. This is substantiated by the potential theory. McGavack and Patrick then postulated that because of a change in the density of the liquid due to negative hydrostatic pressure, the change in X^* at lower (p/p_s) which occurs in Equation 7 could be explained and corrected by multiplying the (p/p_s) term by the surface tension, σ, of the liquid since it is known that the greater the surface tension, the less the compressibility. The modified equation is therefore (28):

$$X^* = k(\sigma p/p_s)^{1/n'} \qquad (8)$$

where: k = an empirical constant.

Although the derivation of Equation 8 cannot be completely justified theoretically, it has been justified empirically as seen for sulfur dioxide on silica gel described above. This leads to the conclusion that the assumption made regarding the

volume occupied by the adsorbed phase was the same at the same values of (p/p_s) regardless of the temperature is valid. Since Equation 8 does not hold, however, for all systems, it must therefore be concluded that Equation 8 is strictly an empirical equation and does not prove or disprove the capillary condensation theory, but is a useful tool when it is valid.

Hysteresis

Theoretically, adsorption-desorption curves should coincide. This is not always the case, however, and the resulting phenomena is termed "hysteresis." Although no mechanism has been proposed which fits all the experimental data, most investigators associate hysteresis with capillary condensation (27).

Cohan (8) classified the proposed theories regarding hysteresis as: 1) the incomplete wetting theory, 2) the ink bottle theory, and 3) the open pore theory. The incomplete wetting theory was proposed by Zsigmondy (44). He believed that a film of gas on the surface of the capillaries caused incomplete wetting. However, if this explanation were valid, the presence of air or any other impurity would cause the hysteresis loop to occur from one end of the isotherm to the other and be eliminated when the impurity was removed. This does not occur and therefore the incomplete wetting theory is considered invalid (27).

The ink bottle theory postulates that constricted necks near the openings of the capillaries are responsible for hysteresis. Some investigators believe that while the ink bottle theory is not the main cause of hysteresis, it is responsible for some portion of the phenomena (8).

The open pore theory suggests that the clefts and pores of the solid may widen toward their bases and therefore behave as though they were large open areas on the surface of the adsorbent. As the adsorbate is adsorbed, a monomolecular layer of adsorbate is formed on the walls of the pore before it begins to fill due to capillary condensation. This causes a delay in the formation of a meniscus in the pore and accounts for no hysteresis effect to be noted until the monolayer of adsorbate has covered the walls of the pore. It is further postulated that the liquid in the pore has similar properties to that of the liquid in bulk. Therefore, during desorption, the surface tension of the liquid in the pore resists the removal of the liquid from the pore and accounts for the higher values of relative saturation of the adsorbent during desorption.

Using the open pore theory as a basis, Cohan predicted and confirmed that the hysteresis loop begins at a partial pressure corresponding to a capillary radius, calculated from the Kelvin equation, which was twice the thickness of the adsorbed film. He concluded that: 1) hysteresis usually begins at the partial pressure of a unimolecular layer adsorbed

on the capillaries, 2) the surface tension and density of a liquid adsorbed in a capillary are similar in magnitude to those properties of the liquid in bulk if the capillary radius is equal to or greater than twice the radius of the adsorbed molecule, 3) the formation of a monomolecular layer on the pore wall is accompanied by capillary condensation, and 4) the radii of such pores can be calculated from the Kelvin equation (8).

Heat of adsorption

Since adsorption decreases with a rise in temperature, it is expected that it should take place with the evolution of heat. This is substantiated by examining the thermodynamic equation:

$$\Delta F = \Delta H - T\Delta S \qquad (9)$$

where: F = free energy.

H = heat of adsorption.

S = entropy.

It is therefore apparent that adsorption is an exothermic process. The heat of adsorption is defined as the decrease in the heat content of the system undergoing adsorption (27). It is the sum of the heat of normal condensation and the heat of wetting.

The heat of adsorption may be expressed in one of two ways: either the differential heat of adsorption ($-\Delta H$), or the integral heat of adsorption. The former is given in BTU

per pound mole of adsorbate and is the preferable means of expressing heats of adsorption since the differential heat of adsorption may be easily compared to the latent heat of condensation. The differential heat of adsorption of a gas is defined as the change in enthalpy when a unit quantity of the gas is adsorbed by a relatively large quantity of adsorbent on which a definite concentration of the adsorbed gas already exists. It is also a function of the concentration, and it diminishes with an increase in concentration. As complete saturation of an adsorbent is approached, the differential heat of adsorption approaches that of normal condensation.

The integral heat of adsorption is usually expressed in BTU per pound of adsorbent and it varies with the concentration of the adsorbate, diminishing with an increase in concentration. It is defined as the change in enthalpy per unit weight of adsorbed gas when adsorbed on gas-free or "out-gassed" adsorbent to form a definite concentration of adsorbate (22). It may be calculated from the differential heat of adsorption by using the following equation (39):

$$Q = \int_0^X H dX \qquad (10)$$

The differential heat of adsorption may be calculated from the adsorption isotherms at two different temperatures by using the Clasius-Clapeyron equation which is of the form (15):

$$-\Delta H = \frac{RT_1T_2}{T_2 - T_1} \ln \frac{p_2}{p_1} \qquad (11)$$

where: p_1 and p_2 are the equilibrium pressures at temperatures T_1 and T_2 respectively.

Fixed-Bed Dynamics

From a mechanical viewpoint, adsorption on a large scale may be carried out in one of several ways. These include: 1) dumping the adsorbent into a fluid to be purified and later removing the adsorbent by filtration, 2) moving beds of adsorbent in a continuous, steady state operation, and 3) passing the fluid over a fixed-bed (2). Due to the inconvenience and relatively high cost of transporting solid particles as required in the first two methods listed above, the fixed-bed technique is the most commonly used method of large scale adsorption (30, 39).

In designing a fixed-bed adsorption column, there are several factors which must be determined to evaluate the effectiveness of the adsorbent. The first determination is the rate of adsorption. This information provides an insight into the feasibility of using the particular adsorbent under consideration and basic design information such as column height and flow rate through the column.

The effective rate of adsorption may be determined by one of several steps. The sequence of steps in the adsorption process are (43): 1) mass transfer from the bulk gas to the external surface of the adsorbent particles, 2) pore diffusion

in the fluid phase within the particles, 3) reaction at the phase boundary, 4) diffusion in the adsorbed surface layer, and 5) in cases of moderately high mass transfer with extremely slow flow rates, the breakthrough curves may be broadened by eddy dispersion or molecular diffusion in the longitudinal direction.

From Fick's law of diffusion, a description of the rate of accumulation of a substance at a given point in a medium as a function of time may be obtained. For the isotropic case, the equation is (1):

$$\frac{\partial C}{\partial t} = D(\nabla^2 C) \tag{12}$$

where: D = diffusivity.

The diffusivity must be defined as to whether the term is describing pore diffusion, condensed vapor diffusion, or particle diffusion (43).

The rate of particle diffusion may be approximated by the linear driving force relationship proposed by Glueckauf and Coates (19):

$$\left[\frac{dX}{dt}\right]_{Ws} = k_s a_p (X_i - X) \tag{13}$$

where: X = adsorbate content of adsorbent at time t.

X_i = adsorbate content of adsorbent at external surface of the adsorbent in equilibrium with C.

k_s = solid phase mass transfer coefficient.

a_p = particle surface area.

W_s = dry weight of adsorbent.

It is assumed that all resistances to solid diffusion are located in a very thin shell just inside the surface of the particle. This implies that the concentration of the adsorbate at the surface of the adsorbent, X_i, changes to X immediately upon crossing this shell and there are no additional concentration gradients inside the particle.

The second aspect of fixed-bed column design which must be determined is the column breakthrough curve. This curve provides information regarding effectiveness of the adsorbent in column operations, height and adsorption characteristics of the adsorption zone, and time of usefulness of the column. These pieces of information are all necessary in the design of the adsorption phase of an overall operation.

The shape and position of a breakthrough curve depends on three factors. They are: 1) equilibrium, 2) rate, and 3) stoichiometry. The breakthrough curve is usually S-shaped, as shown in Figure 3, and is a plot of the relative saturation of the adsorbate in the effluent stream during the run. The two main points of interest on the curve are the breakpoint and the bed exhaustion point. The breakpoint occurs at an arbitrary value of relative saturation of the effluent stream which is usually 0.05. This point signifies the emergence of the leading edge of the adsorption zone at the outlet end of the column. The bed exhaustion point is usually set at a relative

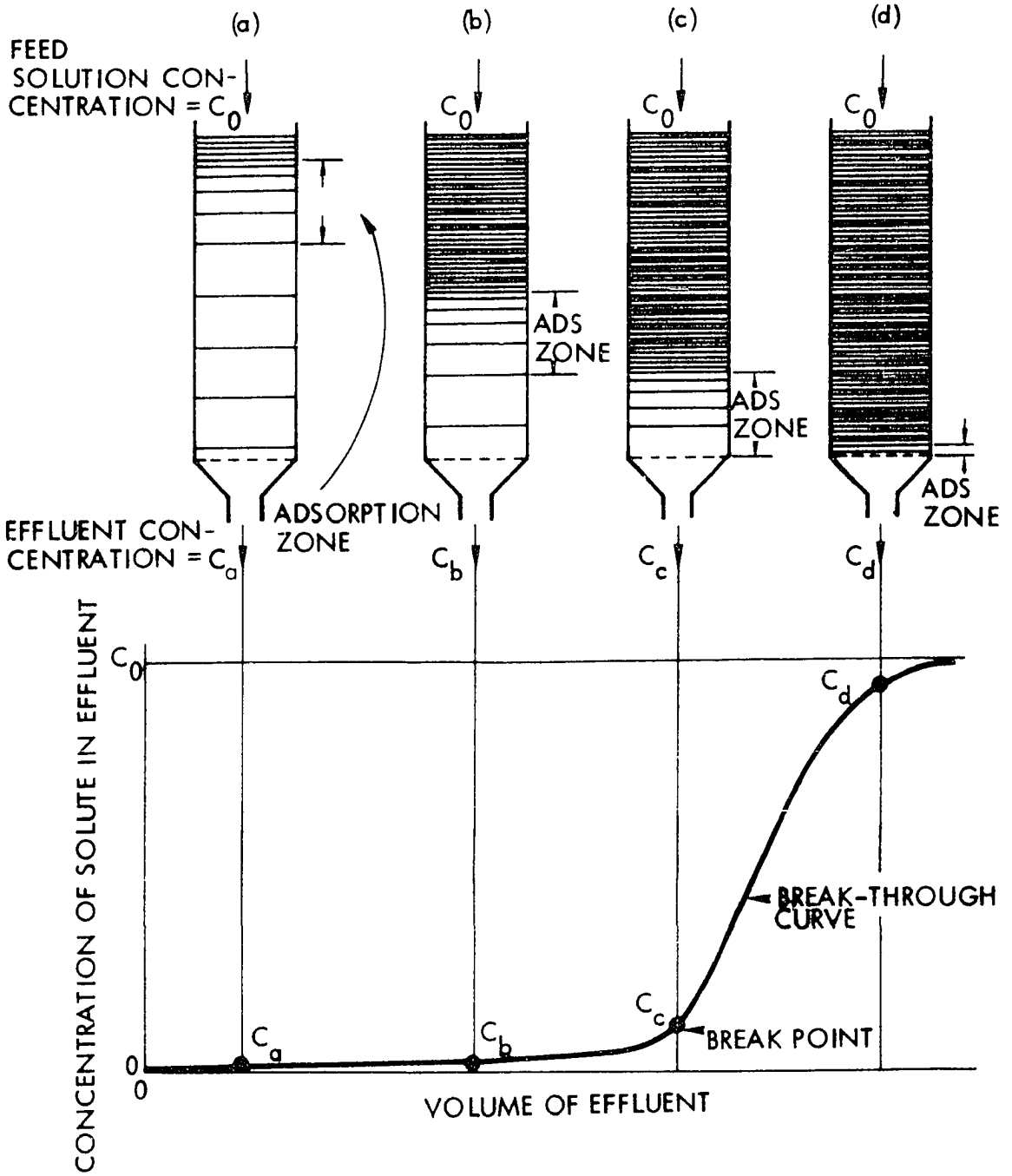

Figure 3. The adsorption wave (39)

saturation of the effluent stream of 0.95 and signifies the time at which the fixed-bed ceases to be effective in the removal of the adsorbate. The slope of the breakthrough curve provides information regarding adsorption characteristics in the adsorption zone and indicates the amount of leeway present in column operations after the breakpoint is reached and before the relative saturation becomes unacceptable.

Figure 3 (39) illustrates the operation of a fixed-bed adsorption column and the development of the breakthrough curve. The fluid containing the adsorbate is passed continually down through a relatively deep bed of adsorbent which is initially free of adsorbate. The uppermost layer of adsorbent first adsorbs the adsorbate rapidly and effectively. The adsorbate which is not adsorbed by the uppermost layers is substantially all removed by the layers of solid in the lower part of the bed. The effluent which leaves the bottom part of the bed is practically adsorbate-free as represented by C_a in Figure 3. The distribution of adsorbate in the bed is represented by the density of the horizontal lines in Figure 3. When the uppermost layer of the bed is practically saturated, the bulk of the adsorption takes place in a relatively narrow adsorption zone. This zone moves down the bed as the upper part of the zone becomes saturated with adsorbate at a rate very much slower than the linear velocity of the fluid through the bed. At a later time, such as at b in Figure 3, roughly half the bed is saturated with adsorbate while the effluent

stream remains essentially the same. When the lower portion of the adsorption zone has reached the bottom of the bed, as at c in Figure 3, the concentration of the adsorbate in the effluent stream rises to an appreciable value, C_c, for the first time. When this phenomena occurs, the bed is said to have reached the "breakpoint." As the adsorption zone passes out of the column, the concentration of adsorbate in the effluent rises rapidly until the concentration of the influent stream is reached. The breakthrough curve is therefore the concentration history of the adsorbate in the effluent stream between points c and d. If the adsorption process were infinitely rapid, the adsorption zone would be very narrow and the breakthrough curve would be a straight vertical line (39).

Breakthrough curve models

There have been many models attempting to describe the breakthrough curve (43). Each model makes several simplifying assumptions and is applicable to specific adsorption situations. No attempt will be made to report on any models except those applicable to this investigation.

In the case of propane and propylene being adsorbed on activated carbon, a strongly favorable equilibrium situation is present as shown in Figure 2. There are eight models which are applicable to this case. While each model has its own unique assumptions and is applicable to certain types of controlling diffusion, there are several assumptions which are common to

all models. They are: 1) the adsorption process is isothermal, 2) the pressure gradient along the length of the tower can be neglected, 3) there is no diffusion or dispersion in the longitudinal direction, 4) the gas mass velocity is constant, 5) the flowing gas contains a single adsorbing component, 6) the average particle concentration and gas composition do not vary across any given tower cross section, 7) the mass transfer rate constants are not functions of concentration, and 8) the concentration of the adsorbate in the inlet gas is constant (31).

Assumptions 1 to 6 are necessary to develop the differential form of the mass balance, which is one of the necessary equations in each model. One form of the differential mass balance is:

$$\left[\frac{\partial C}{\partial W_s}\right]_t + \frac{\epsilon}{G'}\left[\frac{\partial C}{\partial t}\right]_{W_s} + \frac{1}{G'}\left[\frac{\partial X}{\partial t}\right]_{W_s} = 0 \qquad (14)$$

where: ϵ = void fraction of the fixed-bed.

G' = mass flow rate of the solvent stream.

Thomas (38) made a suitable change in the independent variables which reduced Equation 14 to a simplified form. This was accomplished by substituting the cumulative weight of the pure solvent carrying the adsorbate, W, into Equation 14 by using the following relationship:

$$W = G't - \epsilon W_s \qquad (15)$$

Equation 14 then reduces to the continuity equation:

$$\left[\frac{\partial C}{\partial W_s}\right]_W + \left[\frac{\partial X}{\partial W}\right]_{W_s} = 0 \qquad (16)$$

Equation 16 is applicable for the case of a constant adsorption zone which is independent of the height of the fixed-bed. Integration of Equation 16 yields (42):

$$\frac{C}{C_o} = \psi \frac{X}{X_o^*} \qquad (17)$$

where: X_o^* = adsorbate content of adsorbent in equilibrium with C_o.

ψ = constant.

The first three models to be presented are applicable for the case where fluid-phase or external diffusion is the rate controlling mechanism. Most of the work for this case was conducted by H. Bliss and his associates.

Eagleton and Bliss (13) developed a kinetic model which interprets fixed-bed adsorption data in terms of mass transfer coefficients by using a gas film and solid shell resistance concept. In their development, they made the following assumptions: 1) the adsorption zone is constant as it moves through the bed, 2) no concentration, pressure or temperature gradients perpendicular to the flow, 3) no interparticle diffusion in the direction of flow, 4) the rate equations are linear and of the form of Equation 13, and 5) the isotherm, which in truth is curved and concave toward the solution concentration axis, is in fact concave to the solution

concentration axis, but made up of two straight lines. Their equations are:

$$X^* = \alpha + \left[\frac{X_o^* - \alpha}{C_o}\right] C^* \qquad \text{for } \alpha < X^* < X_o^* \qquad (18)$$

and

$$C^* = 0 \qquad \text{for } 0 < X^* < \alpha \qquad (19)$$

where: C^* = adsorbate concentration in equilibrium with X^*.

X^* = adsorbate concentration of adsorbent in equilibrium with C^*.

α = a constant determined by intercept $\neq 0$ from straight line isotherm.

Using the above assumptions and the method of Glueckauf (18), the following equations were derived to describe the breakthrough curve (13):

for $C_D > C$

$$\ln\left[\frac{C_D/C_o}{C/C_o}\right] = -\left[\frac{C_o k_g a_p}{X_o^* G'}\right] W + \left[\frac{k_g a_p W_s}{G'}\right] + 2 - \frac{C_o}{C_D} \qquad (20)$$

for $C > C_D$

$$\ln\left[\frac{1 - C_D/C_o}{1 - C/C_o}\right] = \left(\frac{C_D/C_o}{1 - C_D/C_o}\right)\left[\left(\frac{C_o k_g a_p}{X_o^* G'}\right) W - \left(\frac{k_g a_p W_s}{G'}\right) - 2 + \frac{C_o}{C_D}\right] \qquad (21)$$

where: C_D = concentration of solvent with respect to adsorbate at point of discontinuity.

$$C_D = \frac{\alpha}{\frac{X_o^*}{C_o} + \frac{k_g a_p}{k_s a_p}} \qquad (22)$$

Thus, for the case of solid shell resistance controlling, the equation for the breakthrough curve is:

$$-\ln (1 - C/C_o) = \left(\frac{\alpha K_s a_p}{X_o^* G'}\right) W - \left(\frac{\alpha k_s a_p W_s}{C_o G'}\right) + 1 \qquad (23)$$

The mass transfer coefficient, $k_g a_p$, is obtained from Equation 20 by plotting $\ln C/C_o$ versus W for low values of C/C_o and measuring the slope. With this value of $k_g a_p$ and a value of $k_s a_p$ determined from Equation 32 or 13, C_D may be determined by use of Equation 22. The slope of a plot of $\ln (1 - C/C_o)$ versus W gives $K_s a_p$ from Equation 23. This method does not apply to runs of high inlet concentration since the width of the adsorption zone is not constant (13).

In another case with external diffusion the rate controlling resistance, Selke and Bliss (36) proposed a solution to the equation for the breakthrough curve to be:

$$\ln \frac{C}{C_o} = \left[\frac{k_g a_p v \rho_b}{G'}\right]\left[\frac{C_o W}{\rho_b X_o^* v} - 1\right] - 1 \qquad (24)$$

where: ρ_b = bulk packed density of the adsorbent.

v = fixed-bed volume.

A simplified method of determining the breakthrough curve was developed by Treybal (39) using the treatment for isothermal ion exchange developed by Michaels (29). Michaels

imposed the following limitations in the use of his method: 1) the adsorption is isothermal from a dilute feed mixture, 2) the isotherm is concave to the solution concentration axis, 3) the adsorption zone is constant in height as it travels through the adsorption column, and 4) the height of the adsorbent bed is large relative to the height of the adsorption zone.

By writing a material balance over the adsorption zone, an operating line is established on the isotherm which when reduced to a differential height of the adsorption zone and graphically integrated give the following equation for the breakthrough curve (39):

$$\frac{t - t_B}{t_E - t_B} = \frac{\int_{C_B}^{C} \frac{dC}{C - C^*}}{\frac{Z_a}{G'/K_g a_p}} \qquad (25)$$

where: t = time.

t_B = time at breakpoint.

C_B = concentration of adsorbate in effluent stream at breakpoint.

Z_a = height of the adsorption zone.

$$Z_a = Z\left[\frac{t_E - t_B}{t_E - (1 - f)(t_E - t_B)}\right] \qquad (26)$$

where: t_E = time at bed exhaustion.

Z = height of fixed-bed.

f = fractional ability of the adsorbent in the adsorption zone to adsorb the adsorbate.

$$f = \frac{U}{C_o(t_E - t_B)} \tag{27}$$

where: U = quantity of adsorbate removed in the adsorption zone from the breakpoint to bed exhaustion point.

Leavit (24) has used the above development to treat the non-isothermal case.

Michaels' solution is also applicable to the case where particle diffusion is the rate controlling mechanism. In addition, models proposed by Glueckauf and Coates (19), Boyd, Meyers, and Adamson (3), and Vermeulen (42) are applicable to this situation. However, before presenting the models for the particle diffusion case, it is necessary to define several terms.

In many cases, it is convenient to form dimensionless groups of the numerous variables. The dimensionless groups allow a reasonable generality in the theoretical analysis. Among these groups is the number of transfer units, N, or the number of apparent reaction units, N_R, which are defined as follows:

$$N = \frac{N_R}{a} = \frac{K_g a_p Z A_X \rho_g}{G'} \tag{28}$$

where: a = correction factor accounting for linearity deviation when diffusional resistances are added.

A_X = cross-sectional area of the bed.

The correction factor, a, in Equation 28 is a function of the ratio of $(K_S a_p / K_g a_p)$ and the radius of the bed, r. It may be defined by the equation:

$$\frac{a}{N_R} = \frac{1}{N_g} + \frac{1}{N_s} \tag{29}$$

where: N = number of transfer units with g and s referring to gas and solid phases respectively (42).

Since the breakthrough curve can reflect the exact behavior of the equilibrium isotherm if step-by-step calculations are made or if the equilibrium is either very favorable or very unfavorable, an effort is generally made to fit the isotherm with a constant separation factor, r^*. This factor is defined by the equation (42):

$$r^* = \frac{C^*/C(X_o^*/X^* - 1)}{(1 - C^*/C_o)} \tag{30}$$

where: C_o = inlet adsorbate concentration.

Using the separation factor as a basis for calculations, the available solutions for breakthrough curves may also be classified into the following categories of equilibrium behavior (43): 1) strongly favorable ($r^* \leqslant 0.3$), 2) irreversible ($r^* = 0$), 3) linear ($r^* = 1$), 4) nonlinear ($0.3 < r^* < 10$), and 5) strongly unfavorable ($r^* \geqslant 10$). The initial slopes of the breakthrough curves increase with a decreasing constant separation factor, r^*. Constant mass transfer zone or adsorption zone, or constant pattern properties are generally exhibited by curves of $r^* \leqslant 0.5$ (42). For propane being adsorbed by activated carbon, $r^* = 0.0669834$ and for propylene the value of r^* is 0.080365. Both cases therefore represent the strongly favorable case and probably are adsorbed in a constant mass

transfer or adsorption zone. This is confirmed by the type A isotherm shown in Figure 2.

Glueckauf and Coates (19) proposed a model based on the linear driving force approximation described in Equation 13. From the differential equation:

$$\frac{dC}{dt} = \frac{60 D_p X_o^* \rho_b}{d_p^2 C_o \epsilon} (C_o - C) \qquad (31)$$

where: D_p = particle phase diffusivity.

d_p = arithmetic mean particle diameter.

Integration of Equation 31 yields:

$$\frac{C}{C_o} = 1 - \exp - \left[\left(\frac{60 D_p X_o^* \rho_b v}{C_o G' d_p^2} \right) \left(\frac{C_o W}{\rho_b X_o^* v} - 1 \right) + 1 \right] \qquad (32)$$

For the irreversible case, $r^* = 0$, Boyd et al. (3) proposed the following exact solution:

$$\frac{C}{C_o} = 1 - \frac{6}{\pi^2} \sum_{n=1}^{\infty} \frac{1}{n^2} \exp - n^2 \left[\left(\frac{4\pi^2 D_p X_o^* \rho_b v}{C_o G' d_p^2} \right) \left(\frac{C_o W}{X_o^* \rho_b v} - 1 \right) + 0.97 \right] \qquad (33)$$

Vermeulen (42) proposed the following solution for the breakthrough curve for solid phase diffusion controlling with a quadratic driving force:

$$\frac{C}{C_o} = \left\{ 1 - \exp - \frac{\pi^2}{\pi^2 r^* + 15(1 - r^*)} \left[\left(\frac{60 D_p X_o^* \rho_b v}{C_o G' d_p^2} \right) \left(\frac{C_o W}{\rho_b X_o^* v} - 1 \right) + 0.93 \right] \right\}^{0.5} \qquad (34)$$

For the case where surface reaction kinetics are the rate controlling mechanism, Sillén and Ekedahl (37) proposed the following equation:

$$\frac{1}{1 - r^*} \ln \left[\frac{C/C_o}{1 - C/C_o} \right] = N_R \left[\frac{C_o W}{\rho_b X_o^* v} - 1 \right] \qquad (35)$$

This model is very useful for r^* values between 0 and 0.5 and for the treatment of the combined-mechanism region and of pore diffusion. It is also very useful for preliminary interpretation of data where the rate controlling mechanism is not known (42).

DESCRIPTION OF EQUIPMENT

Two different types of apparatus were used to obtain data for this investigation. They were the Cahn Electrobalance to obtain equilibrium data and a gas flow apparatus utilizing a thermal conductivity cell to determine the breakthrough data. A description of each system is given below.

Cahn Electrobalance

This apparatus was originally built by Frost (17). It was designed to gravimetrically measure the degree of adsorption by employing a Cahn RG Electrobalance, encased in a vacuum bottle, which continuously recorded the weight of the sample on a Varian Model G-15-L strip chart recorder. The pressure of the system was measured by a Texas Instruments Inc. Model 145 Precision Pressure Gage.

Figure 4 is a schematic diagram and Figure 5 is a photograph of the complete apparatus. The system has been divided into three sections separated by a Vecco FR-150-S high vacuum valve, I in Figure 4, to facilitate description. All lines in the system were 10-mm Pyrex tubing.

Gas handling system

The gas under study was initially admitted into the system through a fine capillary, 0.009 in. ID, designated G in Figure 4. After flowing through the capillary, the gas passed through a dry ice-acetone cold trap before entering a 5-liter

Figure 4. Gravimetric adsorption apparatus

A. Adsorbate gas supply
B. Pressure gauge - 0-30 p.s.i.g.
C. Vecco FR-38-S vacuum valves
D. Dry ice - acetone trap
E. Compound pressure gauge - 30-in. vacuum to 15 p.s.i.g.
F. 5-liter Pyrex gas storage bulb
G. 0.009-in. ID capillary tubing
H. Fore pumps - Welch Duo-Seal
I. Vecco FR-150-S vacuum valve
J. 1-in. ID stainless steel bellows
K. Cahn Electrobalance encased in vacuum bottle
L. Small bore high vacuum stopcock
M. Texas Instruments, Inc. Precision Pressure Gage, Model 145
N. Ion gauge
O. Large bore high vacuum stopcock
P. Liquid nitrogen traps
Q. 3-state mercury diffusion pump-GE M 22DP120
R. Sample hangdown tube
S. Constant temperature water bath

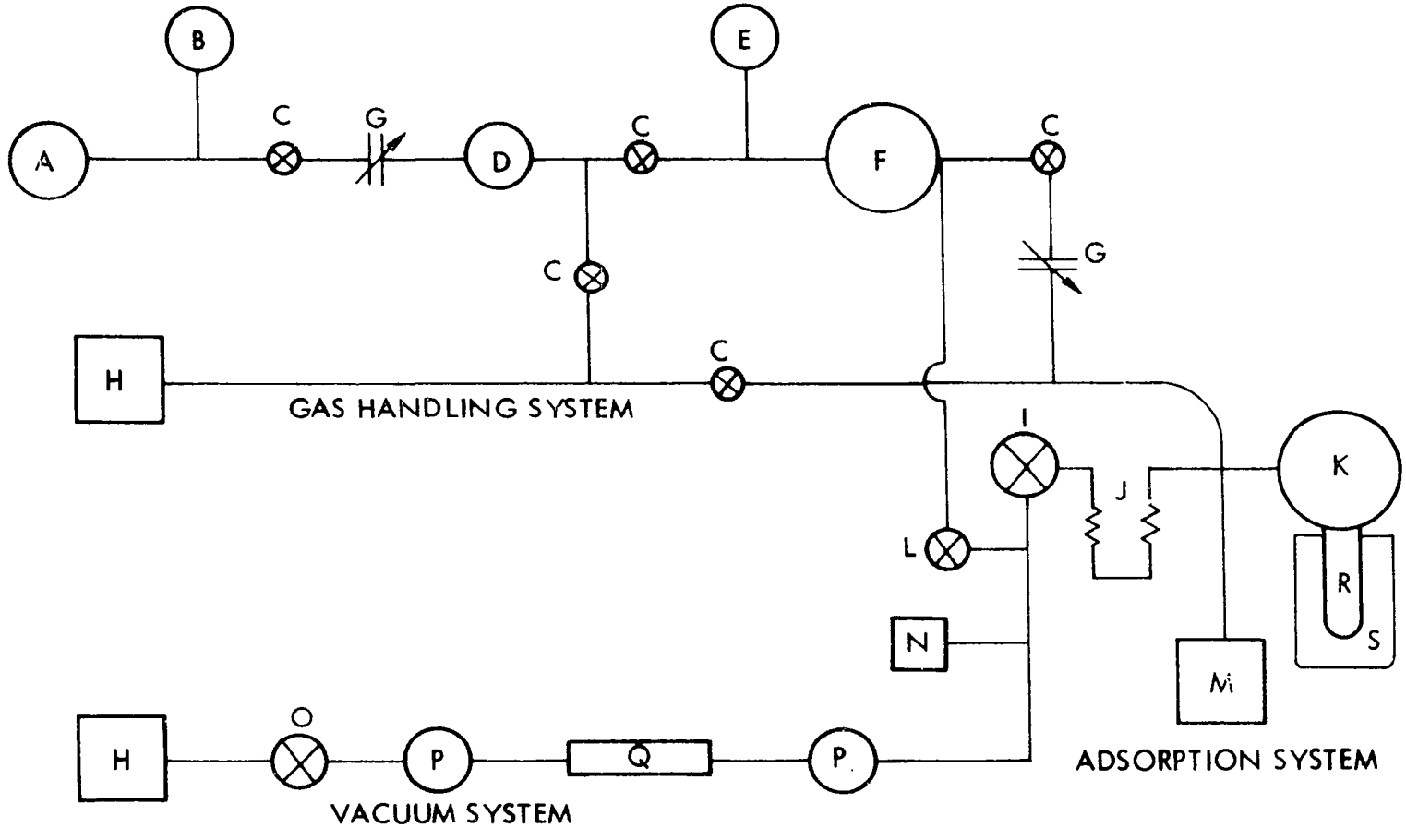
A
B
C
G
D
C
E
F
C
G
C
H
C
GAS HANDLING SYSTEM
I
J
K
L
R
S
N
Mi
ADSORPTION SYSTEM
H
O
P
Q
P
VACUUM SYSTEM

Figure 5. Photograph of gravimetric adsorption apparatus

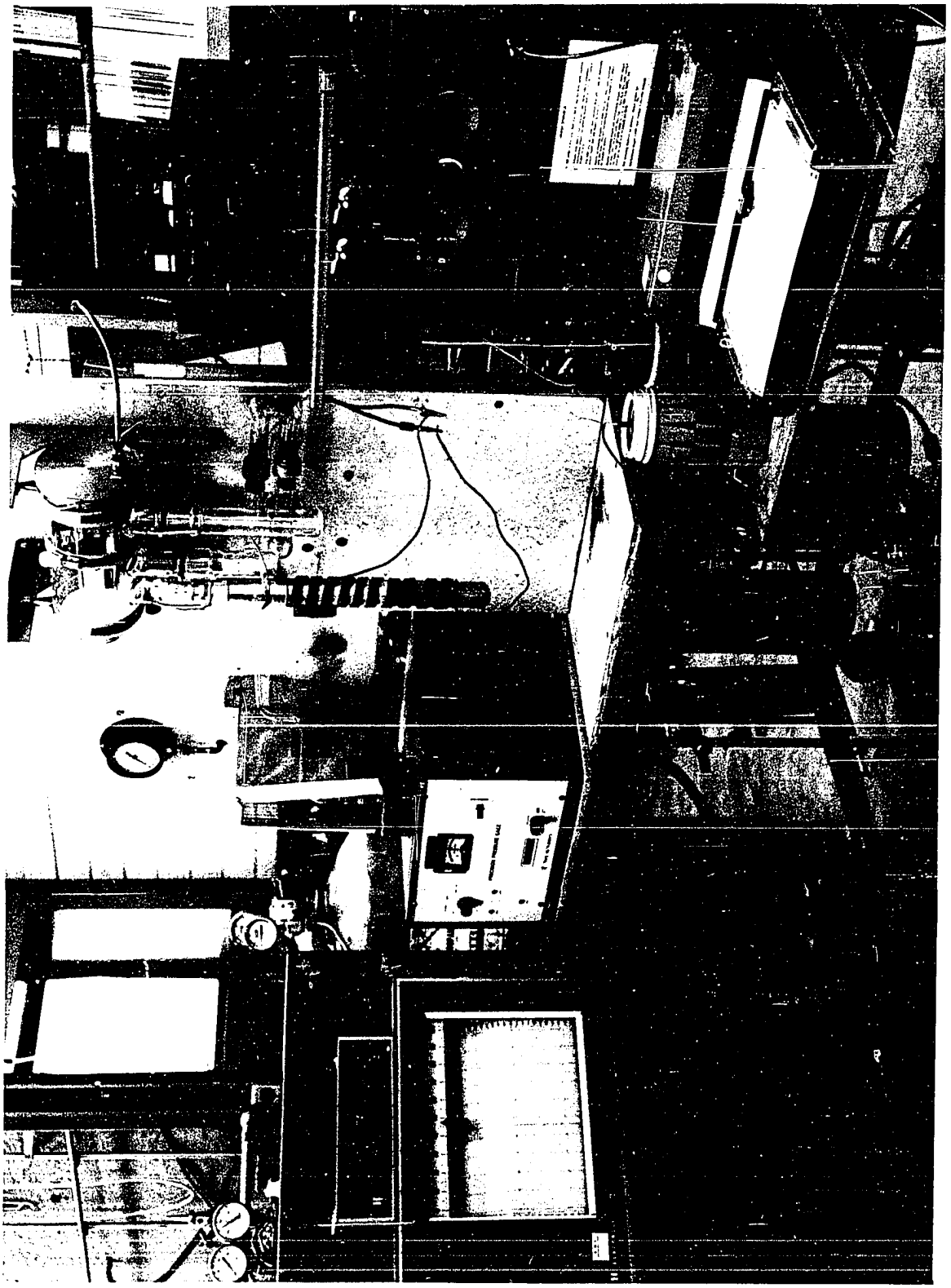

gas storage bulb, D and F respectively in Figure 4. Another section of 0.009-in. ID capillary tubing was located between the gas storage bulb and the Cahn Electrobalance to control the flow rate of the gas entering the adsorption system.

Large quantities of gas were initially removed from the system through a Welch Duo-Seal mechanical vacuum pump located in the gas handling system in order to avoid excessive filling of the cold traps located in the vacuum system.

All valves, designated C in Figure 4, were Vecco FR-38-S high vacuum valves.

Vacuum system

The vacuum system consisted of a 3-stage mercury diffusion pump, Q in Figure 4, which was backed by a Welch Duo-Seal mechanical vacuum pump. Liquid nitrogen cold traps, P in Figure 4, were placed on both sides of the mercury diffusion pump. An ion gauge was used to measure the vacuum in the system and calibrate the Precision Pressure Gage.

Adsorption system

At the entrance to the adsorption system, a Vecco FR-150-S high vacuum valve with an associated bellows constructed of 1-in. ID stainless steel welded to Kovar-Pyrex graded seals was located, I and J in Figure 4. The bellows were necessary to provide flexibility between the valve and pump-out port.

A Texas Instruments Inc. Model 145 Precision Pressure Gage, M in Figure 4, was used to measure the absolute pressure

of the system. A Type 6 Bourdon Tube Capsule with a No. 1 Bourdon Tube, serial No. 1898, was used with the pressure gauge. The effective range of the capsule was 0 to 32 in. Hg. A calibration chart was supplied with the bourdon tube and capsule with points spaced approximately 40 mm apart.

A Cahn RG Electrobalance, K in Figure 4, was used to measure the weight of the sample under study. The Cahn Instrument Company provides a detailed description of the theory and operating procedures for the Cahn RG Electrobalance in the instruction manual (7) for the instrument. Figure 6 shows the elements of the Electrobalance.

The sample under study was placed in the pan held by loop A in Figure 6. A tare weight was placed in the pan held by loop C during calibration of the Electrobalance. A metal "flag" which partially covered a slit between the lamp and the phototube was attached at the end of the balance beam which was suspended in a magnetic field. When a current was passed through the coil, it acted like a DC motor and exerted a force on the beam. As the sample gained weight, the flag moved up exposing the phototube to more light. The current from the phototube was then amplified and passed through the coil which resulted in an electromagnetic force which tended to restore the beam to its original position. This equilibrium position was slightly offset from the original position in order that just the right amount of current could pass through the coil and maintain the heavier load on loop A in a static position.

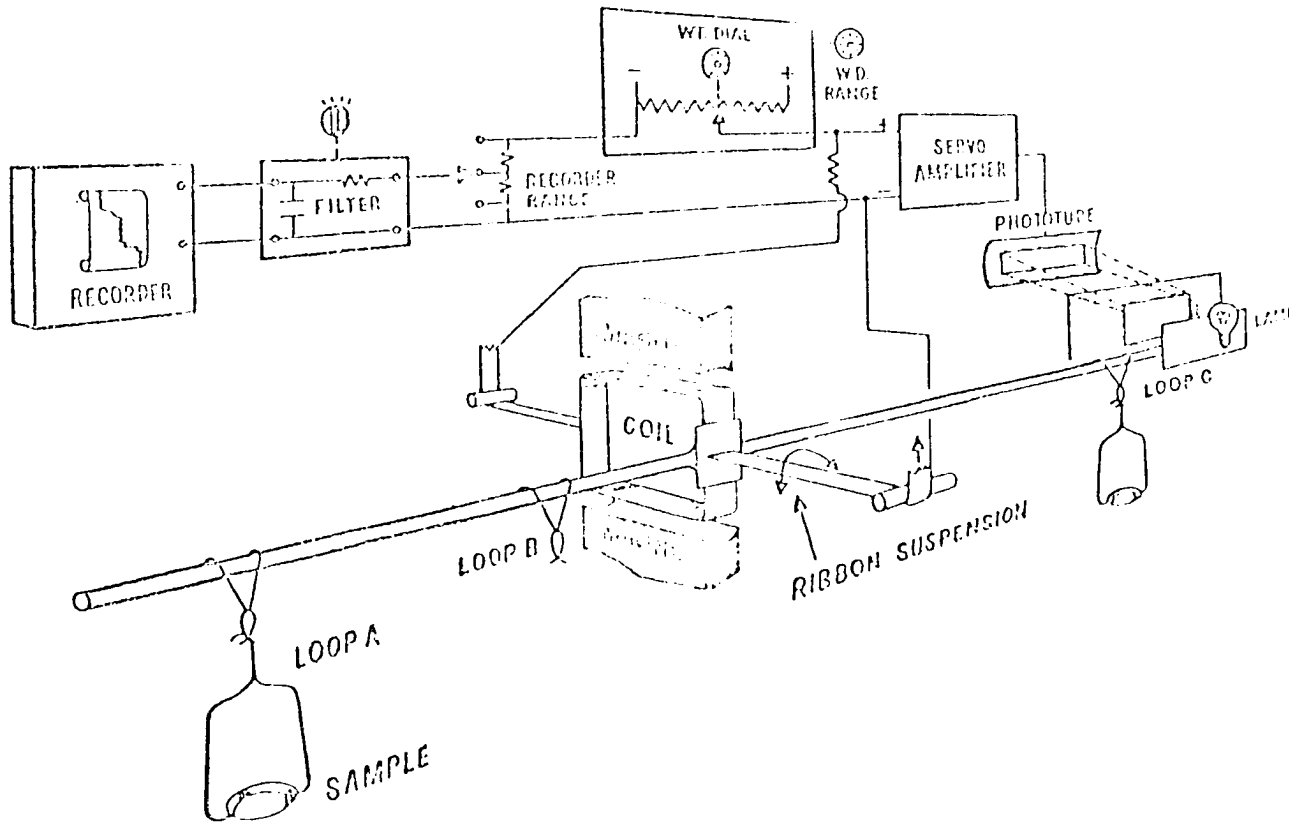

Figure 6. Simplified balance operation (drawing from Cahn Electrobalance Instruction Manual (7)

The resulting change in current reflected the gain in weight of the sample and was measured as a voltage drop across a resistor on a millivolt recorder.

A Varian Model G-15-1 strip chart recorder was used for the measurements. The response time was 0.75 sec for full scale deflection (21) which was much faster than the fastest response which occurred in the experiments, thereby making the error due to time lag negligible.

A copper-constantan thermocouple was located immediately above the sample to measure the sample temperature. This was necessary since the adsorbent sample was not in contact with the hangdown tube surrounding it and thus could not safely be assumed to be at the temperature of the hangdown tube. A reference thermocouple was kept at 0° C. A calibration chart distributed by Leeds and Northrup Company was used after initial calibration of the thermocouples using saturated steam and an ice-water bath was completed.

Temperature control

The desired temperatures were obtained by using a constant temperature water bath with a thermal control unit, model S-84805, manufactured by E. H. Sargent and Company, which was immersed in a 5-gal metal tank with a $\frac{1}{4}$-in. acrylic plastic cover. Water was pumped to a water jacket which surrounded the hangdown tube which contained the sample under study by a model E-1 pump manufactured by Eastern Industries. The water jacket

was constructed from a 100-mm Pyrex tube which was closed at one end. The tube was 11 in. deep, and suitable bottom inlet and top outlet ports were installed to promote circular flow of water in the jacket. The tube was mounted in a sheet metal box, 9 in. square and 14 in. deep with Zonolite insulation between the box and Pyrex tube. The tube was held in place at the top with styrofoam and the water jacket was covered with a styrofoam top. Water was pumped to the water jacket and returned to the constant temperature water bath by gravity flow through 3/8-in. Tygon tubing. In addition, the temperature of the room was set at 25° C.

Calibration runs

Prior to making runs with samples of activated carbon, a series of runs were made with no activated carbon in the pan. It was observed that there was an initial apparent weight gain that gradually tapered off to a value slightly above the original value. Since it was assumed that the same phenomena occurred during actual runs, these corrections were used to determine the actual sorption rate curve as shown in Figure 7. The actual correction shown in Figure 7 is an average of all calibration runs made at a temperature of 25° C.

This weight gain was attributed to buoyancy by the Cahn Electrobalance instruction manual (7). Hanson (21) believed that this phenomena was more likely due to convection effects

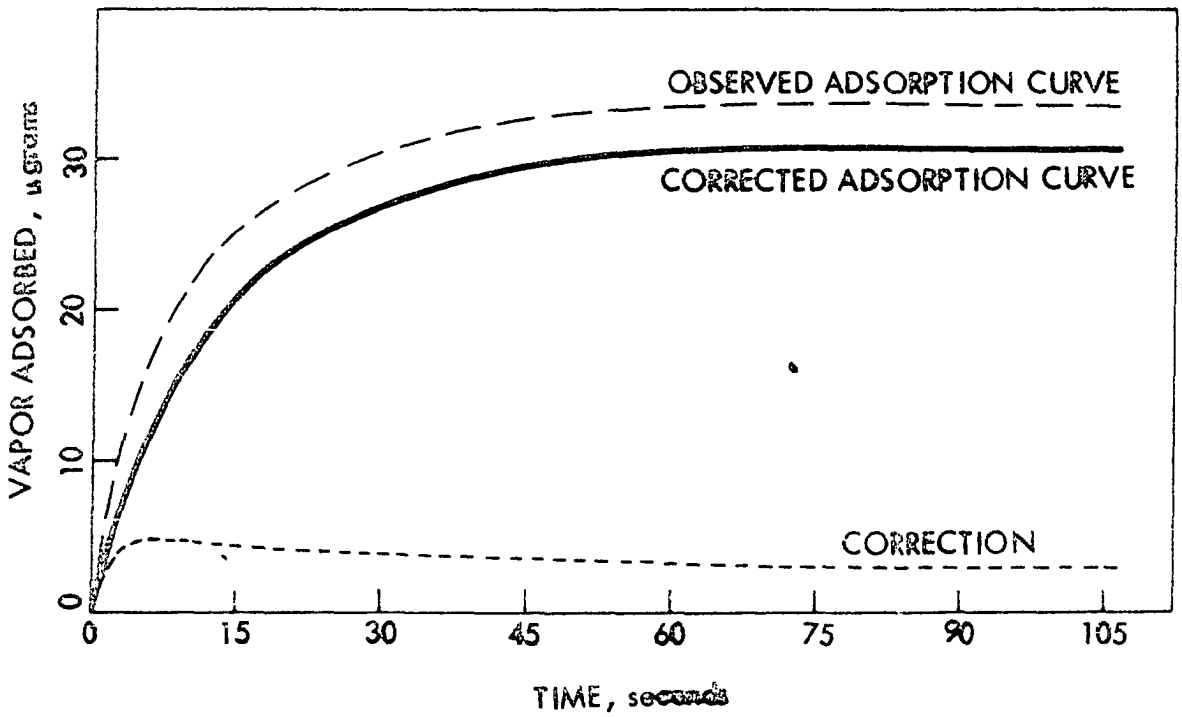

Figure 7. Application of Electrobalance "blank" correction factor to a typical adsorption curve

within the balance chamber. Regardless of the reason, these effects were treated as characteristics of the balance.

Gas Flow Apparatus

The gas flow apparatus was originally designed and built by Leslie v. Szirmay during previous work at Iowa State University. A similar apparatus was also constructed at the University of Denver by v. Szirmay (41).

The apparatus was designed to very accurately measure the difference in thermal conductivity of the two gases under study. To accomplish this, a micro cell, model 470, thermal conductivity cell manufactured by the Gow-Mac Instrument Company was selected as the primary detection instrument since it had the capability to measure a continuously flowing gas stream with a response time of less than 0.5 sec.

Other methods of obtaining concentration data of an effluent stream are described by Tsederberg (40), Frost (17), and Nutter (33). These include the plane horizontal layer method, the concentric cylinder method, the hot wire method, and regular regime method for measurement of thermal conductivity (40).

The sensitivity of the cell was 10^{-10} g/ml. This requires that the cell temperature, pressure, and gas flow rate be very carefully regulated and kept constant in order to insure that all thermal conductivity measurements are made under identical conditions.

The apparatus was constructed as shown in Figures 8 and 9 to meet the above specifications. The temperature was controlled by a constant temperature water bath designated by C in Figure 8. A thermal control unit, model S-84805, manufactured by E. H. Sargent and Company, was used to regulate the temperature of the water bath at $25^{\circ} \pm 0.05^{\circ}$ C. All heat exchangers in the apparatus, including the thermal conductivity cell, were immersed in the water bath, C in Figure 8, except the adsorption column and soap bubble meters which were jacketed and received water pumped from the constant temperature water bath through the jackets by means of a small model E-1 pump manufactured by Eastern Industries. In addition, the ambient temperature of the room was set at $25^{\circ} \pm 0.4^{\circ}$ C.

The pressure from the gas cylinders, A and B in Figure 8, into the apparatus was regulated by two pressure regulating valves. One was located on each of the cylinders with another located just prior to the point where each gas entered the constant temperature water bath.

The gas flow rate was regulated by a series of orifices as shown in Figure 8. At the entrance to each orifice, a manostat and water manometer, E in Figure 8, was situated to provide a constant pressure on the upstream side of the orifice. Each manostat was constructed of 2-in. OD glass tube, 43 inches in length. The tubes were filled with distilled water and a $\frac{1}{4}$-in. OD glass tube with a nozzle at the end was immersed to a predetermined depth in the water to provide the

Figure 8. Gas flow apparatus

A. Propane
B. Propylene
C. Constant temperature water bath
D. Orifice
E. Manostat and water manometer
F. Adsorption column
G. Soap bubble gas flow meter
H. Moisture trap
I. Thermal conductivity cell
J. Recorder
K. Barometer
L. Cartesian Manostat
M. Three-way stopcock

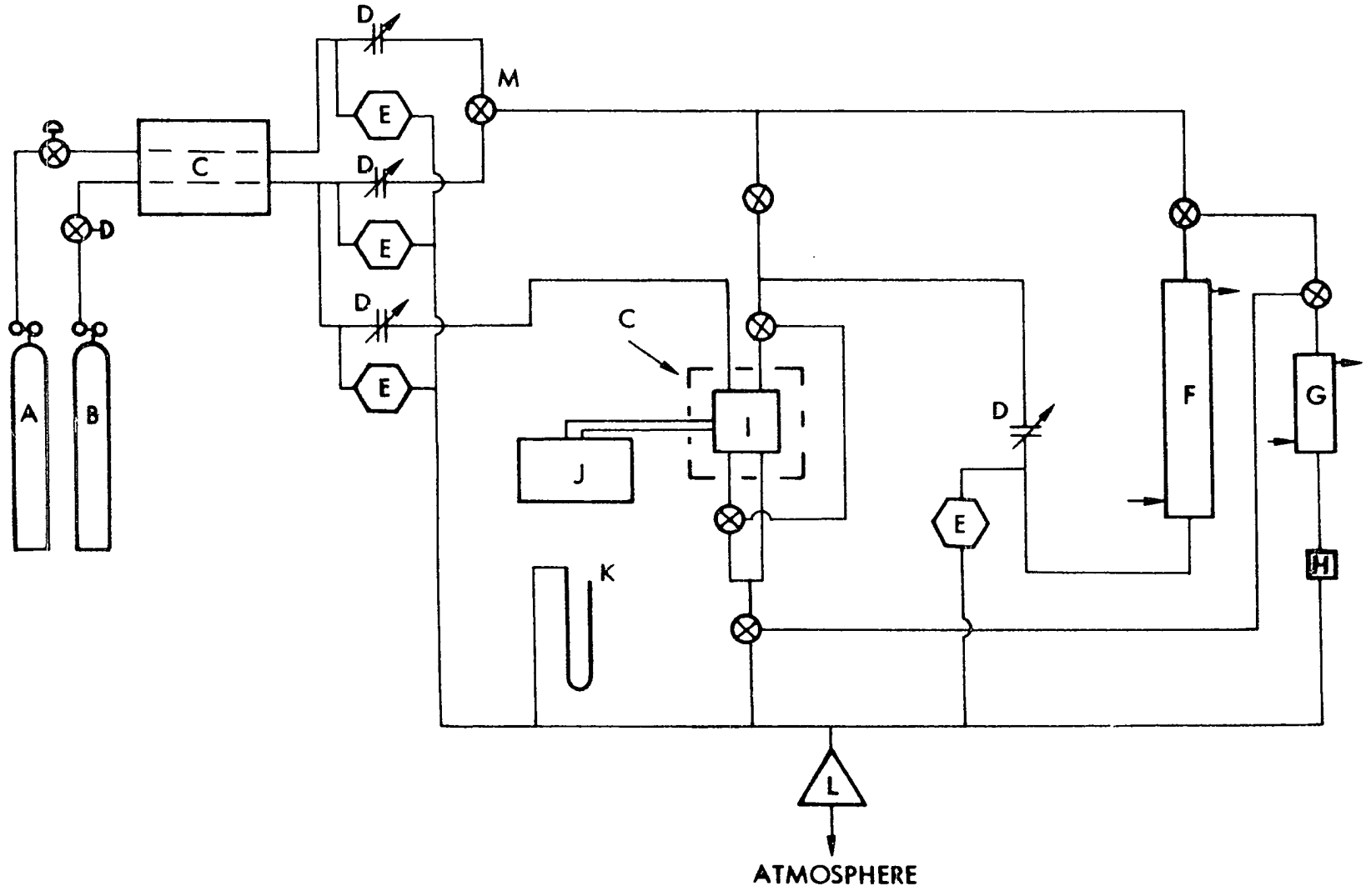
D
M
E
C
D
D
E
D
E
A
B
C
I
J
K
D
E
F
G
H
L
ATMOSPHERE

Figure 9. Photograph of gas flow apparatus

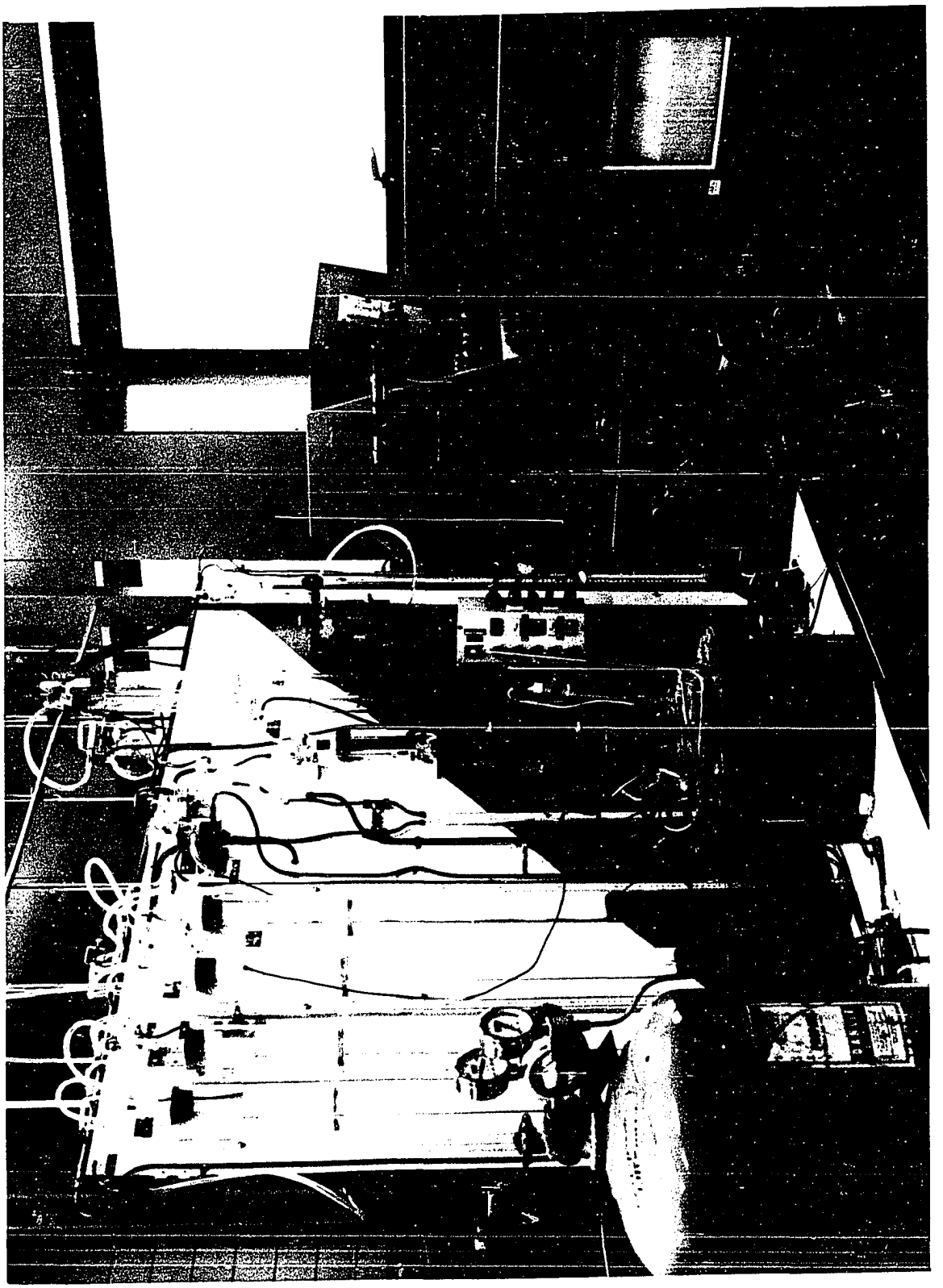

desired upstream pressure at the orifice. The excess gas was bubbled through the water and exhausted into a common manifold. The orifices were constructed of $\frac{1}{4}$-in. OD hard glass tubing where one end was fused over a Bunsen burner flame to obtain the desired orifice size. A pressure of 800 mm H_2O, measured on the manometer adjacent to each manostat, was used for standardization of the orifice flow rates. Fine adjustment of the gas flow rate through a particular orifice was obtained by moving the tube immersed in the manostat up or down, changing the upstream pressure on the orifice, until the desired flow rate was obtained. The flow rate was then measured by timing the rise of soap bubbles in the soap bubble gas flow meter, G in Figure 8. An accuracy of $\pm$ 0.01 ml/min was obtained.

The pressure in the adsorption bed, manifold, and thermal conductivity cell was set and held constant by a Cartesian Manostat, model 8, manufactured by Manostat Corporation. The pressure in the adsorption bed was assumed to be the pressure at the upstream side of the Cartesian Manostat since the pressure drop measured across the adsorption bed was less than 40 mm H_2O and thus considered negligible. The Cartesian Manostat maintained the system pressure at 760 mm $\pm$ 0.2 mm Hg. The gas on the downstream side of the Cartesian Manostat was exhausted into a hood with an exhaust fan in operation. A mercury barometer was used to measure the manifold pressure.

Two column sizes were used in these experiments. Each column was constructed as shown in Figure 10 with a coarse

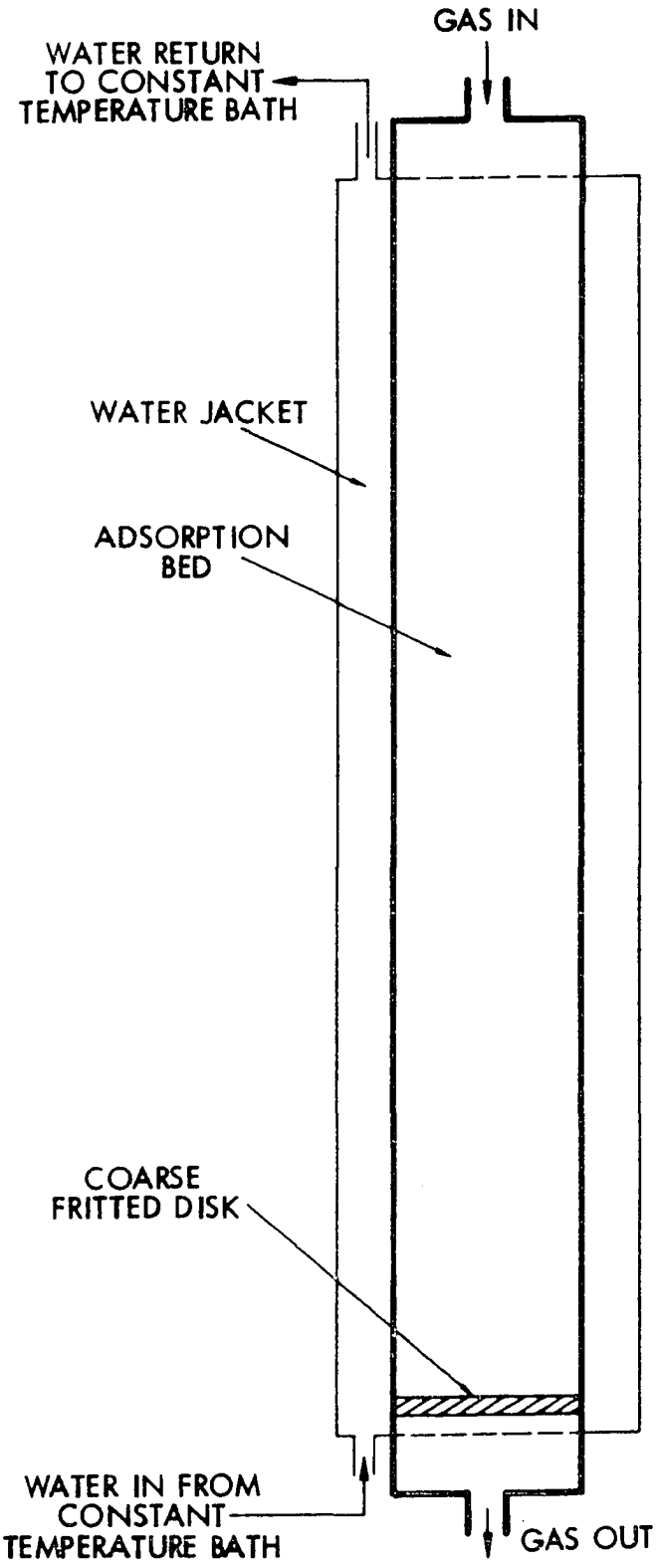

Figure 10. Typical adsorption column

fritted disk installed at the bottom of the column to hold the adsorbent. In addition, each column was surrounded by a 50-mm ID glass tube enclosed at both ends by rubber stoppers which served as constant temperature water jackets for the columns. Water was pumped through the jackets from the constant temperature water bath previously described.

The smaller column was 10-mm ID glass tubing and was 350 mm long. The larger column was 19-mm ID glass tubing and was 550 mm in length. In addition, an identical column to each one described above was constructed with a thermocouple installed as shown in Figure 11. The thermocouples were designed to measure the temperature difference between the two points. These were used in the initial determinations of the temperature rise in the adsorption bed as the adsorption front passed the location of the thermocouples. The change in potential between the copper-constantan thermocouples was measured on a Leeds and Northrup 7555, Type K-5 potentiometer which had the ability to measure a potential difference of 10^{-4} mv. The change in potential between the two thermocouples was measured for a temperature difference of 5° and 10° F using two constant temperature water baths. It was determined that a change in potential of 0.0023 mv represented a change in temperature of 0.1° F.

The signal from the thermal conductivity cell was recorded on a Honeywell Electronik 16 multipoint strip chart recorder.

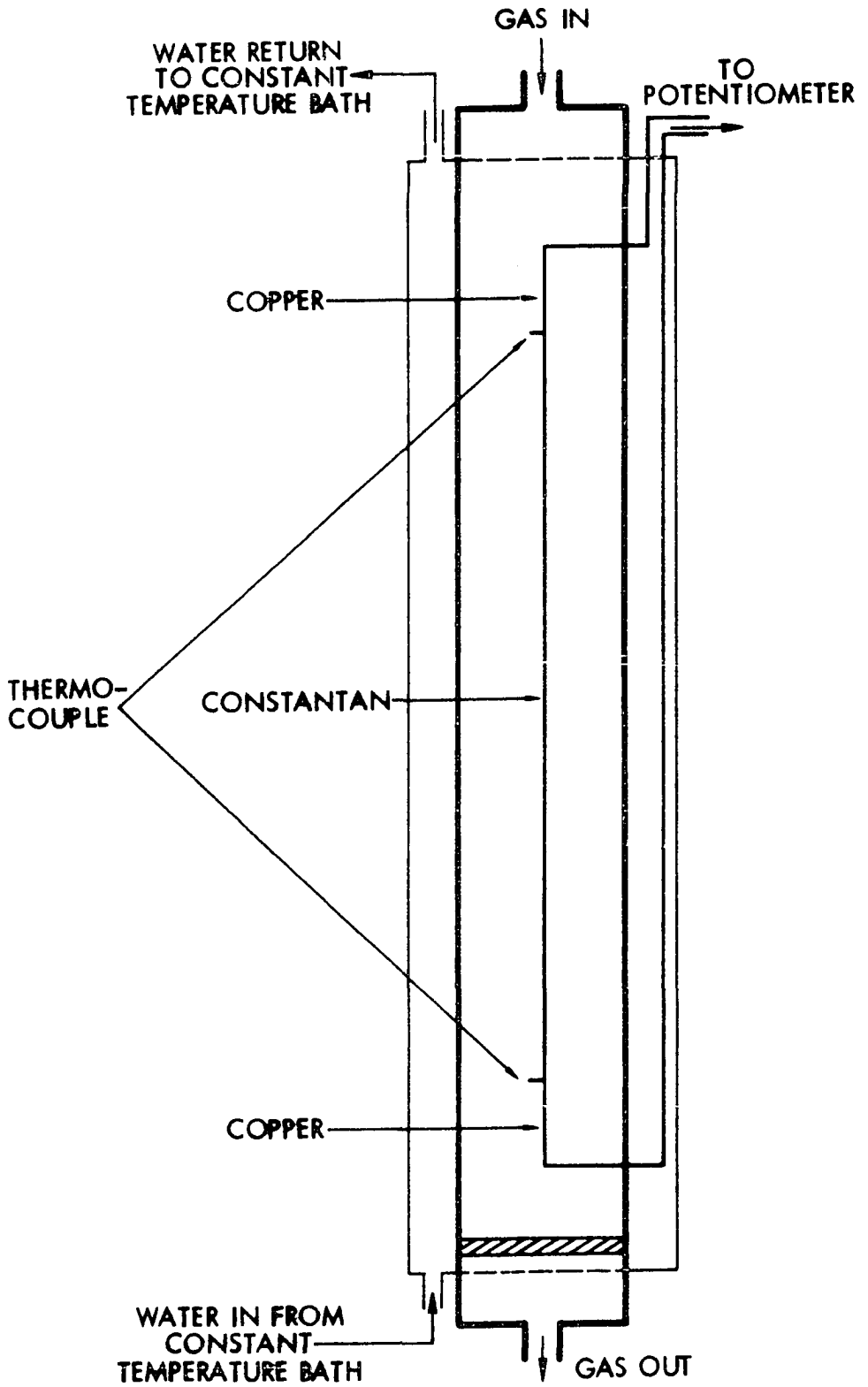

Figure 11. Typical adsorption column with thermocouples installed

Materials used

The gases used were instrument grade (99.5%) propane and C. P. grade (99.0%) propylene. Both gases were obtained from the Matheson Co.

Although several types of activated carbon were initially tested for temperature rise determinations, Columbia LC 20/48, Grade H-63-11 was selected for use in this research since less temperature rise was observed with this type than the others tested. In addition, the heats of adsorption of propane and propylene on Columbia LC activated carbon have been reported by Frost (17). The sample of Columbia LC 20/48, Grade H-63-11 was obtained from the Union Carbide Corporation Carbon Products Division. Table 1 lists the characteristics of this type of activated carbon.

Table 1. Specifications and properties of Columbia LC 20/48, Grade H-63-11 activated carbon

Property	Columbia LC 20/48
Raw material	Coconut shell
Method of activation	High temperature steam
Size distribution	Less than 20 mesh - 3.8% 20 to 48 mesh - 95.1% Thru 48 mesh - 1.1%
Hardness	Greater than 95%
Bulk density	0.5 g/cc
Ash	3.45%
Moisture content	0.00%
Differential heat of adsorption (14) -	
propane	9.294 kcal/g-mole gas
propylene	9.197 kcal/g-mole gas

EXPERIMENTAL PROCEDURE

Cahn Electrobalance

The Electrobalance was first calibrated using the procedures recommended in the instruction manual (7) using the same pan that would be used to hold the sample during the subsequent runs. This calibration could not be checked after a sample had been placed on the pan, so it was assumed that the calibration of the Electrobalance did not change during the period required to make the sorption runs on the sample. This time period was usually for two weeks. A check of the calibration after the sample was removed confirmed the assumption to be valid. The pan used for the runs had the following specifications:

Material - - - - - aluminum

Weight - - - - - - 200 mg

Diameter - - - - - 0.75 in.

In determining the equilibrium isotherms, differential adsorption runs were made. In these runs, the sample, which was initially in equilibrium with the gas adsorbate at a known pressure, was exposed to a higher pressure. The sample then adsorbed the gas until equilibrium was reached at the predetermined temperature and new pressure of the system. The weight gain of the sample was continuously recorded during the unsteady-state period and the equilibrium weight of the sample

was determined when there was no change in the weight of the sample and pressure of the system for a period of 30 min.

To commence a run, the sample of adsorbent, approximately 1 mg of activated carbon which ranged in size from 150 to 200 mesh on the Tyler Standard Screen scale, was evenly distributed over the surface of the 200 mg aluminum pan which had been previously used in the initial calibration runs. The glass hangdown tube was carefully replaced over the pan since any static electricity in the glass caused the aluminum pan to be attracted to it which resulted in spilling the contents of the pan. This often required the procedure to be started over with calibration since the pan usually picked up some foreign matter such as stopcock grease which had to be removed from the pan before proceeding further.

The sample was then outgassed by evacuating the system to less than 10^{-6} mm mercury pressure, measured on the ion gauge, and heated to a temperature of approximately 500° C using an electric tube furnace for a period of 2 days. The tube furnace was 10 inches in length and was placed around the portion of the hangdown tube which contained the sample. This procedure established a true weight of the pure sample of activated carbon. The temperature of the system was then set at 25° C by using the constant temperature water bath previously described. The potential difference between the thermocouples was continuously recorded to insure no temperature fluctuations occurred during a run.

Prior to exposing the sample to gas at a higher pressure, valve I and stopcock L in Figure 4 were closed to isolate the vacuum system from the adsorption and gas handling systems. Gas was then admitted to the system until the pressure of the gas handling system was at a predetermined value. The recorder was checked to insure it was properly operating at 1/3 in. per min. When all conditions were satisfactory, gas was admitted to the adsorption system. When steady state was reached on the Precision Pressure Gage and recorder, the new sample weight and system pressure were recorded and preparations made for the next differential adsorption run.

The series of differential adsorption runs were continued until a pressure of approximately 750 mm mercury was reached. A pressure difference of approximately 200 mm mercury was used for each run except at very low pressures where the degree of adsorption per pressure change was the greatest.

Upon completion of a series of runs, the system was evacuated and the sample heated to approximately 250° C using a neoprene heating tape wrapped around the hangdown tube containing the sample until the initial weight of the pure sample was reached. The entire process was then repeated for the sample being investigated.

For each run, the following data were recorded: 1) pressure of the system, 2) temperature of the system, and 3) weight versus time as continuously recorded on the recorder. No

desorption runs were made since equilibrium data of this type were not needed for subsequent breakthrough runs.

Gas Flow Apparatus

Prior to collecting any data, a series of calibration runs were made to determine the flow rates of the orifices and the relationship between the mole fraction of propane and propylene and the indicated change in potential from the thermal conductivity cell.

The initial orifice calibration runs were made using nitrogen, as a test for leaks in the system was conducted at the same time. A pressure drop of 800 mm H_2O was used for these runs. The flow rates were calculated in ml/min by observing the velocity of the gas traveling through the soap bubble gas flow meter at 25° C. The gas flow was also checked prior to each run and adjusted as necessary by moving the glass tube in the manostat up or down to achieve the desired flow rate.

Since the thermal conductivity of a binary mixture is not usually a linear function of concentration, it was necessary to prepare a calibration curve using various known point concentrations of the two gases. This was achieved by using various combinations of orifices in the two gas flow streams, passing the mixed gas through the thermal conductivity cell, and recording the resulting change in potential on the Honeywell recorder. A maximum change of 49.50 mv was observed

between pure propane and pure propylene with various mixtures giving intermediate values. Figure 12 shows the results. The following expression was derived to describe the curve shown in Figure 12:

$$YA_{C_3H_6} = (17.216 - (YI_{C_3H_6} - 3.401)^2)^{\frac{1}{2}} - 2.377 \qquad (36)$$

where: $YA_{C_3H_6}$ = actual mole fraction propylene.

$YI_{C_3H_6}$ = indicated mole fraction propylene.

The mole fraction of propane was 1.0 minus the mole fraction of propylene after the correction for nonlinearity had been made.

The time for the breakthrough curve to appear was measured on the recorder chart from the time the new adsorbate was admitted through a three-way stopcock into the system (M, Figure 8) until the breakthrough curve actually appeared on the chart. There were two corrections which were then needed to account for the time the gas flowed from the three-way stopcock to the entrance of the bed and from the exit of the bed to the thermal conductivity cell. The volume of tubing between the three-way stopcock and the bed entrance was found to be 50.27 ml. This value was subtracted from the product of the volumetric flow rate and time elapsed.

The correction for the portion of the system between the bed exit and the thermal conductivity cell was found to be a function of flow rate. This was due to the inclusion of the manostat and capillary tubing associated with the thermal

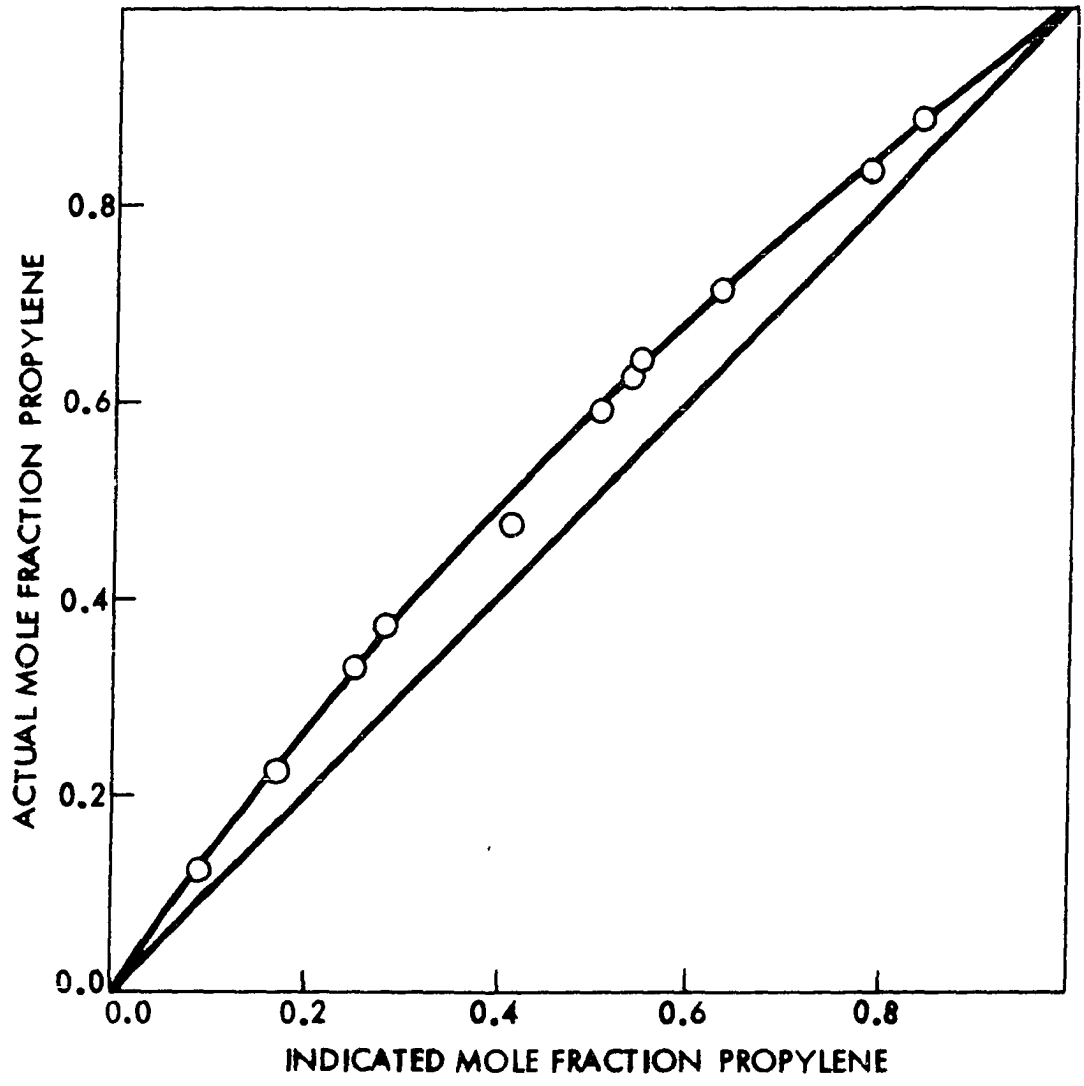

Figure 12. Thermal conductivity cell calibration curve

conductivity cell in this section of the apparatus. The relationship is shown in Figure 13 and the following equation was derived using a least squares analysis to describe the correlation:

$$t_D = 6.773V_f^{-0.182} \tag{37}$$

where: V_f = volumetric flow rate, ml/min.

t_D = time of delay between the bed exit and thermal conductivity cell, min.

Prior to commencing a run, the apparatus must be allowed to reach steady state in all respects. Due to the extreme sensitivity of the thermal conductivity cell, any small change in temperature, system pressure, or gas flow rate resulted in erroneous results.

Once steady state was reached, the electronic circuit was standarized by the following procedure:

1. The recorder pen was set to zero by shorting the two input leads to the recorder. This procedure established a reference point for the next step.

2. The reference gas (propane) flow rate was established and the gas was then circulated through both the reference gas and sample gas sides of the thermal conductivity cell by manipulating the two three-way stopcocks at the entrance and exit of the thermal conductivity cell.

3. The recorder pen was then reset to zero by adjusting the bridge circuit. This procedure balanced both sides of the thermal conductivity cell to zero.

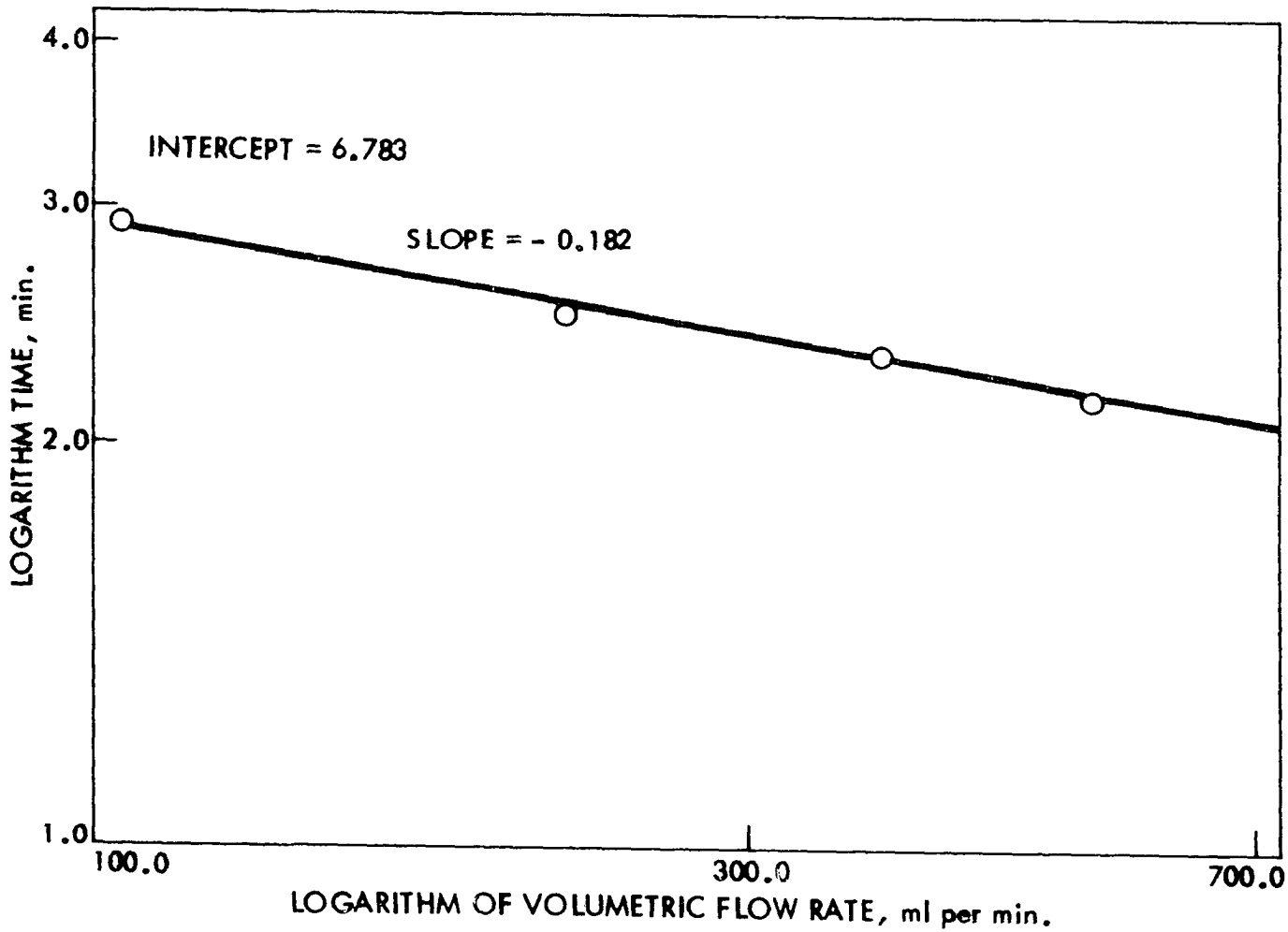

Figure 13. Correction curve for time delay between outlet of adsorption bed and thermal conductivity cell

4. The recirculation of the propane was terminated and the sample gas was admitted to the sample side of the thermal conductivity cell by manipulation of the same two three-way stopcocks previously mentioned.

5. The gas flow rate of the sample gas, which was pure propane, was then adjusted until the recorder again read zero. The gas flow rates on both the reference and sample side of the thermal conductivity cell were thus identical and the system ready to commence a run.

A run was commenced by turning the three-way stopcock which controls the selection of gases to be admitted to the adsorption column. The run was continued until the breakthrough curve appeared and a constant value of potential from the thermal conductivity cell was recorded for 15 min. A reverse run was then conducted which was terminated when the recorder pen reached a steady value of zero for 15 min.

The data collected during each run, in addition to the breakthrough curve, were the temperature profile when of interest, type of activated carbon used, gas flow rate, ambient temperature, temperature of water bath, pressure drop across each orifice and adsorption bed, and system pressure.

EXPERIMENTAL RESULTS AND DISCUSSION

Heat Effects

One of the initial objectives was to determine whether or not truly isothermal conditions existed for the system under study. To accomplish this, 22 runs were made using several types of activated carbon of particle size 30 to 35 U. S. Standard Series mesh. Some of the samples were dried for 24 hr in a 150° C oven prior to use while others were not. The adsorption column shown in Figure 11 was used for these runs. Table 2 gives the results of these runs.

Table 2. Preliminary run temperature determinations

Run no.	Type carbon	Gas flow rate, ml/min	Initial temp.rise °F	Max. run temp.diff. °F	% of initial rise
5-6	Columbia L	38.8	141.30	3.6217	2.56
7-10	Pittsburgh, Type CAL	38.8	125.00	1.8200	1.46
11-12	Columbia L, (dried)	38.8	136.10	2.7000	1.98
13-16	Barnebey Cheney, SK	38.8	125.00	4.7391	3.79
17-20	Columbia L, LC 20/48, Grade H-63-11	38.8	142.00	1.687	1.19
21-22	Silica gel, 6-12 mesh	38.8	39.00	17.826	45.71

Several interesting phenomena were observed during these runs. First, the adsorption wave could be visually detected traveling down through the bed when activated carbon samples, which had not been previously dried, were saturated with

propane or propylene. This visible wave consisted of the moisture which had been driven off the activated carbon. A wave was not observed with samples which had been dried prior to use.

The second interesting phenomena observed was the very high temperature rise recorded in the bed during the initial saturation phase. Values of 125° to 142° F change in temperature between the two thermocouples were recorded. While these temperature rises were not precise, due to the nonlinearity of the thermccouples in this range of temperature differences, the values reported were felt to be correct within ± 5° F. Calibration of the thermocouples was for temperatures between 75° and 80° F. Previous drying of the samples did not appreciably lower the temperature rise observed.

A temperature rise of 160° F was calculated for the initial saturation of activated carbon assuming that: 1) the system was adiabatic, 2) propane acted as an ideal gas, and 3) all activated carbon had a heat capacity similar to that of coke. This calculated value is believed to be in consonance with the observed values.

A typical temperature profile for replacement of propane by propylene is shown in Figure 14. It should be noted that the second peak is less than the first. This is caused by the proximity of the two thermocouples which results in a cancellation of part of the maximum temperature at the second or lower thermocouple due to the bed still cooling at the first

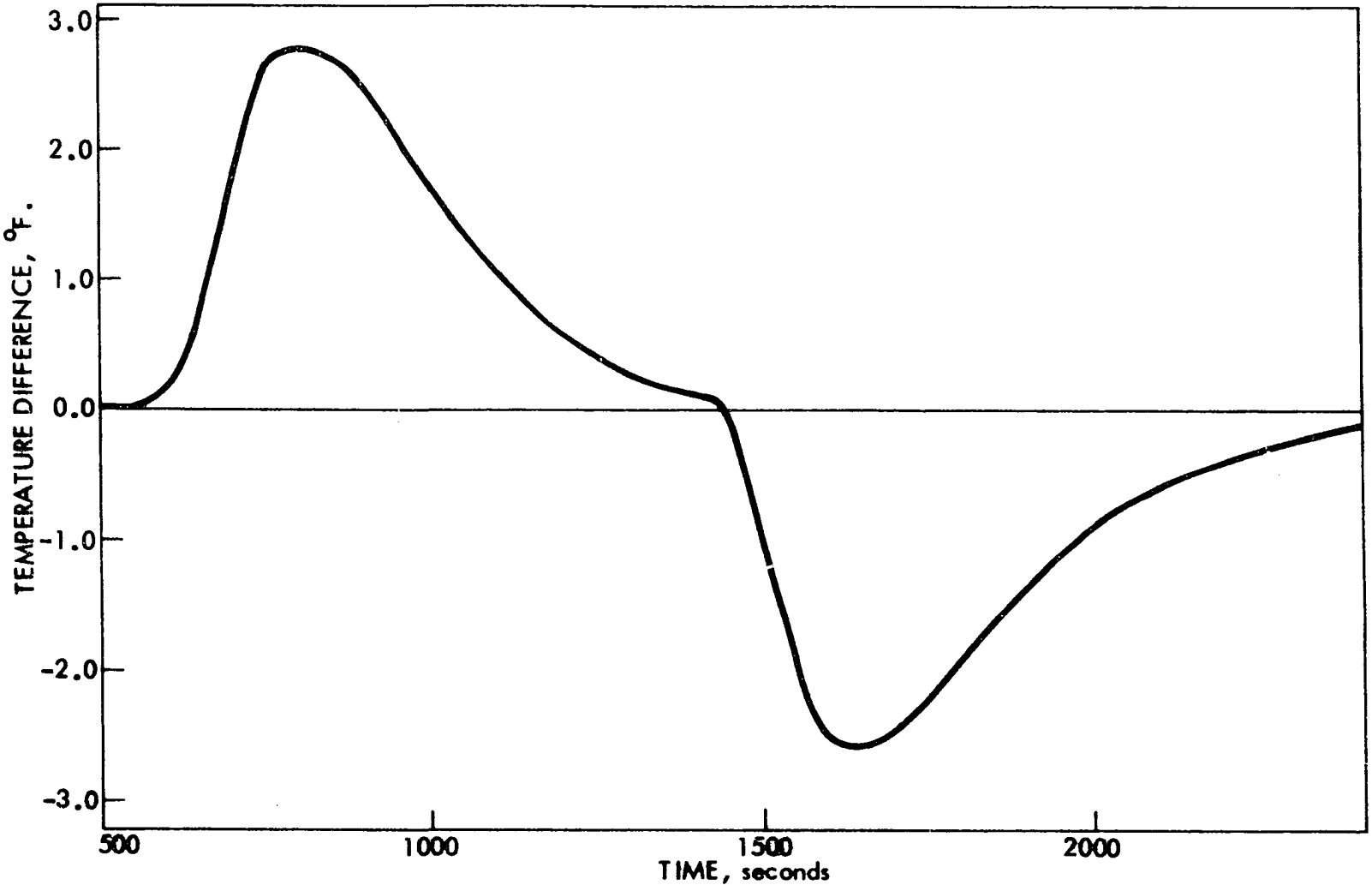

Figure 14. Typical temperature rise profile for propylene replacing propane on Columbia L, 20/48 activated carbon

thermocouple. All temperature profiles observed were of similar shape for both initial saturation runs and adsorption of propane or propylene on a bed previously saturated with the other gas.

It was also observed that for propane being adsorbed by a bed previously saturated with propylene, a temperature rise occurred while there was a temperature drop when the gases were reversed. These observations were expected as the heat of adsorption of propylene is slightly less than that of propane as seen in Table 1. This would thus account for this phenomena.

Runs were also made using 6 - 12 mesh silica gel and Type 4A molecular sieve. The temperature rise observed was much greater for the runs using silica gel as the adsorbent than for any samples of activated carbon. Type 4A molecular sieve did not adsorb either propane or propylene.

From the results shown in Table 2, Columbia LC 20/48, Grade H-63-11 was chosen as the principal adsorbent for use in the remaining runs of this project. In addition, it was further believed that a reduction in the heat of adsorption for a particular system by nearly 99% (run compared to initial temperature rise) constituted an "isothermal" system.

An attempt to correlate the maximum temperature rise observed and the slope of the breakthrough curve was made for cases where either propane and propylene was the gas being adsorbed. Figure 15 shows the correlation for propane being adsorbed by activated carbon and Figure 16 for propylene.

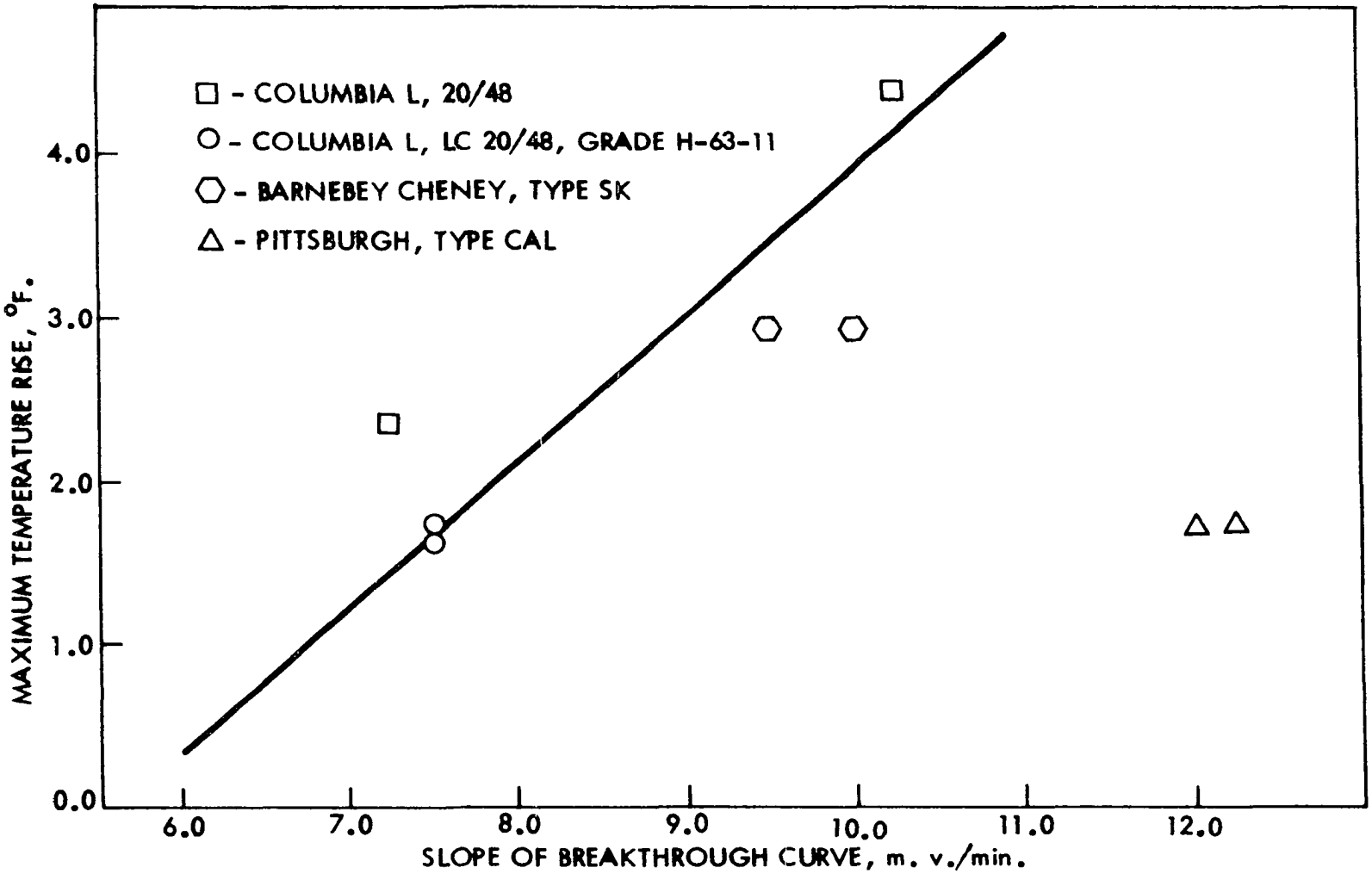

Figure 15. Maximum temperature rise versus slope of the breakthrough curve for propane replacing propylene on various types of activated carbon

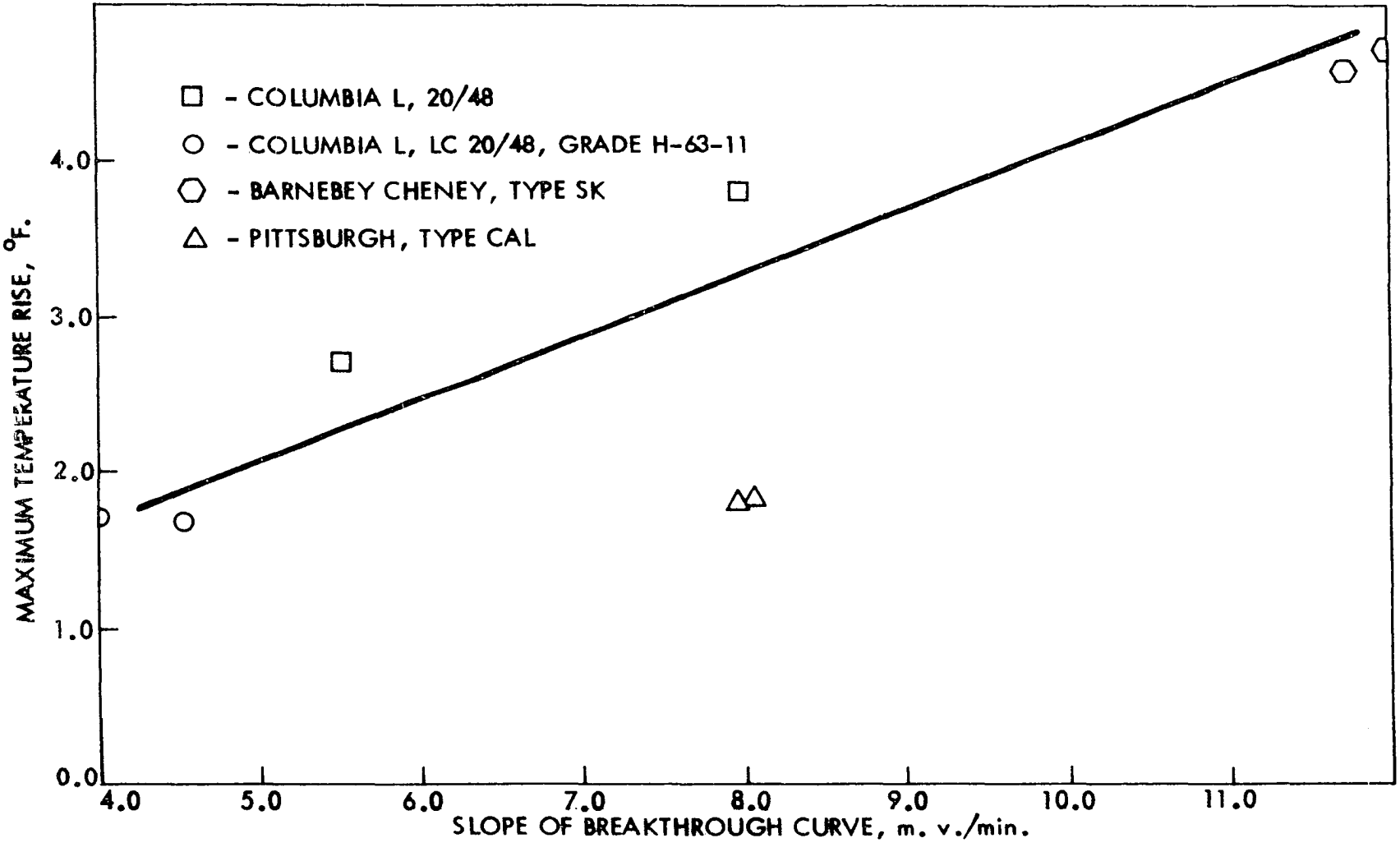

Figure 16. Maximum temperature rise versus slope of the breakthrough curve for propylene replacing propane on various types of activated carbon

In each case, the bed had been previously saturated with the other gas. While neither correlation is good, the points which show the poorest agreement represent a very old sample of Pittsburgh, Type CAL activated carbon of questionable quality.

Since equilibrium data were not available for the specific activated carbons used, no attempt was made to test the models to be investigated during these preliminary runs.

Several runs were next made to determine the relationship between bed temperature rise and concentration of adsorbate in the carrier gas. Both propane and propylene were used as the adsorbate and helium as the carrier gas. The data are given in Table 3 and plotted in Figure 17. It is noted that for this system, a mixture of 7.25 mole percent of either propane or propylene and helium will establish isothermal bed conditions (zero temperature rise) for the adsorption process.

Table 3. Mole fraction of propane or propylene in binary mixture with helium and maximum observed temperature rise in bed above 77.0° F for Columbia LC 20/48, Grade H-63-11, activated carbon

Propane			Propylene		
Run no.	Mole fraction	Temperature rise, °F	Run no.	Mole fraction	Temperature rise, °F
301	0.2027	58.7	310	1.0000	144.4
302	0.5893	107.3	311	0.1389	36.5
303	0.2231	33.4	312	0.3609	82.6
304	0.1362	34.9	313	0.4455	101.5
305	0.3543	85.2	314	0.6169	104.8
306	0.4397	103.0	315	0.1720	51.1
307	1.0000	149.6			

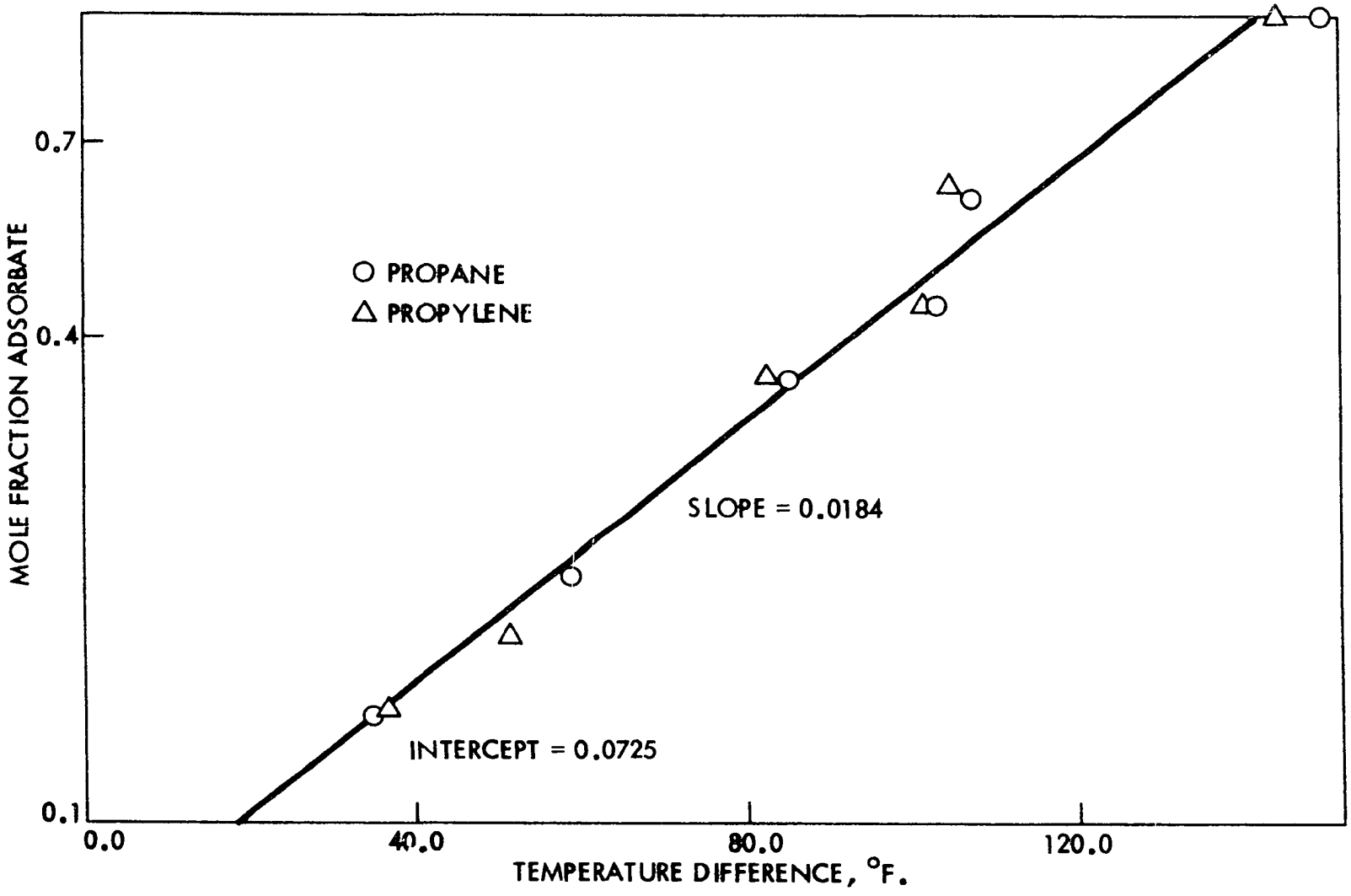

Figure 17. Logarithm of the mole fraction of adsorbate gas in helium carrier stream versus observed bed temperature rise above 77° F for Columbia LC 20/48, Grade H-63-11, activated carbon

These temperature rise data appeared to be very consistent for both gases and were found to be easily reproducible. It is felt that the close agreement between the values of the temperature rise for a given mole fraction of either propane or propylene in a mixture with helium is due to the similarity between the two gases in heats of adsorption, molecular size, viscosity and other properties.

The following relationship was derived from the data given in Table 3 to describe this correlation:

$$\ln Y_A = 0.0725 + 0.184\Delta T \qquad (38)$$

where: Y_A = mole fraction adsorbate.

ΔT = temperature rise in bed from initial temperature of 77.0° F, °F.

Equilibrium Isotherms

The equilibrium isotherms for propane and propylene on Columbia LC 20/48, Grade H-63-11, activated carbon were determined on three samples of activated carbon at 25° C. The results are given in Table 4 and are plotted in Figures 18 and 19.

Table 4. Equilibrium values for propane and propylene adsorbed on Columbia LC 20/48, Grade H-63-11, activated carbon at 25° C

Propane			Propylene		
Sample number	X* g propane/ g carbon	p, mm Hg.	Sample number	X* g propylene/ g carbon	p, mm Hg.
1	0.0526	4.3668	1	0.0641	6.3707
1	0.0974	22.0995	1	0.1111	27.3438
1	0.1416	45.8111	1	0.1660	90.0714
1	0.1986	133.6745	1	0.2234	284.0490
1	0.2327	295.9782	1	0.2586	645.7343
1	0.2540	479.3044	1	0.2678	743.0375
1	0.2611	672.8293	2	0.0666	6.0034
1	0.2709	731.1206	2	0.1021	22.0587
2	0.0501	6.0809	2	0.1683	92.6833
2	0.1483	38.4854	2	0.2233	281.3310
2	0.1902	97.9174	2	0.2585	631.0830
2	0.2375	269.7038	2	0.2687	738.2422
2	0.2634	597.0747	3	0.0699	7.0604
2	0.2686	714.5632	3	0.1095	22.4668
2	0.2701	739.4257	3	0.1730	92.3731
3	0.0930	10.3906	3	0.2281	280.9556
3	0.1266	27.6009	3	0.2583	614.1870
3	0.1886	103.5922	3	0.2633	740.5686
3	0.2364	294.5622			
3	0.2564	528.3967			
3	0.2612	690.8190			
3	0.2643	743.2619			

A determination of the constants in each of the five theoretical descriptions of a type A isotherm was also made. These constants were found by rearranging each of the theoretical models into the form of an equation of a straight line. The data were then applied to the equations and the slope and intercept of the resulting plot were calculated using a least squares analysis as described by Draper and Smith (12). Figures 20 through 25 show these correlations. Table 5 gives the calculated values of these constants and Tables 6 and 7

Figure 18. Equilibrium isotherm for propane on Columbia LC 20/48, Grade H-63-11, activated carbon at 25° C

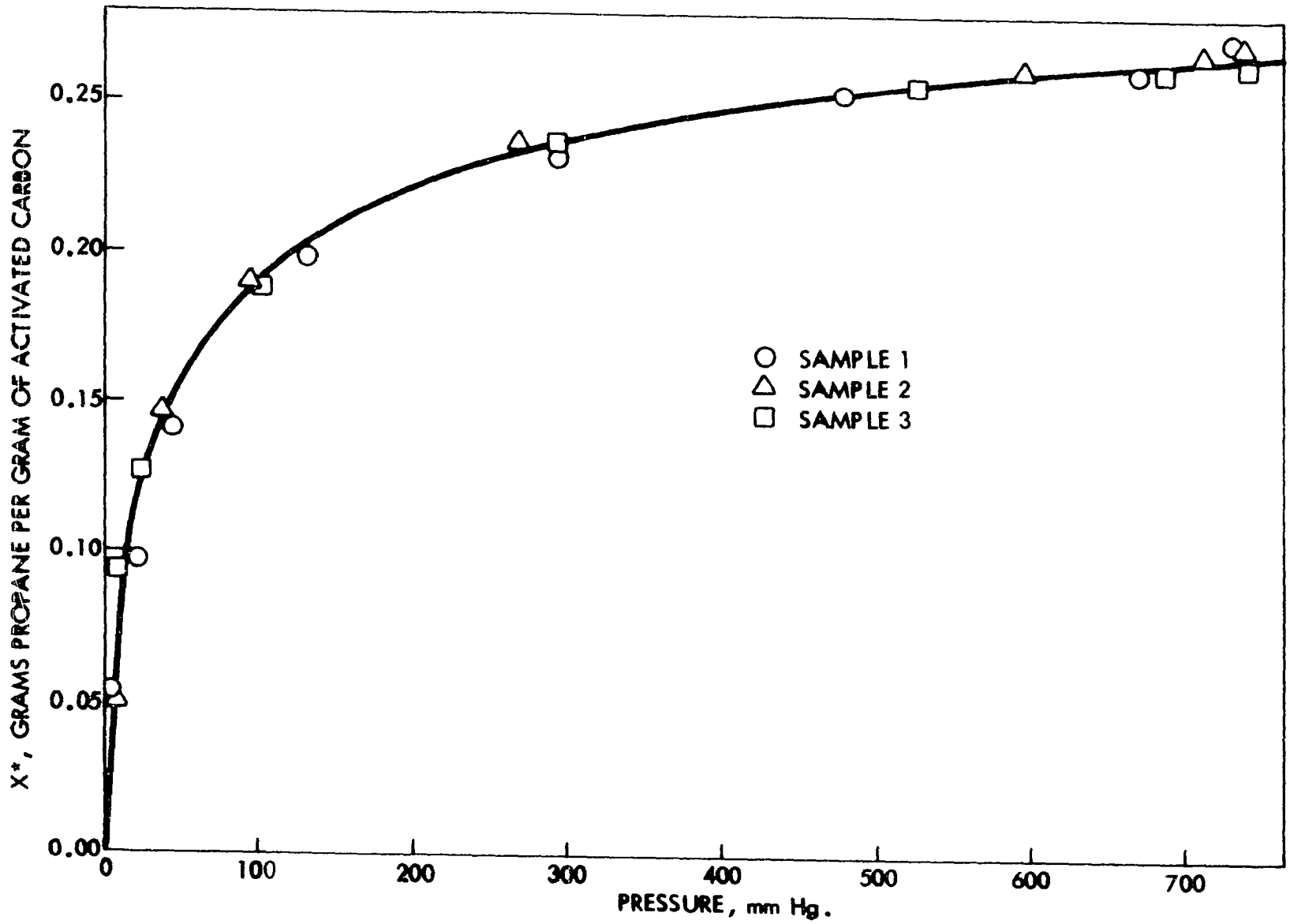
X*, GRAMS PROPANE PER GRAM OF ACTIVATED CARBON
0.25
0.20
0.15
0.10
0.05
0.00
0
100
200
300
400
500
600
700
PRESSURE, mm Hg.
SAMPLE 1
SAMPLE 2
SAMPLE 3

Figure 19. Equilibrium isotherm for propylene on Columbia LC 20/48, Grade H-63-11, activated carbon at 25° C

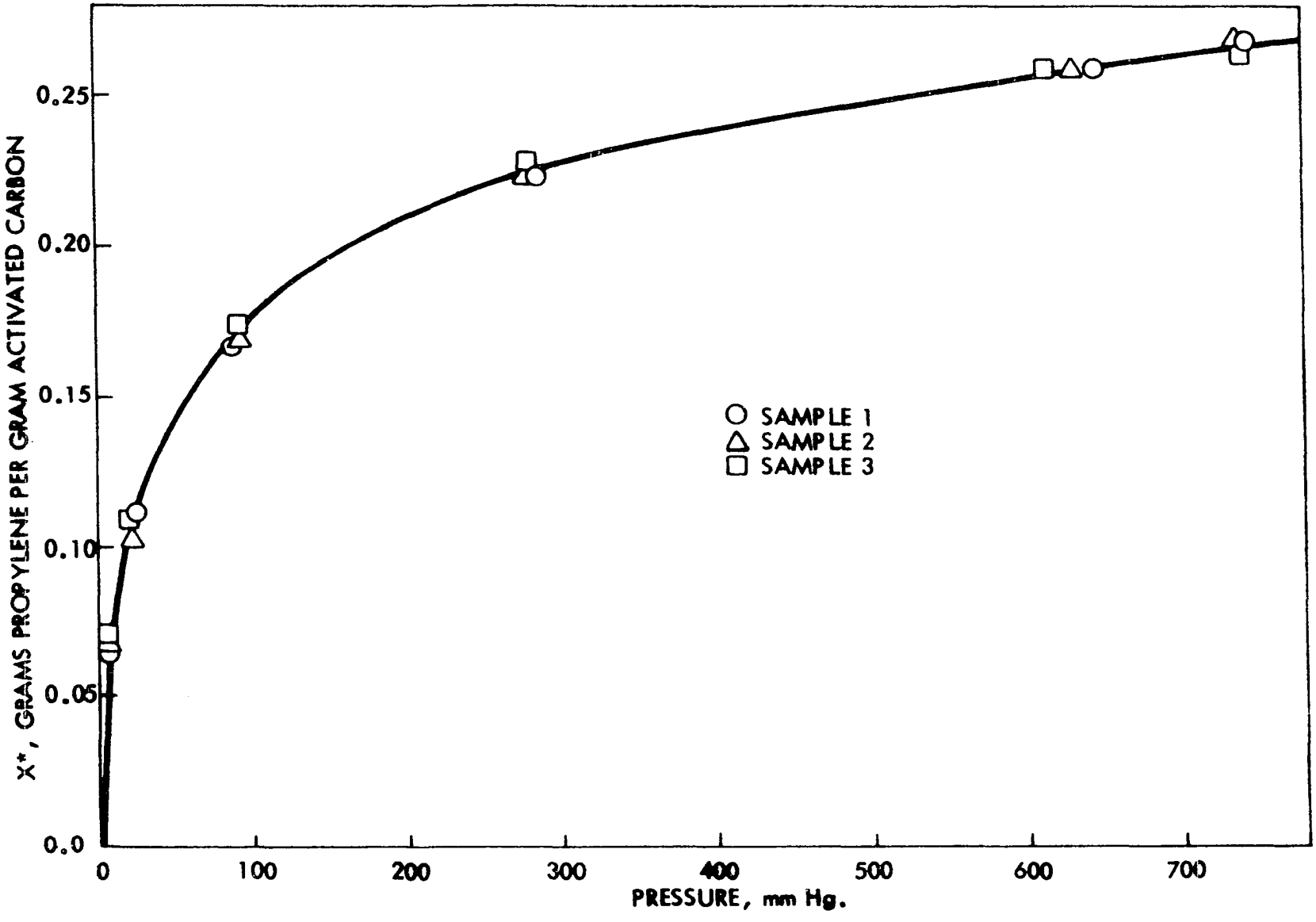
X*, GRAMS PROPYLENE PER GRAM ACTIVATED CARBON
0.0
0.05
0.10
0.15
0.20
0.25
0
100
200
300
400
500
600
700
PRESSURE, mm Hg.
SAMPLE 1
SAMPLE 2
SAMPLE 3

Figure 20. Plot of variables for Freundlich equation for propane on Columbia LC 20/48, Grade H-63-11, activated carbon at 25° C

Figure 21. Plot of variables for Freundlich equation for propylene on Columbia LC 20/48, Grade H-63-11, activated carbon at 25° C

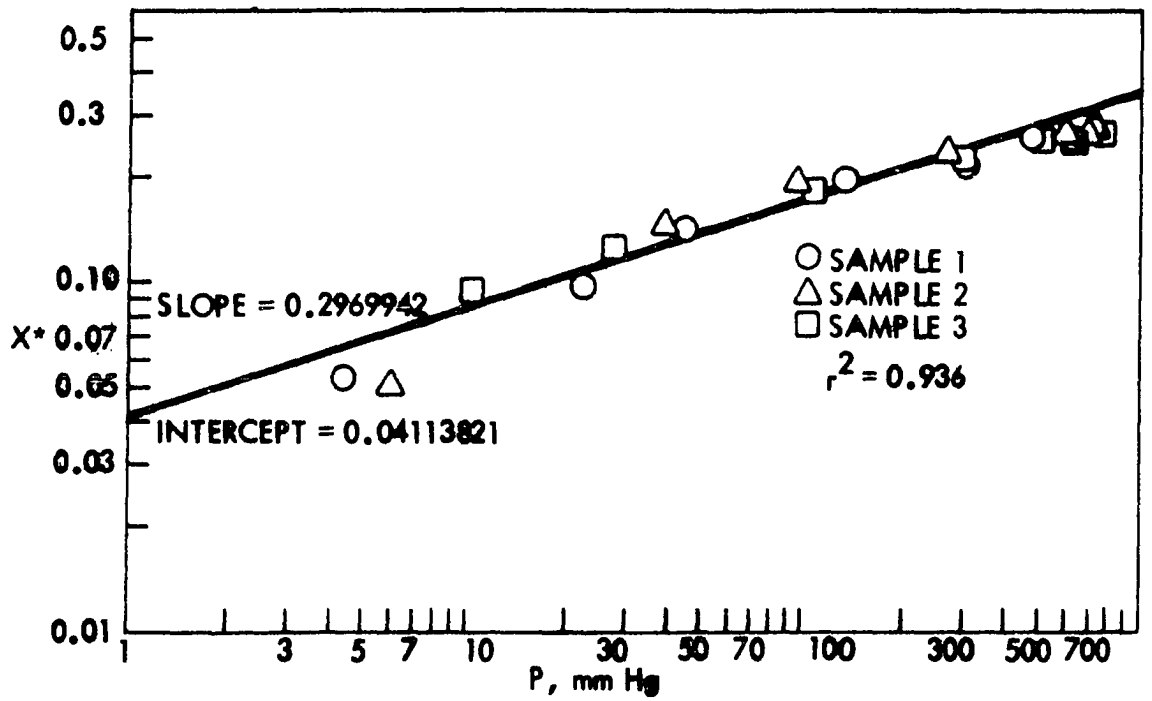
0.5
0.3
0.10
X* 0.07
0.05
0.03
0.01
SLOPE = 0.2969942
INTERCEPT = 0.04113821
SAMPLE 1
SAMPLE 2
SAMPLE 3
r2 = 0.936
1
3
5
7
10
30
50
70
100
300
500
700
P, mm Hg

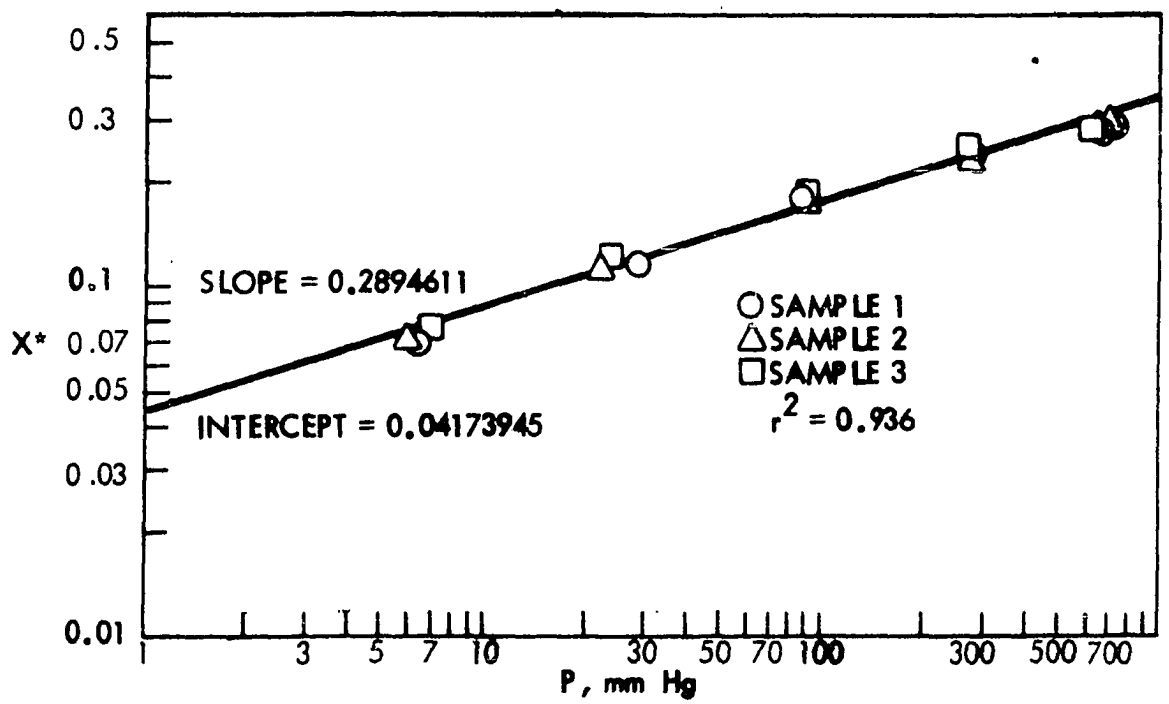
0.5
0.3
0.1
X* 0.07
0.05
0.03
0.01
SLOPE = 0.2894611
INTERCEPT = 0.04173945
SAMPLE 1
SAMPLE 2
SAMPLE 3
r2 = 0.936
1
3
5
7
10
30
50
70
100
300
500
700
P, mm Hg

Figure 22. Plot of variables for Langmuir and monomolecular layer form of B.E.T. equations for propane on Columbia LC 20/48, Grade H-63-11, activated carbon at 25° C

Figure 23. Plot of variables for Langmuir and monomolecular layer form of B.E.T. equations for propylene on Columbia LC 20/48, Grade H-63-11, activated carbon at 25° C

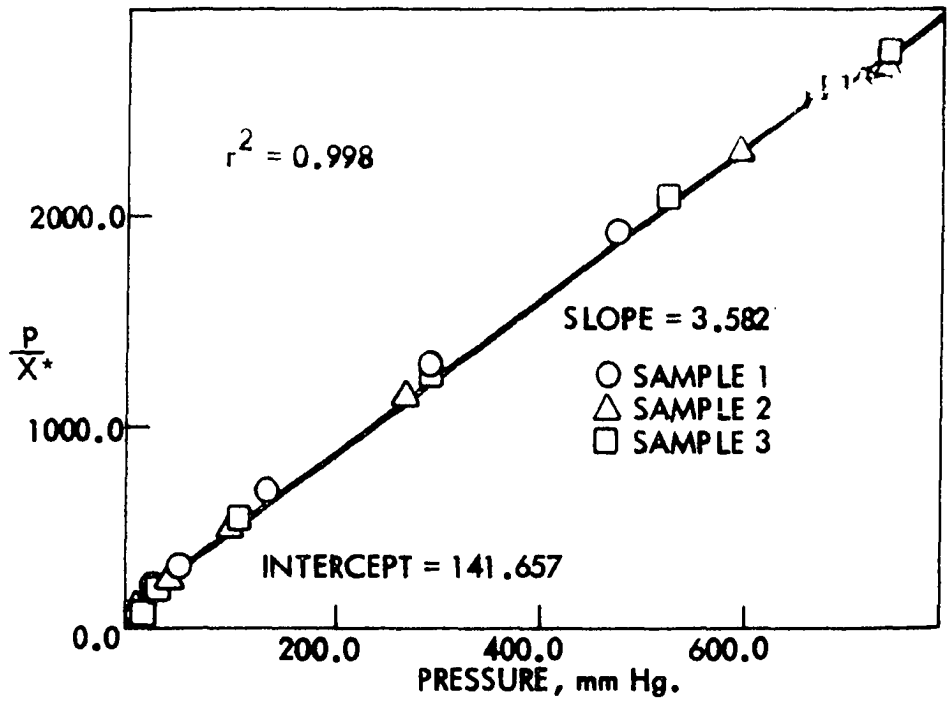
$r^2 = 0.998$
SLOPE = 3.582
SAMPLE 1
SAMPLE 2
SAMPLE 3
INTERCEPT = 141.657
$\frac{P}{X^*}$
2000.0
1000.0
0.0
200.0
400.0
600.0
PRESSURE, mm Hg.

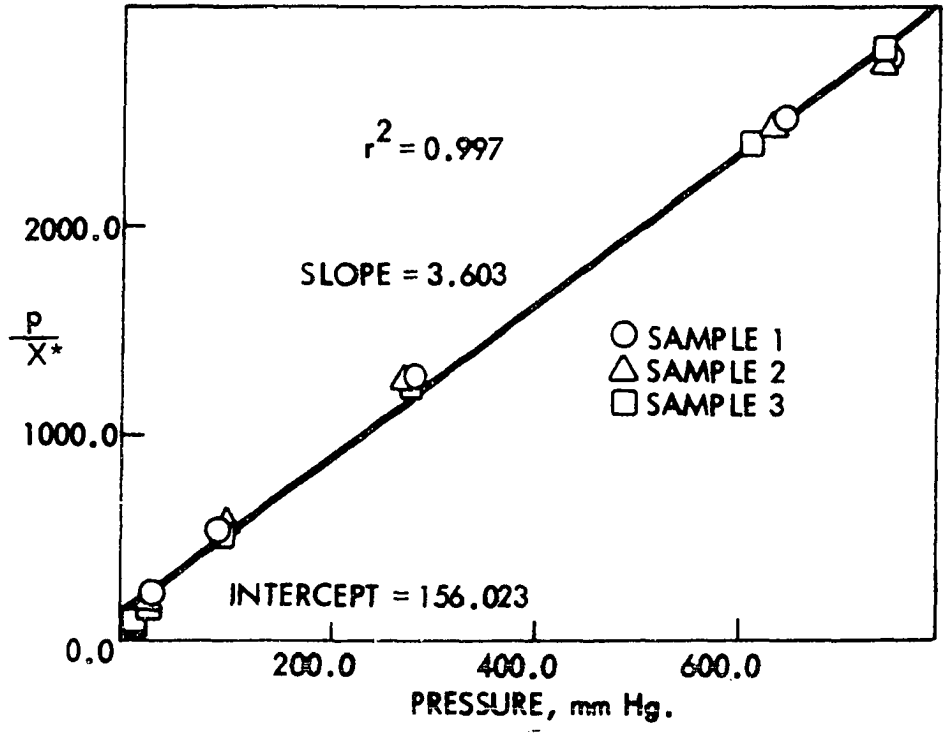
$r^2 = 0.997$
SLOPE = 3.603
SAMPLE 1
SAMPLE 2
SAMPLE 3
INTERCEPT = 156.023
$\frac{P}{X^*}$
2000.0
1000.0
0.0
200.0
400.0
600.0
PRESSURE, mm Hg.

Figure 24. Plot of variables in B.E.T. equation for propane on Columbia LC 20/48, Grade H-63-11, activated carbon at 25° C

Figure 25. Plot of variables in B.E.T. equation for propylene on Columbia LC 20/48, Grade H-63-11, activated carbon at 25° C

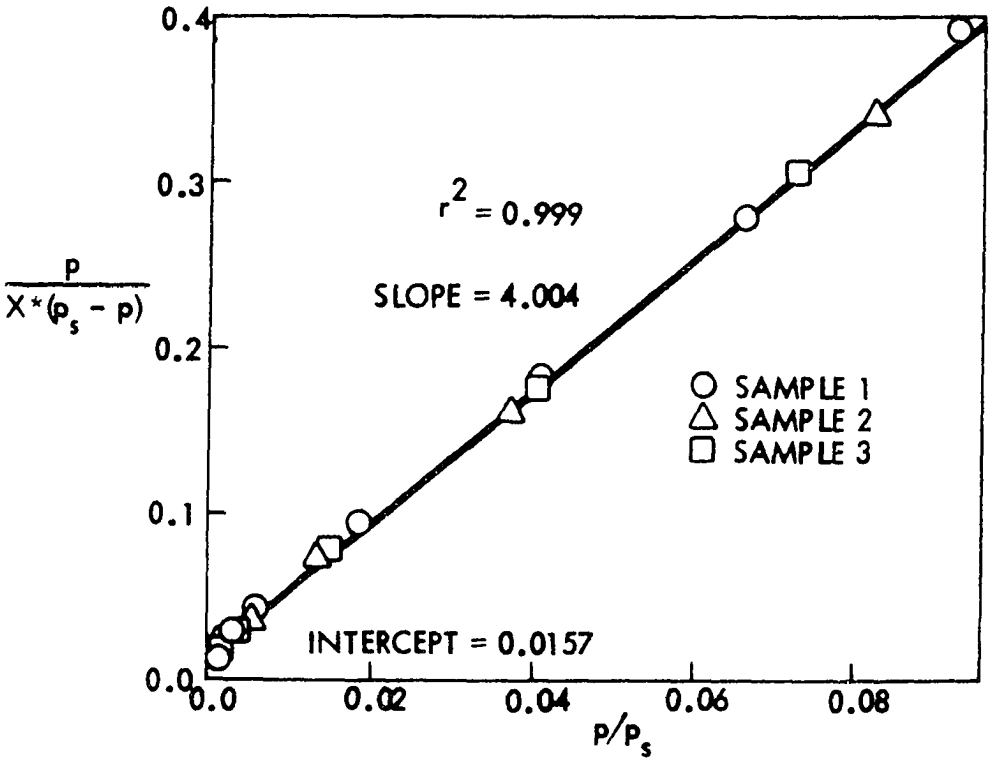
0.4
0.3
0.2
0.1
0.0
$\frac{P}{X^*(P_s - P)}$
$r^2 = 0.999$
SLOPE = 4.004
SAMPLE 1
SAMPLE 2
SAMPLE 3
INTERCEPT = 0.0157
0.0
0.02
0.04
0.06
0.08
P/P_s

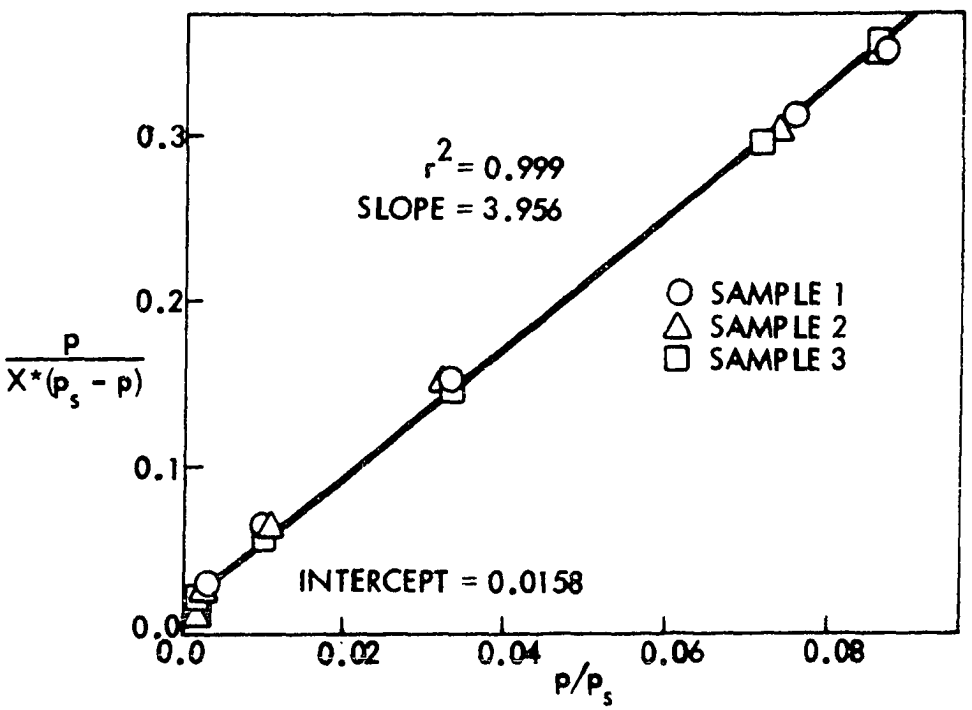
0.3
0.2
0.1
0.0
$\frac{P}{X^*(P_s - P)}$
$r^2 = 0.999$
SLOPE = 3.956
SAMPLE 1
SAMPLE 2
SAMPLE 3
INTERCEPT = 0.0158
0.0
0.02
0.04
0.06
0.08
P/P_s

Table 5. Calculated constants of theoretical equilibrium isotherm models for propane and propylene being adsorbed on Columbia LC 20/48, Grade H-63-11, activated carbon at 25° C

Model	Constant	Propane isotherm	Propylene isotherm
Freundlich	k	0.0411	0.0417
Freundlich	1/n'	0.2970	0.2895
Langmuir	X_m	0.2791	0.2775
Langmuir	B	0.0253	0.0231
Modified B.E.T.	X_m	0.2776	0.2761
Modified B.E.T.	A	0.0254	0.0232
McGavack and Patrick	k	0.5767	0.5743
McGavack and Patrick	1/n'	0.2970	0.2895
B.E.T.	b	255.9986	250.7228
B.E.T.	X_m	0.2488	0.2518

Table 6. Calculated equilibrium isotherm values for propane on Columbia LC 20/48, Grade H-63-11, activated carbon at 25° C

	X*, g propane/g carbon				
p, mm Hg.	Freundlich solution	Langmuir solution	Modified B.E.T. solution	McGavack & Patrick solution	B.E.T. solution
50.0	0.1315	0.1559	0.1558	0.1315	0.1602
100.0	0.1615	0.2000	0.2000	0.1615	0.1971
150.0	0.1822	0.2209	0.2209	0.1822	0.2143
200.0	0.1984	0.2331	0.2330	0.1984	0.2248
250.0	0.2120	0.2410	0.2410	0.2120	0.2322
300.0	0.2238	0.2466	0.2466	0.2238	0.2379
350.0	0.2343	0.2508	0.2508	0.2343	0.2427
400.0	0.2438	0.2540	0.2540	0.2438	0.2467
450.0	0.2525	0.2566	0.2566	0.2525	0.2504
500.0	0.2605	0.2587	0.2587	0.2605	0.2538
550.0	0.2680	0.2604	0.2604	0.2680	0.2569
600.0	0.2750	0.2619	0.2618	0.2750	0.2599
650.0	0.2816	0.2631	0.2631	0.2816	0.2628
700.0	0.2879	0.2642	0.2642	0.2879	0.2656
750.0	0.2938	0.2652	0.2651	0.2938	0.2683
760.0	0.2950	0.2653	0.2653	0.2950	0.2689

Table 7. Calculated equilibrium isotherm values for propylene on Columbia LC 20/48, Grade H-63-11, activated carbon at 25° C

p, mm Hg.	X*, g propylene/g carbon				
	Freundlich solution	Langmuir solution	Modified B.E.T. solution	McGavack & Patrick solution	B.E.T. solution
50.0	0.1295	0.1487	0.1487	0.1295	0.1507
100.0	0.1583	0.1937	0.1937	0.1583	0.1904
150.0	0.1780	0.2154	0.2154	0.1780	0.2093
200.0	0.1934	0.2281	0.2281	0.1934	0.2209
250.0	0.2064	0.2366	0.2365	0.2064	0.2289
300.0	0.2176	0.2425	0.2425	0.2176	0.2350
350.0	0.2275	0.2470	0.2470	0.2275	0.2400
400.0	0.2364	0.2504	0.2504	0.2364	0.2442
450.0	0.2447	0.2532	0.2532	0.2447	0.2479
500.0	0.2522	0.2554	0.2554	0.2522	0.2512
550.0	0.2593	0.2573	0.2573	0.2593	0.2542
600.0	0.2659	0.2588	0.2588	0.2659	0.2570
650.0	0.2721	0.2602	0.2602	0.2721	0.2598
700.0	0.2780	0.2614	0.2614	0.2780	0.2624
750.0	0.2836	0.2624	0.2624	0.2836	0.2649
760.0	0.2847	0.2626	0.2626	0.2847	0.2654

give the calculated isotherm values for the various models for propane and propylene respectively. Plots of these calculated values are compared with the experimental data in Figures 26 and 27.

Examination of Figures 26 and 27 reveals that the B.E.T. model fits the data over the range of the isotherm determined better than any of the other models tested. This is further substantiated by the values of the correlation coefficients, r^2, shown in Figures 20 through 25. The values for the B.E.T. model were the highest.

That the B.E.T. model seemed to fit the data best was unexpected since this model is applicable to the multimolecular

Figure 26. Comparison between experimental and theoretical isotherms for propane on Columbia LC 20/48, Grade H-63-11, activated carbon at 25° C

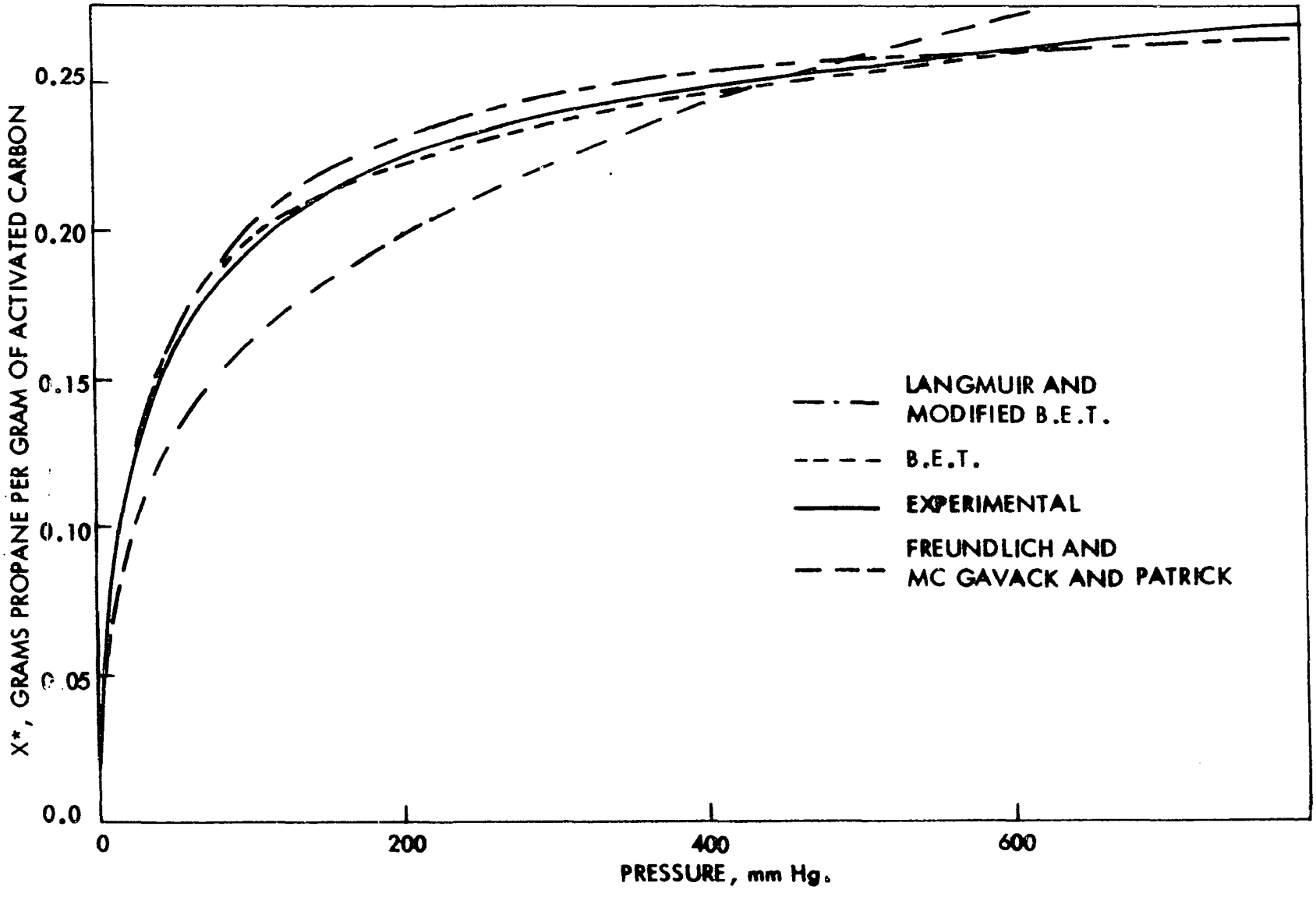
0.25
0.20
0.15
0.10
0.05
0.0
X*, GRAMS PROPANE PER GRAM OF ACTIVATED CARBON
0
200
400
600
PRESSURE, mm Hg.
LANGMUIR AND MODIFIED B.E.T.
B.E.T.
EXPERIMENTAL
FREUNDLICH AND MC GAVACK AND PATRICK

Figure 27. Comparison between experimental and theoretical isotherms for propylene on Columbia LC 20/48, Grade H-63-11, activated carbon at 25° C

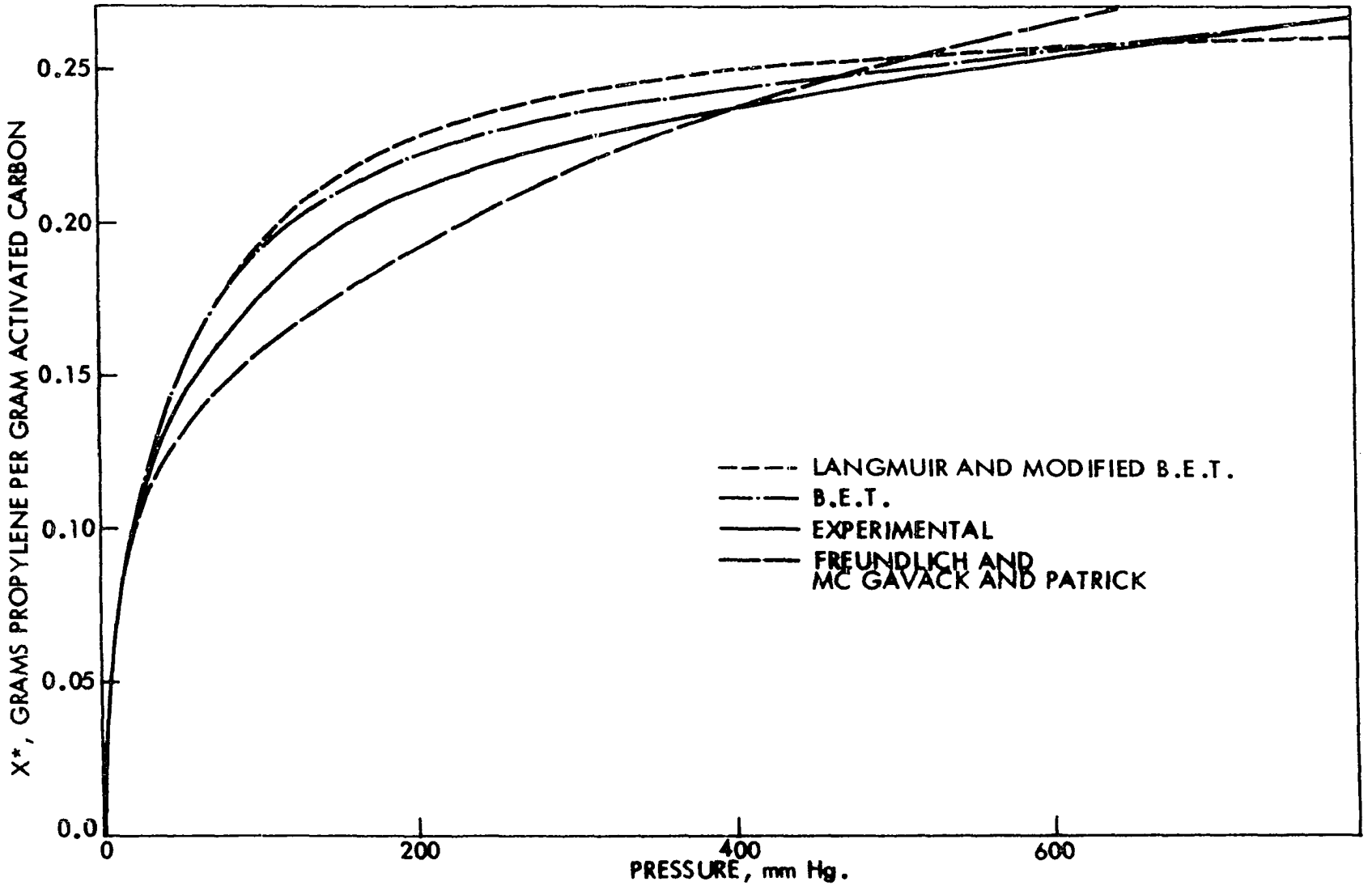
0.25
0.20
0.15
0.10
0.05
0.0
X*, GRAMS PROPYLENE PER GRAM ACTIVATED CARBON
0
200
400
600
PRESSURE, mm Hg.
LANGMUIR AND MODIFIED B.E.T.
B.E.T.
EXPERIMENTAL
FREUNDLICH AND MC GAVACK AND PATRICK

adsorption case. From the calculated values of the monomolecular layer capacity of the carbon, X_m, the B.E.T. model indicated that a multimolecular layer of gas had begun to form at the primary point of interest, 760 mm Hg. This is perhaps explained by the fact that each isotherm was determined for only about the first 15% of the carbon saturation capacity and thus did not represent the entire isotherm for propane and propylene on Columbia LC 20/48, Grade H-63-11, activated carbon at 25° C. Had entire isotherms been determined, the fit of the models might have been different. It is believed that these isotherms were type A and represented the monomolecular layer adsorption capacity of the adsorbent over the entire range of saturation. This is based upon isotherm data found in the literature (25) for these two gases on other activated carbons.

From the data, values of X_o^* were determined to be 0.2660 g propane/g carbon for propane and 0.2630 g propylene/g carbon for propylene. These values were subsequently used in the determination of fit of the various models representing the breakthrough curves.

Breakthrough Data

Sixty-four exchange adsorption runs were made to determine the characteristics of the breakthrough curves for the cases of propane replacing propylene (32 runs) and propylene replacing propane (31 runs). One run was discarded due to a malfunction of the recorder during the run.

The results of these runs are given in Appendix A. In addition to the raw data, values are given for each of the variables calculated for the models previously discussed by the methods shown in Appendix B. Figures 28 and 29 give the calculated breakthrough curves for two runs for each of the models tested. These values were calculated on an IBM 360, model 65 digital computer using the program shown in Appendix B. Figure 28 shows a run in which propane is replacing propylene and Figure 29 shows a run in which propylene is replacing propane. Figures 30 and 31 show these same calculated values plotted against the experimental data taken from Appendix A. It is noted that in both cases, two models appear to fit the data in both shape and prediction of the time of the breakpoint. These are the Eagleton and Bliss and the Glueckauf and Coates models. The other models fail in either predicting the shape of the breakthrough curve or the time of the breakpoint. Some of the models fail both criteria.

The two models which did fit the data were found to predict the shape of the breakthrough curve and in a majority of cases to predict accurately the time of the breakpoint. The reasons for failure, in at least some instances, to predict the time of the breakpoint will be discussed later.

Both the Eagleton and Bliss and Glueckauf and Coates models make essentially the same assumptions. These assumptions may be found in the section on Adsorption Theory. One significant assumption common to both models is that there is

Figure 28. Calculated breakthrough curves from various models for propane replacing propylene on Columbia LC 20/48, Grade H-63-11, activated carbon at 25° C and a mass flow rate of 0.0502 g/min/cm^2

RUN NUMBER 208

PROPANE REPLACING PROPYLENE

C/CO	EB-1	EB-2	EB-3	SB	GC	VM	SE	BOYD	TREY
0.05	12.471	12.674	12.643	12.741	12.643	12.692	12.579	12.466	11.921
0.10	12.612	12.703	12.672	12.882	12.672	12.733	12.723	12.470	12.331
0.15	12.695	12.734	12.702	12.965	12.702	12.776	12.812	12.474	12.572
0.20	12.753	12.766	12.735	13.023	12.735	12.822	12.880	12.477	12.731
0.25	12.799	12.800	12.769	13.069	12.769	12.871	12.935	12.490	12.875
0.30	12.836	12.837	12.806	13.106	12.806	12.923	12.984	12.507	12.979
0.35	12.867	12.876	12.845	13.137	12.845	12.979	13.028	12.535	13.073
0.40	12.894	12.919	12.887	13.164	12.887	13.039	13.069	12.571	13.147
0.45	12.918	12.965	12.934	13.188	12.934	13.105	13.109	12.618	13.218
0.50	12.940	13.016	12.984	13.210	12.984	13.177	13.147	12.662	13.278
0.55	12.959	13.072	13.040	13.229	13.040	13.257	13.186	12.723	13.341
0.60	12.977	13.134	13.103	13.247	13.103	13.346	13.226	12.784	13.395
0.65	12.993	13.205	13.174	13.263	13.174	13.447	13.267	12.872	13.440
0.70	13.008	13.287	13.256	13.278	13.256	13.563	13.311	12.975	13.492
0.75	13.022	13.384	13.353	13.292	13.353	13.701	13.360	13.124	13.542
0.80	13.035	13.503	13.471	13.306	13.471	13.870	13.415	13.284	13.589
0.85	13.048	13.655	13.624	13.318	13.624	14.087	13.483	13.509	13.643
0.90	13.059	13.871	13.840	13.329	13.840	14.394	13.572	13.839	13.701
0.95	13.070	14.239	14.208	13.340	14.208	14.918	13.716	14.378	13.778

LEGEND

EB-1 - EAGLETON-BLISS SOLUTION FOR C < CD
EB-2 - EAGLETON-BLISS SOLUTION FOR C > CD
EB-3 - EAGLETON-BLISS SOLUTION FOR SOLID FILM CONTROLLING
SB - SELKE-BLISS SOLUTION
GC - GLUECKAUF-COATES SOLUTION
VM - VERMEULEN SOLUTION
SE - SILLEN-EKEDAHL SOLUTION
BOYD - BOYD, MEYERS, AND ADAMSON SOLUTION
TREY - TREYBAL SOLUTION

Figure 29. Calculated breakthrough curves from various models for propylene replacing propane on Columbia LC 20/48, Grade H-63-11, activated carbon at 25° C and a mass flow rate of 0.1010 g/min/cm^2

RUN NUMBER 207

PROPYLENE REPLACING PROPANE

C/CO	EB-1	EB-2	EB-3	SB	GC	VM	SE	BOYD	TREY
0.05	11.226	11.244	11.237	12.682	11.237	11.407	12.541	10.495	9.913
0.10	11.340	11.345	11.338	12.796	11.338	11.548	12.660	10.548	10.991
0.15	11.407	11.452	11.445	12.862	11.445	11.698	12.733	10.562	11.561
0.20	11.455	11.565	11.558	12.910	11.558	11.857	12.789	10.610	11.999
0.25	11.491	11.686	11.679	12.946	11.679	12.027	12.835	10.667	12.352
0.30	11.521	11.815	11.808	12.976	11.808	12.208	12.875	10.738	12.551
0.35	11.547	11.953	11.946	13.002	11.946	12.402	12.911	10.835	12.772
0.40	11.569	12.103	12.096	13.024	12.096	12.612	12.945	10.976	12.976
0.45	11.588	12.265	12.258	13.043	12.258	12.841	12.978	11.124	13.168
0.50	11.605	12.443	12.436	13.060	12.436	13.091	13.010	11.291	13.338
0.55	11.621	12.640	12.633	13.076	12.633	13.367	13.042	11.498	13.500
0.60	11.635	12.860	12.854	13.090	12.853	13.676	13.075	11.744	13.648
0.65	11.649	13.110	13.103	13.104	13.103	14.027	13.109	11.548	13.771
0.70	11.661	13.398	13.391	13.116	13.391	14.431	13.145	11.388	13.883
0.75	11.672	13.739	13.732	13.127	13.732	14.910	13.185	11.868	14.021
0.80	11.683	14.156	14.149	13.138	14.149	15.495	13.231	13.473	14.159
0.85	11.693	14.693	14.686	13.148	14.686	16.250	13.286	14.241	14.319
0.90	11.702	15.451	15.444	13.157	15.444	17.314	13.360	15.399	14.520
0.95	11.711	16.746	16.740	13.166	16.740	19.133	13.479	17.395	14.771

LEGEND

EB-1 - EAGLETON-BLISS SOLUTION FOR C < CD
EB-2 - EAGLETON-BLISS SOLUTION FOR C > CD
EB-3 - EAGLETON-BLISS SOLUTION FOR SOLID FILM CONTROLLING
SB - SELKE-BLISS SOLUTION
GC - GLUECKAUF-COATES SOLUTION
VM - VERMEULEN SOLUTION
SE - SILLEN-EKEDAHL SOLUTION
BOYD - BOYD, MEYERS, AND ADAMSON SOLUTION
TREY - TREYBAL SOLUTION

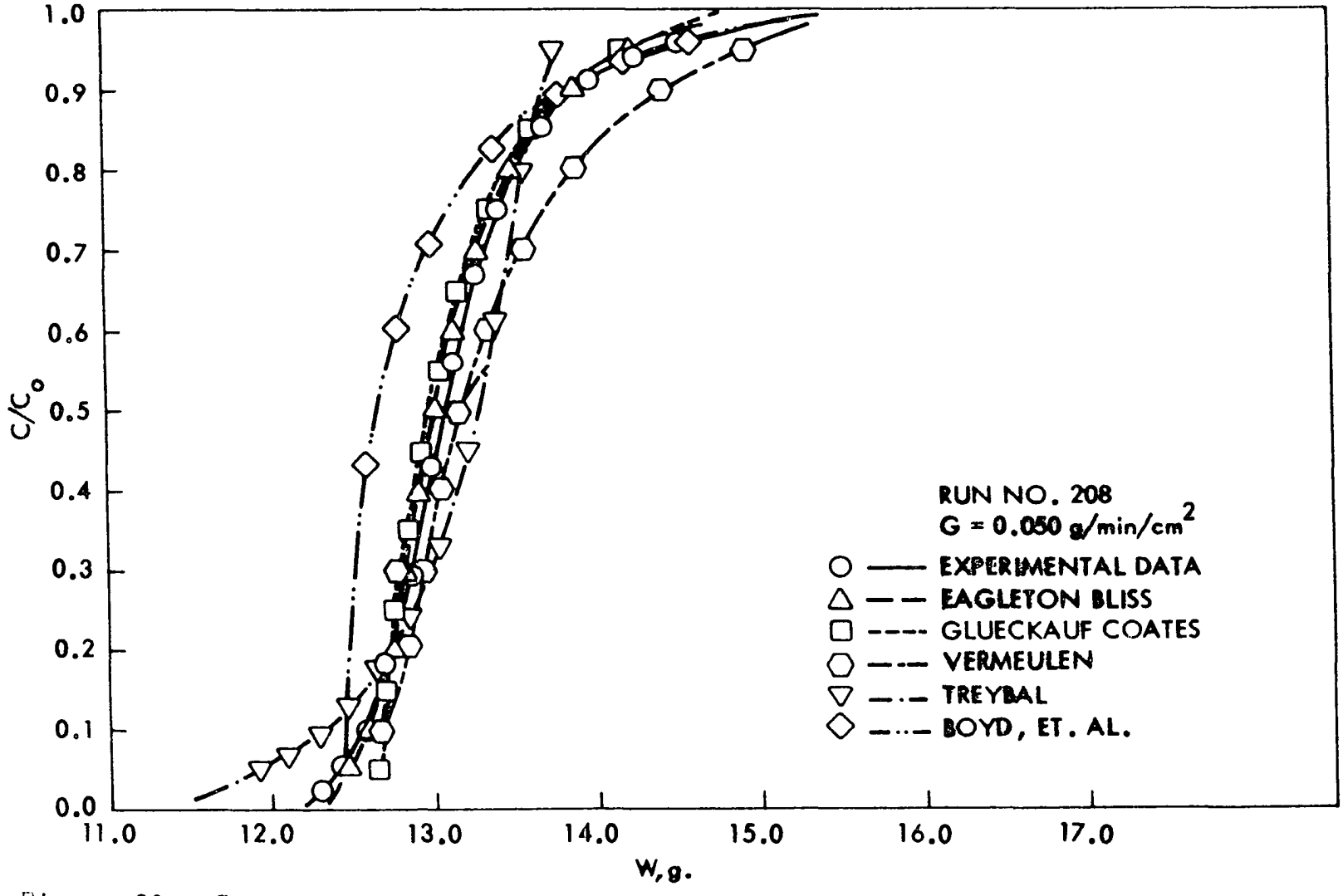

Figure 30. Comparison between experimental data and various models predicting the breakthrough curve for propane replacing propylene on Columbia LC 20/48, Grade H-63-11, activated carbon at 25° C and 1 atm pressure

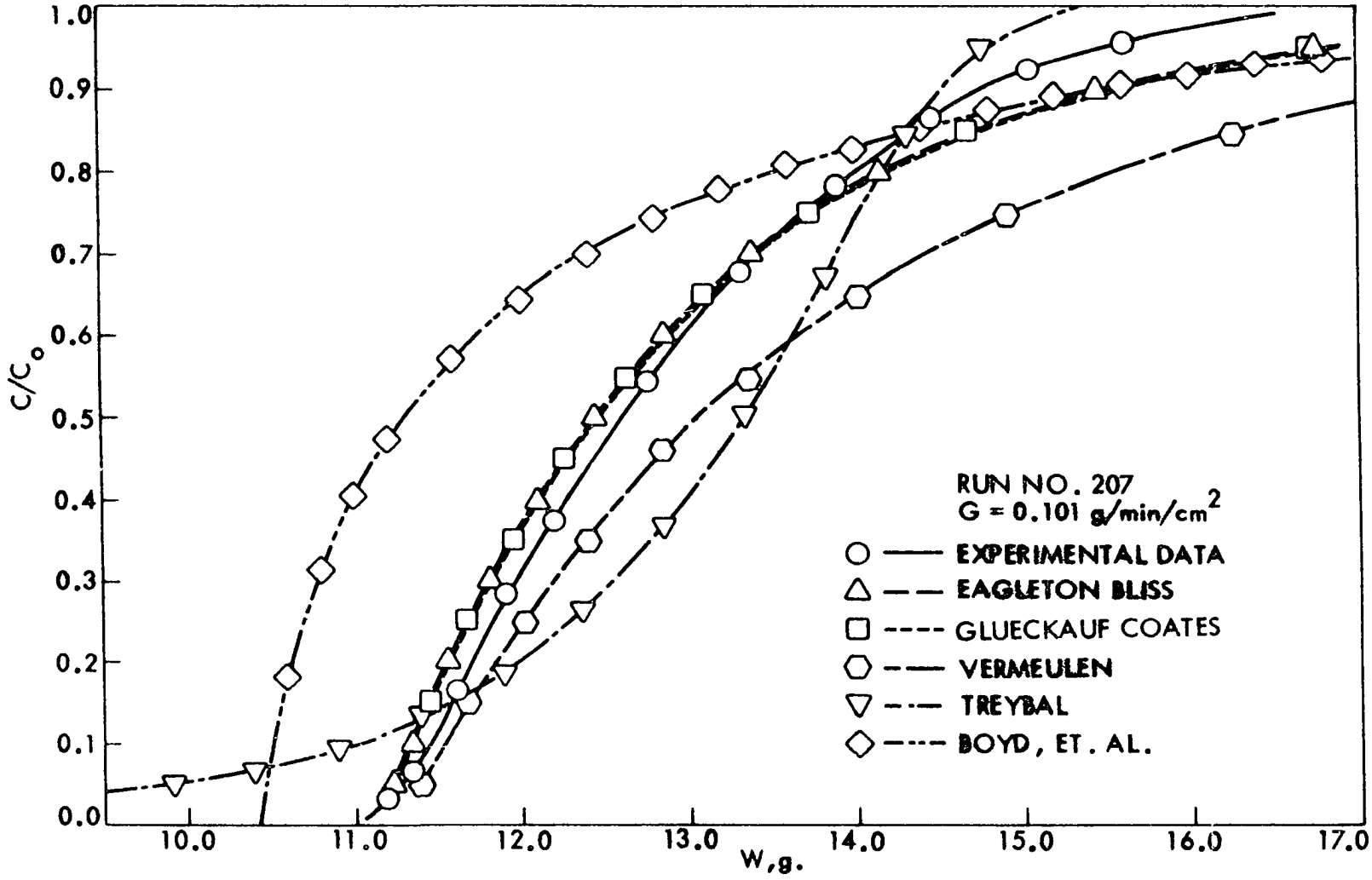

Figure 31. Comparison between experimental data and various models predicting the breakthrough curve for propylene replacing propane on Columbia LC 20/48, Grade H-63-11, activated carbon at 25° C and 1 atm pressure

a linear driving force, described by Equation 13, with particle diffusion the rate controlling mechanism. The primary differences between these two models are that the Eagleton and Bliss model assumes that there is a gas film resistance and that the isotherms are made up of two straight lines. These assumptions affect the shape of the curve at its initial turn upward (19). This is taken into account in Equation 20 and explains the more gradual upswing as the breakthrough curve begins to appear in the Eagleton and Bliss model. This effect becomes negligible when the concentration of the adsorbate in the adsorbent becomes larger and exceeds the concentration of the adsorbate in the adsorbent at the point of discontinuity, C_D. Equation 21 is then applicable for describing the remainder of the breakthrough curve.

Both Equation 21, the Eagleton and Bliss model for $C > C_D$, and Equation 32, the Glueckauf and Coates model, have the same general form in that they relate the relative concentration of the effluent stream to 1.0 minus an exponential function with the cumulative weight of the effluent stream, W, as the independent variable. The Glueckauf and Coates model, the earlier derived, is the simpler insofar as the number of terms is concerned since it does not have any correction terms to more accurately describe the shape of the equilibrium isotherm and thus the driving forces. It was found that the correction terms, such as C_D and α for the Eagleton and Bliss model,

either do not improve the fit of the models to the data or make it much worse.

Figures 32 and 33 show the breakthrough curves for each adsorbate replacing the other for the mass flow rates used in this study and the particle size of the bed held constant. Figures 34 and 35 show the breakthrough curves for each adsorbate at a constant flow rate and the particle size of the bed varied. It is apparent from these plots that the slope of the breakthrough curve for each adsorbate increases as the mass flow rate and particle size decreases. This phenomena was predicted by Glueckauf and Coates (19). They stated that for the case of only one solute with a type A isotherm, there is more sharpening in the breakthrough curves as the particle size and flow rate are reduced. This occurrence almost seems obvious since for the case of the smaller particle and lower flow rate, equilibrium would be established quicker as there is less distance to travel into the particle and thus less resistance. In addition, the adsorbate molecules would not pass the solid particles as quickly and hence could be adsorbed easier. These two phenomena would tend to decrease the length of the adsorption zone and cause the slope of the breakthrough curve to be sharper as witnessed and predicted.

Comparison of the equilibrium isotherms, shown in Figures 18 and 19, for these two gases discloses that the equilibrium isotherm for propane is more concave toward the adsorbate concentration or pressure axis than the propylene equilibrium

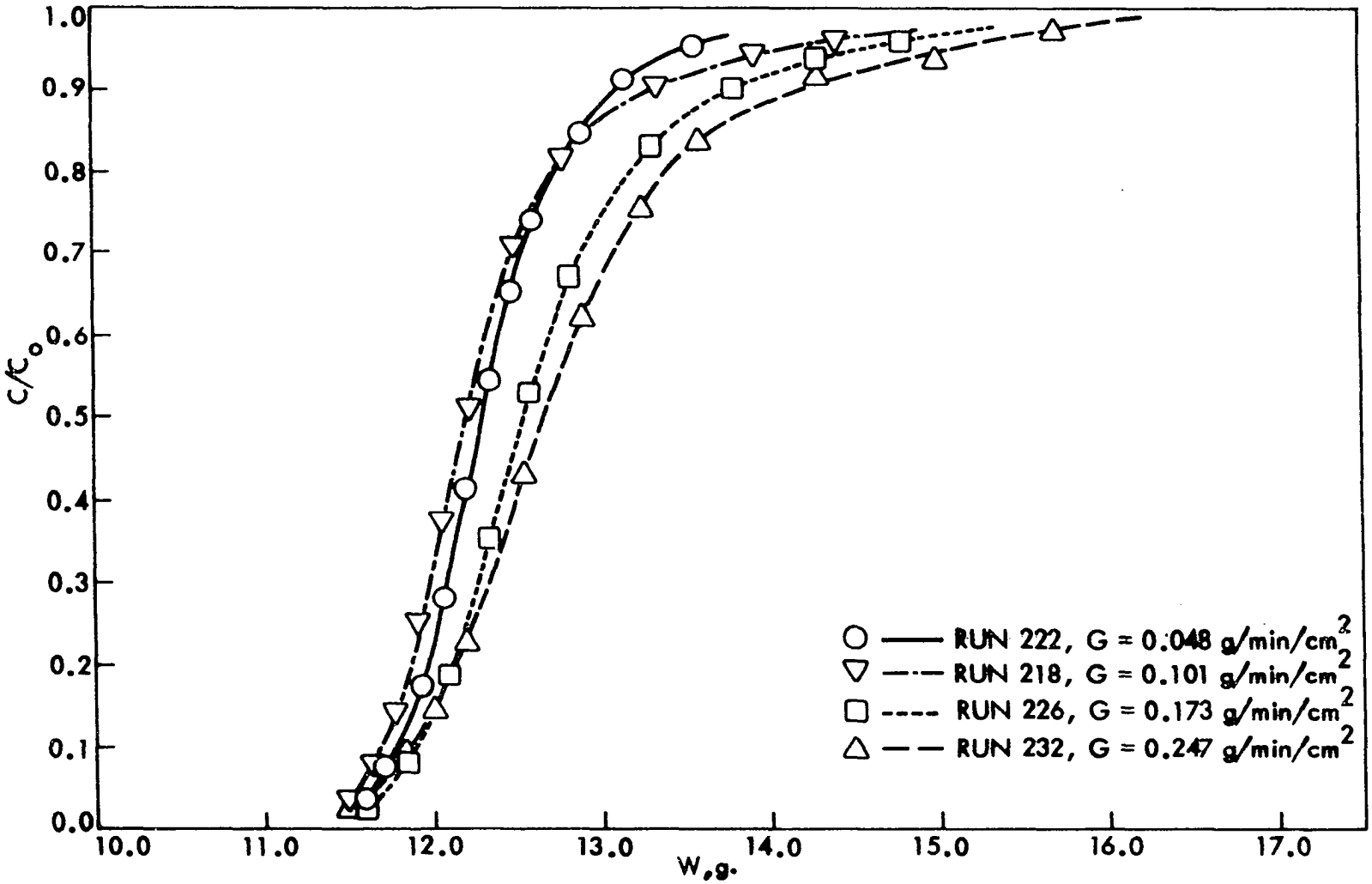

Figure 32. Comparison of breakthrough curves for propane replacing propylene on 25-30 mesh, U. S. Standard Sieve Series, Columbia LC 20/48, Grade H-63-11, activated carbon at various mass flow rates

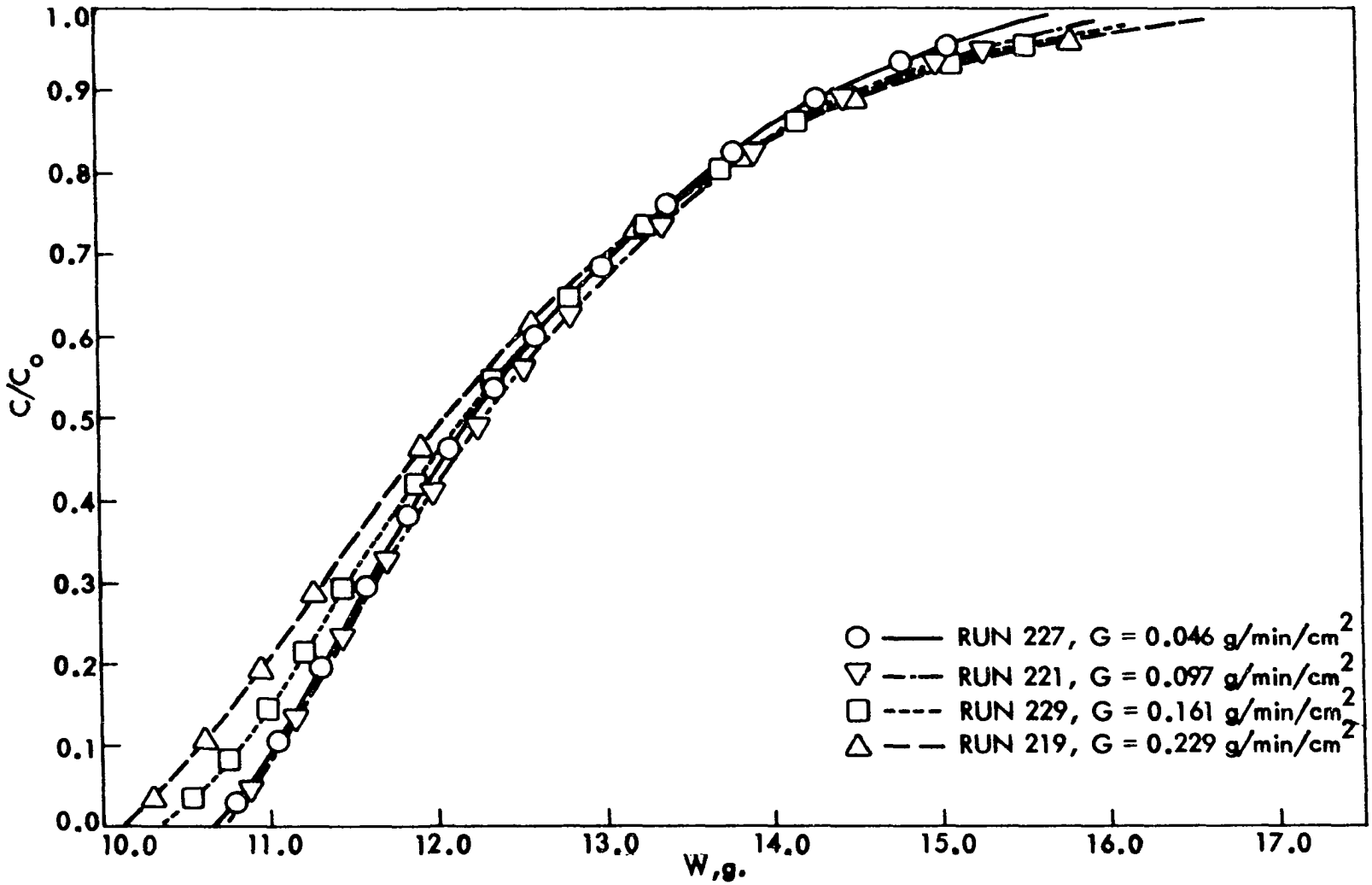

Figure 33. Comparison of breakthrough curves for propylene replacing propane on 25-30 mesh, U. S. Standard Sieve Series, Columbia LC 20/48, Grade H-63-11, activated carbon at various mass flow rates

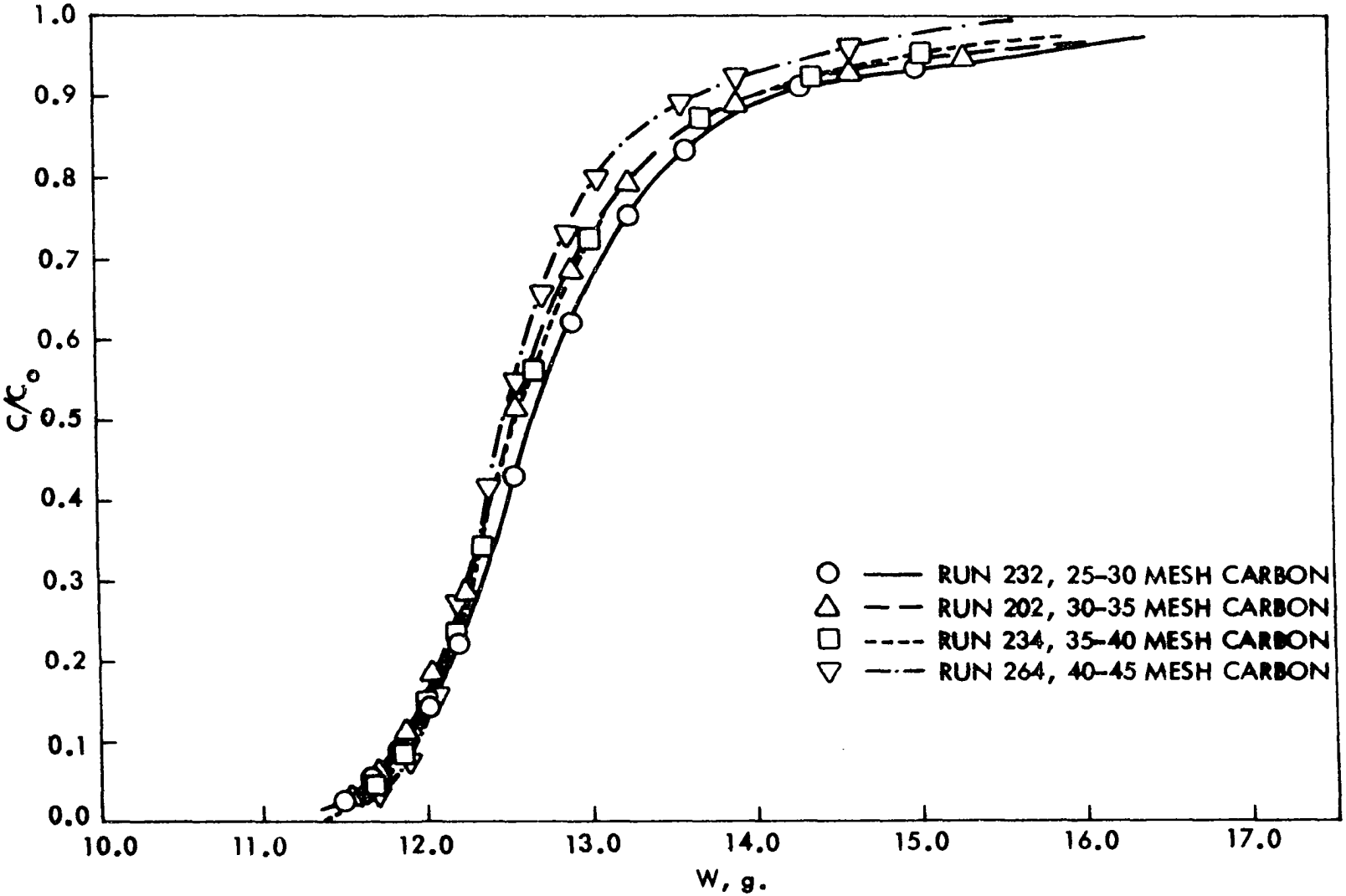

Figure 34. Comparison of breakthrough curves for propane replacing propylene on various particle sizes of Columbia LC 20/48, Grade H-63-11, activated carbon at a mass flow rate of 0.24 g/min/cm^2

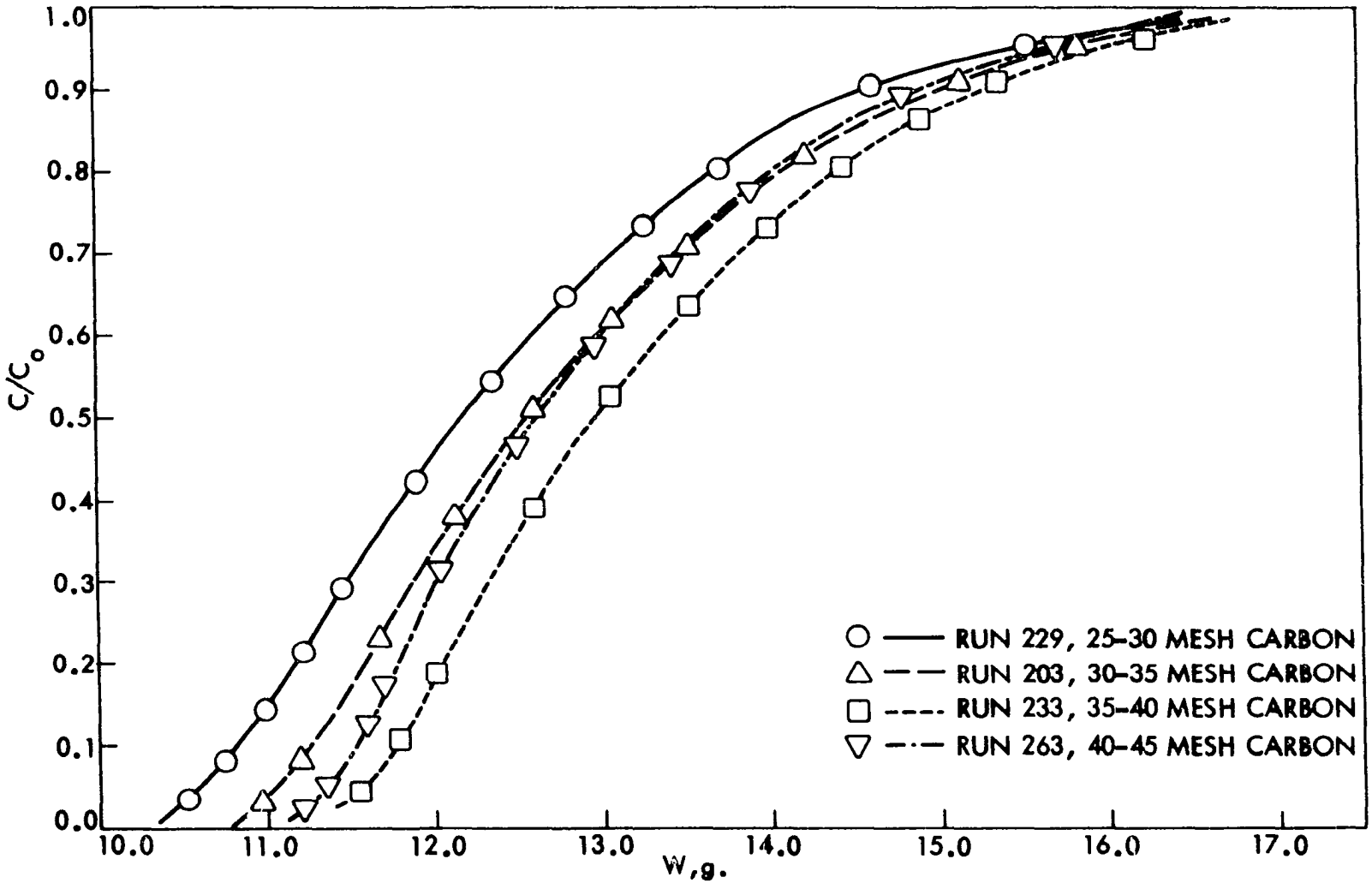

Figure 35. Comparison of breakthrough curves for propylene replacing propane on various particle sizes of Columbia LC 20/48, Grade E-63-11, activated carbon at a mass flow rate of 0.16 g/min/cm^2

isotherm. It is also noted that the heat of adsorption of propane is slightly higher than that of propylene. These observations indicate that propane is more strongly adsorbed on the surface of the carbon than propylene and thus the length of the adsorption zone in a fixed-bed would be shorter for the case where propane was the adsorbate. An examination of the breakthrough curves shown in Figures 32 through 35 reveals that the slopes of the curves for propane replacing propylene are always much steeper than when conditions of the run are identical except that propylene is the adsorbate. This confirms the expectation that the adsorption zone is shorter when propane is the adsorbate.

The shape of the experimental curves is in consonance with the hypothesis of deVault (11). He stated that for a system with only one solute present, and the isotherm is type A, the front boundary of the band will be sharp and will constantly tend to sharpen itself in spite of diffusion while the rear boundary will be broad and gradual.

Flow rate corrections

Due to an oversight on the part of the author concerning the effect of bed resistance on the volumetric flow rate, it was necessary to establish a correction between the pressure drop across the bed and the change in volumetric flow rate of the gas when the bed resistance was introduced into the system. Data were taken from three of the four volumetric

flow rates used in the actual adsorption runs. The fourth flow rate controlling orifice was broken prior to making these calibration runs. These runs were made at each of the particle sizes of the carbon used in this study. Table 8 gives the results of these runs and Figure 36 is a plot of this data. The slopes and intercepts shown on Figure 36 were determined using a method of least squares described in Draper and Smith (12).

Table 8. Pressure drop across adsorption bed versus change in flow rate when bed resistance is injected into gas flow stream for propane and propylene on Columbia LC 20/48, Grade H-63-11 activated carbon at 25° C

Adsorption bed particle size, U. S. Standard Sieve Series	Adsorbate	Pressure drop, mm H_2O	Change in volumetric flow rate, ml/min
25-30	Propane	4.0	33.90
25-30	Propane	10.5	71.14
25-30	Propane	22.5	122.41
25-30	Propylene	4.0	36.22
25-30	Propylene	12.0	75.25
25-30	Propylene	22.5	128.76
30-35	Propane	5.0	37.08
30-35	Propane	15.0	76.53
30-35	Propane	26.0	128.05
30-35	Propylene	5.5	37.47
30-35	Propylene	13.5	73.75
30-35	Propylene	25.5	122.89
35-40	Propane	6.0	34.85
35-40	Propane	19.5	71.24
35-40	Propane	32.5	127.16
35-40	Propylene	6.0	36.63
35-40	Propylene	17.5	76.69
35-40	Propylene	33.5	132.60
40-45	Propane	7.5	34.31
40-45	Propane	18.0	73.12
40-45	Propane	34.0	123.88
40-45	Propylene	7.5	36.31
40-45	Propylene	20.0	73.28
40-45	Propylene	35.0	130.68

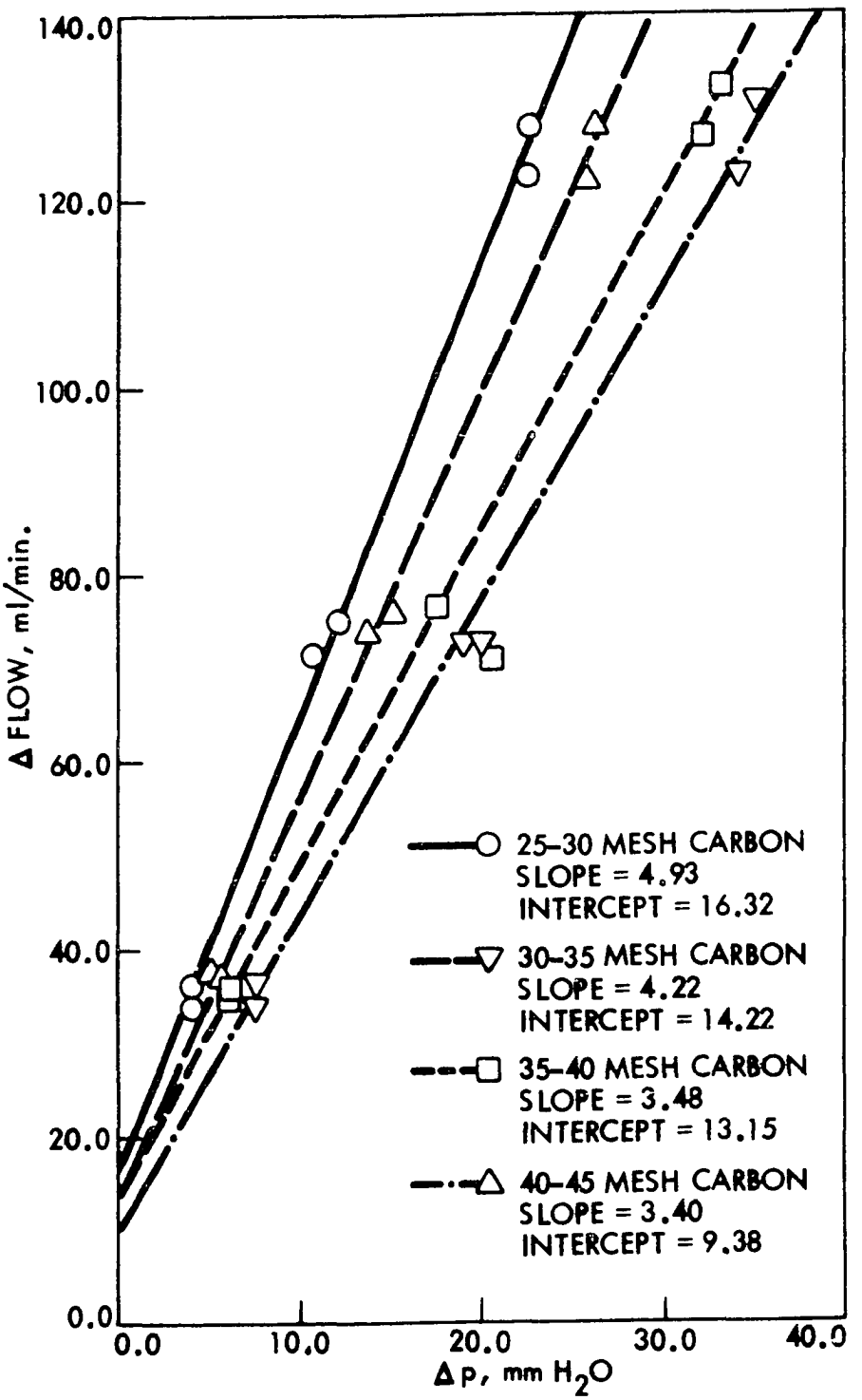

Figure 36. Flow rate correction for bed resistance versus bed pressure drop for propane and propylene flowing through Columbia LC 20/48, Grade H-63-11, activated carbon at 25° C

From the above data, the following general formula was derived to determine the flow rate correction to apply to each run based on the observed pressure drop for that run:

$$\Delta\text{flow} = \text{Intercept} + \text{Slope } X\Delta p \qquad (39)$$

This correction was subsequently subtracted from the observed unobstructed volumetric flow rate to establish a "corrected" volumetric flow rate for the run. It was found that this was an extremely sensitive correction as an error in the pressure drop reading of 0.5 mm H_2O had a significant effect on the "corrected" volumetric flow rate in some cases.

An examination of the pressure drop measurements revealed that several were in error. This was determined by the fact that one of the two readings could not possibly be the counterpart of the other since the amount of fluid in the manometer and the resulting possible manometer readings were known. In these runs, the calculated values of the cumulative flow rate of the effluent stream, W, did not appear to be correct as they did not compare favorably with other runs made under similar conditions or the predicted values from the models.

Mass transfer relationships

Figures 37 through 44 show the correlations found between the mass transfer coefficients, $k_g a_p$, $k_s a_p$, $K_g a_p$, $K_s a_p$, and the mass flow rate for both propane and propylene on Columbia LC 20/48, Grade H-63-11, activated carbon. These mass transfer

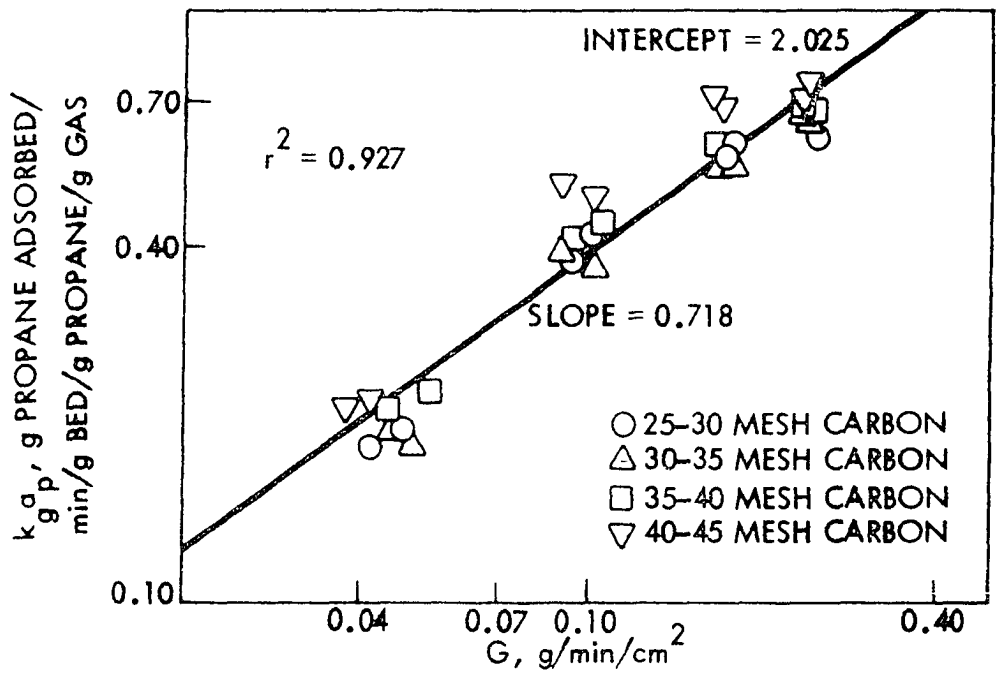

Figure 37. Gas phase mass transfer coefficient versus mass flow rate for propane on Columbia LC 20/48, Grade H-63-11, activated carbon at 25° C

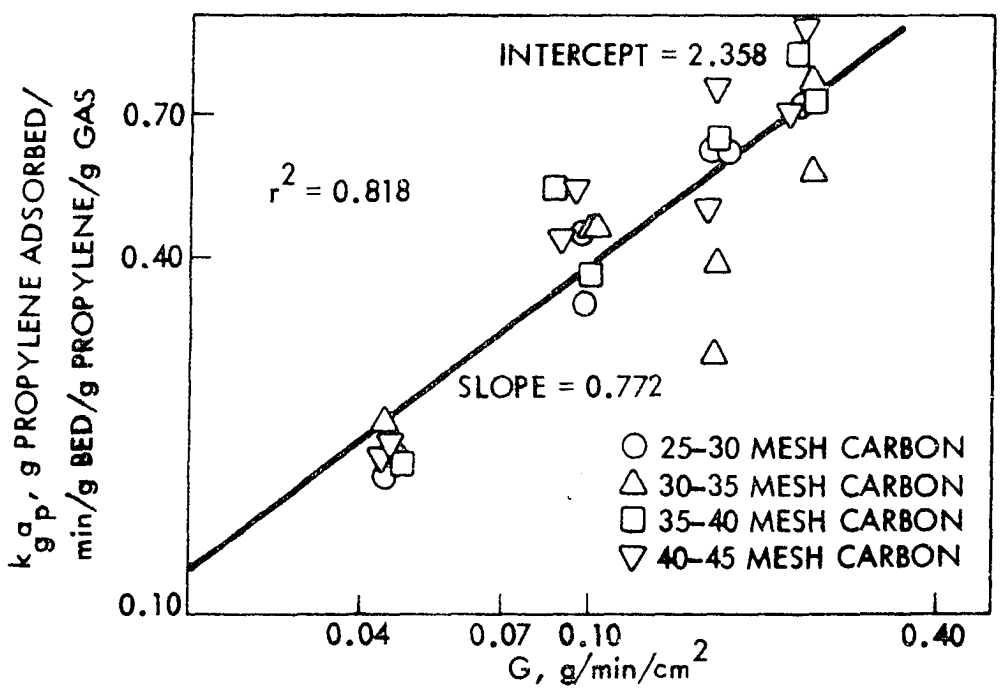

Figure 38. Gas phase mass transfer coefficient versus mass flow rate for propylene on Columbia LC 20/48, Grade H-63-11, activated carbon at 25° C

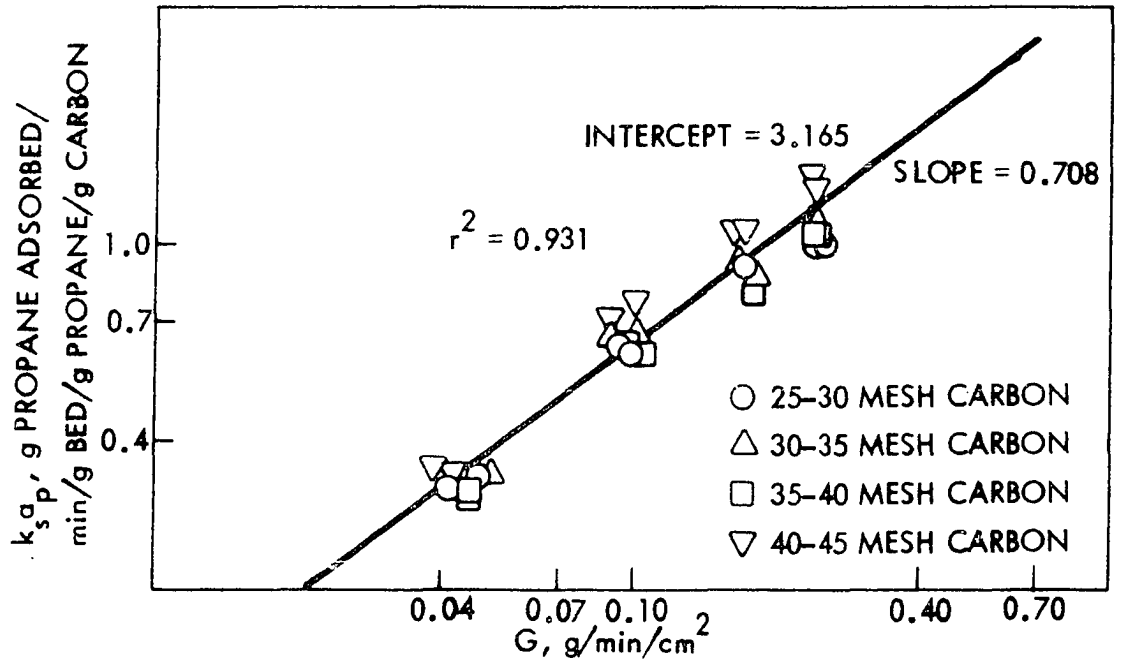

Figure 39. Solid phase mass transfer coefficient versus mass flow rate for propane on Columbia LC 20/48, Grade H-63-11, activated carbon at 25° C

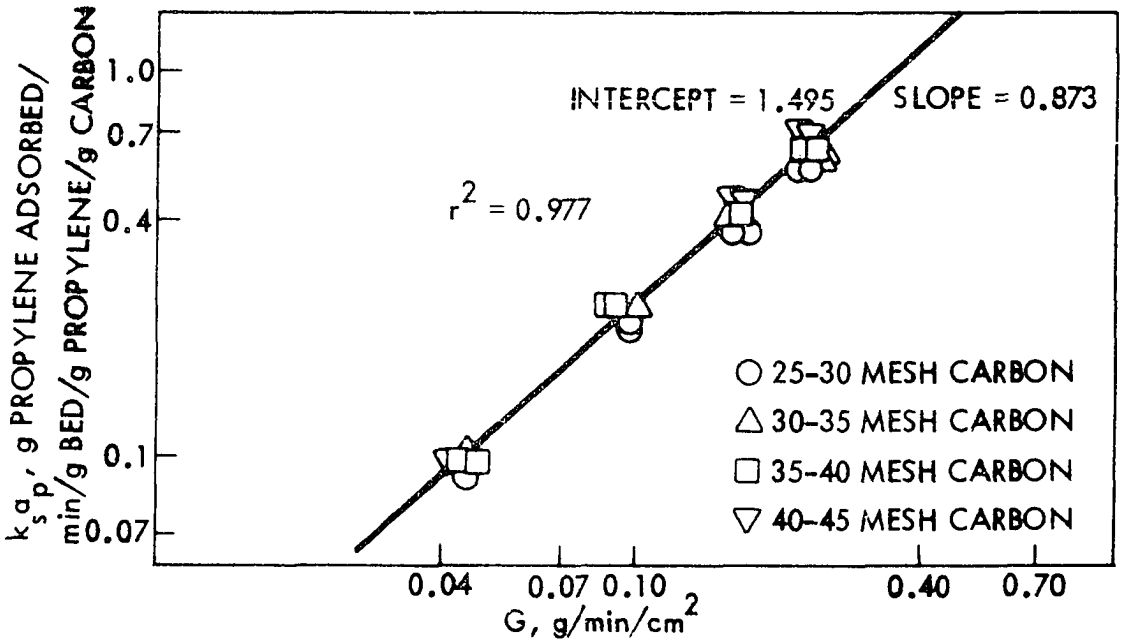

Figure 40. Solid phase mass transfer coefficient versus mass flow rate for propylene on Columbia LC 20/48, Grade H-63-11, activated carbon at 25° C

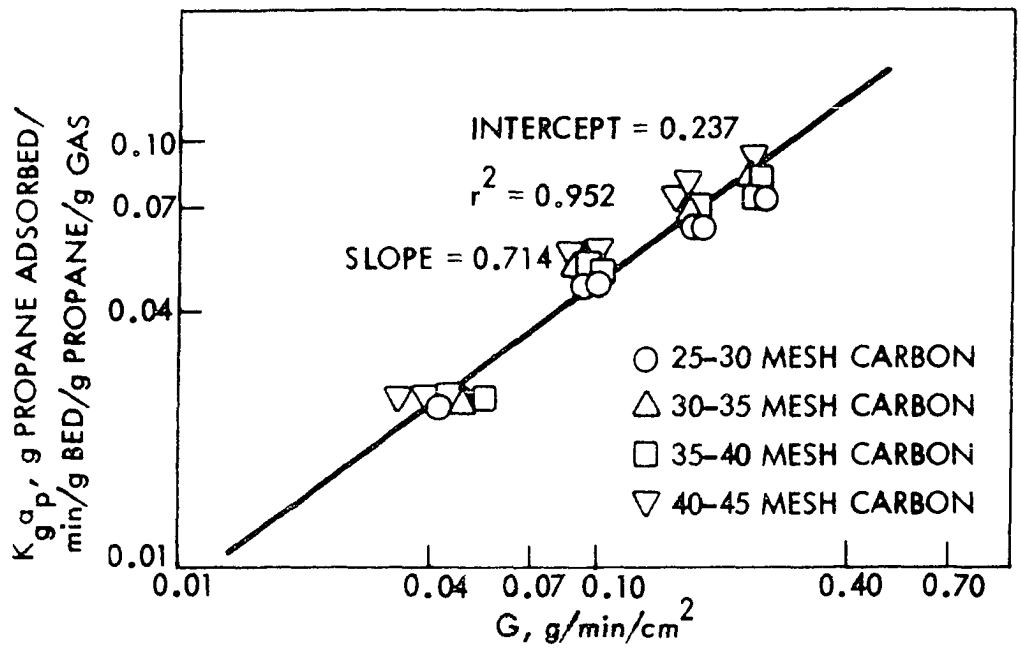

Figure 41. Overall gas phase mass transfer coefficient versus mass flow rate for propane on Columbia LC 20/48, Grade H-63-11, activated carbon at 25° C

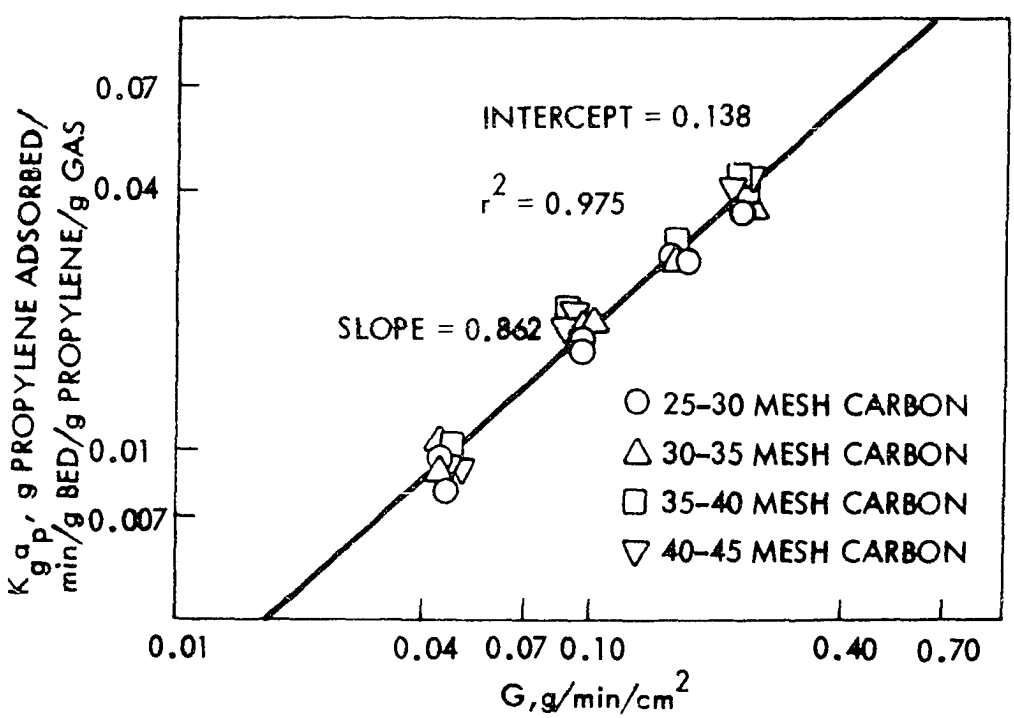

Figure 42. Overall gas phase mass transfer coefficient versus mass flow rate for propylene on Columbia LC 20/48, Grade H-63-11, activated carbon at 25° C

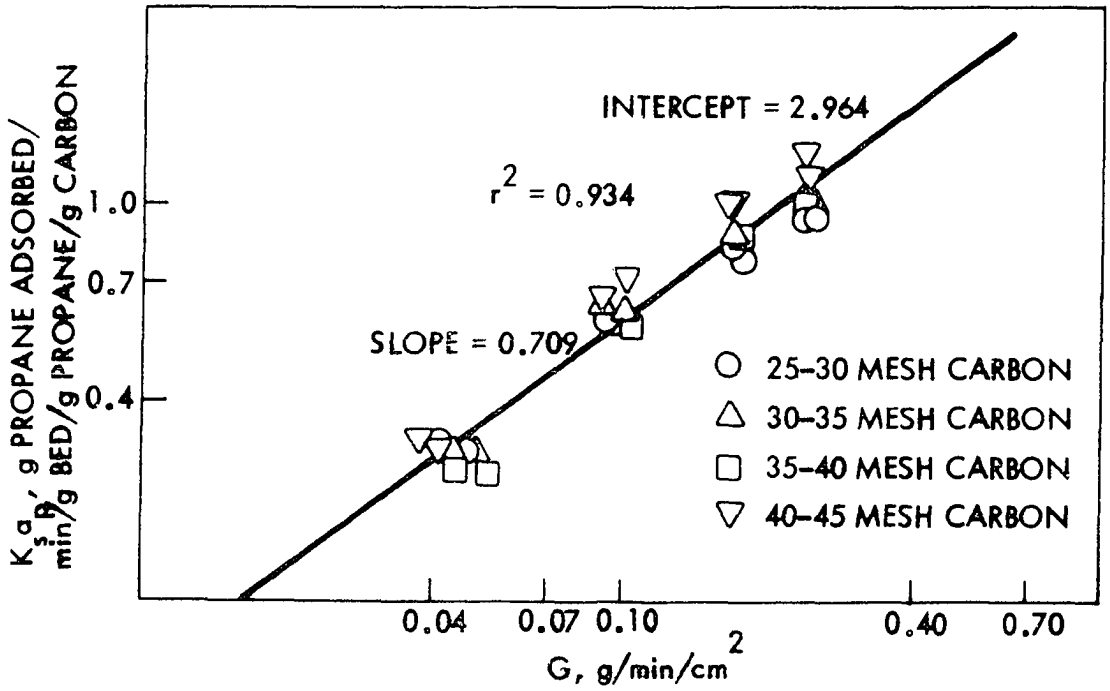

Figure 43. Overall solid phase mass transfer coefficient versus mass flow rate for propane on Columbia LC 20/48, Grade H-63-11, activated carbon at 25° C

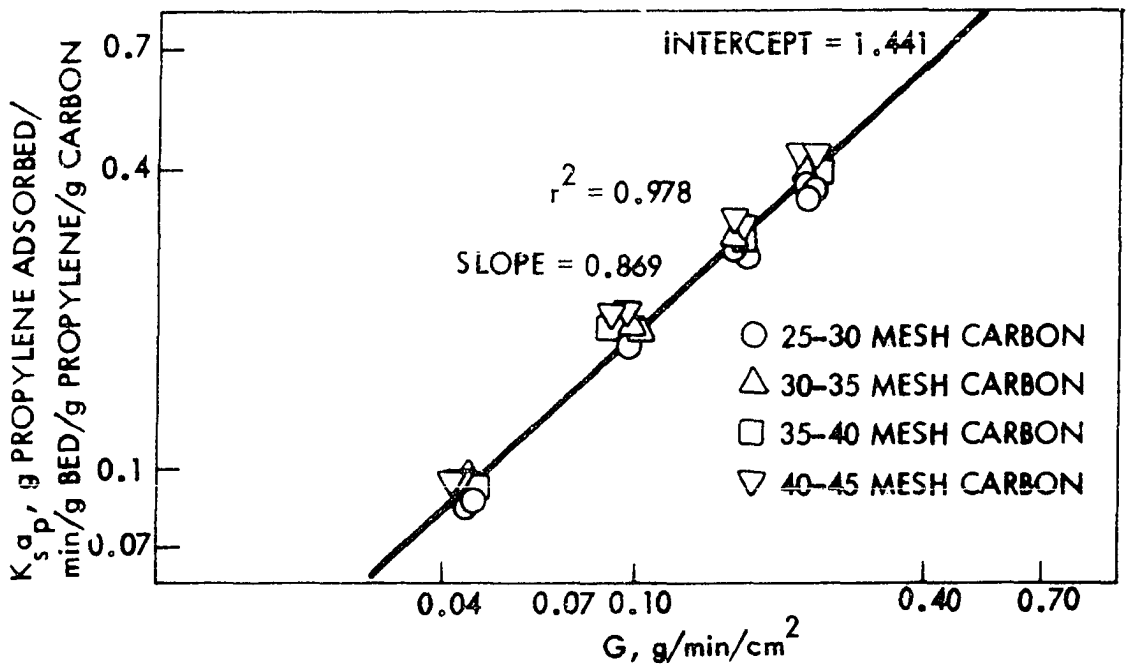

Figure 44. Overall solid phase mass transfer coefficient versus mass flow rate for propylene on Columbia LC 20/48, Grade H-63-11, activated carbon at 25° C

coefficients were determined independently of each other by methods shown in Appendix B.

It is noted that all correlations were found to be log-log relationships as determined by the highest value of the multiple correlation coefficient, r^2, and acceptable F values for lack of fit when a statistical analysis was conducted on the data as outlined in Draper and Smith (12). All of the log-log correlations were statistically significant within a 95% confidence level when the F test for lack of fit was applied. Each correlation was analyzed for fit in curvilinear, semilogarithmic, and log-log coordinates. From these plots, the following relationships were derived:

Propane:

$$k_g a_p = 2.025\ G^{0.718} \quad (40)$$

$$k_s a_p = 3.165\ G^{0.708} \quad (41)$$

$$K_g a_p = 0.237\ G^{0.714} \quad (42)$$

$$K_s a_p = 2.964\ G^{0.709} \quad (43)$$

Propylene:

$$k_g a_p = 2.358\ G^{0.772} \quad (44)$$

$$k_s a_p = 1.495\ G^{0.873} \quad (45)$$

$$K_g a_p = 0.138\ G^{0.862} \quad (46)$$

$$K_s a_p = 1.441\ G^{0.869} \quad (47)$$

It is noted that the gas phase mass transfer coefficients calculated increase as the mass flow rate increases which is consistent with theoretical predictions (39). The solid phase

mass transfer coefficients were also found to be directly proportional to mass flow rate.

Although other investigators (13, 19, 33, 39, 41) have calculated solid phase mass transfer coefficients from experimental breakthrough data, no general correlations were found. Many of the reported values for the solid phase mass transfer coefficient were calculated for systems operating at much higher flow rates than used in this study (13, 33). In these cases, there appeared to be no correlation between mass flow rate and the solid phase mass transfer coefficient. In this work, as indicated later by the direct linear relationship between pressure drop across the adsorption bed and flow rate, the flow rates used were in the very low laminar region, thus assuring plug flow through the adsorption bed. This suggests that a limiting value for the solid phase mass transfer coefficient had not been reached due to the very low flow rates used.

There are several other hypotheses (13, 39, 43) which attempt to explain the relationship between the solid phase mass transfer coefficients and the mass flow rate. Some possible explanations for the observed phenomena are:

1. An increase in mass flow rate would increase the concentration of the adsorbate at the surface of the adsorbent particle due to increased turbulence around the particle, thus increasing the adsorption rate and mass transfer coefficient.

2. An increase in mass flow rate would increase the pressure drop across a particle and thus increase the

superficial flow rate within the cracks and crevices which might act as pores of a nonhomogeneous particle at lower mass flow rates.

3. The use of solid phase mass transfer coefficients with an implied linear driving force is not strictly correct owing to the rigidity of each solid particle and the unsteady-state diffusional conditions existing within each particle.

4. In cases of moderately high transfer with extremely slow flow rates, the breakthrough curves may be broadened by eddy dispersion or molecular diffusion in the longitudinal direction. These phenomena would also be reflected in the solid phase mass transfer coefficient, and their effect would be reduced as mass flow rate is increased.

5. Since a solid phase mass transfer coefficient calculated from breakthrough data is an average for a wide range of driving forces, the calculated values would be functions of the system, including the mass flow rate which affects the steepness of the breakthrough curve as shown earlier. For a major part of the breakthrough curve the driving force is so large that it minimizes the effect of the solid phase mass transfer coefficient.

From the above discussion, it is believed that the calculated values of solid phase mass transfer coefficients would be better defined as "effective" solid phase mass transfer coefficients since they are functions of the systems for which they are calculated.

An analysis of the ratios of the gas and solid phase mass transfer coefficients to their respective overall mass transfer

coefficients indicates that solid phase diffusion is the apparent rate controlling mechanism by a value of nine to one. This supports the hypotheses of the two models which best fit the experimental data regarding the rate controlling mechanism.

Diffusivities

The calculated values of the particle diffusivities as defined by Glueckauf and Coates (19) are given in Appendix A. Figures 45 and 46 show these values plotted against the mass flow rate. It is noted that the values appear to be functions of particle size as well as mass flow rate.

Since diffusivity is normally considered to be a property of a given system, these results are somewhat surprising. A review of the definition of particle diffusivity, D_p, and its relationship to the solid phase mass transfer coefficient (19, 42) leads one to suspect that this is not a true diffusivity, but an "effective" diffusivity, since it appears to be "structure sensitive" (39). This structure sensitivity might be explained by the following hypothesis: an increase in the available surface area within the bed as particle size is increased would in some instances decrease the length of travel within an adsorbent particle. In addition, mass flow rate would affect the particle diffusivity in the same manner as it does the solid phase mass transfer coefficient since both are descriptions of the "effective" resistance to diffusion. This would cause the particle diffusivity to increase with mass flow rate. Thus the "effective" particle diffusivity would be a direct function of the solid phase mass transfer

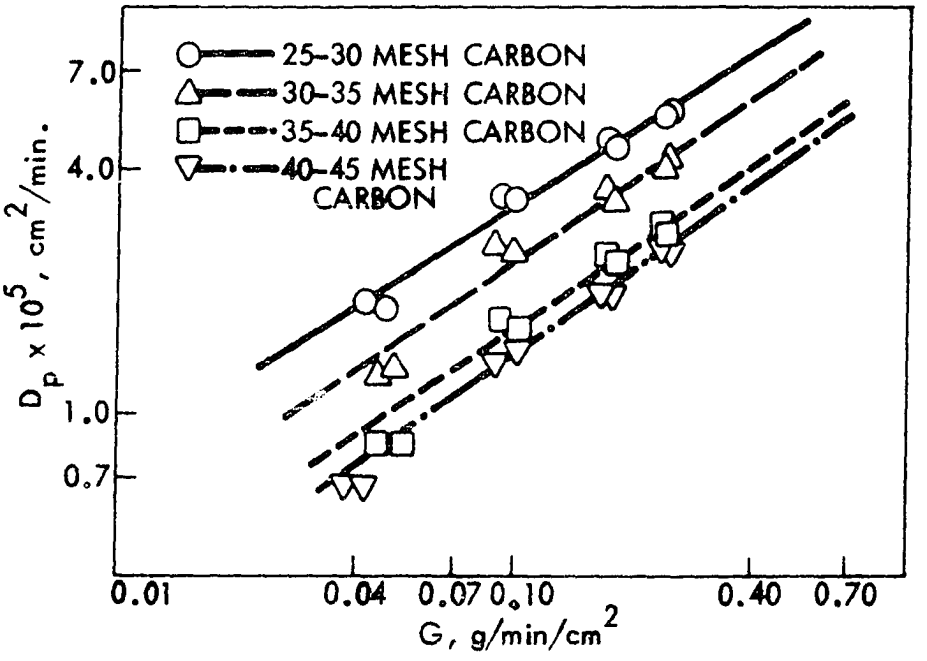

Figure 45. "Effective" particle diffusivities versus mass flow rate for propane on Columbia LC 20/48, Grade H-63-11, activated carbon at 25° C

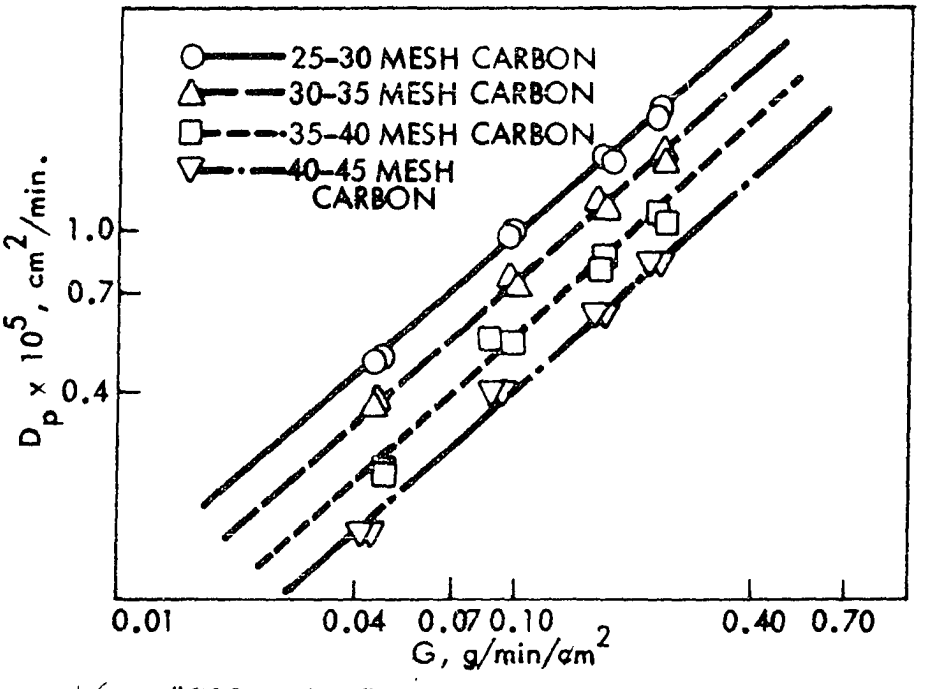

Figure 46. "Effective" particle diffusivities versus mass flow rate for propylene on Columbia LC 20/48, Grade H-63-11, activated carbon at 25° C

coefficient and the particle size which is in consonance with its definition (19).

The calculated values of particle diffusivity of propylene replacing propane compare well in magnitude with the values reported by v. Szirmay (41) for ethylene replacing ethane. However, the values of the particle diffusivity for ethane replacing ethylene are two orders of magnitude greater than those found for propane replacing propylene. It was noted, however, that v. Szirmay's values for particle diffusivity for ethane replacing ethylene did not appear to hold to any correlation as flow rate was increased while the values for the case of ethylene replacing ethane had a similar correlation as for propylene replacing propane. Similar flow rates were used in both studies.

Concentration at discontinuity

Figures 47 and 48 show the values of the concentration of the adsorbate at the point of discontinuity, C_D, plotted versus mass flow rate. No direct correlation was found. The values did appear to fall within a general range which was different for each gas replacing the other. Average values of 0.2491 for propane replacing propylene and 0.939 for propylene replacing propane were found.

The above findings are substantiated by the higher ratio of the gas phase to solid phase mass transfer coefficients for propylene replacing propane as C_D is defined as the value at

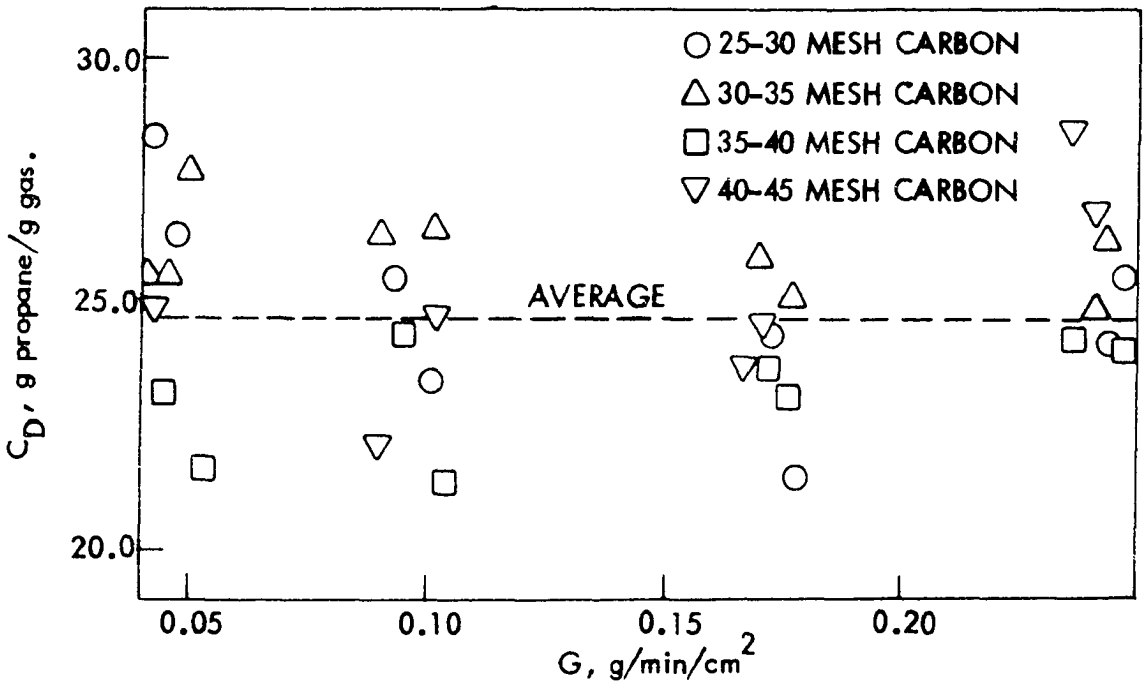

Figure 47. Concentration at discontinuity versus mass flow rate for propane on Columbia LC 20/48, Grade H-63-11, activated carbon at 25° C

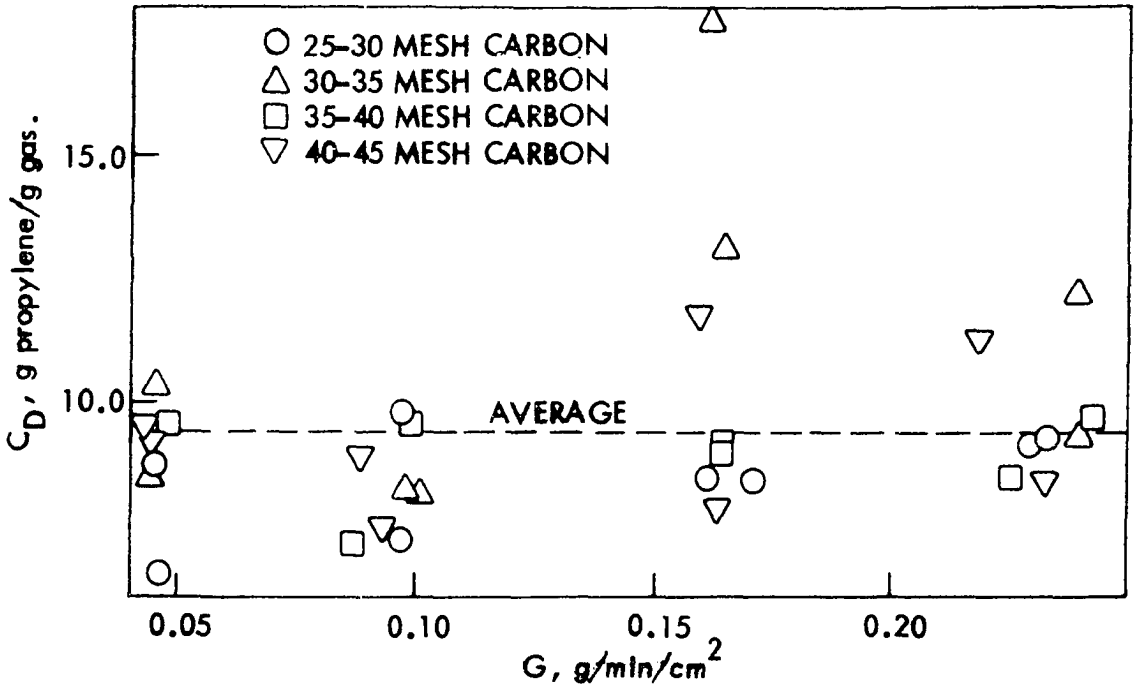

Figure 48. Concentration at discontinuity versus mass flow rate for propylene on Columbia LC 20/48, Grade H-63-11, activated carbon at 25° C

which a line with a slope of $-k_g a_p/k_s a_p$ and intercept inter-sects a linear operating line between the origin and the point of bed operation on the equilibrium isotherm. Thus, the higher the $k_g a_p/k_s a_p$ ratio, the greater the slope and the lower the value of C_D.

Pressure drop

Figure 49 shows the relationship between pressure drop across the bed and uncorrected volumetric flow rate. As expected, this plot shows that pressure drop increases with an increase in flow rate and a decrease in particle size since with smaller particles, there is less void space in the bed.

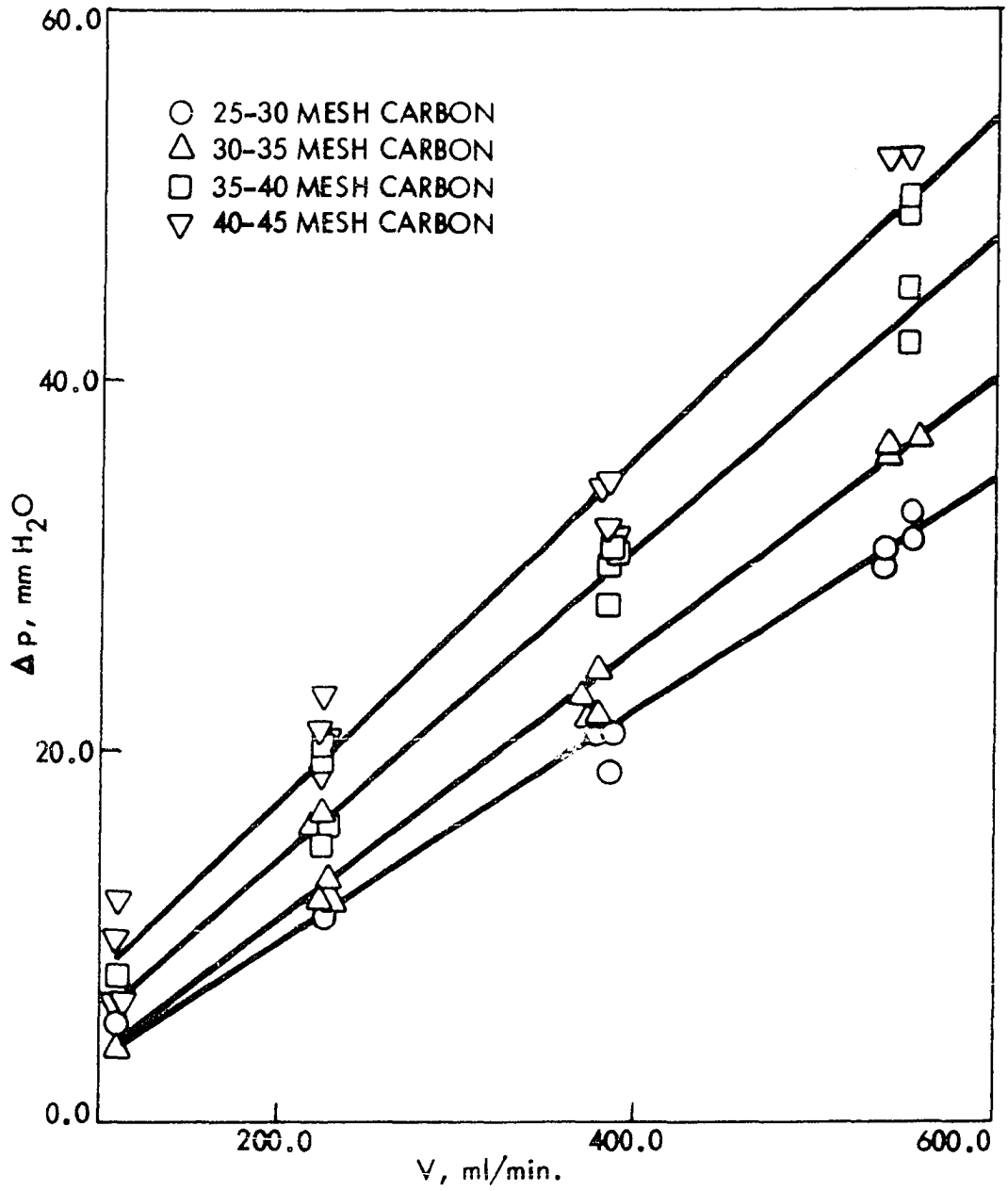

Figure 49. Volumetric flow rate versus pressure drop across adsorption bed

CONCLUSIONS

The following conclusions have been reached as a result of this research:

1. Essentially, isothermal adsorption may be obtained by selecting a gas-pair which has nearly equal heats of adsorption.

2. The resulting breakthrough curves for isothermal exchange adsorption may be predicted by appropriate mathematical models.

3. For the gas-pair propane and propylene, the Glueckauf and Coates model (19) and the Eagleton and Bliss model (13) fit the data. From the assumptions of these models and ratios of calculated mass transfer coefficients, the rate controlling mechanism for the exchange adsorption between the gas-pair propane and propylene is particle diffusion.

4. The Glueckauf and Coates model (19) which assumes a linear driving force, adequately describes the change in concentration of the adsorbate on the adsorbent with respect to time for the case of exchange adsorption between propane and propylene on Columbia LC 20/48, Grade H-63-11, activated carbon.

5. A log-log correlation exists between the mass flow rate of the gas stream and the gas and solid mass transfer coefficients and the overall gas and solid phase mass transfer coefficients.

6. The gas and solid phase mass transfer coefficients and the overall gas and solid phase mass transfer coefficients

increase as the mass flow rate increases.

7. The calculated particle diffusivities increase with mass flow rate and adsorbent particle size.

8. Since the calculated particle diffusivities are functions of mass flow rate and particle size, they are not properties of the system but are "effective" particle diffusivities since they appear to be "structure sensitive."

9. The length of the adsorption zone decreases as the mass flow rate and carbon particle size increase. This phenomena is in consonance with the theory of Glueckauf and Coates (19).

10. The concentration at discontinuity as defined by Eagleton and Bliss (13) is characteristic of the adsorbate-adsorbent system and appears not to be a function of the flow rate or adsorbent particle size.

11. At low flow rates, there is a linear relationship between the pressure drop across the adsorption bed and the mass flow rate. The slope of this relationship depends upon the bed particle size and increases as the particle size increases.

12. The more concave the equilibrium isotherms are toward the adsorbate concentration axis, the steeper or sharper the slope of the breakthrough curve for the case of exchange adsorption as well as normal binary adsorption.

13. Equilibrium isotherms representing adsorption of propane and propylene on activated carbon vary from carbon to

carbon and method of activation.

14. The shape of the equilibrium isotherms for propane and propylene on Columbia LC 20/48, Grade H-63-11, activated carbon represent monomolecular layer adsorption for the range of the isotherm determined.

15. The B.E.T. equation predicts the shape of the equilibrium isotherm at 25° C for propane and propylene on Columbia LC 20/48, Grade H-63-11, activated carbon up to 760 mm Hg better than other models tested.

16. A linear relationship exists between the temperature rise in the bed during the adsorption process and the mole fraction of the adsorbate in an inert helium gas carrier stream at constant flow rate.

17. Heat of adsorption data may be used to reasonably predict the temperature increase or decrease in the adsorption zone as exchange adsorption takes place.

18. Isothermal conditions in an adsorption bed may be approximated when the concentration of the adsorbate in an inert carrier gas stream is sufficiently dilute.

RECOMMENDATIONS

The following recommendations are made to serve as a guide for further research in the field of adsorption:

1. Further studies should be conducted to examine the relationship between bed temperature rise due to heat of adsorption and concentration of the adsorbate in an inert carrier gas stream, bed diameter, mass flow rate, and adsorbent particle size.

2. An investigation should be made into the feasibility of removing heat generated within an adsorption bed during the adsorption process for use as an energy source for the desorption process.

3. Additional breakthrough data should be obtained for other gas-pairs with similar heats of adsorption but with other types of equilibrium isotherms in order to determine the applicability of other isothermal breakthrough models to this process.

4. The effects of diluting the adsorbate in some inert carrier gas on the shape and predictability of breakthrough curves should be studied.

5. An investigation should be made into the actual effect of the mass transfer coefficients and diffusivities over the range of the breakthrough curve.

NOMENCLATURE

A	empirical constant.
A_x	bed cross-sectional area, cm^2.
a	correction factor accounting for linearity deviation when diffusional resistances are added.
B	temperature dependent constant characteristic of the adsorbent.
b	empirical constant.
C	effluent stream concentration of the adsorbate at time t, g adsorbate/g carrier gas.
C_B	effluent stream concentration of the adsorbate at the breakpoint, g adsorbate/g carrier gas.
C_D	gas stream concentration of adsorbate at point of discontinuity, g adsorbate/g carrier gas.
C_o	influent stream concentration of adsorbate, g adsorbate/g carrier gas.
C^*	gas stream concentration of the adsorbate in equilibrium with X^*, g adsorbate/g carrier gas.
D	diffusivity, cm^2/min.
D_p	particle phase diffusivity, cm^2/min.
d_p	arithmetic mean particle diameter, cm.
F	thermodynamic property free energy, cal/g-mole.
f	fractional ability of adsorbent in the adsorption zone to still adsorb the adsorbate.

G	mass flow rate of gas stream per cross-sectional area of bed, $g/min/cm^2$.
G'	mass flow rate of gas stream, g/min.
$-\Delta H$	differential heat of adsorption, cal/g-mole.
K, K_g, K_s	overall mass transfer coefficient, min^{-1} (subscripts g and s refer to gas phase and solid phase respectively).
k, k_1, k_2, k_3, k''	empirical constants.
k_g	gas film mass transfer coefficient, $g/min\text{-}cm^2$.
k_s	solid phase mass transfer coefficient, $g/min\text{-}cm^2$.
M	molecular weight.
m	slope of the adsorption isotherm at influent stream conditions.
N, N_g, N_s	number of transfer units (subscripts s and g refer to gas phase and solid phase respectively) (see Equation 28).
N_R	number of apparent reaction units (see Equation 28).
n	integer.
n'	empirical constant with a value greater than unity.
p	adsorbate vapor pressure, mm Hg.
p_s	saturation vapor pressure at temperature T, mm Hg.
Q	integral heat of adsorption, cal/g-mole.
r	radius, cm.
r^2	multiple correlation coefficient.
r_c	capillary radius, cm.

r^* equilibrium parameter, (see Equation 29).

S thermodynamic property entropy, cal/g-mole.

T absolute temperature.

t time, min.

t_B time of appearance of the breakpoint, min.

t_D time of delay between bed exit and thermal conductivity cell, min.

t_E time of appearance of bed exhaustion point, min.

U quantity of adsorbate removed in the adsorption zone from the breakpoint to the time of bed exhaustion, g.

V molar volume of adsorbate, cm^3/g-mole.

V_f volumetric flow rate, ml/min.

v fixed-bed volume, cm^3.

W cumulative pure solvent passed up to time t, g.

W_S weight of adsorbent in bed, g.

X adsorbate content of adsorbent at time t, g adsorbate/g adsorbent.

X_i adsorbate content of adsorbent at external surface of adsorbent particle or interface, g adsorbate/g adsorbent.

X_m monolayer capacity of adsorbent, g adsorbate/g adsorbent.

X^* adsorbate content of adsorbent in equilibrium with C^*, g adsorbate/g adsorbent.

X_o^*	adsorbate content of adsorbent in equilibrium with C_o, g adsorbate/g adsorbent.
Y_A	mole fraction of adsorbate.
$YA_{C_3H_6}$	actual mole fraction propylene.
$YI_{C_3H_6}$	indicated mole fraction propylene.
Z	height of fixed-bed, cm.
Z_a	height of adsorption zone, cm.
	intercept value of X^* for linear isotherm approximation, g adsorbate/g adsorbent.
β_i	adsorption potential at a point where the density of the adsorbed substance is ρ_i, g.
ϵ	void fraction of fixed-bed.
θ	contact angle.
ρ_b	bulk packed density of fixed-bed, g/cm^3.
ρ_f	density of the influent stream, g/cm^3.
ρ_g	density of the adsorbate, g/cm^3.
ρ_i	density of the adsorbed substance when the adsorption potential is β_i, g/cm^3.
ρ_x	density of the gas phase, g/cm^3.
σ	surface tension of the condensed vapor, g/min^2.
ψ	constant.

LITERATURE CITED

1. Barrer, R. M. Diffusion in and through solids. Cambridge, England, University Press. 1941.

2. Barry, H. M. Fixed-bed adsorption. Chemical Engineering 67, No. 3: 105-120. 1960.

3. Boyd, G. E., Meyers, L. S., Jr. and Adamson, A. W. The exchange adsorption of ions from aqueous solutions by organic zeolites. II. American Chemical Society Journal 69: 2836-2858. 1947.

4. Brunauer, S. The adsorption of gases and vapors. Vol. 1. Princeton, New Jersey, Princeton University Press. 1943.

5. Brunauer, S., Deming, L. S., Deming, W. E. and Teller, E. On a theory of the van der Waals adsorption of gases. Chemical Society Journal 62: 1723-1732. 1940.

6. Brunauer, S., Emmett, P. H. and Teller, E. Adsorption of gases in multimolecular layers. American Chemical Society Journal 60: 309-319. 1938.

7. Cahn, R. G. Automatic electrobalance instruction manual. Paramount, California, Cahn Instrument Company. ca. 1964.

8. Cohan, L. H. Sorption hysteresis and the vapor pressure of concave surfaces. American Chemical Society Journal 60: 433-435. 1938.

9. deBoer, J. H. The dynamical character of adsorption. 2nd ed. Oxford, England, The Clarendon Press. 1968.

10. de Saussure, N. T. Observations l'absorption des gaz par differents corps. Gilbert's Annalen der Physik 47: 113-183. 1814. Original not available: cited in McBain, J. W. The sorption of gases and vapours by solids. P. 2. London, England, George Routledge and Sons, Ltd. 1932.

11. deVault, D. Theory of chromatography. American Chemical Society Journal 65: 532-540. 1943.

12. Draper, N. R. and Smith, H. Applied regression analysis. New York, New York, John Wiley and Sons, Inc. 1966.

13. Eagleton, L. C. and Bliss, H. Drying of air in fixed beds. Chemical Engineering Progress 49: 543-548. 1953.

14. Eucken, A. Theory of adsorption (translated title). Verhandlungen der Deutschen physikalischen Gesellschaft 16: 345-362. 1914. Original not available: abstracted in Chemical Abstracts 8: 3390. 1914.

15. Foster, A. G. Low pressure isothermals and heats of sorption. Chemical Society (London) Journal 147: 360-366. 1945.

16. Freundlich, H. Colloid and capillary chemistry. London, England, Methuen and Co., Ltd. 1926.

17. Frost, R. R. Evaluation of surface areas from chromatographic and gravimetric adsorption data. Unpublished Ph.D. thesis. Ames, Iowa, Library, Iowa State University. 1968.

18. Glueckauf, E. Theory of chromatography. II. Chromatographs of a single solute. Chemical Society (London) Journal 149: 1302-1308. 1947.

19. Glueckauf, E. and Coates, J. Theory of chromatography. IV. The influence of incomplete equilibrium on the front boundary of chromatograms and on the effectiveness of separation. Chemical Society (London) Journal 149: 1315-1321. 1947.

20. Graham, D. Adsorption equilibria. Chemical Engineering Progress Symposium Series 55, No. 24: 17-23. 1959.

21. Hanson, T. P. Diffusion coefficient measurements for the water vapor-corn starch granule system. Unpublished M.S. thesis. Ames, Iowa, Library, Iowa State University. 1967.

22. Jain, L. K., Gehrhardt, H. M. and Kyle, B. G. Liquid phase adsorption equilibria with molecular sieve adsorbent. Journal of Chemical and Engineering Data 10, No. 2: 202-204. 1965.

23. Langmuir, I. Adsorption of gases on plane surfaces of glass mica, and platinum. American Chemical Society Journal 40: 1361-1403. 1918.

24. Leavit, F. W. Non-isothermal adsorption in large fixed-beds. Chemical Engineering Progress 58, No. 8: 54-59. 1962.

25. Lewis, W. K., Gilliland, E. R., Chertow, B., and Cadogan, W. P. Pure gas isotherms. Industrial and Engineering Chemistry 42, No. 7: 1326-1332. 1950.

26. Magnus, A. Theory of gas adsorption (translated title). Zeitschrift für physikalische Chemie 142,A: 401-430. 1929. Original available but not translated; abstracted in Chemical Abstracts 23: 5379. 1929.

27. Mantell, C. L. Adsorption. New York, New York, McGraw-Hill Book Co., Inc. 1951.

28. McGavack, J. and Patrick, W. A. The adsorption of sulfur dioxide by the gel of silicic acid. American Chemical Society Journal 42: 946-978. 1920.

29. Michaels, A. S. Simplified method of interpreting kinetic data in fixed-bed ion exchange. Industrial and Engineering Chemistry 44: 1922-1928. 1952.

30. Monet, G. P. and Vermeulen, T. Progress in separation by sorption operations - adsorption, dialysis, and ion exchange. Chemical Engineering Progress Symposium Series 55, No. 25: 109-133. 1959.

31. Needham, R. B., Campbell, J. M. and McLeod, H. O. Critical evaluation of mathematical models used for dynamic adsorption of hydrocarbons. Industrial and Engineering Chemistry-Process Design and Development 5, No. 2: 122-128. 1966.

32. Norman, R. L. Propylene-propane adsorption in a packed silica gel adsorption bed. Microfilm copy No. 63-0414. Unpublished Ph.D. thesis. Ann Arbor, Michigan, Library, University of Michigan. Ann Arbor, Michigan, University Microfilms. 1962.

33. Nutter, J. I. Drying of air by fixed bed adsorption using molecular sieves. Unpublished Ph.D. thesis. Ames, Iowa, Library, Iowa State University. 1964.

34. Polanyi, M. Neueres über adsorption und ursache der adsorptionskräfte. Zeitschrift fur Elektrochemie [illegible]: 370-374. 1920. Original available but not translated; abstracted in Chemical Abstracts 14: 3557. 1920.

35. Polanyi, M. Adsorption from the point of view of the third law of thermodynamics (translated title). Verhandlungen der Deutschen physikalischen Gesellschaft 16: 1012-1016. 1914. Original not available; abstracted in Chemical Abstracts 9: 1870. 1915.

36. Selke, W. A. and Bliss, R. H. Application of ion exchange. Chemical Engineering Progress 46: 509-516. 1950.

37. Sillén, L. G. and Ekedahl, E. On filtration through a sorbent layer. Arkiv för kemi, minealogi och geologi 22 A, No. 16: 1-12. 1946.

38. Thomas, H. C. Heterogeneous ion exchange in a flowing system. American Chemical Society Journal 66: 1664-1666. 1944.

39. Treybal, R. E. Mass transfer operations. 2nd ed. New York, New York, McGraw-Hill Book Co., Inc. 1968.

40. Tsederberg, N. V. Thermal conductivity of gases and liquids. Cambridge, Massachusetts, The M. I. T. Press. 1965.

41. v. Szirmay, L. Adsorption transient correlations and relative diffusivities from ethane-ethylene adsorption measurements on activated carbon. Unpublished Ph.D. thesis. Denver, Colorado, Library, University of Denver. 1969.

42. Vermeulen, T. Separation by adsorption methods. Advances in Chemical Engineering 2: 147-208. 1956.

43. Vermeulen, T. and Hiester, N. K. Kinetic relationships for ion exchange processes. Chemical Engineering Progress Symposium Series 55, No. 24: 61-69. 1959.

44. Zsigmondy, A. Über die Struktur des Gels der Kieselsaure Theorie der Entwasserung. Zeitschrift fur anorganische und allgemeine chemie 71: 356-377. 1911.

ACKNOWLEDGMENTS

The author wishes to express his appreciation to the following people without whose help this work would not have been possible:

To Dr. George Burnet for establishing the project and devoting much time, advice, and encouragement during the investigation.

To the members of the faculty of the Department of Chemical Engineering for their many useful suggestions and advice during my three years at Iowa State University.

To my wife, Patricia, for her continued interest, encouragement, and support throughout our tenure at Iowa State University.

APPENDIX A - BREAKTHROUGH DATA AND CALCULATED PARAMETERS

The following raw data, time and concentration of the effluent stream, were extracted from a continuous recorder plot of the output signal from the thermal conductivity cell shown in Figure 8. The values of C/C_o and W were obtained from Equations 36, 37, and 15 respectively.

The calculated parameters for each run were obtained by the methods given in Appendix B.

Listed alphabetically below is the nomenclature used to describe the calculated parameters:

BIG KGAP — Overall gas phase mass transfer coefficient times the effective mass transfer area, $K_g a_p$.

BIG KSAP — Overall solid phase mass transfer coefficient times the effective mass transfer area, $K_s a_p$.

C — Uncorrected concentration of the adsorbate in the effluent stream.

C/CO — Corrected relative concentration of the adsorbate in the effluent stream.

CD — Concentration at discontinuity, C_D.

KGAP — Gas phase mass transfer coefficient times the effective mass transfer area, $k_g a_p$.

KSAP — Solid phase mass transfer coefficient times the effective mass transfer area, $k_s a_p$.

RUN NUMBER 201

ADSORBATE - PROPYLENE
CARBON PARTICLE SIZE - 30-35 MESH US STD. SIEVE
BED WEIGHT - 49.55 G CARBON
UNCORRECTED VOL. FLOW RATE - 370.6599 ML/MIN
PRESSURE DROP - 23.0 MM H2O
MASS FLOW RATE - 0.1611 G/MIN-CM2
KGAP - 0.2814 G C3H6/MIN-G BED-G C3H6/G GAS
KSAP - 0.3190 G C3H6/MIN-G BED-G C3H6/G SOLID
BIG KGAP - 0.0264 G C3H6/MIN-G BED-G C3H6/G GAS
BIG KSAP - 0.2994 G C3H6/MIN-G BED-G C3H6/G SOLID
EFFECTIVE PARTICLE DIFFUSIVITY - 1.16 X 10-5 CM2/MIN
CO - 0.1791 G C3H6/G GAS

POINT	TIME, MIN.	C	CUM. WEIGHT	C/CO
1	25.00	0.008	10.081	0.0114
2	25.50	0.009	10.309	0.0128
3	26.00	0.011	10.537	0.0157
4	26.50	0.031	10.764	0.0438
5	27.00	0.065	10.992	0.0904
6	27.50	0.119	11.220	0.1618
7	28.00	0.179	11.448	0.2375
8	28.50	0.242	11.675	0.3133
9	29.00	0.307	11.903	0.3878
10	29.50	0.368	12.131	0.4546
11	30.00	0.430	12.358	0.5196
12	30.50	0.487	12.586	0.5769
13	31.00	0.540	12.814	0.6283
14	31.50	0.591	13.042	0.6760
15	32.00	0.641	13.269	0.7213
16	32.50	0.687	13.497	0.7617
17	33.00	0.730	13.725	0.7983
18	33.50	0.770	13.952	0.8316
19	34.00	0.807	14.180	0.8615
20	34.50	0.836	14.408	0.8846
21	35.00	0.862	14.636	0.9048
22	35.50	0.888	14.863	0.9248
23	36.00	0.907	15.091	0.9392
24	36.50	0.925	15.319	0.9526
25	37.00	0.940	15.547	0.9637
26	37.50	0.948	15.774	0.9696
27	38.00	0.957	16.002	0.9762
28	38.50	0.963	16.230	0.9806
29	39.00	0.969	16.457	0.9849
30	39.50	0.971	16.685	0.9864

RUN NUMBER 201 CONTINUED

POINT	TIME, MIN.	C	CUM. WEIGHT	C/CO
31	40.00	0.974	16.913	0.9885
32	40.50	0.979	17.141	0.9921
33	41.00	0.980	17.368	0.9928
34	41.50	0.982	17.596	0.9943
35	42.00	0.984	17.824	0.9957

RUN NUMBER 202

ADSORBATE - PROPANE
CARBON PARTICLE SIZE - 30-35 MESH US STD. SIEVE
BED WEIGHT - 49.55 G CARBON
UNCORRECTED VOL. FLOW RATE - 378.9080 ML/MIN
PRESSURE DROP - 22.0 MM H2O
MASS FLOW RATE - 0.1766 G/MIN-CM2
KGAP - 0.5504 G C3H8/MIN-G BED-G C3H8/G GAS
KSAP - 0.8883 G C3H8/MIN-G BED-G C3H8/G SOLID
BIG KGAP - 0.0664 G C3H8/MIN-G BED-G C3H8/G GAS
BIG KSAP - 0.8302 G C3H8/MIN-G BED-G C3H8/G SOLID
EFFECTIVE PARTICLE DIFFUSIVITY - 3.43 X 10-5 CM2/MIN
CO - 0.2509 G C3H6/G GAS

POINT	TIME, MIN.	C	CUM. WEIGHT	C/CO
1	25.75	0.012	11.444	0.0014
2	26.00	0.016	11.569	0.0043
3	26.25	0.020	11.694	0.0072
4	26.50	0.028	11.818	0.0129
5	26.75	0.042	11.943	0.0231
6	27.00	0.063	12.068	0.0385
7	27.25	0.100	12.193	0.0661
8	27.50	0.149	12.318	0.1037
9	27.75	0.220	12.442	0.1603
10	28.00	0.309	12.567	0.2349
11	28.50	0.511	12.817	0.4211
12	29.00	0.678	13.067	0.5955
13	29.50	0.790	13.316	0.7247
14	30.00	0.855	13.566	0.8050
15	31.00	0.921	14.065	0.8908
16	32.00	0.952	14.564	0.9328
17	33.00	0.968	15.063	0.9549
18	34.00	0.977	15.563	0.9674
19	35.00	0.982	16.062	0.9744
20	36.00	0.987	16.561	0.9815

RUN NUMBER 203

ADSORBATE - PROPYLENE
CARBON PARTICLE SIZE - 30-35 MESH US STD. SIEVE
BED WEIGHT - 49.55 G CARBON
UNCORRECTED VOL. FLOW RATE - 371.3318 ML/MIN
PRESSURE DROP - 22.0 MM H2O
MASS FLOW RATE - 0.1641 G/MIN-CM2
KGAP - 0.4002 G C3H6/MIN-G BED-G C3H6/G GAS
KSAP - 0.3080 G C3H6/MIN-G BED-G C3H6/G SOLID
BIG KGAP - 0.0278 G C3H6/MIN-G BED-G C3H6/G GAS
BIG KSAP - 0.2949 G C3H6/MIN-G BED-G C3H6/G SOLID
EFFECTIVE PARTICLE DIFFUSIVITY - 1.14 X 10-5 CM2/MIN
CO - 0.1313 G C3H6/G GAS

POINT	TIME, MIN.	C	CUM. WEIGHT	C/CO
1	25.00	0.003	10.279	0.0043
2	25.50	0.006	10.511	0.0086
3	26.00	0.009	10.743	0.0128
4	26.50	0.022	10.975	0.0312
5	27.00	0.058	11.207	0.0809
6	27.50	0.112	11.439	0.1527
7	28.00	0.175	11.671	0.2326
8	28.50	0.238	11.903	0.3086
9	29.00	0.302	12.135	0.3822
10	29.50	0.362	12.367	0.4482
11	30.00	0.422	12.599	0.5113
12	30.50	0.480	12.831	0.5700
13	31.00	0.532	13.063	0.6206
14	31.50	0.584	13.295	0.6696
15	32.00	0.632	13.527	0.7133
16	32.50	0.676	13.759	0.7521
17	33.00	0.715	13.991	0.7857
18	33.50	0.758	14.223	0.8217
19	34.00	0.793	14.455	0.8503
20	34.50	0.824	14.687	0.8751
21	35.00	0.850	14.919	0.8955
22	35.50	0.875	15.151	0.9149
23	36.00	0.893	15.383	0.9286
24	36.50	0.912	15.615	0.9429
25	37.00	0.927	15.847	0.9541
26	37.50	0.938	16.079	0.9623
27	38.00	0.945	16.311	0.9674
28	38.50	0.952	16.543	0.9725
29	39.00	0.956	16.775	0.9755
30	39.50	0.959	17.007	0.9777

RUN NUMBER 203 CONTINUED

POINT	TIME, MIN.	C	CUM. WEIGHT	C/CO
31	40.00	0.962	17.239	0.9798
32	40.50	0.969	17.471	0.9849
33	41.00	0.969	17.703	0.9849
34	41.50	0.971	17.935	0.9864
35	42.00	0.972	18.167	0.9871

RUN NUMBER 204

ADSORBATE - PROPANE
CARBON PARTICLE SIZE - 30-35 MESH US STD. SIEVE
BED WEIGHT - 49.55 G CARBON
UNCORRECTED VOL. FLOW RATE - 378.9080 ML/MIN
PRESSURE DROP - 24.5 MM H2O
MASS FLOW RATE - 0.1697 G/MIN-CM2
KGAP - 0.5488 G C3H8/MIN-G BED-G C3H8/G GAS
KSAP - 0.9286 G C3H8/MIN-G BED-G C3H8/G SOLID
BIG KGAP - 0.0683 G C3H8/MIN-G BED-G C3H8/G GAS
BIG KSAP - 0.8652 G C3H8/MIN-G BED-G C3H8/G SOLID
EFFECTIVE PARTICLE DIFFUSIVITY - 3.58 X 10-5 CM2/MIN
CO - 0.2593 G C3H6/G GAS

POINT	TIME, MIN.	C	CUM. WEIGHT	C/CO
1	26.00	0.013	11.104	0.0021
2	26.25	0.018	11.224	0.0057
3	26.50	0.023	11.344	0.0093
4	26.75	0.037	11.464	0.0194
5	27.00	0.055	11.584	0.0326
6	27.25	0.089	11.704	0.0578
7	27.50	0.131	11.824	0.0897
8	27.75	0.192	11.944	0.1376
9	28.00	0.268	12.064	0.2000
10	28.50	0.467	12.304	0.3784
11	29.00	0.648	12.544	0.5626
12	29.50	0.772	12.784	0.7032
13	30.00	0.842	13.023	0.7886
14	31.00	0.912	13.503	0.8788
15	32.00	0.945	13.983	0.9232
16	33.00	0.962	14.463	0.9465
17	34.00	0.972	14.943	0.9604
18	35.00	0.979	15.423	0.9702
19	36.00	0.982	15.903	0.9744
20	37.00	0.986	16.382	0.9801

RUN NUMBER 205

ADSORBATE - PROPYLENE
CARBON PARTICLE SIZE - 30-35 MESH US STD. SIEVE
BED WEIGHT - 49.55 G CARBON
UNCORRECTED VOL. FLOW RATE - 227.5282 ML/MIN
PRESSURE DROP - 13.0 MM H2O
MASS FLOW RATE - 0.0984 G/MIN-CM2
KGAP - 0.4576 G C3H6/MIN-G BED-G C3H6/G GAS
KSAP - 0.2033 G C3H6/MIN-G BED-G C3H6/G SOLID
BIG KGAP - 0.0200 G C3H6/MIN-G BED-G C3H6/G GAS
BIG KSAP - 0.1982 G C3H6/MIN-G BED-G C3H6/G SOLID
EFFECTIVE PARTICLE DIFFUSIVITY - 0.76 X 10-5 CM2/MIN
CD - 0.0816 G C3H6/G GAS

POINT	TIME, MIN.	C	CUM. WEIGHT	C/CO
1	41.00	0.004	10.476	0.0057
2	41.50	0.012	10.615	0.0171
3	42.00	0.030	10.754	0.0424
4	42.50	0.056	10.893	0.0782
5	43.00	0.091	11.032	0.1252
6	43.50	0.133	11.171	0.1798
7	44.00	0.179	11.310	0.2375
8	45.00	0.265	11.588	0.3401
9	46.00	0.352	11.867	0.4374
10	47.00	0.433	12.145	0.5227
11	48.00	0.506	12.423	0.5955
12	49.00	0.577	12.701	0.6631
13	50.00	0.640	12.980	0.7204
14	51.00	0.700	13.258	0.7729
15	52.00	0.754	13.536	0.8184
16	53.00	0.803	13.814	0.8583
17	54.00	0.842	14.092	0.8893
18	55.00	0.879	14.371	0.9179
19	56.00	0.906	14.649	0.9384
20	57.00	0.929	14.927	0.9556
21	58.00	0.943	15.205	0.9659
22	59.00	0.957	15.484	0.9762
23	60.00	0.965	15.762	0.9820
24	61.00	0.968	16.040	0.9842
25	62.00	0.973	16.318	0.9878

RUN NUMBER 206

ADSORBATE - PROPANE
CARBON PARTICLE SIZE - 30-35 MESH US STD. SIEVE
BED WEIGHT - 49.55 G CARBON
UNCORRECTED VOL. FLOW RATE - 108.3264 ML/MIN
PRESSURE DROP - 5.5 MM H2O
MASS FLOW RATE - 0.0461 G/MIN-CM2
KGAP - 0.1975 G C3H8/MIN-G BED-G C3H8/G GAS
KSAP - 0.3283 G C3H8/MIN-G BED-G C3H8/G SOLID
BIG KGAP - 0.0243 G C3H8/MIN-G BED-G C3H8/G GAS
BIG KSAP - 0.3062 G C3H8/MIN-G BED-G C3H8/G SOLID
EFFECTIVE PARTICLE DIFFUSIVITY - 1.27 X 10-5 CM2/MIN
CO - 0.2561 G C3H6/G GAS

POINT	TIME, MIN.	C	CUM. WEIGHT	C/CO
1	87.00	0.014	10.732	0.0029
2	88.00	0.019	10.862	0.0064
3	89.00	0.029	10.992	0.0136
4	90.00	0.051	11.122	0.0297
5	91.00	0.090	11.253	0.0653
6	92.00	0.173	11.383	0.1225
7	93.00	0.282	11.513	0.2118
8	94.00	0.423	11.643	0.3369
9	95.00	0.561	11.773	0.4712
10	96.00	0.679	11.904	0.5966
11	97.00	0.767	12.034	0.6973
12	98.00	0.829	12.164	0.7724
13	99.00	0.869	12.294	0.8228
14	100.00	0.900	12.424	0.8630
15	101.00	0.920	12.555	0.8894
16	102.00	0.937	12.685	0.9123
17	103.00	0.948	12.815	0.9273
18	104.00	0.957	12.945	0.9396
19	105.00	0.966	13.075	0.9521
20	106.00	0.974	13.206	0.9632

RUN NUMBER 207

ADSORBATE - PROPYLENE
CARBON PARTICLE SIZE - 30-35 MESH US STD. SIEVE
BED WEIGHT - 49.55 G CARBON
UNCORRECTED VOL. FLOW RATE - 227.5282 ML/MIN
PRESSURE DROP - 12.0 MM H2O
MASS FLOW RATE - 0.1010 G/MIN-CM2
KGAP - 0.4557 G C3H6/MIN-G BED-G C3H6/G GAS
KSAP - 0.2007 G C3H6/MIN-G BED-G C3H6/G SOLID
BIG KGAP - 0.0197 G C3H6/MIN-G BED-G C3H6/G GAS
BIG KSAP - 0.1958 G C3H6/MIN-G BED-G C3H6/G SOLID
EFFECTIVE PARTICLE DIFFUSIVITY - 0.76 X 10-5 CM2/MIN
CO - 0.0809 G C3H6/G GAS

POINT	TIME, MIN.	C	CUM. WEIGHT	C/CO
1	41.00	0.002	10.763	0.0029
2	41.50	0.003	10.906	0.0043
3	42.00	0.008	11.049	0.0114
4	42.50	0.022	11.191	0.0312
5	43.00	0.047	11.334	0.0659
6	43.50	0.079	11.477	0.1092
7	44.00	0.120	11.620	0.1631
8	45.00	0.218	11.906	0.2849
9	46.00	0.296	12.191	0.3754
10	47.00	0.378	12.477	0.4653
11	48.00	0.456	12.762	0.5460
12	49.00	0.528	13.048	0.6168
13	50.00	0.594	13.334	0.6788
14	51.00	0.657	13.619	0.7355
15	52.00	0.714	13.905	0.7848
16	53.00	0.765	14.191	0.8275
17	54.00	0.813	14.476	0.8663
18	55.00	0.851	14.762	0.8963
19	56.00	0.886	15.047	0.9233
20	57.00	0.911	15.333	0.9422
21	58.00	0.932	15.619	0.9578
22	59.00	0.948	15.904	0.9696
23	60.00	0.958	16.190	0.9769
24	61.00	0.966	16.476	0.9827
25	62.00	0.970	16.761	0.9856

RUN NUMBER 208

ADSORBATE - PROPANE
CARBON PARTICLE SIZE - 30-35 MESH US STD. SIEVE
BED WEIGHT - 49.55 G CARBON
UNCORRECTED VOL. FLOW RATE - 108.3264 ML/MIN
PRESSURE DROP - 4.0 MM H2O
MASS FLOW RATE - 0.0502 G/MIN-CM2
KGAP - 0.1850 G C3H8/MIN-G BED-G C3H8/G GAS
KSAP - 0.3447 G C3H8/MIN-G BED-G C3H8/G SOLID
BIG KGAP - 0.0245 G C3H8/MIN-G BED-G C3H8/G GAS
BIG KSAP - 0.3189 G C3H8/MIN-G BED-G C3H8/G SOLID
EFFECTIVE PARTICLE DIFFUSIVITY - 1.32 X 10-5 CM2/MIN
CO - 0.2768 G C3H6/G GAS

POINT	TIME, MIN.	C	CUM. WEIGHT	C/CO
1	87.00	0.012	11.714	0.0014
2	88.00	0.013	11.856	0.0021
3	89.00	0.018	11.997	0.0057
4	90.00	0.027	12.139	0.0122
5	91.00	0.046	12.281	0.0260
6	92.00	0.084	12.423	0.0541
7	93.00	0.150	12.565	0.1045
8	94.00	0.247	12.706	0.1825
9	95.00	0.380	12.848	0.2975
10	96.00	0.520	12.990	0.4300
11	97.00	0.648	13.132	0.5626
12	98.00	0.745	13.274	0.6715
13	99.00	0.813	13.416	0.7527
14	100.00	0.860	13.557	0.8113
15	101.00	0.895	13.699	0.8564
16	102.00	0.919	13.841	0.8881
17	103.00	0.937	13.983	0.9123
18	104.00	0.949	14.125	0.9286
19	105.00	0.958	14.266	0.9410
20	106.00	0.967	14.408	0.9535
21	107.00	0.972	14.550	0.9604
22	108.00	0.977	14.692	0.9674
23	109.00	0.981	14.834	0.9730

RUN NUMBER 209

ADSORBATE - PROPYLENE
CARBON PARTICLE SIZE - 30-35 MESH US STD. SIEVE
BED WEIGHT - 49.55 G CARBON
UNCORRECTED VOL. FLOW RATE - 110.7805 ML/MIN
PRESSURE DROP - 6.0 MM H2O
MASS FLOW RATE - 0.0442 G/MIN-CM2
KGAP - 0.2118 G C3H6/MIN-G BED-G C3H6/G GAS
KSAP - 0.0980 G C3H6/MIN-G BED-G C3H6/G SOLID
BIG KGAP - 0.0096 G C3H6/MIN-G BED-G C3H6/G GAS
BIG KSAP - 0.0955 G C3H6/MIN-G BED-G C3H6/G SOLID
EFFECTIVE PARTICLE DIFFUSIVITY - 0.37 X 10-5 CM2/MIN
CO - 0.0846 G C3H6/G GAS

POINT	TIME, MIN.	C	CUM. WEIGHT	C/CO
1	86.00	0.012	10.187	0.0171
2	86.50	0.023	10.250	0.0326
3	87.00	0.036	10.313	0.0507
4	87.50	0.050	10.375	0.0700
5	88.00	0.064	10.438	0.0890
6	88.50	0.082	10.500	0.1132
7	89.00	0.103	10.563	0.1410
8	89.50	0.121	10.625	0.1644
9	90.00	0.144	10.688	0.1938
10	92.50	0.248	11.001	0.3203
11	95.00	0.352	11.313	0.4384
12	97.50	0.448	11.626	0.5379
13	100.00	0.537	11.939	0.6254
14	102.50	0.617	12.251	0.6997
15	105.00	0.691	12.564	0.7651
16	107.50	0.757	12.877	0.8209
17	110.00	0.813	13.190	0.8663
18	112.50	0.863	13.502	0.9056
19	115.00	0.901	13.815	0.9347
20	117.50	0.935	14.128	0.9600
21	120.00	0.943	14.441	0.9659
22	122.50	0.968	14.753	0.9842
23	125.00	0.975	15.066	0.9892

RUN NUMBER 210

ADSORBATE - PROPANE
CARBON PARTICLE SIZE - 30-35 MESH US STD. SIEVE
BED WEIGHT - 49.55 G CARBON
UNCORRECTED VOL. FLOW RATE - 539.7173 ML/MIN
PRESSURE DROP - 36.0 MM H2O
MASS FLOW RATE - C.2427 G/MIN-CM2
KGAP - 0.6465 G C3H8/MIN-G BED-G C3H8/G GAS
KSAP - 1.1112 G C3H8/MIN-G BED-G C3H8/G SOLID
BIG KGAP - 0.0813 G C3H8/MIN-G BED-G C3H8/G GAS
BIG KSAP - 1.0342 G C3H8/MIN-G BED-G C3H8/G SOLID
EFFECTIVE PARTICLE DIFFUSIVITY - 4.28 X 10-5 CM2/MIN
CD - 0.2621 G C3H6/G GAS

POINT	TIME, MIN.	C	CUM. WEIGHT	C/CO
1	19.00	0.014	11.260	0.0029
2	19.25	0.020	11.432	0.0072
3	19.50	0.030	11.603	0.0144
4	19.75	0.046	11.775	0.0260
5	20.00	0.080	11.946	0.0511
6	20.25	0.131	12.118	0.0897
7	20.50	0.206	12.289	0.1489
8	21.00	0.425	12.632	0.3388
9	21.50	0.652	12.975	0.5670
10	22.00	0.788	13.319	0.7223
11	23.00	0.903	14.005	0.8669
12	24.00	0.946	14.691	0.9245
13	25.00	0.966	15.377	0.9521
14	26.00	0.978	16.063	0.9688
15	27.00	0.983	16.749	0.9759
16	28.00	0.988	17.435	0.9829

RUN NUMBER 211

ADSORBATE - PROPYLENE
CARBON PARTICLE SIZE - 30-35 MESH US STD. SIEVE
BED WEIGHT - 49.55 G CARBON
UNCORRECTED VOL. FLOW RATE - 111.3100 ML/MIN
PRESSURE DROP - 6.0 MM H2O
MASS FLOW RATE - 0.0446 G/MIN-CM2
KGAP - 0.1707 G C3H6/MIN-G BED-G C3H6/G GAS
KSAP - 0.0999 G C3H6/MIN-G BED-G C3H6/G SOLID
BIG KGAP - 0.0094 G C3H6/MIN-G BED-G C3H6/G GAS
BIG KSAP - 0.0966 G C3H6/MIN-G BED-G C3H6/G SOLID
EFFECTIVE PARTICLE DIFFUSIVITY - 0.37 X 10-5 CM2/MIN
CD - 0.1039 G C3H6/G GAS

POINT	TIME, MIN.	C	CUM. WEIGHT	C/CO
1	86.00	0.023	10.265	0.0326
2	86.50	0.035	10.328	0.0493
3	87.00	0.050	10.391	0.0700
4	87.50	0.063	10.454	0.0877
5	88.00	0.083	10.517	0.1146
6	88.50	0.100	10.580	0.1370
7	89.00	0.123	10.643	0.1669
8	89.50	0.144	10.706	0.1938
9	90.00	0.164	10.769	0.2189
10	92.50	0.272	11.084	0.3481
11	95.00	0.374	11.399	0.4610
12	97.50	0.468	11.714	0.5581
13	100.00	0.555	12.029	0.6425
14	102.50	0.635	12.344	0.7159
15	105.00	0.706	12.659	0.7780
16	107.50	0.772	12.974	0.8332
17	110.00	0.826	13.290	0.8767
18	112.50	0.874	13.605	0.9141
19	115.00	0.910	13.920	0.9414
20	117.50	0.937	14.235	0.9615
21	120.00	0.955	14.550	0.9747
22	122.50	0.966	14.865	0.9827
23	125.00	0.975	15.180	0.9892

RUN NUMBER 212

ADSORBATE - PROPANE
CARBON PARTICLE SIZE - 30-35 MESH US STD. SIEVE
BED WEIGHT - 49.55 G CARBON
UNCORRECTED VOL. FLOW RATE - 539.7173 ML/MIN
PRESSURE DROP - 36.5 MM H2O
MASS FLOW RATE - 0.2413 G/MIN-CM2
KGAP - 0.6713 G C3H8/MIN-G BED-G C3H8/G GAS
KSAP - 1.0648 G C3H8/MIN-G BED-G C3H8/G SOLID
BIG KGAP - 0.0801 G C3H8/MIN-G BED-G C3H8/G GAS
BIG KSAP - 0.9963 G C3H8/MIN-G BED-G C3H8/G SOLID
EFFECTIVE PARTICLE DIFFUSIVITY - 4.12 X 10-5 CM2/MIN
CD - 0.2478 G C3H6/G GAS

POINT	TIME, MIN.	C	CUM. WEIGHT	C/CO
1	18.75	0.013	11.024	0.0021
2	19.00	0.021	11.194	0.0079
3	19.25	0.033	11.365	0.0165
4	19.50	0.056	11.535	0.0333
5	19.75	0.098	11.706	0.0646
6	20.00	0.160	11.876	0.1123
7	20.25	0.249	12.047	0.1841
8	20.50	0.369	12.217	0.2876
9	21.00	0.606	12.558	0.5178
10	21.50	0.760	12.900	0.6891
11	22.00	0.847	13.241	0.7949
12	23.00	0.922	13.923	0.8921
13	24.00	0.952	14.605	0.9328
14	25.00	0.967	15.287	0.9535
15	26.00	0.978	15.969	0.9688
16	27.00	0.983	16.651	0.9759
17	28.00	0.986	17.334	0.9801

RUN NUMBER 213

ADSORBATE - PROPYLENE
CARBON PARTICLE SIZE - 30-35 MESH US STD. SIEVE
BED WEIGHT - 49.55 G CARBON
UNCORRECTED VOL. FLOW RATE - 555.8779 ML/MIN
PRESSURE DROP - 37.0 MM H2O
MASS FLOW RATE - 0.2394 G/MIN-CM2
KGAP - 0.7997 G C3H6/MIN-G BED-G C3H6/G GAS
KSAP - 0.4092 G C3H6/MIN-G BED-G C3H6/G SOLID
BIG KGAP - 0.0395 G C3H6/MIN-G BED-G C3H6/G GAS
BIG KSAP - 0.3975 G C3H6/MIN-G BED-G C3H6/G SOLID
EFFECTIVE PARTICLE DIFFUSIVITY - 1.53 X 10-5 CM2/MIN
CO - 0.0925 G C3H6/G GAS

POINT	TIME, MIN.	C	CUM. WEIGHT	C/CO
1	18.00	0.003	10.449	0.0043
2	18.25	0.006	10.618	0.0086
3	18.50	0.018	10.787	0.0256
4	18.75	0.037	10.956	0.0521
5	19.00	0.062	11.126	0.0863
6	19.25	0.097	11.295	0.1331
7	19.50	0.132	11.464	0.1785
8	20.00	0.220	11.803	0.2872
9	21.00	0.391	12.480	0.4790
10	22.00	0.540	13.156	0.6283
11	23.00	0.674	13.833	0.7504
12	24.00	0.782	14.510	0.8414
13	25.00	0.858	15.187	0.9017
14	26.00	0.909	15.864	0.9407
15	27.00	0.939	16.541	0.9630
16	28.00	0.954	17.218	0.9740
17	29.00	0.961	17.895	0.9791
18	30.00	0.966	18.572	0.9827

RUN NUMBER 214

ADSORBATE - PROPANE
CARBON PARTICLE SIZE - 30-35 MESH US STD. SIEVE
BED WEIGHT - 49.55 G CARBON
UNCORRECTED VOL. FLOW RATE - 222.0905 ML/MIN
PRESSURE DROP - 12.0 MM H2O
MASS FLOW RATE - 0.1021 G/MIN-CM2
KGAP - 0.3711 G C3H8/MIN-G BED-G C3H8/G GAS
KSAP - 0.6489 G C3H8/MIN-G BED-G C3H8/G SOLID
BIG KGAP - 0.0472 G C3H8/MIN-G BED-G C3H8/G GAS
BIG KSAP - 0.6032 G C3H8/MIN-G BED-G C3H8/G SOLID
EFFECTIVE PARTICLE DIFFUSIVITY - 2.49 X 10-5 CM2/MIN
CO - 0.2652 G C3H6/G GAS

POINT	TIME, MIN.	C	CUM. WEIGHT	C/CO
1	43.75	0.013	11.663	0.0021
2	44.00	0.018	11.735	0.0057
3	44.25	0.021	11.807	0.0079
4	44.50	0.025	11.880	0.0108
5	44.75	0.031	11.952	0.0151
6	45.00	0.040	12.024	0.0216
7	45.25	0.053	12.096	0.0311
8	45.50	0.071	12.168	0.0444
9	45.75	0.102	12.241	0.0676
10	46.00	0.139	12.313	0.0959
11	46.25	0.183	12.385	0.1305
12	46.50	0.235	12.457	0.1725
13	47.00	0.375	12.601	0.2930
14	47.50	0.518	12.746	0.4280
15	48.00	0.647	12.890	0.5616
16	49.00	0.806	13.179	0.7441
17	50.00	0.883	13.468	0.8408
18	51.00	0.922	13.756	0.8921
19	52.00	0.945	14.045	0.9232
20	53.00	0.959	14.334	0.9424
21	54.00	0.968	14.623	0.9549
22	55.00	0.973	14.911	0.9618
23	56.00	0.978	15.200	0.9688

RUN NUMBER 215

ADSORBATE - PROPYLENE
CARBON PARTICLE SIZE - 30-35 MESH US STD. SIEVE
BED WEIGHT - 49.55 G CARBON
UNCORRECTED VOL. FLOW RATE - 555.8779 ML/MIN
PRESSURE DROP - 37.0 MM H2O
MASS FLOW RATE - 0.2394 G/MIN-CM2
KGAP - 0.5676 G C3H6/MIN-G BED-G C3H6/G GAS
KSAP - 0.4023 G C3H6/MIN-G BED-G C3H6/G SOLID
BIG KGAP - 0.0369 G C3H6/MIN-G BED-G C3H6/G GAS
BIG KSAP - 0.3865 G C3H6/MIN-G BED-G C3H6/G SOLID
EFFECTIVE PARTICLE DIFFUSIVITY - 1.49 X 10-5 CM2/MIN
CO - 0.1225 G C3H6/G GAS

POINT	TIME, MIN.	C	CUM. WEIGHT	C/CO
1	18.00	0.005	10.449	0.0071
2	18.25	0.008	10.618	0.0114
3	18.50	0.010	10.787	0.0142
4	18.75	0.023	10.956	0.0326
5	19.00	0.045	11.126	0.0631
6	19.25	0.075	11.295	0.1039
7	19.50	0.111	11.464	0.1514
8	20.00	0.195	11.803	0.2571
9	21.00	0.363	12.480	0.4492
10	22.00	0.519	13.156	0.6081
11	23.00	0.655	13.833	0.7337
12	24.00	0.768	14.510	0.8299
13	25.00	0.850	15.187	0.8955
14	26.00	0.904	15.864	0.9369
15	27.00	0.938	16.541	0.9623
16	28.00	0.954	17.218	0.9740
17	29.00	0.962	17.895	0.9798
18	30.00	0.968	18.572	0.9842

RUN NUMBER 216

ADSORBATE - PROPANE
CARBON PARTICLE SIZE - 30-35 MESH US STD. SIEVE
BED WEIGHT - 49.55 G CARBON
UNCORRECTED VOL. FLOW RATE - 222.0905 ML/MIN
PRESSURE DROP - 16.5 MM H2O
MASS FLOW RATE - 0.0898 G/MIN-CM2
KGAP - 0.3924 G C3H8/MIN-G BED-G C3H8/G GAS
KSAP - 0.6800 G C3H8/MIN-G BED-G C3H8/G SOLID
BIG KGAP - 0.0496 G C3H8/MIN-G BED-G C3H8/G GAS
BIG KSAP - 0.6325 G C3H8/MIN-G BED-G C3H8/G SOLID
EFFECTIVE PARTICLE DIFFUSIVITY - 2.62 X 10-5 CM2/MIN
CO - 0.2635 G C3H6/G GAS

POINT	TIME, MIN.	C	CUM. WEIGHT	C/CO
1	43.75	0.016	10.215	0.0043
2	44.00	0.017	10.279	0.0050
3	44.25	0.018	10.342	0.0057
4	44.50	0.021	10.406	0.0079
5	44.75	0.027	10.469	0.0122
6	45.00	0.039	10.533	0.0209
7	45.25	0.050	10.596	0.0289
8	45.50	0.067	10.660	0.0414
9	45.75	0.095	10.723	0.0623
10	46.00	0.128	10.787	0.0874
11	46.50	0.220	10.914	0.1603
12	47.00	0.350	11.041	0.2707
13	47.50	0.499	11.167	0.4093
14	48.00	0.631	11.294	0.5443
15	49.00	0.804	11.548	0.7417
16	50.00	0.888	11.802	0.8473
17	51.00	0.928	12.056	0.9002
18	52.00	0.949	12.310	0.9286
19	53.00	0.963	12.564	0.9479
20	54.00	0.972	12.818	0.9604
21	55.00	0.981	13.071	0.9730
22	56.00	0.988	13.325	0.9829

RUN NUMBER 217

ADSORBATE - PROPYLENE
CARBON PARTICLE SIZE - 25-30 MESH US STD. SIEVE
BED WEIGHT - 47.95 G CARBON
UNCORRECTED VOL. FLOW RATE - 538.1594 ML/MIN
PRESSURE DROP - 30.0 MM H2O
MASS FLOW RATE - 0.2322 G/MIN-CM2
KGAP - 0.7365 G C3H6/MIN-G BED-G C3H6/G GAS
KSAP - 0.3785 G C3H6/MIN-G BED-G C3H6/G SOLID
BIG KGAP - 0.0353 G C3H6/MIN-G BED-G C3H6/G GAS
BIG KSAP - 0.3676 G C3H6/MIN-G BED-G C3H6/G SOLID
EFFECTIVE PARTICLE DIFFUSIVITY - 1.99 X 10-5 CM2/MIN
CO - 0.0928 G C3H6/G GAS

POINT	TIME, MIN.	C	CUM. WEIGHT	C/CO
1	18.00	0.004	10.121	0.0057
2	18.25	0.010	10.285	0.0142
3	18.50	0.022	10.449	0.0312
4	18.75	0.042	10.613	0.0590
5	19.00	0.068	10.777	0.0944
6	19.25	0.100	10.942	0.1370
7	19.50	0.124	11.106	0.1682
8	20.00	0.211	11.434	0.2765
9	21.00	0.369	12.091	0.4557
10	22.00	0.515	12.747	0.6043
11	23.00	0.648	13.404	0.7275
12	24.00	0.757	14.060	0.8209
13	25.00	0.837	14.717	0.8854
14	26.00	0.896	15.374	0.9309
15	27.00	0.929	16.030	0.9556
16	28.00	0.950	16.687	0.9711
17	29.00	0.959	17.343	0.9777
18	30.00	0.966	18.000	0.9827
19	31.00	0.969	18.657	0.9849

RUN NUMBER 218

ADSORBATE - PROPANE
CARBON PARTICLE SIZE - 25-30 MESH US STD. SIEVE
BED WEIGHT - 47.95 G CARBON
UNCORRECTED VOL. FLOW RATE - 226.4182 ML/MIN
PRESSURE DROP - 11.0 MM H2O
MASS FLOW RATE - 0.1012 G/MIN-CM2
KGAP - 0.4209 G C3H8/MIN-G BED-G C3H8/G GAS
KSAP - 0.6111 G C3H8/MIN-G BED-G C3H8/G SOLID
BIG KGAP - 0.0457 G C3H8/MIN-G BED-G C3H8/G GAS
BIG KSAP - 0.5749 G C3H8/MIN-G BED-G C3H8/G SOLID
EFFECTIVE PARTICLE DIFFUSIVITY - 3.34 X 10-5 CM2/MIN
CD - 0.2327 G C3H6/G GAS

POINT	TIME, MIN.	C	CUM. WEIGHT	C/CO
1	42.00	0.012	11.058	0.0014
2	42.25	0.014	11.130	0.0029
3	42.50	0.018	11.201	0.0057
4	42.75	0.025	11.273	0.0108
5	43.00	0.033	11.344	0.0165
6	43.25	0.043	11.416	0.0238
7	43.50	0.061	11.488	0.0370
8	43.75	0.085	11.559	0.0548
9	44.00	0.117	11.631	0.0790
10	44.25	0.157	11.702	0.1099
11	44.50	0.201	11.774	0.1449
12	45.00	0.328	11.917	0.2514
13	45.50	0.467	12.060	0.3784
14	46.00	0.600	12.203	0.5115
15	47.00	0.778	12.489	0.7104
16	48.00	0.865	12.776	0.8177
17	49.00	0.907	13.062	0.8722
18	50.00	0.932	13.348	0.9056
19	51.00	0.945	13.634	0.9232
20	52.00	0.954	13.921	0.9355
21	53.00	0.960	14.207	0.9438
22	54.00	0.964	14.493	0.9493
23	55.00	0.970	14.779	0.9576

RUN NUMBER 219

ADSORBATE - PROPYLENE
CARBON PARTICLE SIZE - 25-30 MESH US STD. SIEVE
BED WEIGHT - 47.95 G CARBON
UNCORRECTED VOL. FLOW RATE - 538.1594 ML/MIN
PRESSURE DROP - 31.0 MM H2O
MASS FLOW RATE - 0.2292 G/MIN-CM2
KGAP - 0.7376 G C3H6/MIN-G BED-G C3H6/G GAS
KSAP - 0.3698 G C3H6/MIN-G BED-G C3H6/G SOLID
BIG KGAP - 0.0346 G C3H6/MIN-G BED-G C3H6/G GAS
BIG KSAP - 0.3594 G C3H6/MIN-G BED-G C3H6/G SOLID
EFFECTIVE PARTICLE DIFFUSIVITY - 1.95 X 10-5 CM2/MIN
CO - 0.0908 G C3H6/G GAS

POINT	TIME, MIN.	C	CUM. WEIGHT	C/CO
1	18.00	0.006	9.981	0.0086
2	18.25	0.012	10.143	0.0171
3	18.50	0.027	10.305	0.0382
4	18.75	0.049	10.467	0.0686
5	19.00	0.077	10.629	0.1065
6	19.25	0.106	10.791	0.1449
7	19.50	0.142	10.953	0.1912
8	20.00	0.218	11.277	0.2849
9	21.00	0.376	11.925	0.4631
10	22.00	0.524	12.573	0.6130
11	23.00	0.653	13.221	0.7319
12	24.00	0.762	13.869	0.8250
13	25.00	0.844	14.517	0.8908
14	26.00	0.900	15.165	0.9339
15	27.00	0.935	15.813	0.9600
16	28.00	0.954	16.461	0.9740
17	29.00	0.964	17.109	0.9813
18	30.00	0.970	17.757	0.9856
19	31.00	0.972	18.405	0.9871

RUN NUMBER 220

ADSORBATE - PROPANE
CARBON PARTICLE SIZE - 25-30 MESH US STD. SIEVE
BED WEIGHT - 47.95 G CARBON
UNCORRECTED VOL. FLOW RATE - 226.4182 ML/MIN
PRESSURE DROP - 13.5 MM H2O
MASS FLOW RATE - 0.0932 G/MIN-CM2
KGAP - 0.3826 G C3H8/MIN-G BED-G C3H8/G GAS
KSAP - 0.6338 G C3H8/MIN-G BED-G C3H8/G SOLID
BIG KGAP - 0.0455 G C3H8/MIN-G BED-G C3H8/G GAS
BIG KSAP - 0.5914 G C3H8/MIN-G BED-G C3H8/G SOLID
EFFECTIVE PARTICLE DIFFUSIVITY - 3.43 X 10-5 CM2/MIN
CO - 0.2555 G C3H6/G GAS

POINT	TIME, MIN.	C	CUM. WEIGHT	C/CO
1	42.00	0.015	10.158	0.0036
2	42.25	0.019	10.224	0.0064
3	42.50	0.022	10.290	0.0086
4	42.75	0.027	10.356	0.0122
5	43.00	0.039	10.422	0.0209
6	43.25	0.050	10.488	0.0289
7	43.50	0.065	10.553	0.0400
8	43.75	0.089	10.619	0.0578
9	44.00	0.123	10.685	0.0836
10	44.25	0.163	10.751	0.1146
11	44.50	0.213	10.817	0.1546
12	45.00	0.337	10.949	0.2592
13	45.50	0.476	11.081	0.3870
14	46.00	0.608	11.212	0.5199
15	47.00	0.784	11.476	0.7175
16	48.00	0.873	11.740	0.8279
17	49.00	0.920	12.003	0.8894
18	50.00	0.946	12.267	0.9245
19	51.00	0.960	12.530	0.9438
20	52.00	0.973	12.794	0.9618
21	53.00	0.980	13.058	0.9716
22	54.00	0.983	13.321	0.9759
23	55.00	0.990	13.585	0.9858

RUN NUMBER 221

ADSORBATE - PROPYLENE
CARBON PARTICLE SIZE - 25-30 MESH US STD. SIEVE
BED WEIGHT - 47.95 G CARBON
UNCORRECTED VOL. FLOW RATE - 226.9681 ML/MIN
PRESSURE DROP - 11.0 MM H2O
MASS FLOW RATE - 0.0971 G/MIN-CM2
KGAP - 0.3386 G C3H6/MIN-G BED-G C3H6/G GAS
KSAP - 0.1846 G C3H6/MIN-G BED-G C3H6/G SOLID
BIG KGAP - 0.0171 G C3H6/MIN-G BED-G C3H6/G GAS
BIG KSAP - 0.1789 G C3H6/MIN-G BED-G C3H6/G SOLID
EFFECTIVE PARTICLE DIFFUSIVITY - 0.97 X 10-5 CM2/MIN
CO - 0.0978 G C3H6/G GAS

POINT	TIME, MIN.	C	CUM. WEIGHT	C/CO
1	41.00	0.003	10.337	0.0043
2	41.50	0.005	10.475	0.0071
3	42.00	0.008	10.612	0.0114
4	42.50	0.014	10.749	0.0199
5	43.00	0.035	10.887	0.0493
6	43.50	0.063	11.024	0.0877
7	44.00	0.098	11.161	0.1344
8	44.50	0.136	11.299	0.1836
9	45.00	0.176	11.436	0.2338
10	46.00	0.255	11.711	0.3285
11	47.00	0.329	11.985	0.4122
12	48.00	0.403	12.260	0.4916
13	49.00	0.472	12.534	0.5620
14	50.00	0.539	12.809	0.6273
15	51.00	0.603	13.084	0.6870
16	52.00	0.662	13.358	0.7399
17	53.00	0.714	13.633	0.7848
18	54.00	0.765	13.908	0.8275
19	55.00	0.811	14.182	0.8648
20	56.00	0.848	14.457	0.8940
21	57.00	0.879	14.732	0.9179
22	58.00	0.904	15.006	0.9369
23	59.00	0.922	15.281	0.9504
24	60.00	0.940	15.556	0.9637
25	61.00	0.951	15.830	0.9718
26	62.00	0.958	16.105	0.9769
27	63.00	0.963	16.380	0.9806
28	64.00	0.968	16.654	0.9842
29	65.00	0.971	16.929	0.9864

RUN NUMBER 222

ADSORBATE - PROPANE
CARBON PARTICLE SIZE - 25-30 MESH US STD. SIEVE
BED WEIGHT - 47.95 G CARBON
UNCORRECTED VOL. FLOW RATE - 110.2509 ML/MIN
PRESSURE DROP - 4.0 MM H2O
MASS FLOW RATE - 0.0482 G/MIN-CM2
KGAP - 0.1957 G C3H8/MIN-G BED-G C3H8/G GAS
KSAP - 0.3394 G C3H8/MIN-G BED-G C3H8/G SOLID
BIG KGAP - 0.0240 G C3H8/MIN-G BED-G C3H8/G GAS
BIG KSAP - 0.3157 G C3H8/MIN-G BED-G C3H8/G SOLID
EFFECTIVE PARTICLE DIFFUSIVITY - 1.83 X 10-5 CM2/MIN
CD - 0.2637 G C3H6/G GAS

POINT	TIME, MIN.	C	CUM. WEIGHT	C/CO
1	87.00	0.014	11.246	0.0029
2	87.50	0.018	11.314	0.0057
3	88.00	0.026	11.382	0.0115
4	88.50	0.033	11.451	0.0165
5	89.00	0.048	11.519	0.0275
6	89.50	0.062	11.587	0.0377
7	90.00	0.083	11.655	0.0533
8	90.50	0.111	11.723	0.0744
9	91.00	0.146	11.791	0.1014
10	92.00	0.236	11.928	0.1734
11	93.00	0.362	12.064	0.2814
12	94.00	0.503	12.200	0.4133
13	95.00	0.631	12.336	0.5443
14	96.00	0.733	12.473	0.6576
15	97.00	0.803	12.609	0.7405
16	98.00	0.853	12.745	0.8024
17	99.00	0.889	12.882	0.8486
18	100.00	0.917	13.018	0.8854
19	101.00	0.937	13.154	0.9123
20	102.00	0.950	13.290	0.9300
21	103.00	0.957	13.427	0.9396
22	104.00	0.966	13.563	0.9521
23	105.00	0.970	13.699	0.9576
24	106.00	0.978	13.836	0.9688
25	107.00	0.982	13.972	0.9744
26	108.00	0.985	14.108	0.9787
27	109.00	0.987	14.244	0.9815
28	110.00	0.992	14.381	0.9886

RUN NUMBER 223

ADSORBATE - PROPYLENE
CARBON PARTICLE SIZE - 25-30 MESH US STD. SIEVE
BED WEIGHT - 47.95 G CARBON
UNCORRECTED VOL. FLOW RATE - 226.9681 ML/MIN
PRESSURE DROP - 11.0 MM H2O
MASS FLOW RATE - 0.0971 G/MIN-CM2
KGAP - 0.4723 G C3H6/MIN-G BED-G C3H6/G GAS
KSAP - 0.1821 G C3H6/MIN-G BED-G C3H6/G SOLID
BIG KGAP - 0.0176 G C3H6/MIN-G BED-G C3H6/G GAS
BIG KSAP - 0.1781 G C3H6/MIN-G BED-G C3H6/G SOLID
EFFECTIVE PARTICLE DIFFUSIVITY - 0.96 X 10-5 CM2/MIN
CD - 0.0718 G C3H6/G GAS

POINT	TIME, MIN.	C	CUM. WEIGHT	C/CO
1	41.00	0.001	10.337	0.0014
2	41.50	0.001	10.475	0.0014
3	42.00	0.001	10.612	0.0014
4	42.50	0.004	10.749	0.0057
5	43.00	0.014	10.887	0.0199
6	43.50	0.035	11.024	0.0493
7	44.00	0.062	11.161	0.0863
8	44.50	0.097	11.299	0.1331
9	45.00	0.136	11.436	0.1836
10	46.00	0.214	11.711	0.2801
11	47.00	0.292	11.985	0.3709
12	48.00	0.369	12.260	0.4557
13	49.00	0.439	12.534	0.5288
14	50.00	0.508	12.809	0.5975
15	51.00	0.572	13.084	0.6584
16	52.00	0.632	13.358	0.7133
17	53.00	0.688	13.633	0.7625
18	54.00	0.740	13.908	0.8067
19	55.00	0.788	14.182	0.8462
20	56.00	0.828	14.457	0.8783
21	57.00	0.861	14.732	0.9041
22	58.00	0.890	15.006	0.9263
23	59.00	0.913	15.281	0.9437
24	60.00	0.932	15.556	0.9578
25	61.00	0.947	15.830	0.9689
26	62.00	0.955	16.105	0.9747
27	63.00	0.962	16.380	0.9798
28	64.00	0.967	16.654	0.9835
29	65.00	0.970	16.929	0.9856

RUN NUMBER 224

ADSORBATE - PROPANE
CARBON PARTICLE SIZE - 25-30 MESH US STD. SIEVE
BED WEIGHT - 47.95 G CARBON
UNCORRECTED VOL. FLOW RATE - 110.5157 ML/MIN
PRESSURE DROP - 6.0 MM H2O
MASS FLOW RATE - 0.0420 G/MIN-CM2
KGAP - 0.1837 G C3H8/MIN-G BED-G C3H8/G GAS
KSAP - 0.3551 G C3H8/MIN-G BED-G C3H8/G SOLID
BIG KGAP - 0.0241 G C3H8/MIN-G BED-G C3H8/G GAS
BIG KSAP - 0.3277 G C3H8/MIN-G BED-G C3H8/G SOLID
EFFECTIVE PARTICLE DIFFUSIVITY - 1.90 X 10-5 CM2/MIN
CO - 0.2836 G C3H6/G GAS

POINT	TIME, MIN.	C	CUM. WEIGHT	C/CO
1	85.00	0.011	9.521	0.0007
2	85.50	0.012	9.580	0.0014
3	86.00	0.014	9.640	0.0029
4	86.50	0.016	9.699	0.0043
5	87.00	0.019	9.758	0.0064
6	87.50	0.024	9.818	0.0100
7	88.00	0.028	9.877	0.0129
8	88.50	0.038	9.936	0.0202
9	89.00	0.049	9.996	0.0282
10	89.50	0.066	10.055	0.0407
11	90.00	0.090	10.114	0.0586
12	90.50	0.129	10.174	0.0882
13	91.00	0.159	10.233	0.1115
14	92.00	0.259	10.352	0.1924
15	93.00	0.393	10.470	0.3093
16	94.00	0.531	10.589	0.4410
17	95.00	0.657	10.708	0.5724
18	96.00	0.753	10.826	0.6808
19	97.00	0.821	10.945	0.7625
20	98.00	0.868	11.064	0.8215
21	99.00	0.901	11.182	0.8643
22	100.00	0.922	11.301	0.8921
23	101.00	0.941	11.420	0.9177
24	102.00	0.955	11.538	0.9369
25	103.00	0.964	11.657	0.9493
26	104.00	0.971	11.776	0.9590
27	105.00	0.977	11.894	0.9674
28	106.00	0.982	12.013	0.9744

RUN NUMBER 225

ADSORBATE - PROPYLENE
CARBON PARTICLE SIZE - 25-30 MESH US STD. SIEVE
BED WEIGHT - 47.95 G CARBON
UNCORRECTED VOL. FLOW RATE - 109.0901 ML/MIN
PRESSURE DROP - 4.0 MM H2O
MASS FLOW RATE - C.0454 G/MIN-CM2
KGAP - 0.1872 G C3H6/MIN-G BED-G C3H6/G GAS
KSAP - 0.0898 G C3H6/MIN-G BED-G C3H6/G SOLID
BIG KGAP - 0.0085 G C3H6/MIN-G BED-G C3H6/G GAS
BIG KSAP - 0.0874 G C3H6/MIN-G BED-G C3H6/G SOLID
EFFECTIVE PARTICLE DIFFUSIVITY - 0.47 X 10-5 CM2/MIN
CO - 0.0873 G C3H6/G GAS

POINT	TIME, MIN.	C	CUM. WEIGHT	C/CO
1	87.00	0.006	10.581	0.0086
2	88.00	0.009	10.709	0.0128
3	89.00	0.024	10.838	0.0340
4	90.00	0.048	10.966	0.0672
5	91.00	0.077	11.094	0.1065
6	92.00	0.110	11.222	0.1501
7	93.00	0.148	11.351	0.1988
8	94.00	0.187	11.479	0.2473
9	95.00	0.227	11.607	0.2956
10	96.00	0.263	11.736	0.3378
11	97.00	0.303	11.864	0.3833
12	98.00	0.338	11.992	0.4221
13	99.00	0.375	12.120	0.4621
14	100.00	0.410	12.249	0.4989
15	101.00	0.445	12.377	0.5349
16	102.00	0.479	12.505	0.5690
17	103.00	0.510	12.633	0.5994
18	104.00	0.541	12.762	0.6292
19	105.00	0.572	12.890	0.6584
20	106.00	0.602	13.018	0.6861
21	107.00	0.632	13.147	0.7133
22	108.00	0.659	13.275	0.7372
23	109.00	0.685	13.403	0.7599
24	110.00	0.711	13.531	0.7823
25	111.00	0.735	13.660	0.8025
26	112.00	0.760	13.788	0.8233
27	113.00	0.783	13.916	0.8422
28	114.00	0.803	14.044	0.8583
29	115.00	0.823	14.173	0.8743
30	116.00	0.842	14.301	0.8893

RUN NUMBER 225 CONTINUED

POINT	TIME, MIN.	C	CUM. WEIGHT	C/CO
31	117.00	0.859	14.429	0.9025
32	118.00	0.875	14.558	0.9149
33	119.00	0.891	14.686	0.9271
34	120.00	0.903	14.814	0.9362
35	121.00	0.916	14.942	0.9459
36	122.00	0.927	15.071	0.9541
37	123.00	0.938	15.199	0.9623
38	124.00	0.946	15.327	0.9681
39	125.00	0.953	15.455	0.9733
40	126.00	0.959	15.584	0.9777
41	127.00	0.964	15.712	0.9813
42	128.00	0.969	15.840	0.9849
43	129.00	0.972	15.969	0.9871
44	130.00	0.976	16.097	0.9900

RUN NUMBER 226

ADSORBATE - PROPANE
CARBON PARTICLE SIZE - 25-30 MESH US STD. SIEVE
BED WEIGHT - 47.95 G CARBON
UNCORRECTED VOL. FLOW RATE - 386.7998 ML/MIN
PRESSURE DROP - 21.0 MM H2O
MASS FLOW RATE - 0.1734 G/MIN-CM2
KGAP - 0.5582 G C3H8/MIN-G BED-G C3H8/G GAS
KSAP - 0.8622 G C3H8/MIN-G BED-G C3H8/G SOLID
BIG KGAP - 0.0633 G C3H8/MIN-G BED-G C3H8/G GAS
BIG KSAP - 0.8081 G C3H8/MIN-G BED-G C3H8/G SOLID
EFFECTIVE PARTICLE DIFFUSIVITY - 4.69 X 10-5 CM2/MIN
CO - 0.2432 G C3H6/G GAS

POINT	TIME, MIN.	C	CUM. WEIGHT	C/CO
1	25.25	0.011	10.985	0.0007
2	25.50	0.013	11.108	0.0021
3	25.75	0.017	11.230	0.0050
4	26.00	0.022	11.353	0.0086
5	26.25	0.033	11.475	0.0165
6	26.50	0.051	11.598	0.0297
7	26.75	0.080	11.721	0.0511
8	27.00	0.121	11.843	0.0821
9	27.50	0.252	12.088	0.1866
10	28.00	0.439	12.333	0.3519
11	28.50	0.618	12.578	0.5305
12	29.00	0.746	12.823	0.6727
13	30.00	0.876	13.314	0.8318
14	31.00	0.929	13.804	0.9015
15	32.00	0.957	14.294	0.9396
16	33.00	0.971	14.784	0.9590
17	34.00	0.982	15.275	0.9744
18	35.00	0.986	15.765	0.9801

RUN NUMBER 227

ADSORBATE - PROPYLENE
CARBON PARTICLE SIZE - 25-30 MESH US STD. SIEVE
BED WEIGHT - 47.95 G CARBON
UNCORRECTED VOL. FLOW RATE - 109.7316 ML/MIN
PRESSURE DROP - 4.0 MM H2O
MASS FLOW RATE - 0.0458 G/MIN-CM2
KGAP - 0.2611 G C3H6/MIN-G BED-G C3H6/G GAS
KSAP - 0.0897 G C3H6/MIN-G BED-G C3H6/G SOLID
BIG KGAP - 0.0088 G C3H6/MIN-G BED-G C3H6/G GAS
BIG KSAP - 0.0879 G C3H6/MIN-G BED-G C3H6/G SOLID
EFFECTIVE PARTICLE DIFFUSIVITY - 0.48 X 10-5 CM2/MIN
CO - 0.0646 G C3H6/G GAS

POINT	TIME, MIN.	C	CUM. WEIGHT	C/CO
1	87.00	0.006	10.676	0.0086
2	88.00	0.022	10.806	0.0312
3	89.00	0.045	10.935	0.0631
4	90.00	0.076	11.064	0.1052
5	91.00	0.109	11.194	0.1488
6	92.00	0.147	11.323	0.1976
7	93.00	0.189	11.453	0.2498
8	94.00	0.227	11.582	0.2956
9	95.00	0.262	11.711	0.3366
10	96.00	0.301	11.841	0.3811
11	97.00	0.338	11.970	0.4221
12	98.00	0.376	12.100	0.4631
13	99.00	0.411	12.229	0.5000
14	100.00	0.447	12.358	0.5369
15	101.00	0.479	12.488	0.5690
16	102.00	0.512	12.617	0.6014
17	103.00	0.543	12.747	0.6311
18	104.00	0.575	12.876	0.6612
19	105.00	0.605	13.005	0.6888
20	106.00	0.635	13.135	0.7159
21	107.00	0.661	13.264	0.7390
22	108.00	0.688	13.394	0.7625
23	109.00	0.713	13.523	0.7840
24	110.00	0.739	13.652	0.8059
25	111.00	0.763	13.782	0.8258
26	112.00	0.788	13.911	0.8462
27	113.00	0.808	14.041	0.8624
28	114.00	0.826	14.170	0.8767
29	115.00	0.844	14.299	0.8908
30	116.00	0.860	14.429	0.9033

RUN NUMBER 227 CONTINUED

POINT	TIME, MIN.	C	CUM. WEIGHT	C/CO
31	117.00	0.878	14.558	0.9172
32	118.00	0.891	14.688	0.9271
33	119.00	0.903	14.817	0.9362
34	120.00	0.915	14.946	0.9452
35	121.00	0.927	15.076	0.9541
36	122.00	0.935	15.205	0.9600
37	123.00	0.944	15.335	0.9667
38	124.00	0.951	15.464	0.9718
39	125.00	0.957	15.593	0.9762
40	126.00	0.961	15.723	0.9791
41	127.00	0.965	15.852	0.9820
42	128.00	0.969	15.982	0.9849
43	129.00	0.972	16.111	0.9871
44	130.00	0.973	16.240	0.9878

RUN NUMBER 228

ADSORBATE - PROPANE
CARBON PARTICLE SIZE - 25-30 MESH US STD. SIEVE
BED WEIGHT - 47.95 G CARBON
UNCORRECTED VOL. FLOW RATE - 383.6023 ML/MIN
PRESSURE DROP - 19.0 MM H2O
MASS FLOW RATE - 0.1777 G/MIN-CM2
KGAP - 0.5945 G C3H8/MIN-G BED-G C3H8/G GAS
KSAP - 0.8180 G C3H8/MIN-G BED-G C3H8/G SOLID
BIG KGAP - 0.0622 G C3H8/MIN-G BED-G C3H8/G GAS
BIG KSAP - 0.7720 G C3H8/MIN-G BED-G C3H8/G SOLID
EFFECTIVE PARTICLE DIFFUSIVITY - 4.48 X 10-5 CM2/MIN
CO - 0.2238 G C3H6/G GAS

POINT	TIME, MIN.	C	CUM. WEIGHT	C/CO
1	25.25	0.011	11.270	0.0007
2	25.50	0.015	11.395	0.0036
3	25.75	0.020	11.521	0.0072
4	26.00	0.030	11.646	0.0144
5	26.25	0.046	11.772	0.0260
6	26.50	0.072	11.898	0.0451
7	26.75	0.113	12.023	0.0760
8	27.00	0.169	12.149	0.1194
9	27.50	0.327	12.400	0.2505
10	28.00	0.516	12.651	0.4260
11	28.50	0.674	12.903	0.5911
12	29.00	0.780	13.154	0.7128
13	30.00	0.888	13.656	0.8473
14	31.00	0.933	14.159	0.9069
15	32.00	0.956	14.661	0.9383
16	33.00	0.968	15.164	0.9549
17	34.00	0.977	15.666	0.9674
18	35.00	0.982	16.169	0.9744

RUN NUMBER 229

ADSORBATE - PROPYLENE
CARBON PARTICLE SIZE - 25-30 MESH US STD. SIEVE
BED WEIGHT - 47.95 G CARBON
UNCORRECTED VOL. FLOW RATE - 379.0811 ML/MIN
PRESSURE DROP - 21.0 MM H2O
MASS FLOW RATE - 0.1610 G/MIN-CM2
KGAP - 0.6266 G C3H6/MIN-G BED-G C3H6/G GAS
KSAP - 0.2860 G C3H6/MIN-G BED-G C3H6/G SOLID
BIG KGAP - 0.0271 G C3H6/MIN-G BED-G C3H6/G GAS
BIG KSAP - 0.2787 G C3H6/MIN-G BED-G C3H6/G SOLID
EFFECTIVE PARTICLE DIFFUSIVITY - 1.51 X 10-5 CM2/MIN
CO - 0.0836 G C3H6/G GAS

POINT	TIME, MIN.	C	CUM. WEIGHT	C/CO
1	25.25	0.002	10.189	0.0029
2	25.50	0.005	10.303	0.0071
3	25.75	0.012	10.416	0.0171
4	26.00	0.024	10.530	0.0340
5	26.25	0.037	10.644	0.0521
6	26.50	0.058	10.758	0.0809
7	26.75	0.080	10.872	0.1106
8	27.00	0.105	10.985	0.1436
9	27.25	0.132	11.099	0.1785
10	27.50	0.162	11.213	0.2164
11	28.00	0.224	11.441	0.2920
12	29.00	0.338	11.896	0.4221
13	30.00	0.455	12.351	0.5450
14	31.00	0.561	12.806	0.6481
15	32.00	0.655	13.261	0.7337
16	33.00	0.739	13.716	0.8059
17	34.00	0.808	14.172	0.8624
18	35.00	0.863	14.627	0.9056
19	36.00	0.903	15.082	0.9362
20	37.00	0.932	15.537	0.9578
21	38.00	0.952	15.992	0.9725
22	39.00	0.963	16.447	0.9806
23	40.00	0.968	16.903	0.9842

RUN NUMBER 230

ADSORBATE - PROPANE
CARBON PARTICLE SIZE - 25-30 MESH US STD. SIEVE
BED WEIGHT - 47.95 G CARBON
UNCORRECTED VOL. FLOW RATE - 552.5684 ML/MIN
PRESSURE DROP - 33.0 MM H2O
MASS FLOW RATE - 0.2426 G/MIN-CM2
KGAP - 0.6586 G C3H8/MIN-G BED-G C3H8/G GAS
KSAP - 1.0051 G C3H8/MIN-G BED-G C3H8/G SOLID
BIG KGAP - 0.0741 G C3H8/MIN-G BED-G C3H8/G GAS
BIG KSAP - 0.9428 G C3H8/MIN-G BED-G C3H8/G SOLID
EFFECTIVE PARTICLE DIFFUSIVITY - 5.47 X 10-5 CM2/MIN
CD - 0.2412 G C3H6/G GAS

POINT	TIME, MIN.	C	CUM. WEIGHT	C/CO
1	18.00	0.011	10.574	0.0007
2	18.25	0.015	10.745	0.0036
3	18.50	0.022	10.917	0.0086
4	18.75	0.038	11.088	0.0202
5	19.00	0.064	11.260	0.0392
6	19.25	0.110	11.431	0.0737
7	19.50	0.177	11.603	0.1257
8	19.75	0.262	11.774	0.1949
9	20.00	0.373	11.946	0.2912
10	20.50	0.588	12.289	0.4990
11	21.00	0.744	12.632	0.6703
12	21.50	0.847	12.974	0.7949
13	22.00	0.887	13.317	0.8460
14	23.00	0.939	14.003	0.9150
15	24.00	0.962	14.689	0.9465
16	25.00	0.973	15.375	0.9618
17	26.00	0.980	16.061	0.9716
18	27.00	0.987	16.747	0.9815
19	28.00	0.989	17.433	0.9843

RUN NUMBER 231

ADSORBATE - PROPYLENE
CARBON PARTICLE SIZE - 25-30 MESH US STD. SIEVE
BED WEIGHT - 47.95 G CARBON
UNCORRECTED VOL. FLOW RATE - 385.1907 ML/MIN
PRESSURE DROP - 19.0 MM H2O
MASS FLOW RATE - 0.1709 G/MIN-CM2
KGAP - 0.6118 G C3H6/MIN-G BED-G C3H6/G GAS
KSAP - 0.2801 G C3H6/MIN-G BED-G C3H6/G SOLID
BIG KGAP - 0.0265 G C3H6/MIN-G BED-G C3H6/G GAS
BIG KSAP - 0.2729 G C3H6/MIN-G BED-G C3H6/G SOLID
EFFECTIVE PARTICLE DIFFUSIVITY - 1.48 X 10-5 CM2/MIN
CO - 0.0838 G C3H6/G GAS

POINT	TIME, MIN.	C	CUM. WEIGHT	C/CO
1	25.50	0.002	10.961	0.0029
2	25.75	0.003	11.082	0.0043
3	26.00	0.006	11.203	0.0086
4	26.25	0.017	11.324	0.0241
5	26.50	0.030	11.444	0.0424
6	26.75	0.049	11.565	0.0686
7	27.00	0.068	11.686	0.0944
8	27.25	0.093	11.807	0.1278
9	27.50	0.122	11.928	0.1657
10	28.00	0.179	12.169	0.2375
11	29.00	0.297	12.653	0.3766
12	30.00	0.413	13.136	0.5020
13	31.00	0.520	13.619	0.6091
14	32.00	0.618	14.102	0.7007
15	33.00	0.706	14.585	0.7780
16	34.00	0.782	15.069	0.8414
17	35.00	0.841	15.552	0.8885
18	36.00	0.887	16.035	0.9240
19	37.00	0.919	16.518	0.9482
20	38.00	0.941	17.001	0.9645
21	39.00	0.954	17.485	0.9740
22	40.00	0.962	17.968	0.9798

RUN NUMBER 232

ADSORBATE - PROPANE
CARBON PARTICLE SIZE - 25-30 MESH US STD. SIEVE
BED WEIGHT - 47.95 G CARBON
UNCORRECTED VOL. FLOW RATE - 552.5684 ML/MIN
PRESSURE DROP - 31.5 MM H2O
MASS FLOW RATE - 0.2474 G/MIN-CM2
KGAP - 0.6178 G C3H8/MIN-G BED-G C3H8/G GAS
KSAP - 1.0122 G C3H8/MIN-G BED-G C3H8/G SOLID
BIG KGAP - 0.0729 G C3H8/MIN-G BED-G C3H8/G GAS
BIG KSAP - 0.9451 G C3H8/MIN-G BED-G C3H8/G SOLID
EFFECTIVE PARTICLE DIFFUSIVITY - 5.48 X 10-5 CM2/MIN
CO - 0.2535 G C3H6/G GAS

POINT	TIME, MIN.	C	CUM. WEIGHT	C/CO
1	18.00	0.012	10.792	0.0014
2	18.25	0.016	10.967	0.0043
3	18.50	0.021	11.142	0.0079
4	18.75	0.032	11.317	0.0158
5	19.00	0.048	11.492	0.0275
6	19.25	0.082	11.667	0.0526
7	19.50	0.132	11.842	0.0905
8	19.75	0.200	12.017	0.1441
9	20.00	0.297	12.191	0.2246
10	20.50	0.521	12.541	0.4310
11	21.00	0.703	12.891	0.6234
12	21.50	0.814	13.241	0.7539
13	22.00	0.880	13.591	0.8369
14	23.00	0.939	14.290	0.9150
15	24.00	0.956	14.990	0.9383
16	25.00	0.980	15.689	0.9716
17	26.00	0.988	16.389	0.9829
18	27.00	0.991	17.088	0.9872
19	28.00	0.994	17.788	0.9914

RUN NUMBER 233

ADSORBATE - PROPYLENE
CARBON PARTICLE SIZE - 35-40 MESH US STD. SIEVE
BED WEIGHT - 50.98 G CARBON
UNCORRECTED VOL. FLOW RATE - 385.1907 ML/MIN
PRESSURE DROP - 31.0 MM H2O
MASS FLOW RATE - 0.1641 G/MIN-CM2
KGAP - 0.6461 G C3H6/MIN-G BED-G C3H6/G GAS
KSAP - 0.3184 G C3H6/MIN-G BED-G C3H6/G SOLID
BIG KGAP - 0.0318 G C3H6/MIN-G BED-G C3H6/G GAS
BIG KSAP - 0.3096 G C3H6/MIN-G BED-G C3H6/G SOLID
EFFECTIVE PARTICLE DIFFUSIVITY - 0.85 X 10-5 CM2/MIN
CO - 0.0894 G C3H6/G GAS

POINT	TIME, MIN.	C	CUM. WEIGHT	C/CO
1	27.00	0.003	11.201	0.0043
2	27.25	0.008	11.317	0.0114
3	27.50	0.018	11.433	0.0256
4	27.75	0.033	11.549	0.0465
5	28.00	0.053	11.665	0.0741
6	28.25	0.079	11.781	0.1092
7	28.50	0.108	11.897	0.1475
8	28.75	0.140	12.013	0.1887
9	29.00	0.174	12.128	0.2313
10	30.00	0.312	12.592	0.3934
11	31.00	0.438	13.056	0.5278
12	32.00	0.551	13.520	0.6387
13	33.00	0.655	13.984	0.7337
14	34.00	0.742	14.448	0.8084
15	35.00	0.814	14.911	0.8671
16	36.00	0.870	15.375	0.9110
17	37.00	0.910	15.839	0.9414
18	38.00	0.938	16.303	0.9623
19	39.00	0.953	16.767	0.9733
20	40.00	0.962	17.230	0.9798

RUN NUMBER 234

ADSORBATE - PROPANE
CARBON PARTICLE SIZE - 35-40 MESH US STD. SIEVE
BED WEIGHT - 50.98 G CARBON
UNCORRECTED VOL. FLOW RATE - 549.2996 ML/MIN
PRESSURE DROP - 49.0 MM H2O
MASS FLOW RATE - 0.2375 G/MIN-CM2
KGAP - 0.6886 G C3H8/MIN-G BED-G C3H8/G GAS
KSAP - 1.0566 G C3H8/MIN-G BED-G C3H8/G SOLID
BIG KGAP - 0.0826 G C3H8/MIN-G BED-G C3H8/G GAS
BIG KSAP - 0.9907 G C3H8/MIN-G BED-G C3H8/G SOLID
EFFECTIVE PARTICLE DIFFUSIVITY - 2.90 X 10-5 CM2/MIN
CO - 0.2421 G C3H6/G GAS

POINT	TIME, MIN.	C	CUM. WEIGHT	C/CO
1	19.00	0.012	11.010	0.0014
2	19.25	0.015	11.178	0.0036
3	19.50	0.026	11.345	0.0115
4	19.75	0.041	11.513	0.0223
5	20.00	0.071	11.681	0.0444
6	20.25	0.125	11.849	0.0851
7	20.50	0.208	12.017	0.1505
8	20.75	0.310	12.185	0.2357
9	21.00	0.432	12.352	0.3453
10	21.50	0.649	12.688	0.5637
11	22.00	0.792	13.024	0.7271
12	23.00	0.909	13.695	0.8748
13	24.00	0.949	14.367	0.9286
14	25.00	0.968	15.038	0.9549
15	26.00	0.979	15.709	0.9702
16	27.00	0.984	16.381	0.9773
17	28.00	0.988	17.052	0.9829
18	29.00	0.990	17.723	0.9858

RUN NUMBER 235

ADSORBATE - PROPYLENE
CARBON PARTICLE SIZE - 35-40 MESH US STD. SIEVE
BED WEIGHT - 50.98 G CARBON
UNCORRECTED VOL. FLOW RATE - 385.1907 ML/MIN
PRESSURE DROP - 31.0 MM H2O
MASS FLOW RATE - 0.1641 G/MIN-CM2
KGAP - 0.6267 G C3H6/MIN-G BED-G C3H6/G GAS
KSAP - 0.3140 G C3H6/MIN-G BED-G C3H6/G SOLID
BIG KGAP - 0.0312 G C3H6/MIN-G BED-G C3H6/G GAS
BIG KSAP - 0.3052 G C3H6/MIN-G BED-G C3H6/G SOLID
EFFECTIVE PARTICLE DIFFUSIVITY - 0.83 X 10-5 CM2/MIN
CO - 0.0908 G C3H6/G GAS

POINT	TIME, MIN.	C	CUM. WEIGHT	C/CO
1	27.00	0.001	11.201	0.0014
2	27.25	0.003	11.317	0.0043
3	27.50	0.006	11.433	0.0086
4	27.75	0.011	11.549	0.0157
5	28.00	0.024	11.665	0.0340
6	28.25	0.041	11.781	0.0576
7	28.50	0.064	11.897	0.0890
8	28.75	0.093	12.013	0.1278
9	29.00	0.122	12.128	0.1657
10	30.00	0.257	12.592	0.3308
11	31.00	0.390	13.056	0.4780
12	32.00	0.508	13.520	0.5975
13	33.00	0.616	13.984	0.6988
14	34.00	0.708	14.448	0.7797
15	35.00	0.788	14.911	0.8462
16	36.00	0.849	15.375	0.8947
17	37.00	0.897	15.839	0.9316
18	38.00	0.927	16.303	0.9541
19	39.00	0.948	16.767	0.9696
20	40.00	0.960	17.230	0.9784
21	41.00	0.967	17.694	0.9835

RUN NUMBER 236

ADSORBATE - PROPANE
CARBON PARTICLE SIZE - 35-40 MESH US STD. SIEVE
BED WEIGHT - 50.98 G CARBON
UNCORRECTED VOL. FLOW RATE - 549.2996 ML/MIN
PRESSURE DROP - 45.0 MM H2O
MASS FLOW RATE - 0.2465 G/MIN-CM2
KGAP - 0.6789 G C3H8/MIN-G BED-G C3H8/G GAS
KSAP - 1.0316 G C3H8/MIN-G BED-G C3H8/G SOLID
BIG KGAP - 0.0809 G C3H8/MIN-G BED-G C3H8/G GAS
BIG KSAP - 0.9679 G C3H8/MIN-G BED-G C3H8/G SOLID
EFFECTIVE PARTICLE DIFFUSIVITY - 2.84 X 10-5 CM2/MIN
CO - 0.2404 G C3H6/G GAS

POINT	TIME, MIN.	C	CUM. WEIGHT	C/CO
1	19.00	0.011	11.447	0.0007
2	19.25	0.013	11.621	0.0021
3	19.50	0.020	11.796	0.0072
4	19.75	0.030	11.970	0.0144
5	20.00	0.047	12.144	0.0267
6	20.25	0.089	12.318	0.0578
7	20.50	0.145	12.492	0.1006
8	20.75	0.231	12.667	0.1693
9	21.00	0.342	12.841	0.2636
10	21.50	0.571	13.189	0.4814
11	22.00	0.746	13.538	0.6727
12	23.00	0.896	14.235	0.8577
13	24.00	0.947	14.932	0.9259
14	25.00	0.967	15.629	0.9535
15	26.00	0.980	16.326	0.9716
16	27.00	0.987	17.023	0.9815
17	28.00	0.990	17.720	0.9858
18	29.00	0.991	18.417	0.9872

RUN NUMBER 237

ADSORBATE - PROPYLENE
CARBON PARTICLE SIZE - 35-40 MESH US STD. SIEVE
BED WEIGHT - 50.98 G CARBON
UNCORRECTED VOL. FLOW RATE - 109.3447 ML/MIN
PRESSURE DROP - 6.0 MM H2O
MASS FLOW RATE - 0.0468 G/MIN-CM2
KGAP - 0.1840 G C3H6/MIN-G BED-G C3H6/G GAS
KSAP - 0.0974 G C3H6/MIN-G BED-G C3H6/G SOLID
BIG KGAP - 0.0096 G C3H6/MIN-G BED-G C3H6/G GAS
BIG KSAP - 0.0945 G C3H6/MIN-G BED-G C3H6/G SOLID
EFFECTIVE PARTICLE DIFFUSIVITY - 0.26 X 10-5 CM2/MIN
CO - 0.0952 G C3H6/G GAS

POINT	TIME, MIN.	C	CUM. WEIGHT	C/CO
1	89.00	0.007	11.181	0.0100
2	90.00	0.012	11.313	0.0171
3	91.00	0.030	11.445	0.0424
4	92.00	0.055	11.578	0.0768
5	93.00	0.091	11.710	0.1252
6	94.00	0.130	11.842	0.1759
7	95.00	0.172	11.974	0.2289
8	96.00	0.217	12.107	0.2837
9	97.00	0.254	12.239	0.3273
10	98.00	0.295	12.371	0.3743
11	99.00	0.336	12.503	0.4199
12	100.00	0.375	12.636	0.4621
13	101.00	0.413	12.768	0.5020
14	102.00	0.448	12.900	0.5379
15	103.00	0.483	13.032	0.5730
16	104.00	0.517	13.165	0.6062
17	105.00	0.551	13.297	0.6387
18	106.00	0.582	13.429	0.6677
19	107.00	0.604	13.561	0.6879
20	108.00	0.643	13.694	0.7231
21	109.00	0.670	13.826	0.7469
22	110.00	0.700	13.958	0.7729
23	111.00	0.726	14.090	0.7950
24	112.00	0.752	14.223	0.8167
25	113.00	0.773	14.355	0.8340
26	114.00	0.795	14.487	0.8519
27	115.00	0.815	14.619	0.8679
28	116.00	0.832	14.752	0.8814
29	117.00	0.852	14.884	0.8971
30	118.00	0.868	15.016	0.9095

RUN NUMBER 237 CONTINUED

POINT	TIME, MIN.	C	CUM. WEIGHT	C/CO
31	119.00	0.883	15.148	0.9210
32	120.00	0.896	15.281	0.9309
33	121.00	0.908	15.413	0.9399
34	122.00	0.920	15.545	0.9489
35	123.00	0.928	15.677	0.9549
36	124.00	0.935	15.810	0.9600
37	125.00	0.941	15.942	0.9645
38	126.00	0.948	16.074	0.9696
39	127.00	0.950	16.206	0.9711
40	128.00	0.956	16.339	0.9755
41	129.00	0.962	16.471	0.9798
42	130.00	0.964	16.603	0.9813
43	131.00	0.967	16.735	0.9835

RUN NUMBER 238

ADSORBATE - PROPANE
CARBON PARTICLE SIZE - 35-40 MESH US STD. SIEVE
BED WEIGHT - 50.98 G CARBON
UNCORRECTED VOL. FLOW RATE - 382.0242 ML/MIN
PRESSURE DROP - 28.0 MM H2O
MASS FLOW RATE - 0.1763 G/MIN-CM2
KGAP - 0.5863 G C3H8/MIN-G BED-G C3H8/G GAS
KSAP - 0.8877 G C3H8/MIN-G BED-G C3H8/G SOLID
BIG KGAP - 0.0697 G C3H8/MIN-G BED-G C3H8/G GAS
BIG KSAP - 0.8330 G C3H8/MIN-G BED-G C3H8/G SOLID
EFFECTIVE PARTICLE DIFFUSIVITY - 2.44 X 10-5 CM2/MIN
CO - 0.2398 G C3H6/G GAS

POINT	TIME, MIN.	C	CUM. WEIGHT	C/CO
1	26.75	0.012	11.924	0.0014
2	27.00	0.020	12.048	0.0072
3	27.25	0.030	12.173	0.0144
4	27.50	0.047	12.297	0.0267
5	27.75	0.076	12.422	0.0481
6	28.00	0.120	12.547	0.0813
7	28.25	0.183	12.671	0.1305
8	28.50	0.267	12.796	0.1991
9	29.00	0.469	13.045	0.3803
10	29.50	0.645	13.294	0.5594
11	30.00	0.768	13.544	0.6985
12	31.00	0.887	14.042	0.8460
13	32.00	0.932	14.540	0.9056
14	33.00	0.955	15.039	0.9369
15	34.00	0.967	15.537	0.9535
16	35.00	0.975	16.036	0.9646
17	36.00	0.980	16.534	0.9716
18	37.00	0.985	17.033	0.9787
19	38.00	0.988	17.531	0.9829
20	39.00	0.990	18.029	0.9858
21	40.00	0.992	18.528	0.9886

RUN NUMBER 240

ADSORBATE - PROPANE
CARBON PARTICLE SIZE - 35-40 MESH US STD. SIEVE
BED WEIGHT - 50.98 G CARBON
UNCORRECTED VOL. FLOW RATE - 382.0242 ML/MIN
PRESSURE DROP - 30.0 MM H2O
MASS FLOW RATE - 0.1718 G/MIN-CM2
KGAP - 0.5792 G C3H8/MIN-G BED-G C3H8/G GAS
KSAP - 0.9087 G C3H8/MIN-G BED-G C3H8/G SOLID
BIG KGAP - 0.0706 G C3H8/MIN-G BED-G C3H8/G GAS
BIG KSAP - 0.8509 G C3H8/MIN-G BED-G C3H8/G SOLID
EFFECTIVE PARTICLE DIFFUSIVITY - 2.49 X 10-5 CM2/MIN
CD - 0.2459 G C3H6/G GAS

POINT	TIME, MIN.	C	CUM. WEIGHT	C/CO
1	26.75	0.013	11.607	0.0021
2	27.00	0.019	11.729	0.0064
3	27.25	0.024	11.850	0.0100
4	27.50	0.037	11.972	0.0194
5	27.75	0.060	12.093	0.0363
6	28.00	0.094	12.214	0.0616
7	28.25	0.145	12.336	0.1006
8	28.50	0.214	12.457	0.1554
9	29.00	0.408	12.700	0.3231
10	29.50	0.597	12.943	0.5084
11	30.00	0.738	13.186	0.6634
12	31.00	0.879	13.671	0.8356
13	32.00	0.931	14.157	0.9042
14	33.00	0.955	14.643	0.9369
15	34.00	0.970	15.128	0.9576
16	35.00	0.980	15.614	0.9716
17	36.00	0.985	16.100	0.9787
18	37.00	0.988	16.585	0.9829
19	38.00	0.990	17.071	0.9858
20	39.00	0.992	17.556	0.9886
21	40.00	0.995	18.042	0.9929

RUN NUMBER 241

ADSORBATE - PROPYLENE
CARBON PARTICLE SIZE - 35-40 MESH US STD. SIEVE
BED WEIGHT - 50.98 G CARBON
UNCORRECTED VOL. FLOW RATE - 224.7787 ML/MIN
PRESSURE DROP - 20.5 MM H2O
MASS FLOW RATE - C.0871 G/MIN-CM2
KGAP - 0.5307 G C3H6/MIN-G BED-G C3H6/G GAS
KSAP - 0.2027 G C3H6/MIN-G BED-G C3H6/G SOLID
BIG KGAP - 0.0208 G C3H6/MIN-G BED-G C3H6/G GAS
BIG KSAP - 0.1983 G C3H6/MIN-G BED-G C3H6/G SOLID
EFFECTIVE PARTICLE DIFFUSIVITY - 0.54 X 10-5 CM2/MIN
CO - 0.0712 G C3H6/G GAS

POINT	TIME, MIN.	C	CUM. WEIGHT	C/CO
1	44.25	0.002	10.039	0.0029
2	44.50	0.004	10.101	0.0057
3	44.75	0.010	10.162	0.0142
4	45.00	0.021	10.224	0.0298
5	45.25	0.030	10.286	0.0424
6	45.50	0.042	10.347	0.0590
7	45.75	0.058	10.409	0.0809
8	46.00	0.078	10.470	0.1079
9	46.25	0.098	10.532	0.1344
10	46.50	0.120	10.593	0.1631
11	46.75	0.141	10.655	0.1900
12	47.00	0.165	10.717	0.2202
13	48.00	0.257	10.963	0.3308
14	49.00	0.344	11.209	0.4287
15	50.00	0.422	11.455	0.5113
16	51.00	0.498	11.702	0.5877
17	52.00	0.566	11.948	0.6528
18	53.00	0.629	12.194	0.7106
19	54.00	0.688	12.441	0.7625
20	55.00	0.741	12.687	0.8076
21	56.00	0.792	12.933	0.8495
22	57.00	0.832	13.180	0.8814
23	58.00	0.869	13.426	0.9103
24	59.00	0.895	13.672	0.9301
25	60.00	0.917	13.919	0.9467
26	61.00	0.937	14.165	0.9615
27	62.00	0.948	14.411	0.9696
28	63.00	0.958	14.658	0.9769
29	64.00	0.962	14.904	0.9798
30	65.00	0.965	15.150	0.9820

RUN NUMBER 242

ADSORBATE - PROPANE
CARBON PARTICLE SIZE - 35-40 MESH US STD. SIEVE
BED WEIGHT - 50.98 G CARBON
UNCORRECTED VOL. FLOW RATE - 109.7316 ML/MIN
PRESSURE DROP - 8.0 MM H2O
MASS FLOW RATE - 0.0446 G/MIN-CM2
KGAP - 0.2132 G C3H8/MIN-G BED-G C3H8/G GAS
KSAP - 0.3077 G C3H8/MIN-G BED-G C3H8/G SOLID
BIG KGAP - 0.0245 G C3H8/MIN-G BED-G C3H8/G GAS
BIG KSAP - 0.2896 G C3H8/MIN-G BED-G C3H8/G SOLID
EFFECTIVE PARTICLE DIFFUSIVITY - 0.85 X 10-5 CM2/MIN
CO - 0.2317 G C3H6/G GAS

POINT	TIME, MIN.	C	CUM. WEIGHT	C/CO
1	87.50	0.016	10.460	0.0043
2	88.00	0.017	10.524	0.0050
3	88.50	0.020	10.587	0.0072
4	89.00	0.028	10.650	0.0129
5	89.50	0.036	10.713	0.0187
6	90.00	0.049	10.776	0.0282
7	90.50	0.068	10.839	0.0422
8	91.00	0.096	10.902	0.0631
9	91.50	0.128	10.965	0.0874
10	92.00	0.169	11.029	0.1194
11	93.00	0.273	11.155	0.2042
12	94.00	0.402	11.281	0.3176
13	95.00	0.532	11.407	0.4419
14	96.00	0.648	11.533	0.5626
15	97.00	0.739	11.660	0.6646
16	98.00	0.805	11.786	0.7429
17	99.00	0.852	11.912	0.8012
18	100.00	0.889	12.038	0.8486
19	101.00	0.911	12.165	0.8775
20	102.00	0.929	12.291	0.9015
21	103.00	0.944	12.417	0.9218
22	104.00	0.953	12.543	0.9341
23	105.00	0.960	12.670	0.9438
24	106.00	0.969	12.796	0.9562
25	107.00	0.972	12.922	0.9604
26	108.00	0.978	13.048	0.9688
27	109.00	0.980	13.174	0.9716
28	110.00	0.981	13.301	0.9730

RUN NUMBER 243

ADSORBATE - PROPYLENE
CARBON PARTICLE SIZE - 35-40 MESH US STD. SIEVE
BED WEIGHT - 50.98 G CARBON
UNCORRECTED VOL. FLOW RATE - 226.4182 ML/MIN
PRESSURE DROP - 16.0 MM H2O
MASS FLOW RATE - 0.0979 G/MIN-CM2
KGAP - 0.3784 G C3H6/MIN-G BED-G C3H6/G GAS
KSAP - 0.2033 G C3H6/MIN-G BED-G C3H6/G SOLID
BIG KGAP - 0.0200 G C3H6/MIN-G BED-G C3H6/G GAS
BIG KSAP - 0.1972 G C3H6/MIN-G BED-G C3H6/G SOLID
EFFECTIVE PARTICLE DIFFUSIVITY - 0.54 X 10-5 CM2/MIN
CD - 0.0965 G C3H6/G GAS

POINT	TIME, MIN.	C	CUM. WEIGHT	C/CO
1	44.50	0.005	11.385	0.0071
2	44.75	0.008	11.454	0.0114
3	45.00	0.009	11.523	0.0128
4	45.25	0.011	11.592	0.0157
5	45.50	0.020	11.662	0.0284
6	45.75	0.032	11.731	0.0451
7	46.00	0.046	11.800	0.0645
8	46.25	0.061	11.869	0.0850
9	46.50	0.079	11.938	0.1092
10	46.75	0.099	12.007	0.1357
11	47.00	0.120	12.077	0.1631
12	48.00	0.215	12.353	0.2813
13	49.00	0.300	12.630	0.3800
14	50.00	0.381	12.907	0.4685
15	51.00	0.459	13.183	0.5490
16	52.00	0.530	13.460	0.6187
17	53.00	0.595	13.737	0.6797
18	54.00	0.657	14.013	0.7355
19	55.00	0.711	14.290	0.7823
20	56.00	0.763	14.567	0.8258
21	57.00	0.809	14.844	0.8632
22	58.00	0.846	15.120	0.8924
23	59.00	0.878	15.397	0.9172
24	60.00	0.903	15.674	0.9362
25	61.00	0.923	15.950	0.9511
26	62.00	0.940	16.227	0.9637
27	63.00	0.953	16.504	0.9733
28	64.00	0.960	16.780	0.9784
29	65.00	0.965	17.057	0.9820

RUN NUMBER 244

ADSORBATE - PROPANE
CARBON PARTICLE SIZE - 35-40 MESH US STD. SIEVE
BED WEIGHT - 50.98 G CARBON
UNCORRECTED VOL. FLOW RATE - 109.2123 ML/MIN
PRESSURE DROP - 4.0 MM H2O
MASS FLOW RATE - 0.0534 G/MIN-CM2
KGAP - 0.2278 G C3H8/MIN-G BED-G C3H8/G GAS
KSAP - 0.3013 G C3H8/MIN-G BED-G C3H8/G SOLID
BIG KGAP - 0.0246 G C3H8/MIN-G BED-G C3H8/G GAS
BIG KSAP - 0.2850 G C3H8/MIN-G BED-G C3H8/G SOLID
EFFECTIVE PARTICLE DIFFUSIVITY - 0.84 X 10-5 CM2/MIN
CO - 0.2174 G C3H6/G GAS

POINT	TIME, MIN.	C	CUM. WEIGHT	C/CO
1	88.50	0.012	12.703	0.0014
2	89.00	0.013	12.778	0.0021
3	89.50	0.019	12.854	0.0064
4	90.00	0.023	12.929	0.0093
5	90.50	0.034	13.004	0.0173
6	91.00	0.047	13.080	0.0267
7	91.50	0.070	13.155	0.0437
8	92.00	0.097	13.231	0.0638
9	92.50	0.129	13.306	0.0882
10	93.00	0.170	13.382	0.1202
11	94.00	0.278	13.532	0.2084
12	95.00	0.405	13.683	0.3203
13	96.00	0.538	13.834	0.4480
14	97.00	0.650	13.985	0.5648
15	98.00	0.738	14.136	0.6634
16	99.00	0.803	14.287	0.7405
17	100.00	0.851	14.438	0.7999
18	101.00	0.886	14.588	0.8447
19	102.00	0.910	14.739	0.8762
20	103.00	0.928	14.890	0.9002
21	104.00	0.941	15.041	0.9177
22	105.00	0.952	15.192	0.9328
23	106.00	0.960	15.343	0.9438
24	107.00	0.967	15.493	0.9535
25	108.00	0.969	15.644	0.9562
26	109.00	0.971	15.795	0.9590
27	110.00	0.976	15.946	0.9660

RUN NUMBER 245

ADSORBATE - PROPYLENE
CARBON PARTICLE SIZE - 35-40 MESH US STD. SIEVE
BED WEIGHT - 50.98 G CARBON
UNCORRECTED VOL. FLOW RATE - 549.2996 ML/MIN
PRESSURE DROP - 42.0 MM H2O
MASS FLOW RATE - 0.2422 G/MIN-CM2
KGAP - 0.7491 G C3H6/MIN-G BED-G C3H6/G GAS
KSAP - 0.4017 G C3H6/MIN-G BED-G C3H6/G SOLID
BIG KGAP - 0.0396 G C3H6/MIN-G BED-G C3H6/G GAS
BIG KSAP - 0.3897 G C3H6/MIN-G BED-G C3H6/G SOLID
EFFECTIVE PARTICLE DIFFUSIVITY - 1.07 X 10-5 CM2/MIN
CD - 0.0964 G C3H6/G GAS

POINT	TIME, MIN.	C	CUM. WEIGHT	C/CO
1	19.25	0.001	11.430	0.0014
2	19.50	0.002	11.602	0.0029
3	19.75	0.004	11.773	0.0057
4	20.00	0.005	11.944	0.0071
5	20.25	0.013	12.115	0.0185
6	20.50	0.032	12.286	0.0451
7	20.75	0.058	12.457	0.0809
8	21.00	0.092	12.629	0.1265
9	21.25	0.130	12.800	0.1759
10	22.00	0.264	13.313	0.3389
11	23.00	0.433	13.998	0.5227
12	24.00	0.579	14.683	0.6649
13	25.00	0.704	15.368	0.7763
14	26.00	0.800	16.052	0.8559
15	27.00	0.871	16.737	0.9118
16	28.00	0.914	17.422	0.9444
17	29.00	0.943	18.107	0.9659
18	30.00	0.957	18.791	0.9762
19	31.00	0.967	19.476	0.9835
20	32.00	0.970	20.161	0.9856

RUN NUMBER 246

ADSORBATE - PROPANE
CARBON PARTICLE SIZE - 35-40 MESH US STD. SIEVE
BED WEIGHT - 50.98 G CARBON
UNCORRECTED VOL. FLOW RATE - 225.8684 ML/MIN
PRESSURE DROP - 19.0 MM H2O
MASS FLOW RATE - 0.0952 G/MIN-CM2
KGAP - 0.4086 G C3H8/MIN-G BED-G C3H8/G GAS
KSAP - 0.6326 G C3H8/MIN-G BED-G C3H8/G SOLID
BIG KGAP - 0.0493 G C3H8/MIN-G BED-G C3H8/G GAS
BIG KSAP - 0.5928 G C3H8/MIN-G BED-G C3H8/G SOLID
EFFECTIVE PARTICLE DIFFUSIVITY - 1.74 X 10-5 CM2/MIN
CO - 0.2436 G C3H6/G GAS

POINT	TIME, MIN.	C	CUM. WEIGHT	C/CO
1	44.50	0.015	11.053	0.0036
2	44.75	0.019	11.121	0.0064
3	45.00	0.023	11.188	0.0093
4	45.25	0.032	11.255	0.0158
5	45.50	0.043	11.323	0.0238
6	45.75	0.061	11.390	0.0370
7	46.00	0.085	11.457	0.0548
8	46.25	0.115	11.525	0.0775
9	46.50	0.157	11.592	0.1099
10	46.75	0.204	11.659	0.1473
11	47.00	0.263	11.726	0.1958
12	47.50	0.399	11.861	0.3148
13	48.00	0.530	11.996	0.4400
14	48.50	0.642	12.130	0.5562
15	49.00	0.736	12.265	0.6611
16	50.00	0.851	12.534	0.7999
17	51.00	0.909	12.803	0.8748
18	52.00	0.938	13.072	0.9137
19	53.00	0.958	13.342	0.9410
20	54.00	0.968	13.611	0.9549
21	55.00	0.977	13.880	0.9674
22	56.00	0.981	14.149	0.9730
23	57.00	0.985	14.418	0.9787

RUN NUMBER 247

ADSORBATE - PROPYLENE
CARBON PARTICLE SIZE - 35-40 MESH US STD. SIEVE
BED WEIGHT - 50.98 G CARBON
UNCORRECTED VOL. FLOW RATE - 549.2996 ML/MIN
PRESSURE DROP - 50.0 MM H2O
MASS FLOW RATE - 0.2249 G/MIN-CM2
KGAP - 0.8984 G C3H6/MIN-G BED-G C3H6/G GAS
KSAP - 0.4150 G C3H6/MIN-G BED-G C3H6/G SOLID
BIG KGAP - 0.0417 G C3H6/MIN-G BED-G C3H6/G GAS
BIG KSAP - 0.4043 G C3H6/MIN-G BED-G C3H6/G SOLID
EFFECTIVE PARTICLE DIFFUSIVITY - 1.11 X 10-5 CM2/MIN
CO - 0.0845 G C3H6/G GAS

POINT	TIME, MIN.	C	CUM. WEIGHT	C/CO
1	20.00	0.002	11.058	0.0029
2	20.25	0.005	11.217	0.0071
3	20.50	0.008	11.376	0.0114
4	20.75	0.030	11.535	0.0424
5	21.00	0.058	11.694	0.0809
6	21.25	0.093	11.853	0.1278
7	21.50	0.136	12.012	0.1836
8	22.00	0.230	12.330	0.2991
9	23.00	0.393	12.966	0.4811
10	24.00	0.547	13.602	0.6349
11	25.00	0.673	14.238	0.7495
12	26.00	0.779	14.873	0.8389
13	27.00	0.853	15.509	0.8979
14	28.00	0.903	16.145	0.9362
15	29.00	0.935	16.781	0.9600
16	30.00	0.951	17.417	0.9718
17	31.00	0.959	18.053	0.9777
18	32.00	0.963	18.688	0.9806
19	33.00	0.968	19.324	0.9842

RUN NUMBER 248

ADSORBATE - PROPANE
CARBON PARTICLE SIZE - 35-40 MESH US STD. SIEVE
BED WEIGHT - 50.98 G CARBON
UNCORRECTED VOL. FLOW RATE - 225.8684 ML/MIN
PRESSURE DROP - 15.0 MM H2O
MASS FLOW RATE - 0.1043 G/MIN-CM2
KGAP - 0.4348 G C3H8/MIN-G BED-G C3H8/G GAS
KSAP - 0.5957 G C3H8/MIN-G BED-G C3H8/G SOLID
BIG KGAP - 0.0482 G C3H8/MIN-G BED-G C3H8/G GAS
BIG KSAP - 0.5623 G C3H8/MIN-G BED-G C3H8/G SOLID
EFFECTIVE PARTICLE DIFFUSIVITY - 1.65 X 10-5 CM2/MIN
CD - 0.2231 G C3H6/G GAS

POINT	TIME, MIN.	C	CUM. WEIGHT	C/CO
1	44.50	0.013	12.134	0.0021
2	44.75	0.015	12.208	0.0036
3	45.00	0.017	12.282	0.0050
4	45.25	0.021	12.355	0.0079
5	45.50	0.030	12.429	0.0144
6	45.75	0.039	12.503	0.0209
7	46.00	0.054	12.576	0.0319
8	46.25	0.073	12.650	0.0459
9	46.50	0.104	12.724	0.0691
10	46.75	0.142	12.798	0.0983
11	47.00	0.188	12.871	0.1345
12	47.50	0.301	13.019	0.2280
13	48.00	0.431	13.166	0.3444
14	48.50	0.560	13.313	0.4702
15	49.00	0.670	13.461	0.5867
16	49.50	0.756	13.608	0.6844
17	50.00	0.818	13.756	0.7588
18	51.00	0.892	14.050	0.8525
19	52.00	0.932	14.345	0.9056
20	53.00	0.953	14.640	0.9341
21	54.00	0.967	14.935	0.9535
22	55.00	0.974	15.229	0.9632
23	56.00	0.977	15.524	0.9674
24	57.00	0.987	15.819	0.9815

RUN NUMBER 249

ADSORBATE - PROPYLENE
CARBON PARTICLE SIZE - 40-45 MESH US STD. SIEVE
BED WEIGHT - 46.85 G CARBON
UNCORRECTED VOL. FLOW RATE - 549.2996 ML/MIN
PRESSURE DROP - 49.0 MM H2O
MASS FLOW RATE - 0.2317 G/MIN-CM2
KGAP - 0.9873 G C3H6/MIN-G BED-G C3H6/G GAS
KSAP - 0.4485 G C3H6/MIN-G BED-G C3H6/G SOLID
BIG KGAP - 0.0415 G C3H6/MIN-G BED-G C3H6/G GAS
BIG KSAP - 0.4371 G C3H6/MIN-G BED-G C3H6/G SOLID
EFFECTIVE PARTICLE DIFFUSIVITY - 0.84 X 10-5 CM2/MIN
CO - 0.0832 G C3H6/G GAS

POINT	TIME, MIN.	C	CUM. WEIGHT	C/CO
1	18.50	0.001	10.425	0.0014
2	18.75	0.002	10.589	0.0029
3	19.00	0.003	10.753	0.0043
4	19.25	0.004	10.917	0.0057
5	19.50	0.013	11.081	0.0185
6	19.75	0.035	11.244	0.0493
7	20.00	0.069	11.408	0.0958
8	20.25	0.112	11.572	0.1527
9	20.50	0.159	11.736	0.2127
10	21.00	0.260	12.063	0.3343
11	22.00	0.442	12.718	0.5318
12	23.00	0.597	13.374	0.6815
13	24.00	0.723	14.029	0.7924
14	25.00	0.820	14.684	0.8719
15	26.00	0.889	15.339	0.9256
16	27.00	0.927	15.994	0.9541
17	28.00	0.947	16.649	0.9689
18	29.00	0.955	17.305	0.9747
19	30.00	0.961	17.960	0.9791
20	31.00	0.964	18.615	0.9813

RUN NUMBER 250

ADSORBATE - PROPANE
CARBON PARTICLE SIZE - 40-45 MESH US STD. SIEVE
BED WEIGHT - 46.85 G CARBON
UNCORRECTED VOL. FLOW RATE - 225.8684 ML/MIN
PRESSURE DROP - 23.0 MM H2O
MASS FLOW RATE - 0.0898 G/MIN-CM2
KGAP - 0.5111 G C3H8/MIN-G BED-G C3H8/G GAS
KSAP - 0.6935 G C3H8/MIN-G BED-G C3H8/G SOLID
BIG KGAP - 0.0517 G C3H8/MIN-G BED-G C3H8/G GAS
BIG KSAP - 0.6550 G C3H8/MIN-G BED-G C3H8/G SOLID
EFFECTIVE PARTICLE DIFFUSIVITY - 1.35 X 10-5 CM2/MIN
CD - 0.2215 G C3H6/G GAS

POINT	TIME, MIN.	C	CUM. WEIGHT	C/CO
1	42.75	0.015	9.958	0.0036
2	43.00	0.018	10.022	0.0057
3	43.25	0.027	10.085	0.0122
4	43.50	0.037	10.149	0.0194
5	43.75	0.054	10.212	0.0319
6	44.00	0.082	10.275	0.0526
7	44.25	0.122	10.339	0.0828
8	44.50	0.175	10.402	0.1241
9	44.75	0.244	10.466	0.1800
10	45.00	0.325	10.529	0.2487
11	45.50	0.500	10.656	0.4103
12	46.00	0.640	10.783	0.5540
13	46.50	0.749	10.910	0.6762
14	47.00	0.821	11.037	0.7625
15	48.00	0.889	11.291	0.8486
16	49.00	0.935	11.544	0.9096
17	50.00	0.953	11.798	0.9341
18	51.00	0.967	12.052	0.9535
19	52.00	0.974	12.306	0.9632
20	53.00	0.979	12.559	0.9702
21	54.00	0.981	12.813	0.9730
22	55.00	0.983	13.067	0.9759

RUN NUMBER 251

ADSORBATE - PROPYLENE
CARBON PARTICLE SIZE - 40-45 MESH US STD. SIEVE
BED WEIGHT - 46.85 G CARBON
UNCORRECTED VOL. FLOW RATE - 538.1594 ML/MIN
PRESSURE DROP - 52.0 MM H2O
MASS FLOW RATE - 0.2185 G/MIN-CM2
KGAP - 0.7054 G C3H6/MIN-G BED-G C3H6/G GAS
KSAP - 0.4508 G C3H6/MIN-G BED-G C3H6/G SOLID
BIG KGAP - 0.0398 G C3H6/MIN-G BED-G C3H6/G GAS
BIG KSAP - 0.4348 G C3H6/MIN-G BED-G C3H6/G SOLID
EFFECTIVE PARTICLE DIFFUSIVITY - 0.83 X 10-5 CM2/MIN
CO - 0.1122 G C3H6/G GAS

POINT	TIME, MIN.	C	CUM. WEIGHT	C/CO
1	18.75	0.001	9.958	0.0014
2	19.00	0.002	10.112	0.0029
3	19.25	0.005	10.266	0.0071
4	19.50	0.008	10.421	0.0114
5	19.75	0.015	10.575	0.0213
6	20.00	0.039	10.730	0.0549
7	20.25	0.074	10.884	0.1025
8	20.50	0.115	11.038	0.1566
9	20.75	0.162	11.193	0.2164
10	21.00	0.220	11.347	0.2872
11	22.00	0.399	11.965	0.4874
12	23.00	0.557	12.583	0.6444
13	24.00	0.691	13.200	0.7651
14	25.00	0.800	13.818	0.8559
15	26.00	0.875	14.436	0.9149
16	27.00	0.920	15.053	0.9489
17	28.00	0.946	15.671	0.9681
18	29.00	0.958	16.289	0.9769
19	30.00	0.964	16.906	0.9813
20	31.00	0.967	17.524	0.9835

RUN NUMBER 252

ADSORBATE - PROPANE
CARBON PARTICLE SIZE - 40-45 MESH US STD. SIEVE
BED WEIGHT - 46.85 G CARBON
UNCORRECTED VOL. FLOW RATE - 223.6892 ML/MIN
PRESSURE DROP - 17.0 MM H2O
MASS FLOW RATE - 0.1016 G/MIN-CM2
KGAP - 0.4871 G C3H8/MIN-G BED-G C3H8/G GAS
KSAP - 0.7674 G C3H8/MIN-G BED-G C3H8/G SOLID
BIG KGAP - 0.0547 G C3H8/MIN-G BED-G C3H8/G GAS
BIG KSAP - 0.7183 G C3H8/MIN-G BED-G C3H8/G SOLID
EFFECTIVE PARTICLE DIFFUSIVITY - 1.48 X 10-5 CM2/MIN
CO - 0.2466 G C3H6/G GAS

POINT	TIME, MIN.	C	CUM. WEIGHT	C/CO
1	42.75	0.013	11.316	0.0021
2	43.00	0.016	11.387	0.0043
3	43.25	0.019	11.459	0.0064
4	43.50	0.022	11.531	0.0086
5	43.75	0.030	11.603	0.0144
6	44.00	0.045	11.675	0.0253
7	44.25	0.065	11.746	0.0400
8	44.50	0.098	11.818	0.0646
9	44.75	0.142	11.890	0.0983
10	45.00	0.197	11.962	0.1417
11	45.50	0.352	12.106	0.2725
12	46.00	0.520	12.249	0.4300
13	46.50	0.661	12.393	0.5768
14	47.00	0.765	12.536	0.6949
15	48.00	0.879	12.824	0.8356
16	49.00	0.929	13.111	0.9015
17	50.00	0.955	13.398	0.9369
18	51.00	0.969	13.686	0.9562
19	52.00	0.979	13.973	0.9702
20	53.00	0.983	14.260	0.9759
21	54.00	0.990	14.547	0.9858
22	55.00	0.995	14.835	0.9929

RUN NUMBER 253

ADSORBATE - PROPYLENE
CARBON PARTICLE SIZE - 40-45 MESH US STD. SIEVE
BED WEIGHT - 46.85 G CARBON
UNCORRECTED VOL. FLOW RATE - 223.1495 ML/MIN
PRESSURE DROP - 21.0 MM H2O
MASS FLOW RATE - 0.0884 G/MIN-CM2
KGAP - 0.4319 G C3H6/MIN-G BED-G C3H6/G GAS
KSAP - 0.2120 G C3H6/MIN-G BED-G C3H6/G SOLID
BIG KGAP - 0.0194 G C3H6/MIN-G BED-G C3H6/G GAS
BIG KSAP - 0.2061 G C3H6/MIN-G BED-G C3H6/G SOLID
EFFECTIVE PARTICLE DIFFUSIVITY - 0.40 X 10-5 CM2/MIN
CD - 0.0891 G C3H6/G GAS

POINT	TIME, MIN.	C	CUM. WEIGHT	C/CO
1	42.50	0.004	9.750	0.0057
2	43.00	0.007	9.875	0.0100
3	43.50	0.018	10.000	0.0256
4	44.00	0.047	10.125	0.0659
5	44.50	0.087	10.250	0.1199
6	45.00	0.130	10.375	0.1759
7	46.00	0.235	10.624	0.3051
8	47.00	0.322	10.874	0.4045
9	48.00	0.401	11.124	0.4895
10	49.00	0.478	11.374	0.5680
11	50.00	0.550	11.624	0.6378
12	51.00	0.615	11.874	0.6979
13	52.00	0.677	12.123	0.7530
14	53.00	0.734	12.373	0.8017
15	54.00	0.784	12.623	0.8430
16	55.00	0.828	12.873	0.8783
17	56.00	0.864	13.123	0.9064
18	57.00	0.894	13.373	0.9294
19	58.00	0.918	13.622	0.9474
20	59.00	0.937	13.872	0.9615
21	60.00	0.951	14.122	0.9718
22	61.00	0.958	14.372	0.9769
23	62.00	0.965	14.622	0.9820
24	63.00	0.970	14.872	0.9856

RUN NUMBER 254

ADSORBATE - PROPANE
CARBON PARTICLE SIZE - 40-45 MESH US STD. SIEVE
BED WEIGHT - 46.85 G CARBON
UNCORRECTED VOL. FLOW RATE - 108.7031 ML/MIN
PRESSURE DROP - 12.0 MM H2O
MASS FLOW RATE - 0.0380 G/MIN-CM2
KGAP - 0.2137 G C3H8/MIN-G BED-G C3H8/G GAS
KSAP - 0.3548 G C3H8/MIN-G BED-G C3H8/G SOLID
BIG KGAP - 0.0248 G C3H8/MIN-G BED-G C3H8/G GAS
BIG KSAP - 0.3310 G C3H8/MIN-G BED-G C3H8/G SOLID
EFFECTIVE PARTICLE DIFFUSIVITY - 0.68 X 10-5 CM2/MIN
CO - 0.2559 G C3H6/G GAS

POINT	TIME, MIN.	C	CUM. WEIGHT	C/CO
1	85.00	0.012	8.592	0.0014
2	85.50	0.014	8.646	0.0029
3	86.00	0.017	8.699	0.0050
4	86.50	0.021	8.753	0.0079
5	87.00	0.027	8.807	0.0122
6	87.50	0.038	8.860	0.0202
7	88.00	0.048	8.914	0.0275
8	88.50	0.068	8.968	0.0422
9	89.00	0.098	9.022	0.0646
10	89.50	0.131	9.075	0.0897
11	90.00	0.177	9.129	0.1257
12	91.00	0.304	9.236	0.2306
13	92.00	0.458	9.344	0.3698
14	93.00	0.600	9.451	0.5115
15	94.00	0.714	9.558	0.6359
16	95.00	0.795	9.666	0.7308
17	96.00	0.852	9.773	0.8012
18	97.00	0.889	9.881	0.8486
19	98.00	0.916	9.988	0.8841
20	99.00	0.935	10.095	0.9096
21	100.00	0.950	10.203	0.9300
22	101.00	0.959	10.310	0.9424
23	102.00	0.968	10.418	0.9549
24	103.00	0.972	10.525	0.9604
25	104.00	0.975	10.632	0.9646
26	105.00	0.979	10.740	0.9702

RUN NUMBER 255

ADSORBATE - PROPYLENE
CARBON PARTICLE SIZE - 40-45 MESH US STD. SIEVE
BED WEIGHT - 46.85 G CARBON
UNCORRECTED VOL. FLOW RATE - 223.1495 ML/MIN
PRESSURE DROP - 19.0 MM H2O
MASS FLOW RATE - 0.0926 G/MIN-CM2
KGAP - 0.5252 G C3H6/MIN-G BED-G C3H6/G GAS
KSAP - 0.2109 G C3H6/MIN-G BED-G C3H6/G SOLID
BIG KGAP - 0.0198 G C3H6/MIN-G BED-G C3H6/G GAS
BIG KSAP - 0.2061 G C3H6/MIN-G BED-G C3H6/G SOLID
EFFECTIVE PARTICLE DIFFUSIVITY - 0.40 X 10-5 CM2/MIN
CO - 0.0745 G C3H6/G GAS

POINT	TIME, MIN.	C	CUM. WEIGHT	C/CO
1	42.50	0.001	10.231	0.0014
2	43.00	0.003	10.362	0.0043
3	43.50	0.007	10.493	0.0100
4	44.00	0.023	10.624	0.0326
5	44.50	0.053	10.755	0.0741
6	45.00	0.092	10.886	0.1265
7	45.50	0.139	11.017	0.1874
8	46.00	0.195	11.147	0.2571
9	47.00	0.281	11.409	0.3594
10	48.00	0.368	11.671	0.4546
11	49.00	0.449	11.933	0.5389
12	50.00	0.521	12.195	0.6101
13	51.00	0.589	12.456	0.6742
14	52.00	0.651	12.718	0.7302
15	53.00	0.710	12.980	0.7814
16	54.00	0.762	13.242	0.8250
17	55.00	0.809	13.504	0.8632
18	56.00	0.849	13.765	0.8947
19	57.00	0.881	14.027	0.9195
20	58.00	0.909	14.289	0.9407
21	59.00	0.929	14.551	0.9556
22	60.00	0.945	14.813	0.9674
23	61.00	0.954	15.074	0.9740
24	62.00	0.963	15.336	0.9806
25	63.00	0.968	15.598	0.9842

RUN NUMBER 256

ADSORBATE - PROPANE
CARBON PARTICLE SIZE - 40-45 MESH US STD. SIEVE
BED WEIGHT - 46.85 G CARBON
UNCORRECTED VOL. FLOW RATE - 108.8253 ML/MIN
PRESSURE DROP - 10.0 MM H2O
MASS FLOW RATE - 0.0425 G/MIN-CM2
KGAP - 0.2187 G C3H8/MIN-G BED-G C3H8/G GAS
KSAP - 0.3484 G C3H8/MIN-G BED-G C3H8/G SOLID
BIG KGAP - 0.0247 G C3H8/MIN-G BED-G C3H8/G GAS
BIG KSAP - 0.3259 G C3H8/MIN-G BED-G C3H8/G SOLID
EFFECTIVE PARTICLE DIFFUSIVITY - 0.67 X 10-5 CM2/MIN
CO - 0.2486 G C3H6/G GAS

POINT	TIME, MIN.	C	CUM. WEIGHT	C/CO
1	85.50	0.011	9.700	0.0007
2	86.00	0.013	9.761	0.0021
3	86.50	0.019	9.821	0.0064
4	87.00	0.021	9.881	0.0079
5	87.50	0.031	9.941	0.0151
6	88.00	0.041	10.001	0.0223
7	88.50	0.057	10.061	0.0341
8	89.00	0.083	10.121	0.0533
9	89.50	0.116	10.181	0.0782
10	90.00	0.160	10.241	0.1123
11	90.50	0.211	10.301	0.1530
12	91.00	0.276	10.361	0.2067
13	92.00	0.425	10.481	0.3388
14	93.00	0.573	10.601	0.4835
15	94.00	0.693	10.721	0.6122
16	95.00	0.780	10.842	0.7128
17	96.00	0.839	10.962	0.7848
18	97.00	0.883	11.082	0.8408
19	98.00	0.910	11.202	0.8762
20	99.00	0.931	11.322	0.9042
21	100.00	0.947	11.442	0.9259
22	101.00	0.957	11.562	0.9396
23	102.00	0.966	11.682	0.9521
24	103.00	0.969	11.802	0.9562
25	104.00	0.972	11.923	0.9604
26	105.00	0.977	12.043	0.9674

RUN NUMBER 257

ADSORBATE - PROPYLENE
CARBON PARTICLE SIZE - 40-45 MESH US STD. SIEVE
BED WEIGHT - 46.85 G CARBON
UNCORRECTED VOL. FLOW RATE - 107.9394 ML/MIN
PRESSURE DROP - 8.0 MM H2O
MASS FLOW RATE - 0.0443 G/MIN-CM2
KGAP - 0.1956 G C3H6/MIN-G BED-G C3H6/G GAS
KSAP - 0.0980 G C3H6/MIN-G BED-G C3H6/G SOLID
BIG KGAP - 0.0090 G C3H6/MIN-G BED-G C3H6/G GAS
BIG KSAP - 0.0952 G C3H6/MIN-G BED-G C3H6/G SOLID
EFFECTIVE PARTICLE DIFFUSIVITY - 0.18 X 10-5 CM2/MIN
CO - 0.0908 G C3H6/G GAS

POINT	TIME, MIN.	C	CUM. WEIGHT	C/CO
1	86.00	0.002	10.200	0.0029
2	87.00	0.008	10.326	0.0114
3	88.00	0.012	10.451	0.0171
4	89.00	0.033	10.576	0.0465
5	90.00	0.071	10.701	0.0985
6	91.00	0.109	10.826	0.1488
7	92.00	0.150	10.952	0.2014
8	93.00	0.201	11.077	0.2644
9	94.00	0.243	11.202	0.3145
10	95.00	0.279	11.327	0.3561
11	96.00	0.319	11.453	0.4012
12	97.00	0.358	11.578	0.4438
13	98.00	0.397	11.703	0.4853
14	99.00	0.435	11.828	0.5247
15	100.00	0.470	11.954	0.5600
16	101.00	0.504	12.079	0.5936
17	102.00	0.537	12.204	0.6254
18	103.00	0.570	12.329	0.6566
19	104.00	0.602	12.455	0.6861
20	105.00	0.633	12.580	0.7141
21	106.00	0.661	12.705	0.7390
22	107.00	0.689	12.830	0.7634
23	108.00	0.713	12.956	0.7840
24	109.00	0.740	13.081	0.8067
25	110.00	0.764	13.206	0.8266
26	111.00	0.788	13.331	0.8462
27	112.00	0.810	13.457	0.8640
28	113.00	0.830	13.582	0.8798
29	114.00	0.847	13.707	0.8932
30	115.00	0.863	13.832	0.9056

RUN NUMBER 257 CONTINUED

POINT	TIME, MIN.	C	CUM. WEIGHT	C/CO
31	116.00	0.881	13.958	0.9195
32	117.00	0.895	14.083	0.9301
33	118.00	0.907	14.208	0.9392
34	119.00	0.919	14.333	0.9482
35	120.00	0.929	14.459	0.9556
36	121.00	0.938	14.584	0.9623
37	122.00	0.947	14.709	0.9689
38	123.00	0.951	14.834	0.9718
39	124.00	0.958	14.960	0.9769
40	125.00	0.961	15.085	0.9791
41	126.00	0.965	15.210	0.9820
42	127.00	0.969	15.335	0.9849

RUN NUMBER 258

ADSORBATE - PROPANE
CARBON PARTICLE SIZE - 40-45 MESH US STD. SIEVE
BED WEIGHT - 46.85 G CARBON
UNCORRECTED VOL. FLOW RATE - 382.0242 ML/MIN
PRESSURE DROP - 32.0 MM H2O
MASS FLOW RATE - 0.1713 G/MIN-CM2
KGAP - 0.6896 G C3H8/MIN-G BED-G C3H8/G GAS
KSAP - 1.0787 G C3H8/MIN-G BED-G C3H8/G SOLID
BIG KGAP - 0.0770 G C3H8/MIN-G BED-G C3H8/G GAS
BIG KSAP - 1.0102 G C3H8/MIN-G BED-G C3H8/G SOLID
EFFECTIVE PARTICLE DIFFUSIVITY - 2.08 X 10-5 CM2/MIN
CO - 0.2454 G C3H6/G GAS

POINT	TIME, MIN.	C	CUM. WEIGHT	C/CO
1	25.50	0.011	10.968	0.0007
2	25.75	0.012	11.089	0.0014
3	26.00	0.014	11.210	0.0029
4	26.25	0.019	11.331	0.0064
5	26.50	0.025	11.453	0.0108
6	26.75	0.043	11.574	0.0238
7	27.00	0.073	11.695	0.0459
8	27.25	0.128	11.816	0.0874
9	27.50	0.210	11.937	0.1521
10	27.75	0.325	12.058	0.2487
11	28.00	0.451	12.179	0.3632
12	28.25	0.569	12.300	0.4794
13	28.50	0.665	12.421	0.5812
14	28.75	0.740	12.542	0.6657
15	29.00	0.800	12.663	0.7368
16	29.50	0.870	12.905	0.8241
17	30.00	0.909	13.148	0.8748
18	31.00	0.948	13.632	0.9273
19	32.00	0.967	14.116	0.9535
20	33.00	0.977	14.600	0.9674
21	34.00	0.980	15.085	0.9716
22	35.00	0.983	15.569	0.9759

RUN NUMBER 259

ADSORBATE - PROPYLENE
CARBON PARTICLE SIZE - 40-45 MESH US STD. SIEVE
BED WEIGHT - 46.85 G CARBON
UNCORRECTED VOL. FLOW RATE - 107.9394 ML/MIN
PRESSURE DROP - 9.5 MM H2O
MASS FLOW RATE - 0.0411 G/MIN-CM2
KGAP - 0.1850 G C3H6/MIN-G BED-G C3H6/G GAS
KSAP - 0.0976 G C3H6/MIN-G BED-G C3H6/G SOLID
BIG KGAP - 0.0089 G C3H6/MIN-G BED-G C3H6/G GAS
BIG KSAP - 0.0948 G C3H6/MIN-G BED-G C3H6/G SOLID
EFFECTIVE PARTICLE DIFFUSIVITY - 0.18 X 10-5 CM2/MIN
CO - 0.0950 G C3H6/G GAS

POINT	TIME, MIN.	C	CUM. WEIGHT	C/CO
1	87.00	0.003	9.569	0.0043
2	88.00	0.008	9.685	0.0114
3	89.00	0.014	9.801	0.0199
4	90.00	0.033	9.917	0.0465
5	91.00	0.066	10.034	0.0917
6	92.00	0.102	10.150	0.1397
7	93.00	0.143	10.266	0.1925
8	94.00	0.190	10.382	0.2510
9	95.00	0.233	10.499	0.3027
10	96.00	0.268	10.615	0.3435
11	97.00	0.309	10.731	0.3900
12	98.00	0.348	10.848	0.4330
13	99.00	0.387	10.964	0.4748
14	100.00	0.425	11.080	0.5144
15	101.00	0.459	11.196	0.5490
16	102.00	0.494	11.313	0.5838
17	103.00	0.527	11.429	0.6158
18	104.00	0.560	11.545	0.6472
19	105.00	0.590	11.662	0.6751
20	106.00	0.623	11.778	0.7052
21	107.00	0.652	11.894	0.7311
22	108.00	0.680	12.010	0.7556
23	109.00	0.707	12.127	0.7789
24	110.00	0.732	12.243	0.8000
25	111.00	0.757	12.359	0.8209
26	112.00	0.781	12.476	0.8406
27	113.00	0.802	12.592	0.8575
28	114.00	0.822	12.708	0.8735
29	115.00	0.840	12.824	0.8877
30	116.00	0.858	12.941	0.9017

RUN NUMBER 259 CONTINUED

POINT	TIME, MIN.	C	CUM. WEIGHT	C/CO
31	117.00	0.874	13.057	0.9141
32	118.00	0.888	13.173	0.9248
33	119.00	0.900	13.289	0.9339
34	120.00	0.914	13.406	0.9444
35	121.00	0.923	13.522	0.9511
36	122.00	0.934	13.638	0.9593
37	123.00	0.941	13.755	0.9645
38	124.00	0.949	13.871	0.9703
39	125.00	0.953	13.987	0.9733
40	126.00	0.958	14.103	0.9769
41	127.00	0.961	14.220	0.9791
42	128.00	0.966	14.336	0.9827
43	129.00	0.969	14.452	0.9849
44	130.00	0.971	14.569	0.9864

RUN NUMBER 260

ADSORBATE - PROPANE
CARBON PARTICLE SIZE - 40-45 MESH US STD. SIEVE
BED WEIGHT - 46.85 G CARBON
UNCORRECTED VOL. FLOW RATE - 382.0242 ML/MIN
PRESSURE DROP - 34.5 MM H2O
MASS FLOW RATE - 0.1658 G/MIN-CM2
KGAP - 0.7195 G C3H8/MIN-G BED-G C3H8/G GAS
KSAP - 1.0734 G C3H8/MIN-G BED-G C3H8/G SOLID
BIG KGAP - 0.0778 G C3H8/MIN-G BED-G C3H8/G GAS
BIG KSAP - 1.0082 G C3H8/MIN-G BED-G C3H8/G SOLID
EFFECTIVE PARTICLE DIFFUSIVITY - 2.07 X 10-5 CM2/MIN
CO - 0.2373 G C3H6/G GAS

POINT	TIME, MIN.	C	CUM. WEIGHT	C/CO
1	25.75	0.011	10.719	0.0007
2	26.00	0.013	10.836	0.0021
3	26.25	0.017	10.953	0.0050
4	26.50	0.025	11.070	0.0108
5	26.75	0.041	11.187	0.0223
6	27.00	0.070	11.304	0.0437
7	27.25	0.125	11.421	0.0851
8	27.50	0.207	11.539	0.1497
9	27.75	0.322	11.656	0.2461
10	28.00	0.445	11.773	0.3575
11	28.25	0.561	11.890	0.4712
12	28.50	0.660	12.007	0.5757
13	28.75	0.736	12.124	0.6611
14	29.00	0.795	12.242	0.7308
15	29.50	0.869	12.476	0.8228
16	30.00	0.908	12.710	0.8735
17	31.00	0.946	13.179	0.9245
18	32.00	0.963	13.648	0.9479
19	33.00	0.977	14.116	0.9674
20	34.00	0.980	14.585	0.9716
21	35.00	0.985	15.054	0.9787

RUN NUMBER 261

ADSORBATE - PROPYLENE
CARBON PARTICLE SIZE - 40-45 MESH US STD. SIEVE
BED WEIGHT - 46.85 G CARBON
UNCORRECTED VOL. FLOW RATE - 380.4558 ML/MIN
PRESSURE DROP - 34.0 MM H2O
MASS FLOW RATE - 0.1586 G/MIN-CM2
KGAP - 0.4962 G C3H6/MIN-G BED-G C3H6/G GAS
KSAP - 0.3344 G C3H6/MIN-G BED-G C3H6/G SOLID
BIG KGAP - 0.0292 G C3H6/MIN-G BED-G C3H6/G GAS
BIG KSAP - 0.3219 G C3H6/MIN-G BED-G C3H6/G SOLID
EFFECTIVE PARTICLE DIFFUSIVITY - 0.62 X 10-5 CM2/MIN
CO - 0.1174 G C3H6/G GAS

POINT	TIME, MIN.	C	CUM. WEIGHT	C/CO
1	26.00	0.002	10.366	0.0029
2	26.25	0.005	10.478	0.0071
3	26.50	0.007	10.591	0.0100
4	26.75	0.009	10.703	0.0128
5	27.00	0.013	10.815	0.0185
6	27.25	0.031	10.927	0.0438
7	27.50	0.054	11.039	0.0755
8	27.75	0.083	11.151	0.1146
9	28.00	0.120	11.263	0.1631
10	29.00	0.269	11.711	0.3447
11	30.00	0.400	12.160	0.4885
12	31.00	0.521	12.608	0.6101
13	32.00	0.628	13.056	0.7097
14	33.00	0.724	13.505	0.7933
15	34.00	0.800	13.953	0.8559
16	35.00	0.861	14.401	0.9041
17	36.00	0.902	14.850	0.9354
18	37.00	0.933	15.298	0.9586
19	38.00	0.950	15.747	0.9711
20	39.00	0.960	16.195	0.9784
21	40.00	0.965	16.643	0.9820
22	41.00	0.969	17.092	0.9849

RUN NUMBER 262

ADSORBATE - PROPANE
CARBON PARTICLE SIZE - 40-45 MESH US STD. SIEVE
BED WEIGHT - 46.85 G CARBON
UNCORRECTED VOL. FLOW RATE - 549.2996 ML/MIN
PRESSURE DROP - 52.0 MM H2O
MASS FLOW RATE - 0.2357 G/MIN-CM2
KGAP - 0.7084 G C3H8/MIN-G BED-G C3H8/G GAS
KSAP - 1.3727 G C3H8/MIN-G BED-G C3H8/G SOLID
BIG KGAP - 0.0910 G C3H8/MIN-G BED-G C3H8/G GAS
BIG KSAP - 1.2664 G C3H8/MIN-G BED-G C3H8/G SOLID
EFFECTIVE PARTICLE DIFFUSIVITY - 2.60 X 10-5 CM2/MIN
CO - 0.2841 G C3H6/G GAS

POINT	TIME, MIN.	C	CUM. WEIGHT	C/CO
1	18.50	0.012	10.592	0.0014
2	18.75	0.014	10.759	0.0029
3	19.00	0.018	10.925	0.0057
4	19.25	0.023	11.092	0.0093
5	19.50	0.035	11.258	0.0180
6	19.75	0.060	11.425	0.0363
7	20.00	0.114	11.592	0.0767
8	20.25	0.210	11.758	0.1521
9	20.50	0.351	11.925	0.2716
10	20.75	0.502	12.091	0.4123
11	21.00	0.636	12.258	0.5497
12	21.25	0.735	12.425	0.6599
13	21.50	0.809	12.591	0.7478
14	21.75	0.854	12.758	0.8037
15	22.00	0.887	12.924	0.8460
16	22.50	0.926	13.258	0.8975
17	23.00	0.947	13.591	0.9259
18	24.00	0.972	14.257	0.9604
19	25.00	0.982	14.924	0.9744
20	26.00	0.990	15.590	0.9858
21	27.00	0.993	16.257	0.9900

RUN NUMBER 263

ADSORBATE - PROPYLENE
CARBON PARTICLE SIZE - 40-45 MESH US STD. SIEVE
BED WEIGHT - 46.85 G CARBON
UNCORRECTED VOL. FLOW RATE - 378.9080 ML/MIN
PRESSURE DROP - 31.5 MM H2O
MASS FLOW RATE - 0.1629 G/MIN-CM2
KGAP - 0.7736 G C3H6/MIN-G BED-G C3H6/G GAS
KSAP - 0.3291 G C3H6/MIN-G BED-G C3H6/G SOLID
BIG KGAP - 0.0307 G C3H6/MIN-G BED-G C3H6/G GAS
BIG KSAP - 0.3212 G C3H6/MIN-G BED-G C3H6/G SOLID
EFFECTIVE PARTICLE DIFFUSIVITY - 0.62 X 10-5 CM2/MIN
CD - 0.0784 G C3H6/G GAS

POINT	TIME, MIN.	C	CUM. WEIGHT	C/CO
1	26.25	0.002	10.775	0.0029
2	26.50	0.003	10.890	0.0043
3	26.75	0.004	11.005	0.0057
4	27.00	0.005	11.120	0.0071
5	27.25	0.016	11.235	0.0227
6	27.50	0.037	11.350	0.0521
7	27.75	0.061	11.465	0.0850
8	28.00	0.092	11.581	0.1265
9	28.25	0.129	11.696	0.1747
10	29.00	0.246	12.041	0.3180
11	30.00	0.376	12.502	0.4631
12	31.00	0.500	12.962	0.5897
13	32.00	0.608	13.423	0.6916
14	33.00	0.704	13.883	0.7763
15	34.00	0.786	14.344	0.8446
16	35.00	0.848	14.805	0.8940
17	36.00	0.896	15.265	0.9309
18	37.00	0.928	15.726	0.9549
19	38.00	0.949	16.186	0.9703
20	39.00	0.959	16.647	0.9777
21	40.00	0.964	17.107	0.9813
22	41.00	0.970	17.568	0.9856

RUN NUMBER 264

ADSORBATE - PROPANE
CARBON PARTICLE SIZE - 40-45 MESH US STD. SIEVE
BED WEIGHT - 46.85 G CARBON
UNCORRECTED VOL. FLOW RATE - 549.2996 ML/MIN
PRESSURE DROP - 49.5 MM H2O
MASS FLOW RATE - 0.2413 G/MIN-CM2
KGAP - 0.7478 G C3H8/MIN-G BED-G C3H8/G GAS
KSAP - 1.3276 G C3H8/MIN-G BED-G C3H8/G SOLID
BIG KGAP - 0.0909 G C3H8/MIN-G BED-G C3H8/G GAS
BIG KSAP - 1.2328 G C3H8/MIN-G BED-G C3H8/G SOLID
EFFECTIVE PARTICLE DIFFUSIVITY - 2.53 X 10-5 CM2/MIN
CO - 0.2679 G C3H6/G GAS

POINT	TIME, MIN.	C	CUM. WEIGHT	C/CO
1	18.75	0.012	11.022	0.0014
2	19.00	0.017	11.192	0.0050
3	19.25	0.022	11.363	0.0086
4	19.50	0.031	11.533	0.0151
5	19.75	0.056	11.704	0.0333
6	20.00	0.117	11.875	0.0790
7	20.25	0.216	12.045	0.1570
8	20.50	0.355	12.216	0.2751
9	20.75	0.505	12.386	0.4152
10	21.00	0.635	12.557	0.5486
11	21.25	0.735	12.727	0.6599
12	21.50	0.802	12.898	0.7392
13	21.75	0.852	13.068	0.8012
14	22.00	0.882	13.239	0.8395
15	22.50	0.921	13.580	0.8908
16	23.00	0.947	13.921	0.9259
17	24.00	0.973	14.603	0.9618
18	25.00	0.987	15.285	0.9815
19	26.00	0.991	15.967	0.9872
20	27.00	0.992	16.649	0.9886

APPENDIX B - SAMPLE CALCULATIONS

The following programs were used to evaluate the calculated values of the breakthrough curves for the models tested. The first program listed is for the case of propane replacing propylene and the second, for the reverse case. Input data to these programs were: 1) the run number, 2) slopes from plots such as Figure 50 for propane replacing propylene and Figure 51 for the opposite case, and 3) the volumetric flow rate. Calculated values from the various breakthrough models using the input data from Figure 50 in the propane correlation program are given in Figure 28 and plotted in Figure 30. Figure 29 gives the calculated values using the input data from Figure 51 and the propylene correlation program. These values are plotted in Figure 31.

These programs were written in Basic Programming Support Fortran IV Language for the IBM series 360, model 65 digital computer. Listed alphabetically below is the programming nomenclature:

AEB	Expected slope of Eagleton and Bliss model.
AGC	Expected slope of Glueckauf and Coates model.
AHT/CL	Height of adsorption bed.
AHTG	Height of gas transfer unit (39).
AHTOG	Overall height of gas transfer unit (39).
AHTS	Height of solid transfer unit (39).

AKSAP	Solid phase mass transfer coefficient times effective mass transfer area calculated from Glueckauf and Coates model.
ALFA	Linear isotherm intercept.
ANTOG	Overall number of gas transfer units (39).
AREA/AX	Cross-sectional area of adsorption bed.
BKGAP	Overall gas phase mass transfer coefficient times the effective mass transfer area.
CD	Concentration of adsorbate at discontinuity.
DP	Effective particle diffusivity.
DP2	Average particle diameter squared.
EPSI	Void fraction.
G2	Mass flow rate per unit area of bed cross section.
GPRIM	Mass flow rate.
PHI	Porosity of bed.
RHOB	Bulk density of bed.
RHOG	Density of gas.
RSTR	Separation factor (42).
RKGAP	Gas phase mass transfer coefficient times effective mass transfer area times bulk density.
RKSAP	Solid phase mass transfer coefficient times effective mass transfer area times bulk density.
SKGAP	Gas phase mass transfer coefficient times effective mass transfer area.
SKSAP	Solid phase mass transfer coefficient times effective mass transfer area.

SNR Number of reaction units (42).

U Soluted adsorbed in the adsorption zone (39).

W1(I) Cumulative weight of effluent gas from Eagleton and Bliss model, $C < C_D$.

W2(I) Cumulative weight of effluent gas from Eagleton and Bliss model, $C > C_D$.

W2(I) Cumulative weight of effluent gas from Boyd, Meyers, and Adamson model.

W3(I) Cumulative weight of effluent gas from Eagleton and Bliss model, solid film controlling.

W4(I) Cumulative weight of effluent gas from Selke and Bliss model.

W5(I) Cumulative weight of effluent gas from Glueckauf and Coates model.

W6(I) Cumulative weight of effluent gas from Vermeulen model.

W7(I) Cumulative weight of effluent gas from Sillen and Ekedahl model.

WA Weight of effluent gas during breakthrough curve.

WB Weight of effluent gas at breakpoint.

WC Weight of adsorbate adsorbed on adsorbent at bed exhaustion.

WE Weight of effluent gas at bed exhaustion.

XA Ratio of gas phase mass transfer coefficient to Glueckauf and Coates solid phase mass transfer coefficient.

XC Ratio of gas phase mass transfer coefficient to Eagleton and Bliss solid phase mass transfer coefficient.

XOSTR Equilibrium adsorbate capacity of adsorbent.

ZA Height of adsorption zone.

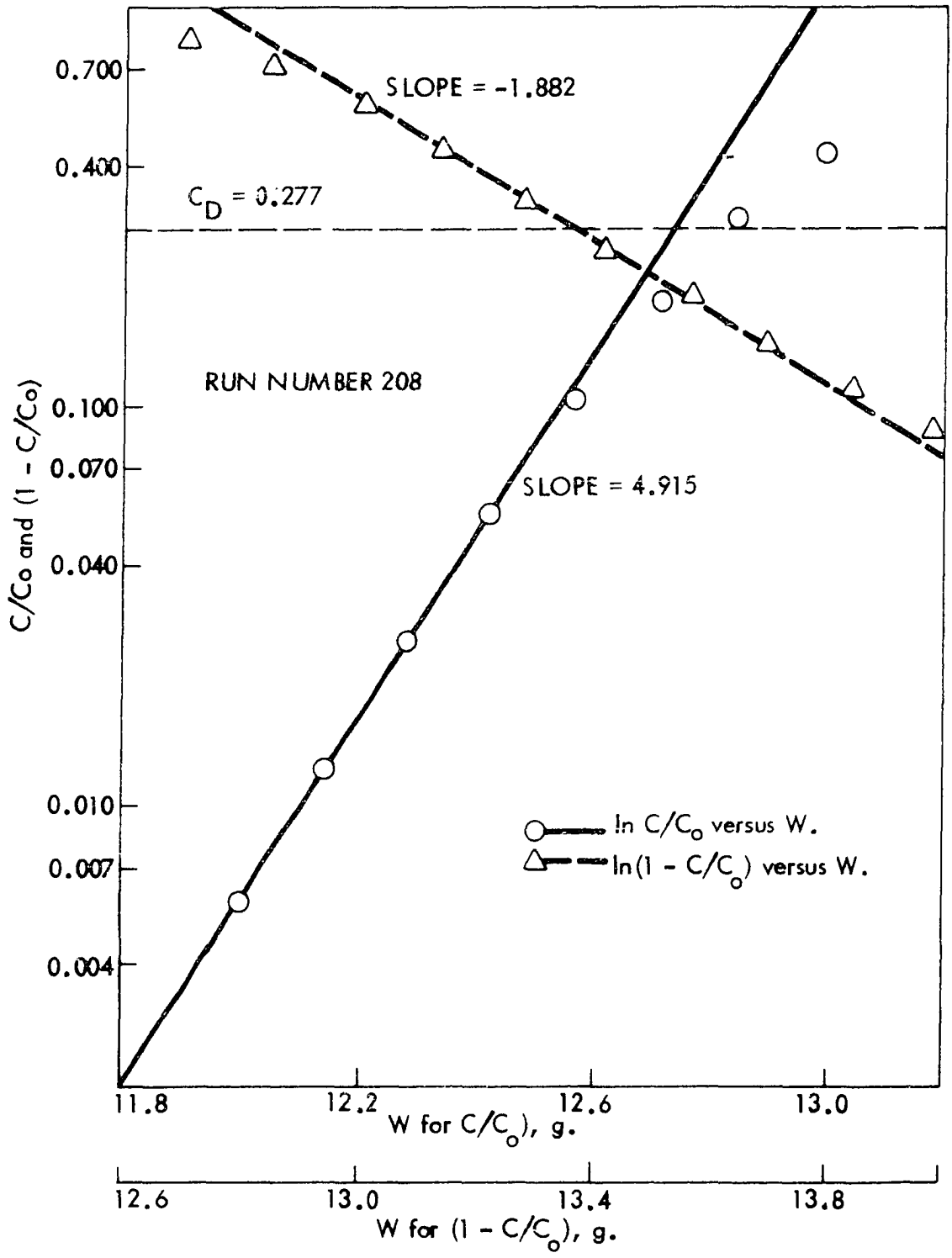

Figure [illegible]. C/C_o and $(1 - C/C_o)$ versus W for propane on Columbia LC 20/40, Grade [illegible]-11, activated carbon at 25° C. (Run number 208)

```
C
C
C
C    PROPANE CORRELATION
C
C
      DIMENSION C(99), W1(99), W2(99), W3(99), W4(99), W5(99)
     1, W6(99), W7(99), SL01(99),SL02(99), SL03(99), FLOW(99)
     2, SL04(99)
    1 FORMAT (I10,4F15.8,F10.7)
   10 FORMAT (1H ,10X,2F15.9)
   11 FORMAT (1H0,10X,'DP=',F14.9,'  CM2/MIN',5X,'BIG KSAP=',
     1F14.9,' MIN -1',5X,'KSAP1 =',F14.9,' MIN -1')
   15 FORMAT (1H1,10X,'BOYD ET. AL.')
   17 FORMAT(1H0,10X,'R1 =',F10.6,10X,'R2 =',F10.6,10X,'G/ARE
     1A = ',F10.6)
   19 FORMAT (////,20X,'TREYBAL SOLUTION')
   20 FORMAT(1H0,10X,'NUMBER',I2,6X,'BREAKPOINT=',F8.4,' GRAM
     1S',6X,'BED EXHAUSTION =',F8.4,' GRAMS',5X,'BIG KGAP =',
     2F10.6)
   23 FORMAT (///,3X,'G PRIM=',F8.4,'G/MIN',5X,'KGAP=',F10.6,
     15X,'KSAP =',F10.6,5X,'CD =',F7.5,5X,'V FLOW =',F10.4,5X
     2,'NR =',F10.5)
   24 FORMAT (1H1, 4X,'RUN NUMBER',I4)
   25 FORMAT(1H0,3X,F10.8,5X,F10.5,5X,F10.5,5X,F10.5,5X,F10.5
     1,5X,F10.5,5X,F10.5,5X,F10.5)
   26 FORMAT(////,5X,'C/CO',14X,'EB1',11X,'EB2',12X,'EBOA',13
     1X,'SB',12X,'GC',13X,'MV',13X,'SE')
   41 FORMAT (I10,5F12.8)
   42 FORMAT (I5, 7F10.7)
      V=135.14
      XOSTR=0.2660
      CO=1.0
      ALFA=0.222
      RSTR=0.0669834
      PI=3.1415926536
      PHI=61.90/V
      DO 601 N=1,32
      IF (N.LE.8)  GO TO 650
      IF (N.LE.16) GO TO 651
      IF (N.LE.24) GO TO 652
      WS=46.85
      DP2=0.00147456
      GO TO 660
  650 WS=49.55
      DP2=0.0029648025
      GO TO 660
  651 WS=47.95
      DP2=0.00416025
      GO TO 660
```

```
652 WS=50.98
    DP2=0.0021022225
660 CONTINUE
    RHOB=WS/V
    RHOG=1.0/544.54321
    EPSI=PHI*RHOG/RHOB
    READ(1,1) M,SLO1(N), SLO2(N),SLO3(N), FLOW(N)
    GPRIM=FLOW(N)*RHOG
    SKGAP=SLO1(N)*GPRIM*XOSTR/CO
    Z=-(SLO2(N)*XOSTR*GPRIM)/CO/SKGAP
    AHT=47.8
    AREA=V/AHT
    G2=GPRIM/AREA
    CD=Z*CO/(1.0+Z)
    SKSAP=SKGAP/(ALFA/CD-XOSTR/CO)
    AKSAP=-SLO2(N)*GPRIM
    XA=SKGAP/AKSAP
    XB=XOSTR/CO
    XC=SKGAP/SKSAP
    A=RHOB*XOSTR*V/CO
    B=CO*GPRIM/AKSAP/XOSTR/RHOB/V
    D=(((PI**2)*(RSTR**2)+15.0*(1.0-RSTR))/(PI**2))
    F=SKGAP*WS/GPRIM
    PSI=4.0*(PI**2)/60.0
    SNR=SLO3(N)*A/(1.0-RSTR)
    BKSAP=-(SLO2(N)*XOSTR*GPRIM/ALFA)
    DP=AKSAP*DP2/60.0
    ANP=60.0*DP*XOSTR*RHOB*V/CO/GPRIM/DP2
    E1=CO/CD
    E2=(1.0-CD/CO)/(CD/CO)
    AEB=CO*SKGAP/XOSTR/GPRIM/E2
    BEB=(-SKGAP*WS/GPRIM-2.0+CO/CD)/E2
    AGC=-SLO2(N)
    BGC=(SLO2(N)*XOSTR*RHOB*V/CO-1.0)
    C(1)=0.05
    WRITE(3,24)M
    WRITE(3,23) GPRIM,SKGAP,SKSAP,CD,FLOW(N),SNR
    WRITE (3,11) DP,BKSAP,AKSAP
    WRITE (3,17) XC,XA,G2
    WRITE (3,26)
    DO 600 I=1,19
    C1=ALOG((CD/CO)/(C(I)/CO))
    C2=ALOG((1.0-CD/CO)/(1.0-C(I)/CO))
    C3=ALOG(C(I)/CO)
    C4=ALOG(C(I)/CO/(1.0-C(I)/CO))
    C5=ALOG(1.0-C(I)/CO)
    C6=(C(I)/CO**2)
    C7=-ALOG(1.0-C6)
    W1(I)=(F+2.0-C1-E1)/SLO1(N)
    W2(I)=(C2*E2+F+2.0-E1)/SLO1(N)
```

```
      W3(I)=(SLO2(N)*XOSTR*WS/CO+C5+1.0)/SLO2(N)
      W4(I)=(C3+F+1.0)/SLO1(N)
      W5(I)=A*(1.0-B*(1.0+C5))
      W6(I)=A*(B*(D*C7-0.93)+1.0)
      W7(I)=(C4/(1.0-RSTR)/SNR+1.0)*A
      C(I+1)=C(I)+0.05
  600 WRITE (3,25) C(I), W1(I), W2(I), W3(I), W4(I), W5(I),
     1W6(I),W7(I)
      WRITE (3,15)
      W1(1)=10.0
      DO 100 J=1,30
      Z=CO*W1(J)/XOSTR/RHOB/V
      SUM=0.0
      DO 101 I=1,5
      AN=I
      W2(I)=1.0/AN/(EXP((AN**2)*(PSI*ANP*(Z-1.0)+0.97)))
  101 SUM=SUM+W2(I)
      C(J)=1.0-6.0/(PI**2)*SUM
      W1(J+1)=W1(J)+0.2
  100 WRITE (3,10) C(J),W1(J)
      WRITE (3,19)
      RKGAP=SKGAP*RHOB
      RKSAP=SKSAP*RHOB
      CL=47.8
      AX=V/CL
      FF=0.637
      GS=GPRIM/AX
      ALS=CO*GS/XOSTR
      ANTOG=3.488
      AHTG=GS/RKGAP
  501 AHTS=ALS/RKSAP
  502 AHTOG=AHTG+3.29*GS*AHTS/ALS
      ZA=AHTOG*ANTOG
      BKGAP=ANTOG*GS/ZA
      DSBP=(CL-ZA*FF)/CL
      WB=DSBP*WS*XOSTR
      WC=WS*XOSTR
      U=WC-WB
      WA=U/FF/CO
      WE=WA+WB
      K=1
  500 WRITE(3,20) K,WB,WE,BKGAP
  601 CONTINUE
      STOP
      END
```

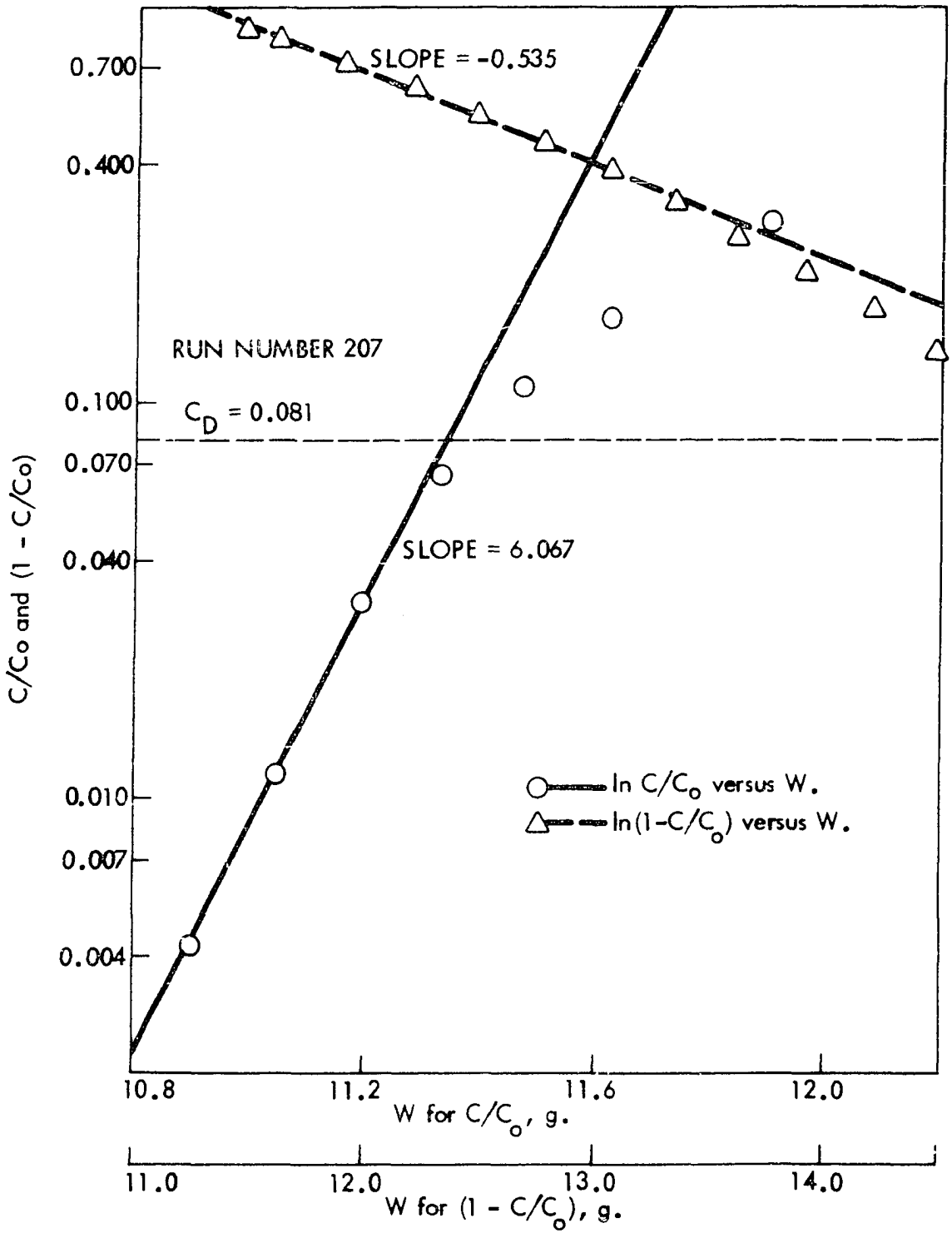

Figure 51. C/C_o and (1 - C/C_o) versus W for propylene on Columbia LC 20/48, Grade H-6[illegible]-11 activated carbon at 25° C. (Run number 207)

```
C
C
C
C   PROPYLENE CORRELATION
C
C
      DIMENSION C(99), W1(99), W2(99), W3(99), W4(99), W5(99)
     1, W6(99), W7(99), SLO1(99),SLO2(99), SLO3(99), FLOW(99)
     2, SLO4(99)
    1 FORMAT (I10,4F15.8,F10.7)
   15 FORMAT (1H1,10X,'BOYD ET. AL.')
   10 FORMAT (1H ,10X,2F15.9)
   11 FORMAT (1H0,10X,'DP=',F14.9,'  CM2/MIN',5X,'BIG KSAP=',
     1F14.9,' MIN -1',5X,'KSAP1 =',F14.9,' MIN -1')
   17 FORMAT(1H0,10X,'R1 =',F10.6,10X,'R2 =',F10.6,10X,'G/ARE
     1A = ',F10.6)
   19 FORMAT (////,20X,'TREYBAL SOLUTION')
   20 FORMAT(1H0,10X,'NUMBER',I2,6X,'BREAKPOINT=',F8.4,' GRAM
     1S',6X,'BED EXHAUSTION =',F8.4,' GRAMS',5X,'BIG KGAP =',
     2F10.6)
   23 FORMAT (///,3X,'G PRIM=',F8.4,'G/MIN',5X,'KGAP=',F10.6,
     15X,'KSAP =',F10.6,5X,'CD =',F7.5,5X,'V FLOW =',F10.4,5X
     2,'NR =',F10.5)
   24 FORMAT (1H1, 4X,'RUN NUMBER',I4)
   25 FORMAT(1H0,3X,F10.8,5X,F10.5,5X,F10.5,5X,F10.5,5X,F10.5
     1,5X,F10.5,5X,F10.5,5X,F10.5)
   26 FORMAT(////,5X,'C/C0',14X,'EB1',11X,'EB2',12X,'EB0A',13
     1X,'SB',12X,'GC',13X,'MV',13X,'SE')
   41 FORMAT (I10,5F12.8)
   42 FORMAT (I5, 7F10.7)
      V=135.14
      X0STR=0.2630
      C0=1.0
      ALFA=0.205
      RSTR=0.080365
      PI=3.1415926536
      PHI=61.90/V
      DO 601 N=1,31
      IF (N.LE.8)  GO TO 650
      IF (N.LE.16) GO TO 651
      IF (N.LE.23) GO TO 652
      WS=46.85
      DP2=0.00147456
      GO TO 660
  650 WS=49.55
      DP2=0.0029648025
      GO TO 660
  651 WS=47.95
      DP2=0.00416025
      GO TO 660
```

```
652 WS=50.98
    DP2=0.0021022225
660 CONTINUE
    RHOB=WS/V
    RHOG=1.0/569.5057
    EPSI=PHI*RHOG/RHOB
    READ(1,1) M,SLO1(N), SLO2(N),SLO3(N), FLOW(N)
    GPRIM=FLOW(N)*RHOG
    SKGAP=SLO1(N)*GPRIM*XOSTR/CO
    Z=-(SLO2(N)*XOSTR*GPRIM)/CO/SKGAP
    AHT=47.8
    AREA=V/AHT
    G2=GPRIM/AREA
    CD=Z*CO/(1.0+Z)
    SKSAP=SKGAP/(ALFA/CD-XOSTR/CO)
    AKSAP=-SLO2(N)*GPRIM
    XA=SKGAP/AKSAP
    XB=XOSTR/CO
    XC=SKGAP/SKSAP
    A=RHOB*XOSTR*V/CO
    D=(((PI**2)*(RSTR**2)+15.0*(1.0-RSTR))/(PI**2))
    F=SKGAP*WS/GPRIM
    PSI=4.0*(PI**2)/60.0
    SNR=SLO3(N)*A/(1.0-RSTR)
    BKSAP=-(SLO2(N)*XOSTR*GPRIM/ALFA)
    B=CO*GPRIM/AKSAP/XOSTR/RHOB/V
    DP=AKSAP*DP2/60.0
    ANP=60.0*DP*XOSTR*RHOB*V/CO/GPRIM/DP2
    E1=CO/CD
    E2=(1.0-CD/CO)/(CD/CO)
    AEB=CO*SKGAP/XOSTR/GPRIM/E2
    BEB=(-SKGAP*WS/GPRIM-2.0+CO/CD)/E2
    AGC=-SLO2(N)
    BGC=(SLO2(N)*XOSTR*RHOB*V/CO-1.0)
    C(1)=0.05
    WRITE(3,24)M
    WRITE(3,23) GPRIM,SKGAP,SKSAP,CD,FLOW(N),SNR
    WRITE (3,11) DP,BKSAP,AKSAP
    WRITE (3,17) XC,XA,G2
    WRITE (3,26)
    DO 600 I=1,19
    C1=ALOG((CD/CO)/(C(I)/CO))
    C2=ALOG((1.0-CD/CO)/(1.0-C(I)/CO))
    C3=ALOG(C(I)/CO)
    C4=ALOG(C(I)/CO/(1.0-C(I)/CO))
    C5=ALOG(1.0-C(I)/CO)
    C6=(C(I)/CO**2)
    C7=-ALOG(1.0-C6)
    W1(I)=(F+2.0-C1-E1)/SLO1(N)
    W2(I)=(C2*E2+F+2.0-E1)/SLO1(N)
```

```
      W3(I)=(SLO2(N)*XOSTR*WS/CO+C5+1.0)/SLO2(N)
      W4(I)=(C3+F+1.0)/SLO1(N)
      W5(I)=A*(1.0-B*(1.0+C5))
      W6(I)=A*(B*(D*C7-0.93)+1.0)
      W7(I)=(C4/(1.0-RSTR)/SNR+1.0)*A
      C(I+1)=C(I)+0.05
  600 WRITE (3,25) C(I), W1(I), W2(I), W3(I), W4(I), W5(I),
     1W6(I),W7(I)
      WRITE (3,15)
      W1(1)=9.6
      DO 100 J=1,32
      Z=CO*W1(J)/XOSTR/RHOB/V
      SUM=0.0
      DO 101 I=1,5
      AN=I
      W2(I)=1.0/AN/(EXP((AN**2)*(PSI*ANP*(Z-1.0)+0.97)))
  101 SUM=SUM+W2(I)
      C(J)=1.0-6.0/(PI**2)*SUM
      W1(J+1)=W1(J)+0.2
  100 WRITE (3,10) C(J),W1(J)
      WRITE (3,19)
      RKGAP=SKGAP*RHOB
      RKSAP=SKSAP*RHOB
      CL=47.8
      AX=V/CL
      FF=0.6605
      GS=GPRIM/AX
      ALS=CO*GS/XOSTR
      ANTOG=3.301
      AHTG=GS/RKGAP
  501 AHTS=ALS/RKSAP
  502 AHTOG=AHTG+3.29*GS*AHTS/ALS
      ZA=AHTOG*ANTOG
      BKGAP=ANTOG*GS/ZA
      DSBP=(CL-ZA*FF)/CL
      WB=DSBP*WS*XOSTR
      WC=WS*XOSTR
      U=WC-WB
      WA=U/FF/CO
      WE=WA+WB
      K=1
  500 WRITE(3,20) K,WB,WE,BKGAP
  601 CONTINUE
      STOP
      END
```